主論文

THESIS

A Study on Nature and Origin of Strongly Stablized Metallic State in Organic Charge-Transfer Complexes of BEDO-TTF

Sachio Horiuchi

Title: A Study on Nature and Origin of Strongly Stabilized Metallic State in Organic Charge-Transfer Complexes of BEDO-TTF

Contents.

Chapter 1 General Introduction

The designs of molecular conductors based on π-electronic systems have been developed both on single component materials and on charge-transfer (CT) complexes.[1] The creation of metals and superconductors requires the formation of partially filled electronic bands. In the case of single component systems, stable open-shell (free radical) species are thus candidates of the molecular conductors. If the component has the closed-shell electronic structure, it is necessary to overlap the bands of highest occupied (HOMO) and lowest unoccupied molecular orbitals (LUMO) each other by reducing their energy separation and increasing the band widths. In spite of extensive work on single component conductors,[2] even molecular metals have not been obtained so far by the above two methods at ambient pressure.

On the other hand for CT complexes, R. S. Mulliken presented the theory on the intermolecular CT interactions in 1951,[3] explaining the presence of either quasi neutral or ionic ground state and the appearance of CT bands in the optical spectra. Utilizing this CT interaction, Akamatu *et al.* discovered the highly conducting perylene-bromide complex in 1954 during the pioneering design on organic semiconductors.[4] The perylene molecules oxidized by bromine exist as cation radicals, serving electric conduction in this complex. The extensive research brought about several major breakthroughs in the development of molecular conductors of CT complexes: (i) the synthesis of TCNQ (for this and other chemical abbreviations in text, see the last part of this thesis) and its highly conducting anion radical salts,[5] (ii) the discovery of novel donor TTF and its TCNQ complex, the first molecular metal,[6] (iii) the finding of molecular superconductor, $(TMTSF)_2X$,[7] (iv) the development of molecular metals[8] and superconductors[9] based on BEDT-TTF with raised dimensionality (two-dimensional, 2D) and critical transition temperatures (Tc >

10 K), (v) the discovery of high-T_c 3D superconductors based on C_{60}.[10] It should be also noted that some ionic CT complexes also serve as the molecular magnets by utilizing the spins on the radical molecules.[11]

The CT complexes are classifiable into two main groups. The first is a donor(D)-acceptor(A) type complex derived from closed-shell organic electron donor and acceptor molecules, as exemplified by TTF-TCNQ. The second group is comprised of radical salts which are made up of the radical ion of an organic donor or acceptor molecule and a closed-shell counterion.

Since most of the components are planar π-molecules, the structure of their CT complexes are low-dimensional. The molecular packing patterns are rather rich in variety, but in most cases, they are roughly classified into two major types; an alternating stack of donor and acceptor molecules and a segregated columnar stack or layered structure of the component molecules. The complexes of the former type have the insulating ground state, but in some cases they accompanied with several interesting properties such as the neutral-ionic transition induced by cooling and/or pressure,[12] switching effect,[13] negative-resistance effect,[14] and spin-Peierls transition.[15] To obtain molecular metals, it is necessary that donor and/or acceptor molecules form a uniform segregated columnar structure and have a partial CT ground state.[16] Particularly in formation of DA-type complexes, relative strength of the components plays a critical role in the conducting properties.[17] Due to the low-dimensional electronic structure, the metallic complexes often experience a metal-insulator transition driven by charge- or spin-density wave (CDW or SDW) instability, which has been attracting an interest also in solid state physics.[18] To stabilize the metallic state, various chemical modifications have been made to the π-molecules, either by introducing weak disorder into the crystals, or by increasing the dimensionality of their electronic structures. The latter modification, e.g., substitution of the sulfur atoms for heavier atoms

(Se and Te)[19] and/or addition of further peripheral chalcogen atoms to the TTF skeleton[8] has yielded fruitful results. The most successful examples are TMTSF and BEDT-TTF, both of which have produced a number of molecular superconductors and low-temperature metals.

Most molecular superconductors are obtained as radical salts.[7,20] The superconducting transition temperature (*Tc*) has markedly increased as the dimensionality of the electronic structure has been raised from quasi-one-dimensional (1D) (e.g. $(TMTSF)_2X$ salts[7]) to two-dimensional (2D) (e.g. κ-$(BEDT\text{-}TTF)_2X$ salts[9,20]).[21] At the same time, the above structural requirement for molecular metals was modified; not only columnar, but also a layered structure of D or A molecules can enable the metallic state when intermolecular interactions are sufficient. For example, the κ-type salts reveal the 2D layers assembled of the dimers of donor molecules instead of columns.

BEDT-TTF derivatives thus seem to be good candidates for higher-dimensional conductors of the DA-type, as well as for superconductors. In fact, 2D donor layers and 1D acceptor columns appear in triclinic (BEDT-TTF)(TCNQ) complex.[22] However, such metallic examples are still few[22,23] among over 20 DA-type BEDT-TTF complexes currently known,[22-24] the physical properties of which greatly depend on the nature of the counter molecules.

As one of the various kinds of BEDT-TTF analogues designed with the aim of increasing *Tc* of superconductivity, the oxygen analog donor, BEDO-TTF (Scheme 1) was synthesized in 1989 by Suzuki *et al.*[25] Since then, its cation radical salts have been prepared with about 30 inorganic anions.[26] Only three of these are semiconducting, and most of the rests are metals, including two superconductors with *Tc* of about 1 K.[27] Their structural and physical properties are poorly characterized for these radical salts, and nothing for

DA-type complexes before this work.

The present research explores BEDO-TTF complexes with a number of counter component molecules, the most of which are organic acceptors. In contrast to the anions of closed-shell electronic structure, the organic acceptors in DA-type complexes themselves are potential building blocks for conducting columns or magnetic chains. In addition, their molecular shape, size, and electron accepting ability, which are easily controlled by chemical modifications, are also expected to play important roles in structural and physical properties and electronic states of the respective complexes. The early part of this thesis will discuss the transport, optical, and magnetic properties of the BEDO-TTF complexes. Through examining the effect of acceptor molecules, these properties are emphasized as unusual particularly for the accessibility to formation of molecular metals. In the latter part, the physical properties of the complexes are discussed in relation with the crystal and electronic band structures. The primary goal is to offer a deeper understanding of the origin of the stable metallic states.

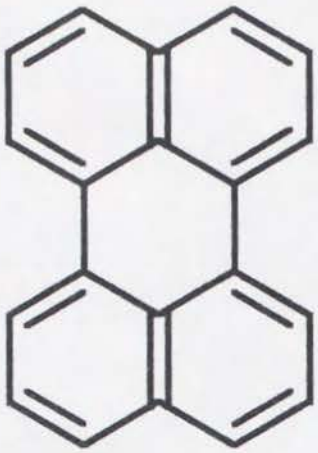

Perylene

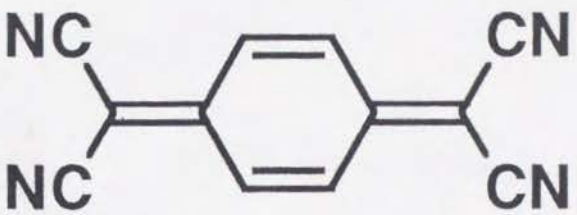

TCNQ

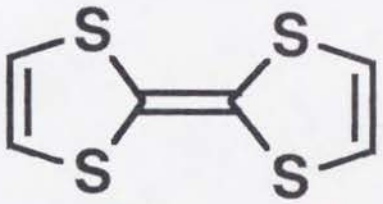

TTF

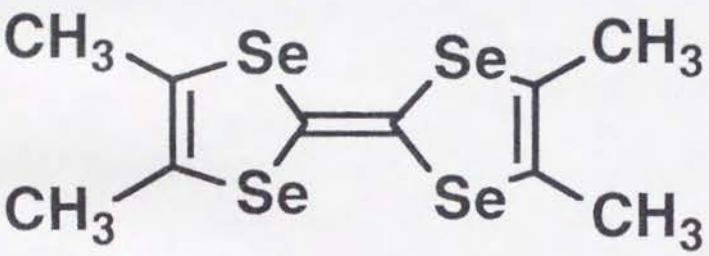

TMTSF

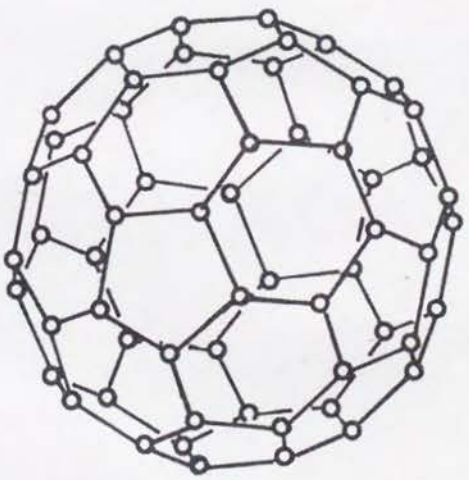

C_{60}

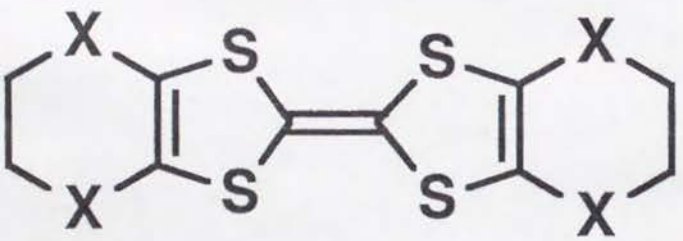

X=O: BEDO-TTF

X=S: BEDT-TTF

Chart 1-1.

Chapter 2 Experimental

2-1 Synthesis of BEDO-TTF

BEDO-TTF was synthesized according to the procedures outlined in Chart 2-1. The chlorination of dioxane and subsequent reactions were performed according to the Refs. 25 and 28, respectively, except the synthesis of III in Chart 2-1. Each reaction product was identified by ^{1}H-NMR spectra recorded on a VARIAN-GEMINI200 spectrometer (200 MHz).

2,3-Dichloro-1,4-dioxane (I). To a 2 l, 3-necked round-bottomed flask equipped with a magnetic stirrer, thermometer and condenser, 1,4-dioxane (1005 g, 11.41 mol, Nakalai) was introduced through a basic alumina column (Super I, ICN). Iodine (6.43 g, 25.3 mmol, Wako) was added before the stirred mixture was bubbled with argon from an inlet tube for 50 min. After the introduction of chlorine gas (several bubbles per one second) was started under slow argon gas flow (one bubble per two minutes), the mixture was heated on an oil bath. The reaction mixture was refluxed for 53 h until the 1,4-dioxane was much decreased in the ^{1}H-NMR spectra. After stopping the insertion of chlorine, the resultant black mixture was cooled to room temperature under bubbling argon for 2 h, poured onto ether (200 ml), and washed with ion-exchanged water (200 ml) and with aq $Na_2S_2O_3$ solution (600 ml). The organic layer was separated and dried with $MgSO_4$ overnight. Ether was removed under reduced pressure, and the residue was distilled at 88 °C /22 Torr to yield I (650 g, 36.4 %) as a pale pink liquid. ^{1}H-NMR ($CDCl_3$) δ 5.97 (2H, s, ClCH), 4.40 (2H, m, OCH_2), 3.74 (2H, m, OCH_2).

(1,4-Dioxane-2,3-diyl)-bis(N,N-dimethyldithiocarbamate) (II). The suspension of I (100 g, 0.637 mol) and N,N-dimethyldithiocarbamic acid disodium salt

dihydrate (245 g, 1.37 mol, Tokyo Kasei) in acetonitrile (1.9 l) was refluxed in 2 l 3-necked round-bottomed flask for 6 h. After cooled by ice bath, the precipitate was collected by filtration, washed with ion-exchanged water (1 l), ethanol (80 ml), and ether (280 ml). After dried *in vacuo*, II was obtained as a colorless solid (125.9 g, 60.3 %). ^{1}H-NMR ($CDCl_3$) δ 6.5 (2H, s, SCH), 3.8 (4H, m, OCH_2), 3.5 (6H, s, CH_3), 3.4 (6H, s, CH_3).

(5,6-Dihydro-1,4-dioxin-2-yl)-N,N-dimethyldithiocarbamate (III). In a 300 ml 3-necked round-bottomed flask equipped with a magnetic stirrer, a thermometer and a L-shaped glass tube connected to a 200 ml round-bottomed flask, II (125.9g, 0.386 mol) was heated by an oil bath (160 °C) with stirring under nitrogen gas flow. The white solid gradually decomposed into a reddish brown oil. After heating for 40 min, the reaction mixture was allowed to cool to the room temperature. The residue dissolved in benzene (50 ml) was chromatographed on a silica gel (70-230 mesh) eluting with benzene to yield III as a reddish brown solid (46.1 g, 58.1 %), which was used in the next step without further purification. ^{1}H-NMR ($CDCl_3$) δ 6.49 (1H, s, OCH=), 4.25 (4H, s, OCH_2), 3.53 (3H, s, CH_3), 3.39 (3H, s, CH_3).

1-Bromo-8-dimethylamino-2,5-dioxa-7,9-dithiabicyclo[4.3.0]nonan-8-ylium bromide (IV). A solution of bromine (14.4 ml, 0.28 mol) in dichloromethane (60 ml) was added dropwise over 1 h to a solution of III (55.87 g, 0.272 mol) in dry dichloromethane (distilled over CaH_2 under nitrogen prior to use) in 1 l 3-necked round-bottomed flask, which was cooled (below 3 °C) by ice bath. After stirring under cooling for further 1.5 h, the resultant precipitates were collected by filtration, washed with dichloromethane (150 ml), and dried *in vacuo* to yield salt IV as a white solid (105 g, 105 %), which was used in the next step without further purification. ^{1}H-NMR (DMSO-d_6) δ 7.16 (1H, s, SCH), 4.27 (4H, br s, OCH_2), 3.62 (3H, s, CH_3), 3.56 (3H, s, CH_3).

8-Dimethylamino-2,5-dioxa-7,9-dithiabicyclo[4.3.0]non-1(6)-en-8-ylium bromide

(V). IV (105 g, 0.288 mol) in 500 ml round-bottomed flask was stirred with magnetic stirrer and heated by oil bath (110 °C) under reduced pressure (20 Torr) for 2 h. The resultant yellow solid V (74 g, 91 %) was used for the next reaction without further purification. ^{1}H-NMR (DMSO-d_6) δ 4.52 (4H, s, OCH_2), 3.48 (6H, s, CH_3).

4,5-(Ethylenedioxy)-1,3-dithiole-2-selenone (VI). V (23.1 g, 81.1 mmol) was dissolved in methanol (200 ml) in 500 ml 3-necked round-bottomed flask equipped with an inlet tube and two aq NaOH traps for unreacted H_2Se gas. After bubbling nitrogen for 10 min, H_2Se gas (Taiyosanso) was introduced to the stirred solution. A slightly exothermic reaction immediately started, and the brownish solution turned to a brownish red suspension. The introduction of H_2Se gas was continued for 35 min until the unreacted gas appeared to bubble in the aq NaOH traps. Nitrogen gas was bubbled into the reaction mixture for 2 h before pouring onto water (900 ml). The resultant precipitate was filtered, washed with water (200 ml), and extracted with boiling cyclohexane (2.3 l). After filtration, the extract was concentrated and dried *in vacuo* to yield VI (15.45 g, 79.6 %) as a brownish red solid. ^{1}H-NMR ($CDCl_3$) δ 4.36 (4H, s).

Bis(ethylenedioxy)tetrathiafulvalene (BEDO-TTF). Trimethyl phosphite (6.39 g, 51.5 mmol, distilled from Na under N_2) was rapidly added under nitrogen to a boiling solution of VI (9.57 g, 40 mmol) in benzene (30 ml, distilled from CaH_2 under N_2) in 200 ml 3-necked round-bottomed flask equipped with a condenser. The dark red solution immediately turned to black. After refluxing for 1 h, benzene was removed under reduced pressure. The residue dissolved in dichloromethane (120 ml) was chromatographed on a silica gel (70-230 mesh) eluting with *n*-hexane-dichloromethane (2:1) to yield BEDO-TTF as red needles (3.41 g, 48.7 %), mp 178-183 °C dec. BEDO-TTF was further purified by twice recrystallization from distilled cyclohexane, for preparations

of its CT complexes. ^{1}H-NMR ($CDCl_3$) δ 4.26 (8H, s). Anal. Calcd for $C_{10}H_8O_4S_4$: C, 37.49; H, 2.52; O, 19.97; S, 40.04 %. Found: C, 37.46; H, 2.67; O, 20.22; S, 40.03 %.

2-2 Preparation of BEDO-TTF Complexes.

DDQ, TCNQ, TCNE, QCl_4, QF_4, H_2CHA, H_2BRA, $Q(OH)_2$, TNF, K(CF), and I_2 were purchased. The following acceptors and electrolytes have been synthesized in my laboratory according to the literatures: HCBD,[29a] F_4TCNQ,[29b] DBDQ,[29c] F_2TCNQ,[23] FTCNQ,[23] DTENF,[29d] DCNQ,[29e] Me_2TCNQ,[29f] Et_2TCNQ,[29f] $(MeO)_2$TCNQ,[29f] QBr_4,[29g] BTDA-TCNQ,[29h] DTNF,[29i] TENF,[29j] TNBP,[29k] DNBP,[29l] $(TPA)_2$HCTMM,[29m] $K_2(SQA)(H_2O)$,[29n] (TBA)PIC,[29o] (TBA)PCA,[29p] $(TBA)_2$HCP,[29q] $(TEA)_2MnBr_4$,[29r] $(TEA)_2CoCl_4$,[29s] and $(TEA)_2CoBr_4$.[29s] $(TBA)_2$HCTMM was prepared from Ba(HCTMM) [29m] and (TBA)Br. $(TEA)_2CHA(H_2O)_x$ (x = 5-6) was prepared from H_2CHA and 20 % aq (TEA)OH solution (1:2 molar ratio) in ethanol. All these acceptors and electrolytes were purified by recrystallization and/or gradient sublimation and identified by elemental analysis. DHBTCNQ and THBTCNQ were kindly supplied by Prof. K. Nakasuji, and C_{10}TCNQ and C_{14}TCNQ by Prof. T. Nakamura. Chart 2-2 shows the chemical structures of organic acceptors and anions used in this work.

Solvents were purified prior to use for preparation of BEDO-TTF complexes; CH_3CN and benzene were distilled under nitrogen from CaH_2, followed by from P_2O_5, and from K_2CO_3; PhCN was twice washed with conc HCl, neutralized by dil $NaHCO_3$ and dried with K_2CO_3 overnight, followed by distillation from P_2O_5 and K_2CO_3 under reduced pressure; TCE was washed with conc H_2SO_4 several times, neutralized with dil $NaHCO_3$, dried with $CaCl_2$ overnight, passed through the alumina column (B, Super I, ICN), distilled under nitrogen, and passed through the alumina column again just before use; THF was distilled from

CaH_2, followed by from Na under argon; EtOH was distilled from magnesium ethoxide under nitrogen.

Two kinds of procedures were employed for preparations of the CT complexes, all of which are given with entry numbers in Table 2–1 and will be represented by these numbers hereafter. This work has produced a number of new BEDO–TTF complexes except 31,[26d] 38a,[26e] and 41.[26a] The first procedure is the direct complex formation, which was applied for the preparations of complexes with organic acceptors or iodine (1–30, 42–44). After mixing two hot solutions of each component, some complexes were precipitated out immediately or upon cooling to the room temperature, whereas the further cooling was required for precipitation of the others. They were collected by filtration, washed with the same solvent as used for the preparation, and dried *in vacuo*. The conditions of these preparations are summarized in Table 2–1. F_4TCNQ gave two complexes with different stoichiometry by changing solvents. The oxidation by iodine gave various BEDO–TTF complexes; (BEDO–TTF)I_3 (42) was obtained using 1.5 equiv of iodine, whereas the mixture of two kinds of crystals (BEDO–TTF)$(I_3)_2$ (43, minor phase) and (BEDO–TTF)$(I_5)_2$ (44, major phase) were yielded by cooling the hot solution of BEDO–TTF containing large excess of iodine (11 equiv) slowly (cooling rate < 4 °C/h) under nitrogen atmosphere. Single crystals of 25 were obtained by diffusing the donor and acceptor in the H–shaped glass tube (55 ml) under nitrogen atmosphere at room temperature. The attempts to obtain large single crystals of other metallic DA–type complexes by slow cooling, recrystallization or diffusion method were unsuccessful.

The second technique is the electrocrystallization for preparations of 12 kinds of BEDO–TTF radical salts with organic anions, chloride, bromide, or triiodide (31–41). Using a conventional H–shaped glass cell equipped with a glass frit separating two chambers, the crystals were grown on a Pt electrode

(2 mm diameter) at 10 °C (in Sanyo Incubator) under constant current. Typical conditions of the preparations are given in Table 2-2. Two kinds of HCTMM salts were obtained using different electrolytes and solvents.

Table 2-1 summarizes their stoichiometry, appearance and decomposition points (*D*p). The stoichiometries of 25, 27, 29, 31, 33, 34, 37, and 39 were determined by X-ray structural analysis (see below), crystal densities, and elemental analyses (Kyoto University). The stoichiometries of 40 and 43 were determined solely from X-ray analyses. The elementary analyses of 40 and 44 were not satisfactory maybe due to the contamination of other minor crystal phases. The stoichiometry of other complexes were determined solely by elemental analyses. Although the stoichiometries of complexes 8 and 44 remain somewhat ambiguous due to the large difference between observed and calculated contents, those of other BEDO-TTF complexes were determined satisfactorily (± 0.3% for C, H, N, O, S and halogen, see Table 2-3). The stoichiometry of 44 will be nominally formulated as (BEDO-TTF)$(I_5)_2$, merely on the basis of its IR spectrum suggesting the divalent state of BEDO-TTF molecule.

2-3 General.

Melting points measured on Yanako MP-500D were not corrected.

Cyclic voltammetry. Electrochemical measurements at 10 mV/s were performed in acetonitrile solution containing 0.1 M (TBA)BF_4 electrolyte with Pt working and counter electrodes vs SCE (saturated calomel electrode) under argon. Voltammogramms were recorded on a Yanaco Polarographic Analyzer P-1100.

Optical measurements. Optical spectra were measured using the KBr disk method on Perkin-Elmer 1600 Series FT-IR (resolution 4 cm^{-1}) for infrared (IR)

and near-infrared region (400-7800 cm^{-1}), and on SHIMADZU UV-3100 spectrometer for near-infrared, visible, and ultraviolet (UV-VIS-NIR) region (3800-42000 cm^{-1}). Electronic absorption spectra were also measured in acetonitrile solution. IR spectra (650-4000 cm^{-1}) with higher resolution (0.5 cm^{-1}) were recorded on Nicolet Magna-IR 750 spectrometer.

Crystal densities were determined using the floating method with a mixture of carbontetrachloride and 1,2-dibromoethane.

D.C. conductivities were measured with either a standard four- or two-probe technique, using gold paint (Tokuriki Kagaku) to attach gold wires (10 μm diameter) to the samples. The powdered samples were compressed under a pressure of 500 MPa, cut to form an orthorhombic shape, and attached with gold wires (25 μm diameter) using gold paint before the measurements. The temperature was measured with a Pt and a Ge resistance.

Thermoelectric Power. An Au-0.07%Fe wire and a chromel wire were attached to each end of a single crystal with gold paint. One end of the crystal was attached on a heat sink which consists of an insulating Cu block with a heater glued using GE varnish. Thermoelectric power of a sample measured with Au-Fe wires and chromel ones were recorded independently, and temperature gradient was calculated from their difference. The absolute thermoelectric power of the sample was obtained by subtracting that of chromel (calibrated by using Pb) from the measured value with the chromel wires.

ESR Measurements. ESR spectrum of a single crystal or a randomly oriented polycrystalline sample was collected on a JEOL JES-TE200 X-band ESR spectrometer equipped with a cylindrical cavity of TE_{011} mode. The static magnetic field (H) and microwave frequency was measured by ECHO Electronics ES-FC5 field meter and a frequency counter build in the spectrometer, respectively. The determination of g tensor of BEDO-TTF^{+} radical was performed by the angular dependent measurement on a large single crystal

(dimensions, 1.7x1.7x0.6 mm^3) of $(BEDO\text{-}TTF)_5HCTMM(PhCN)_2$ (31), all the donor molecules in which are aligned in parallel. After ESR measurements, the crystallographic axes were checked by X-ray diffractions.

Static Magnetic Susceptibility. Magnetization measurements were performed by using a Quantum Design MPMS2 SQUID magnetometer. The polycrystalline sample (ca 10-15 mg) wrapped by polyethylene film was placed inside a polyethylene straw. A fixed magnetic field of 0.1 T or 0.3 T (1 T = 10000 G) was applied to collect data between 2 and 300 K (or 350 K). All the spin susceptibility data are corrected for the magnetization of the blank film and the core diamagnetism using the compilation of Pascal's constants.[30]

2-4 Crystal Structure Determinations.

Crystal structures were determined for 11 BEDO-TTF complexes (25, 27, 29, 31, 33, 34, 37, 39, 40, 42, 43). Intensity data were collected on the automatic four-circle (RIGAKU AFC-4, AFC-5, Mac Science MXC$^{\chi}$, or MXC18K) diffractometer at room temperature. For 25 and 42, the structure solutions by direct method and full-matrix least squares refinements were done using crystanG package program.[31] For the other complexes, the structures were solved by direct methods using the SHELXS-86 program,[32] and refined by a block-diagonal least squares method (UNICS)[33] (27, 31) or a full matrix least squares method (SHELX-76)[32] (29, 33, 34, 37, 39, 40, 43). Table 2-4 summarizes the parameters for crystals, data collection and refinement. Atomic parameters were refined by adopting anisotropic temperature factors for non-hydrogen atoms of the donor molecules in all crystals and for the counter component molecules in 25, 27, 29, 40, 42, and 43. The positions were determined by differential synthesis and following refinement with isotropic temperature factors for all hydrogen atoms in 27 and those of the OH groups of TNBP in

29. Other hydrogen atoms in 29 were refined with isotropic temperature factors under a fixed C–H bond length of 1.08 Å. The positions of hydrogen atoms of the donor molecules were calculated for 25, 31, 33, 34, 37, 39, 40, 42, and 43.[34] The refined and calculated atomic parameters are deposited as supplementary material. Other details specific to each structure determination are given below.

(BEDO–TTF)[Q(OH)$_2$]$_2$ (27). During the X-ray measurement, the surface of this black crystal gradually decomposed to form an orange solid. To avoid this, the crystal was coated with silicon grease.

For the complexes 32, 38a, and 44, only unit cell parameters were measured on a four-circle diffractometer. Table 2-5 summarizes these unit cell parameters. From the unit cell parameters, the complex 38a is regarded as the identical phase to that reported by D. Schweitzer *et al.*[26e]

(BEDO–TTF)$_5$(HCTMM)(PhCN)$_2$ (31). The cell was determined with the aid of oscillation and Weissenberg photographs. Severe disorder of counter components prevented the determination of their positions.

(BEDO–TTF)$_{10}$(CF)$_4$(H$_2$O)$_3$ (33). The positions of counter molecules could not be determined because the obtained cell was too small for them. No superlattices were detected, even by oscillation or Weissenberg photograph, suggesting that anion and water molecules were too randomly disordered to reveal their periodicity.

(BEDO–TTF)$_4$(SQA)(H$_2$O)$_6$ (34). The unit cell parameters, especially parameter *c* were not enough to accommodate the squarate molecule (vide infra). Oscillation and Weissenberg photographs revealed a supercell of (a, $-b+c$, $-2c$) whose corresponding reflections were, however, too weak to determine the definite structure; only 903 and 1521 out of 5882 independent reflections satisfied the criterions, $F > 3\sigma(F)$ and $F > 2\sigma(F)$, respectively. The structure

described here is thus the averaged one. (A similar situation has also been reported in the case of (BEDO–TTF)$_2$ClO$_4$.[26c]) The non-hydrogen atoms of the water and squarate were refined with isotropic temperature factors. The occupancy factors of the squarate and two water molecules were fixed to 1/2, while those of the other two water molecules were unity.

(BEDO–TTF)$_5$(HCP)(PhCN)$_{0.2}$ (37). The cell parameter b described in the present study is too short to accommodate the anion and solvent molecules. The precise cell is (a, $5b$, c), but weakness of the reflections from its correspondent supercell prevented our solving the definite structure; only 314 and 595 out of 2908 independent reflections ($2\theta < 60^\circ$, CuKα) satisfied the criterions, $F > 3\sigma(F)$ and $F > 2\sigma(F)$, respectively. Thus, the crystal structure given here is also the averaged one. In the refinement of the donor molecule, the differential Fourier map presented the peaks corresponding to anions along the $x = 0$ plane. The peak pattern was accounted for by the assumption that two HCP anions were located on the 2-fold screw axis in the period of $5b$. Therefore, the occupancy factor was fixed to 1/5 for the anion atoms. Their positional and isotropic thermal parameters were refined with their bond lengths fixed correspondent to HCP dianion.[35] Although the Fourier map showed very weak remaining peaks related to the solvent molecule in the openings of the anion layer, this molecule was too diluted in the crystal to allow the refinement of its positions.

(BEDO–TTF)$_2$Br(H$_2$O)$_3$ (39). Although the obtained cell was too small for this formula unit, no superlattices were detected even by the measurements on an imaging plate. Atomic parameters were refined adopting isotropic temperature factors for water and bromide. In the refinement of donor molecules, the differential Fourier map presented the counter components, which were distributed as an infinite chain of peaks along the a axis. The strongest peaks were assumed to be bromide anions, and the remainder peaks to be

water molecules. Since the bromide anions and water molecules are disordered, their occupation factors were smaller than unity.

2-5 Band Electronic Structure Calculations.

The tight-binding band calculations were based on the extended Hückel method.[36] The semiempirical parameters for Slater-type atomic orbitals were taken from Ref. 37. The intermolecular transfer integrals (t) were assumed to be proportional to the corresponding overlap integrals (S) of the highest occupied molecular orbital (HOMO) of BEDO-TTF ($t = -ES$, $E = 10$ eV). In the band calculations of the reported BEDO-TTF complexes, we employed the positional parameters of the non-hydrogen atoms of BEDO-TTF taken from the literatures[26a,c,e,27a,38], as well as those of the hydrogen atoms which, though not available in the above literatures, were obtainable from our calculations.[34]

Table 2–1. Compositions, Appearances, Decomposition Temperatures of BEDO–TTF Complexes

	composition (D:A or X:Solv)	appearance	*Dp*, °C	mixing conditions for preparations D, mg (mmol)	A, mg (mmol)	solvent, ml	yield, %	procedure
Acceptor (A)	D:A:Solv							
1. HCBD	2:1	dark green powder	204-209	68.1 (0.213)	38.6 (0.189)	CH_3CN, 40	66	
2. F_4TCNQ	1:1	dark green powder	196-199	51.8 (0.162)	44.3 (0.160)	CH_3CN, 22	66	
3. F_4TCNQ	9:5:4THF	greenish brown powder	194-198	56.3 (0.176)	48.5 (0.176)	THF, 40	91	
4. DDQ	5:3:1CH_3CN	dark brown powder	162-166	44.4 (0.139)	47.3 (0.208)	CH_3CN, 55	66	
5. DBDQ	11:7:1CH_3CN	reddish brown powder	166-168	41.7 (0.130)	45.5 (0.144)	CH_3CN, 26	83	
6. F_2TCNQ	2:1	dark bluish powder	192-196	68.8 (0.215)	27.2 (0.113)	CH_3CN, 30	94	
7. FTCNQ	4:2:1CH_3CN	dark greenish powder	186-189	64.5 (0.201)	25.3 (0.114)	CH_3CN, 30	82	
8. TCNE	2:1[‡]	greenish brown powder	157-162	84.1 (0.262)	33.5 (0.262)	CH_3CN, 40	37	
9. DTENF	2:1	black powder	188-191	50.4 (0.157)	31.8 (0.078)	benzene, 20	51	
10. TCNQ	1:1	black powder	206-208	44.6 (0.139)	45.5 (0.135)	THF, 40	58	
11. DCNQ	2:1	dark brown powder	164-172	45.5 (0.142)	33.6 (0.161)	CH_3CN, 55	56	
12. $C_{10}TCNQ$	10:4:1H_2O	dark green powder	138-142	99.1 (0.309)	58.8 (0.171)	CH_3CN, 75	76	cooling (-20°C)
13. $C_{14}TCNQ$	9:4:2H_2O	black powder	131-133	98.2 (0.306)	59.9 (0.150)	CH_3CN, 80	76	cooling (-20°C)
14. DHBTCNQ	2:1	black powder	112-115	56.8 (0.177)	33.4 (0.118)	CH_3CN, 35	93	cooling (-20°C)
15. THBTCNQ	2:1	dark green powder	138-141	48.1 (0.150)	20.1 (0.071)	CH_3CN, 30	73	cooling (-20°C)
16. Me_2TCNQ	9:5:1CH_3CN	dark blue powder	186-189	49.1 (0.153)	37.8 (0.163)	CH_3CN, 24	98	
17. Et_2TCNQ	2:1	black powder	190-195	69.7 (0.218)	28.1 (0.108)	CH_3CN, 30	93	
18. $(MeO)_2TCNQ$	2:1	dark bluish green powder	182-185	58.3 (0.182)	50.4 (0.191)	CH_3CN, 75	65	
19. QCl_4	2:1	dark green powder	162-164	63.2 (0.197)	48.8 (0.198)	CH_3CN, 70	42	
20. QF_4	11:5:6H_2O	black powder	151-156	61.0 (0.190)	36.6 (0.203)	CH_3CN, 32	51	cooling (-6°C)
21. QBr_4	9:5:1H_2O	greenish brown powder	151-154	49.7 (0.155)	74.4 (0.176)	CH_3CN, 27	63	cooling (0°C)
22. BTDA-TCNQ	7:4	black powder	197-199	66.3 (0.207)	36.2 (0.113)	CH_3CN, 45	81	
23. DTNF	2:1:1CH_3CN	black powder	138-141	47.9 (0.149)	33.6 (0.161)	CH_3CN, 40	62	
24. H_2BRA	2:1H_2BRA	reddish brown powder	158-163	53.1 (0.166)	98.0 (0.329)	CH_3CN, 50	52	
25. H_2CHA	2:1HCHA	black needles	151-155	65.2 (0.203)	90.0 (0.434)	CH_3CN, 55	21	diffusion
26. TENF	1:1	black powder	174-176	62.3 (0.194)	69.4 (0.193)	CH_3CN, 30	60	
27. $Q(OH)_2$	1:2	black plates	125-134	91.7 (0.286)	83.2 (0.594)	CH_3CN, 90	43	cooling (-20°C)
28. TNF	1:1	reddish brown powder	178-182	45.7 (0.143)	50.4 (0.160)	CH_3CN, 40	29	cooling (-80°C)
29. TNBP	1:1	black plates	170-178	54.7 (0.171)	54.8 (0.150)	CH_3CN, 40	34	cooling (-20°C)
30. DNBP	1:1	bluish gray powder	199-202	60.0 (0.187)	47.7 (0.195)	CH_3CN, 40	63	cooling (-20°C)
Anion (X)	D:X:Solv							
31. HCTMM	5:1:2PhCN	black plates	165-172			(electrocrystallization)		
32. HCTMM	4:1:2TCE	black needles	154-161			(electrocrystallization)		
33. CF	10:4:3H_2O	black needles	110-117			(electrocrystallization)		
34. SQA	4:1:6H_2O	black needles	153-159			(electrocrystallization)		
35. PIC	6:3:1TCE	dark green needles	175-181			(electrocrystallization)		
36. PCA	8:4:1H_2O	brownish green powder	177-183			(electrocrystallization)		
37. HCP	5:1:0.2PhCN	black needles	260-267			(electrocrystallization)		
38a. Cl	2:1:3H_2O	black plates	145-149			(electrocrystallization)		
38b. Cl	2:1:3H_2O	black needles	144-147			(electrocrystallization)		
39. Br	2:1:3H_2O	black plates	102-107			(electrocrystallization)		
40. Br	2:1:$MnBr_2(H_2O)_5$	black plates	206-211			(electrocrystallization)		
41. I_3	2.4:1	greenish lustrous plates	146-154			(electrocrystallization)		
42. I_3	1:1	black plates	155-160	32.5 (0.101)	I_2 39.6(0.156)	CH_3CN, 50	46	
43. I_3	1:2	black plates	157-162	30.2 (0.094)	I_2 267 (1.052)	CH_3CN, 100	(minor)	slow cooling
44. I_5	1:2	black rods	152-155				(major)	

D = BEDO-TTF.

Table 2-2. Typical Conditions of Electrocrystallization of BEDO-TTF Radical Salts

salts (D = BEDO-TTF)		donor, mg	supporting electrolytes, mg	solvents, ml	current, μA	yield, mg
31.	$D_5(HCTMM)(PhCN)_2$	10.8	$(TPA)_2HCTMM$, 68.5	PhCN, 18	0.2	5.4
32.	$D_4(HCTMM)(TCE)_2$	10.4	$(TBA)_2HCTMM$, 76.6	TCE, 16; EtOH 2	0.7	6.3
33.	$D_{10}(CF)_4(H_2O)_3$	19.6	K(CF), 50.8; 18-crown-6, 116.1	PhCN, 18; H_2O 2drops	0.2	3.6
34.	$D_4(SQA)(H_2O)_6$	12.0	$K_2(SQA)(H_2O)$, 52.5; 18-crown-6, 96.9	PhCN, 18; H_2O 2drops	0.1	1.6
35.	$D_6(PIC)_3(TCE)$	13.7	(TBA)PIC, 45.6	TCE, 18	0.1	1.1
36.	$D_8(PCA)_4(H_2O)$	16.6	(TBA)PCA, 54.4	PhCN, 18; H_2O 2drops	0.4	4.4
37.	$D_5(HCP)(PhCN)_{0.2}$	25.2	$(TBA)_2HCP$, 37.4	PhCN, 17; EtOH 1	0.1	1.3
38a,b.	$D_2Cl(H_2O)_3$	12.7	$(TEA)_2CoCl_4$, 73.2	PhCN, 18; H_2O 2drops	0.3	3.7*
39.	$D_2Br(H_2O)_3$	14.5	$(TEA)_2CoBr_4$, 77.7	PhCN, 18; H_2O 2drops	0.3	4.1
40.	$D_2Br[MnBr_2(H_2O)_4](H_2O)$	11.1	$(TEA)_2MnBr_4$, 60.9	PhCN, 18; H_2O 2drops	0.3	4.8
41.	$D_{2.4}I_3$	11.2	$(TEA)I_3$, 31.6	PhCN, 18; H_2O 1drop	1.0	5.4

(*) Mixture of needles and plates.

Table 2-3. Elemental Analyses of BEDO-TTF Complexes

	composition	found (calcd) /%				
		C	H	N	other elements	
Acceptor	D:A:Solv					
1. HCBD	2:1	42.46(42.64)	1.82(1.91)	9.97(9.94)	30.20(30.36)(S)	
2. F_4TCNQ	1:1	44.23(44.29)	1.33(1.35)	9.34(9.39)	12.71(12.74)(F)	
3. F_4TCNQ	9:5:4THF	43.81(43.79)	2.32(2.30)	5.98(6.15)	8.27(8.34)(F)	
4. DDQ	5:3:1CH_3CN	39.10(39.27)	1.69(1.86)	4.21(4.22)	9.32(9.15)(Cl)	
5. DBDQ	11:7:1CH_3CN	34.91(34.93)	1.52(1.59)	3.89(3.64)	19.37(19.36)(Br)	
6. F_2TCNQ	2:1	43.88(43.62)	2.23(2.06)	6.36(6.36)	4.14(4.31)(F)	
7. FTCNQ	4:2:1CH_3CN	44.96(44.86)	2.29(2.45)	7.22(7.13)	2.34(2.15)(F)	
8. TCNE	2:1*	38.98(40.61)	2.09(2.09)	5.43(7.29)	32.77(33.36)(S)	
9. DTENF	2:1	41.08(41.21)	1.85(1.92)	7.72(8.01)	24.57(24.45)(S)	
10. TCNQ	1:1	50.38(50.37)	2.13(2.31)	10.58(10.68)	24.37(24.45)(S)	
11. DCNQ	2:1	45.28(45.27)	2.21(2.37)	3.35(3.30)	30.20(30.22)(S)	
12. C_{10}TCNQ	10:4:1H_2O	49.16(49.08)	3.69(3.90)	4.78(4.87)	27.59(27.88)(S)	
13. C_{14}TCNQ	9:4:2H_2O	51.42(51.52)	4.31(4.55)	5.26(4.96)	25.27(25.53)(S)	
14. DHBTCNQ	2:1	49.37(49.44)	3.00(2.84)	6.20(6.15)	27.62(27.79)(S)	
15. THBTCNQ	2:1	49.61(49.33)	3.01(3.05)	6.15(6.06)	27.69(27.73)(S)	
16. Me_2TCNQ	9:5:1CH_3CN	47.70(47.62)	2.68(2.84)	7.43(7.20)	28.47(28.25)(S)	
17. Et_2TCNQ	2:1	47.99(47.98)	3.18(3.13)	6.17(6.22)	28.44(28.47)(S)	
18. $(MeO)_2$TCNQ	2:1	45.28(45.12)	2.75(2.67)	6.30(6.19)	28.25(28.34)(S)	
19. QCl_4	2:1	35.22(35.22)	1.80(1.82)	—	15.74(15.99)(Cl)	
20. QF_4	11:5:6H_2O	37.19(37.09)	2.37(2.22)	—	8.54(8.38)(F)	
21. QBr_4	9:5:1H_2O	28.97(28.71)	1.49(1.48)	—	22.87(23.00)(S)	31.62(31.83)(Br)
22. BTDA-TCNQ	7:4	40.24(40.21)	1.74(1.60)	12.73(12.72)	32.79(32.76)(S)	
23. DTNF	2:1:1CH_3CN	43.69(43.67)	2.37(2.31)	7.98(8.04)	24.52(24.55)(S)	
24. H_2BRA	2:1H_xBRA	33.11(33.26)	1.99(1.93)	0.00(0.00)	27.52(27.33)(S)	16.75(16.02)(Br)
25. H_2CHA	2:1HCHA	36.72(36.74)	1.98(2.13)	—	29.99(30.19)(S)	8.25(8.34)(Cl)
26. TENF	1:1	40.67(40.59)	2.01(1.78)	8.15(8.23)	19.04(18.85)(S)	
27. $Q(OH)_2$	1:2	43.88(43.99)	2.58(2.68)	—	32.04(31.96)(O)	21.10(21.36)(S)
28. TNF	1:1	43.23(43.46)	1.87(2.06)	6.42(6.61)	20.21(20.18)(S)	
29. TNBP	1:1	38.76(38.48)	1.87(2.05)	8.05(8.16)	32.50(32.62)(S)	18.79(18.68)(S)
30. DNBP	1:1	46.56(46.80)	2.71(2.86)	4.82(4.96)	22.76(22.72)(S)	
Anion (X)	D:X:Solv					
31. HCTMM	5:1:2PhCN	44.14(44.16)	2.35(2.50)	5.38(5.57)	15.62(15.90)(O)	31.72(31.87)(S)
32. HCTMM	4:1:2TCE	36.95(37.00)	2.26(2.19)	4.79(4.79)	29.38(29.27)(S)	12.00(12.14)(Cl)
33. CF	10:4:3H_2O	38.32(38.26)	2.26(2.44)	4.47(4.37)	19.13(19.39)(O)	35.68(35.54)(S)
34. SQA	4:1:6H_2O	35.09(35.18)	3.11(2.95)	0.00(0.00)	27.41(27.69)(O)	34.18(34.16)(S)
35. PIC	6:3:1TCE	34.93(35.06)	2.16(2.10)	4.51(4.60)	26.43(26.27)(O)	28.39(28.09)(S)
36. PCA	8:4:1H_2O	41.32(41.44)	2.16(2.05)	8.55(8.63)	16.30(16.27)(O)	31.65(31.61)(S)
37. HCP	5:1:0.2PhCN	41.33(41.33)	2.09(2.23)	4.55(4.69)	34.69(34.65)(S)	
38a. Cl	2:1:3H_2O	32.62(32.89)	3.00(3.04)	0.00(0.00)	23.89(24.10)(O)	
38b. Cl	2:1:3H_2O	32.70(32.89)	2.83(3.04)	0.00(0.00)	4.52(4.85)(Cl)	
39. Br	2:1:3H_2O	30.92(31.00)	2.72(2.86)	—	10.03(10.31)(Br)	
40. Br	2:1:$MnBr_2(H_2O)_5$	24.47(23.42)	2.52(2.56)	0.00(0.00)	21.46(23.37)(Br)	
41. I_3	2.4:1	25.00(25.07)	1.77(1.68)	0.00(0.00)	13.33(13.36)(O)	33.34(33.11)(I)
42. I_3	1:1	17.14(17.13)	1.14(1.15)	—	9.22(9.33)(O)	54.27(54.30)(I)
44. I_5	1:2	8.06(7.56)	0.58(0.51)	—	3.94(4.03)(O)	79.18(79.84)(I)

Table 2-4. Crystal Data, Data Collection, and Reduction Parameters

	25	27	29	31	33	34	37	39	40	42	43
Anion or acceptor (A)	HCHA	$Q(OH)_2$	TNBP	HCTMM	CF	SQA	HCP	Br	Br	I_3	I_3
BEDO-TTF:A:solvent	2:1	1:2	1:1	5:1:2PhCN	1:0.4:0.3H_2O	2:0.5:3H_2O	1:0.2:0.04PhCN	1:0.5:1.5H_2O	2:1:$MnBr_2(H_2O)_5$	1:1	1:2
formula weight	848.88	600.64	686.65	2012.65	361.88	750.97	370.21	387.43	1282.19	701.16	1081.88
space group	monoclinic, $P2_1/a$	triclinic, $P\bar{1}$	monoclinic, $C2/c$	triclinic, $P\bar{1}$	triclinic, $P\bar{1}$	triclinic, $P\bar{1}$	monoclinic, $P2_1/c$	triclinic, $P\bar{1}$	triclinic, $P\bar{1}$	triclinic, $P\bar{1}$	triclinic, $P\bar{1}$
crystal dimensions, mm^3	0.46x0.11x0.03	0.4 x0.3 x0.2	0.75x0.75x0.05	0.67x0.20x0.04	0.45x0.10x0.05	0.67x0.20x0.04	0.30x0.25x0.03	0.35x0.18x0.06	0.60x0.20x0.07	0.25x0.09x0.05	0.15x0.15x0.05
a, Å	10.058(1)	9.312(3)	15.220(3)	10.855(2)	5.342(2)	10.752(2)	17.075(2)	5.3404(8)	14.001(3)	7.632(1)	7.989(2)
b, Å	37.375(4)	9.785(2)	11.118(2)	19.224(3)	17.225(4)	16.517(4)	4.085(4)	16.774(2)	20.099(4)	7.654(3)	10.566(1)
c, Å	4.0443(9)	7.364(2)	16.426(4)	10.286(2)	4.0307(7)	4.0971(6)	20.462(4)	4.0226(6)	6.1823(7)	16.168(4)	7.2579(9)
α, deg		94.68(3)		91.76(2)	102.85(2)	87.35(1)		87.85(1)	90.06(1)	76.51(2)	96.54(1)
β, deg	98.43(2)	96.99(3)	109.96(2)	107.22(2)	98.59(2)	82.01(2)	96.46(2)	81.58(1)	100.21(1)	82.73(1)	110.48(1)
γ, deg		116.89(2)		91.77(2)	93.47(2)	79.74(2)		85.64(1)	101.42(2)	77.95(2)	92.08(1)
V, $Å^3$	1504.0(4)	586.9(3)	2613(1)	2047.3(7)	355.8(2)	708.9(2)	1418(1)	355.30(8)	1677.2(5)	895.2(4)	568.3(2)
Z	2	1	4	1	1	1	4	1	2	2	1
d_{calcd}, $g.cm^{-3}$	1.87	1.70	1.75	1.63	1.69	1.76	1.71	1.81	2.03	2.60	3.16
d_{obs}, $g.cm^{-3}$	1.87	1.69	1.73	1.62	1.70	1.76	1.72	1.80			
radiation	MoKα	MoKα	MoKα	MoKα	CuKα	MoKα	MoKα	MoKα	MoKα	MoKα	MoKα
diffractometer	MXC18K	AFC-4	AFC-4	AFC-5	AFC-5	AFC-4	AFC-4	MXCχ	AFC-5	MXC18K	AFC-5
scan mode	2θ-ω	2θ-ω	ω	2θ-ω	ω	ω	ω	2θ-ω	2θ-ω	2θ-ω	2θ-ω
$2\theta_{max}$	55	60	60	60	60	65	55	125	60	55	55
no. of intensity meas.	4126	3660	6341	14990	1369	6257	4951	1911	10341	4545	3571
criterion for obsd. reflections	$F > 6\sigma(F)$	$F > 3\sigma(F)$	$F > 3\sigma(F)$	$F > 3\sigma(F)$	$F > 3\sigma(F)$	$F > 3\sigma(F)$	$F > 3\sigma(F)$	$F > 3\sigma(F)$	$F > 3\sigma(F)$	$F > 6\sigma(F)$	$F > 3\sigma(F)$
no. of unique reflections used	2279	2743	3085	4150	997	3180	2102	1416	5309	3002	2400
no. of refined parameters	283	205	236	407	82	187	235	98	406	206	109
R	0.051	0.037	0.074	0.127	0.100	0.050	0.084	0.070	0.079	0.040	0.071
Rw [a]						0.077[b]	0.044[c]	0.080[d]			

[a] Quantity minimized $Rw(Fo - Fc)^2$. [b] $w = a/[\sigma^2(Fo) + b|Fo|]$, $a = 1.7471$, $b = 0.000934$. [c] $w = 1/[\sigma^2(Fo) + a|Fo| + b|Fo|^2]$, $a = -0.01538$, $b = 0.00133$.
[d] $w = a/[\sigma^2(Fo) + b|Fo|]$, $a = 2.0397$, $b = 0.001267$.

Table 2-5. Unit Cell Parameters of Other BEDO-TTF Complexes

	$(BEDO\text{-}TTF)_4HCTMM(TCE)_2$ (32)	$(BEDO\text{-}TTF)_2Cl(H_2O)_3$ (38a)	$(BEDO\text{-}TTF)(I_5)_2$ (44)
	triclinic	monoclinic	triclinic
a, Å	10.705(2)	8.580(1)	10.021(1)
b, Å	20.166(7)	5.0933(7)	11.165(1)
c, Å	8.075(2)	16.223(1)	7.325(1)
α, deg	91.92(3)		94.17(1)
β, deg	98.32(1)	98.097(8)	110.79(1)
γ, deg	102.30(2)		75.985(9)
V, Å^3	1681.5(7)	701.9(1)	743.3(2)

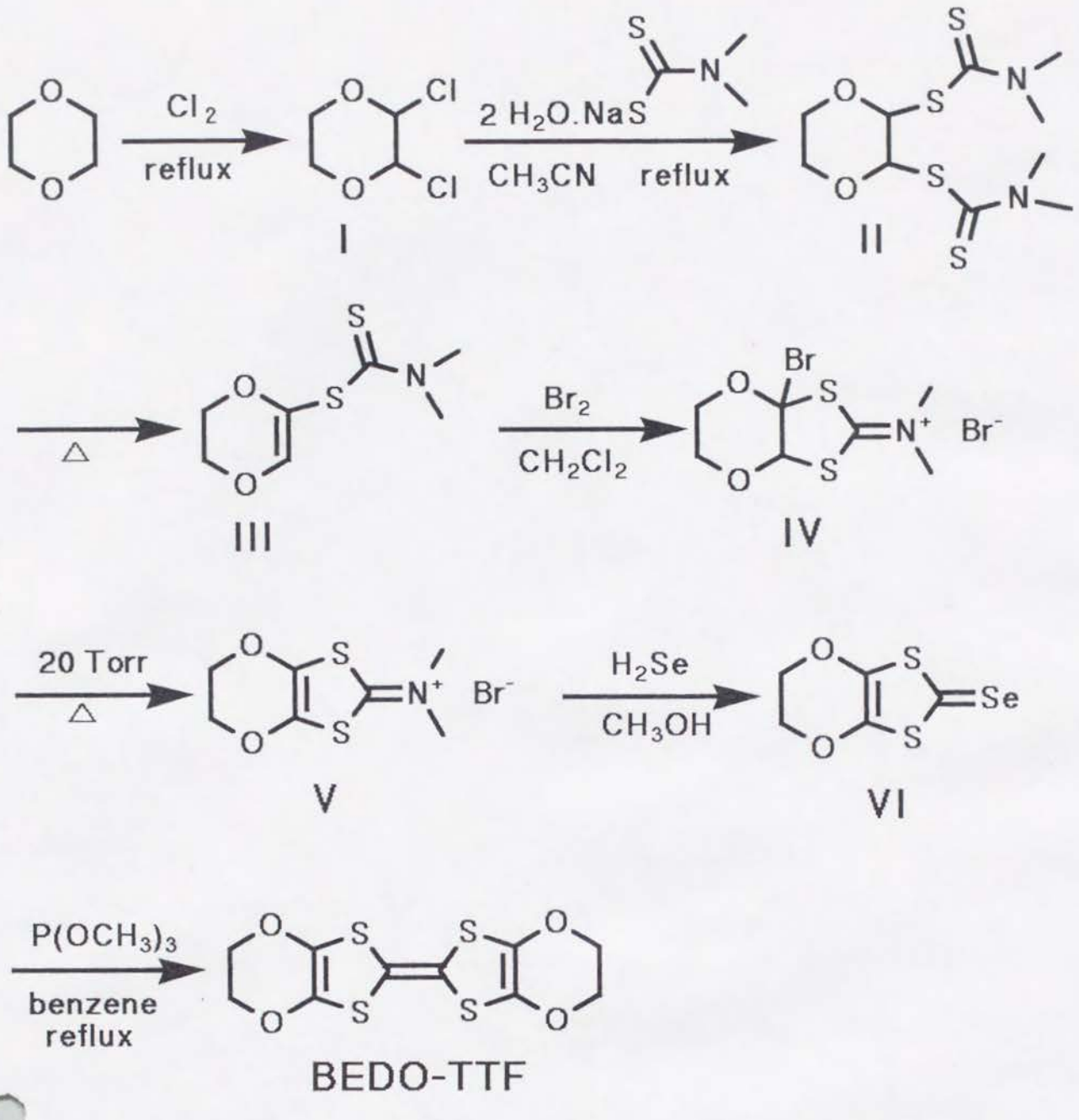

Chart 2-1. Synthetic scheme of BEDO-TTF.

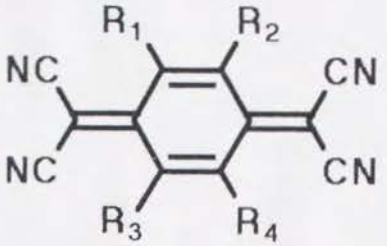

$R_1=R_2=R_3=R_4=F$: F_4TCNQ
$R_1=R_4=F$, $R_2=R_3=H$: F_2TCNQ
$R_1=F$, $R_2=R_3=R_4=H$; FTCNQ
$R_1=R_2=R_3=R_4=H$: TCNQ
$R_1=R_4=CH_3$, $R_2=R_3=H$: Me_2TCNQ
$R_1=R_4=C_2H_5$, $R_2=R_3=H$: Et_2TCNQ
$R_1=R_4=OCH_3$, $R_2=R_3=H$: $(MeO)_2TCNQ$
$R_1=C_nH_{2n+1}$, $R_2=R_3=R_4=H$: C_nTCNQ (n=10,14)

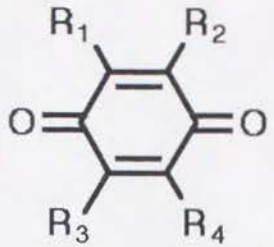

$R_1=R_2=CN$, $R_3=R_4=Cl$:DDQ
$R_1=R_2=CN$, $R_3=R_4=Br$:DBDQ
$R_1=R_2=CN$, $R_3R_4=(CH)_4$:DCNQ
$R_1=R_2=R_3=R_4=X$:QX_4 (X=F, Cl, Br)
$R_1=R_3=Cl$, $R_2=R_4=OH$: H_2CHA
$R_1=R_3=Br$, $R_2=R_4=OH$: H_2BRA
$R_1=R_3=OH$, $R_2=R_4=H$: $Q(OH)_2$

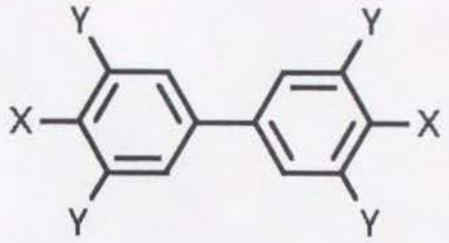

X=OH, Y=NO_2: TNBP
X=NO_2, Y=H: DNBP

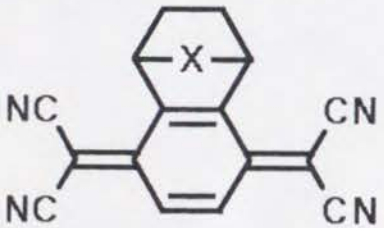

X=CH_2CH_2: THBTCNQ
X=CHCH: DHBTCNQ

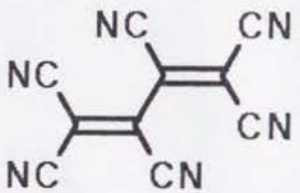

HCBD

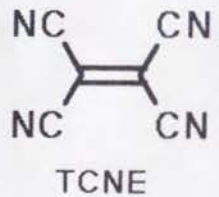

TCNE

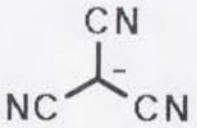

CF^-

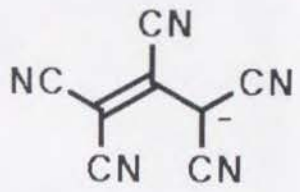

PCA^-

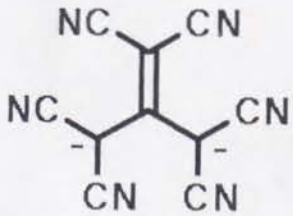

$HCTMM^{2-}$

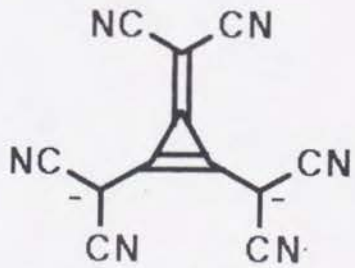

HCP^{2-}

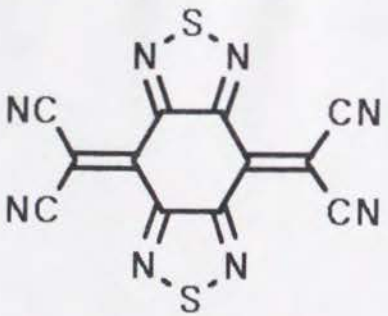

BTDA-TCNQ

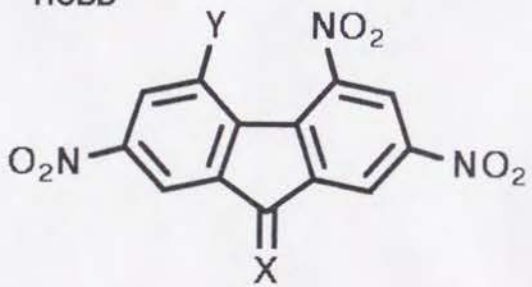

X=O, Y=H :TNF
X=O, Y=NO_2 :TENF
X=$C(CN)_2$, Y=H: DTNF
X=$C(CN)_2$, Y=NO_2: DTENF

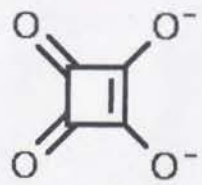

SQA^{2-}

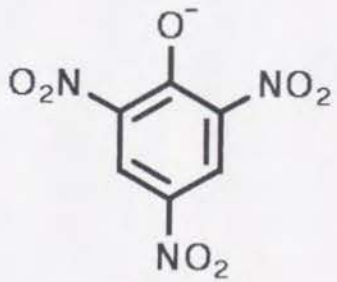

PIC^-

Chart 2-2. Acceptor molecules and organic anions used for preparation of BEDO-TTF complexes

Chapter 3 Physical Properties

3-1 Introduction

This chapter will mainly present the conducting, optical, and magnetic properties of BEDO-TTF complexes. The first section describes the electron-donating ability, which is related to the formation, properties, and electronic states of the complexes. One of the most important observations will appear in the conducting behavior at low temperatures, that is, rather stable metallic state on single crystal and even on the compressed pellet. Another unusual character of these metals is demonstrated in the stoichiometry. The electronic ground state of the complexes are discussed on the basis of the IR and electronic spectra and magnetic susceptibility. The final part of this chapter examines these physical properties as a function of the size, shape, and electron accepting ability of the counter component molecules. It will be emphasized that BEDO-TTF molecule is superior to the conventional donors with respect to the requirement for molecular metals.

3-2 Electron-Donating Property of BEDO-TTF

The difference between ionization potential of a donor and electron affinity of an acceptor is essential for determining the ionicity, and thus the conducting properties, of the CT complex.[16b,17] According to the photoelectron spectroscopy (PES) in the gas phase,[39] both the first vertical and the adiabatic ionization potentials (I_P(D) and I_P^{ad}(D)) increase in the following order: BEDO-TTF (6.46 and 6.12 eV, respectively) < TTF (6.70 and 6.26 eV) ≃ BEDT-TTF (6.7 and 6.30 eV). The order of the last two molecules is, however, different from that of the previously reported I_P^{ad}(D) values (BEDT-

TTF, 6.21 eV; TTF, 6.4 eV).[40] Since the PES spectrum of BEDT-TTF in Ref.39 is more resolved than that in Ref.40, we utilize the ionization potentials of the former for use in the following discussion.

The first oxidation (or reduction) potential $E_{1/2}{}^{1}(D)$ (or $E_{1/2}{}^{1}(A)$) is related to the adiabatic ionization potential (or electron affinity). Our cyclic voltammetry measurements indicate that BEDO-TTF (0.43 V vs. SCE) is stronger than BEDT-TTF (0.53 V), but weaker than TTF (0.37 V) in donating ability, a finding that agrees with reported measurements.[39] However, this order is different from the results for $I_P{}^{ad}(D)$. In Figure 3-1a, we plot $I_P{}^{ad}(D)$ versus $E_{1/2}{}^{1}(D)$ for eight TTF system donors, obtaining the linear relation

$$I_P{}^{ad}(D) = eE_{1/2}{}^{1}(D) + 5.76 \text{ eV}, \qquad (3.1)$$

except for the non-substituted donors (TTF and TSF). While the deviation of TTF may be ascribed to its different solvation energy,[40] the pronounced deviation of TSF requires the reexamination of its $I_P{}^{ad}(D)$ value.

The difference (ΔE) between the $E_{1/2}{}^{1}(D)$ and the second oxidation potential ($E_{1/2}{}^{2}(D)$) is presented in the following order; TTF (0.38 V) > BEDO-TTF (0.26 V) ~ BEDT-TTF (0.25 V). This is indicative of the reduction of on-site Coulomb energy from TTF to BEDO-TTF and BEDT-TTF.

We also measured the CT transition energy ($h\nu_{CT}^{soln}$) of the complex with *s*-trinitrobenzene in chloroform in order to compare donating ability. The $h\nu_{CT}^{soln}$ is usually approximated as,

$$h\nu_{CT}^{soln} = a[I_P(D) - E_A(A)] - C, \qquad (3.2)$$

where $E_A(A)$ is the vertical electron affinity of an acceptor molecule (A), C the Coulomb attractive energy of a D-A pair, and a the constant close to the unity.[41] The plotting of $h\nu_{CT}^{soln}$ versus $I_P(D)$ values (Figure 3-1b) gives a line by least squares fit as

$$h\nu_{CT}^{soln} = aI_P(D) - 3.62 \text{ eV}, \qquad (3.3)$$

where a = 0.836. Based on the Eq(3.3), the difference of the estimated $I_P(D)$ values of BEDO-TTF ($h\nu_{CT}^{soln}$ = 1.86 eV) and BEDT-TTF (1.99 eV) is 0.16 eV, in good agreement with that from the PES measurement (0.2 eV).

All these measurements consistently indicate that the ionization potential of BEDO-TTF is lower than that of BEDT-TTF by 0.1-0.2 eV. Therefore, one can expect metallic BEDO-TTF complexes from combination with weaker acceptors than would be possible for BEDT-TTF.

3-3 Complex Formation of BEDO-TTF

As summarized in Table 3-1, BEDO-TTF gave a large number of complexes with 29 organic acceptors of various shape, size and strength (1-30). In combination with strong acceptors (1-10, $E_{1/2}^{1}$(A) > +0.21 V), immediate complex formation was observed. On the other hand for some complexes of weaker acceptors, their precipitation required cooling below the room temperature.

Electrocrystallization of BEDO-TTF produced 7 radical salts with organic anions. Using the $HCTMM^{2-}$ anion, two kinds of complexes have been obtained as solvated crystals with distinct donor/anion ratios.

Besides, 8 (BEDO-TTF)-halide complexes were yielded by either chemical oxidation or electrocrystallization. During the electrocrystallization in the presence of slight amount of water, the CoX_4^{2-} anion (X = Cl or Br) merely acted as a source of X^- anion, whereas the $MnBr_4^{2-}$ anion yielded a novel salt containing magnetic ions, $(BEDO\text{-}TTF)_2Br[MnBr_2(H_2O)_4](H_2O)$ (40). Without water, these MX_4^{2-} anions did not give single crystals. The Cl salts exhibited two kinds of distinct crystal shapes (plates (38a) and needles (38b)) with the same stoichiometry, $(BEDO\text{-}TTF)_2Cl(H_2O)_3$, showing almost the same conducting

and optical properties. However, different C=C stretching frequency in the IR spectra (1589 and 1596 cm^{-1}, respectively) suggests that these two are different crystal phases.

It is interesting to note that chemical oxidation of BEDO-TTF by iodine in acetonitrile solution produced three new salts with different stoichiometry; (BEDO-TTF)I_3 (42), (BEDO-TTF)$(I_3)_2$ (43), and (BEDO-TTF)$(I_5)_2$ (44). Besides, the oxidation in THF gave a product, the stoichiometry of which is almost identical to that of (BEDO-TTF)$_{2.4}I_3$ (44) obtainable from electrocrystallization. The complexes 43 and 44 are the first examples of divalent BEDO-TTF, as shown later. According to the cyclic voltammetric measurements (in acetonitrile, 0.1 M (TBA)BF_4, 10 mV/s, Pt working electrode), the first reduction half-wave potential of iodine ($E_{1/2}{}^1(I_2)$ = +0.66 V vs SCE) is 0.23 V higher than the $E_{1/2}{}^1$(D) of BEDO-TTF (+0.43 V) and comparable to the $E_{1/2}{}^2$(D) (+0.69 V). Therefore, iodine can oxidize BEDO-TTF not only to +1 but also to +2 state. On the other hand for BEDT-TTF, $E_{1/2}{}^2$(D) (+0.78 V) is 0.12 V higher than $E_{1/2}{}^1(I_2)$, indicating that iodine oxidation of BEDT-TTF is difficult to give +2 state compared with BEDO-TTF. In fact, no dication salts have been reported so far for (BEDT-TTF)-I system, although both chemical and electrochemical oxidation have yielded numerous crystal phases.

In summary, the present work has found out 42 kinds of new BEDO-TTF complexes, emphasizing this donor's good ability of the CT complex formation with various components both by chemical oxidation and by electrocrystallization.

3-4 Conductivity

Table 3-1 summarizes the conducting properties of BEDO-TTF complexes, as well as the $E_{1/2}{}^1$(A) values, where σ_{rt} is the conductivity at room

temperature of the metal (M) or semiconductor (S), $T_{\sigma\,max}$ the temperature at which conductivity reaches the maximum (σ_{max}) for the metal, and *E*a the activation energy of the semiconductor. They show several characteristic features, as follows: i) many have unusual stoichiometries rather than the conventional 1:1, 2:1 or 1:2; ii) 33 out of 45 complexes investigated in this work were found to be metallic; iii) metallic behavior was observed, even on the compressed pellet, for 22 complexes which were obtained only as powder; iv) about three-quarter of the metals retain metallic behavior down to temperature of 20 K or even lower, though below these temperatures they do not show a distinct metal-insulator transition; v) the room temperature conductivity is not very high ($\leq$ 200 $S \cdot cm^{-1}$); vi) the conductivity enhancement is poor even on the single crystal ($\sigma_{max}/\sigma_{rt} < 50$); vii) the acceptor molecules in the metals are rather fertile in the shape, size, and strength.

The conductivity of the metallic 25, 31–35, 38–41 was measured on the single crystals. Two kinds of HCTMM salts with different stoichiometry exhibit contrastive conducting properties; 5:1:2 PhCN salt (31) is a low-temperature molecular metal, while a metal-insulator transition with $T_{\sigma\,max}$ = 235 K was observed for the 4:1:2 TCE salt (32) (Figure 3-2a). Complexes 33–35, 38–41 are metallic down to the lowest temperature measured (1.3–1.4 K or 4 K). The σ_{rt} values are 30–200 $S \cdot cm^{-1}$ for the above four low-temperature molecular metals. The resistivities are simply proportional to T^n ($1 \leq n \leq 2$), a relation typically seen in low-dimensional molecular metals. The conductivity enhancement is only 20–50. The disorder of the anions, as will be seen in the crystal structures of 31, 33, and 39, is considered to be one reason for the high residual resistivity.

Metallic behavior was also found on the compressed pellet of the complexes obtained only as powder. For example, the temperature dependent resistivities of the C_{10}TCNQ (12), $(MeO)_2$TCNQ (18), and QCl_4 (19) complexes are shown in

Figure 3-2b. The 2:1 complex 18 remains metallic down to 5 K, accompanied by a conductivity 15 times that of σ_{rt} (47 S·cm^{-1}). 19 is also metallic to low temperatures (16 K), below which its resistivity increases slightly. Similarly, in metals, 1, 3-9, 11-12, 14-17, 20-24, and 36, resistivities minimize on cooling, but below the cooled temperature exhibit neither the rapid increase characteristic of the Peierls or SDW phase transition, nor the Arrhenius-type temperature dependence; their resistivities at 4-5 K are at most on the same order of the room temperature values. Among these metals, the TCNQ derivative with bulky alkyl chain yielded the least conducting complex 12 (σ_{rt} = 7.3 S·cm^{-1}), with resistivity increasing gradually below 135 K, but remaining low (0.1 S·cm^{-1}) even at 1.6 K (Figure 3-2b). The poor conductivity and high $T_{\sigma\,max}$ may be ascribed to the bulkiness of the acceptor (see below).

The intrinsic temperature-dependent resistivities measured on the compressed pellet of the microcrystalline remain ambiguous because they usually include the resistance due to interparticle contact.[42] By grinding crystals of 31, we were able to actually compared conducting properties on the single crystal and compressed pellet. The compressed sample shows comparable σ_{rt} (~ 100 S·cm^{-1}), but high $T_{\sigma\,max}$ (14 K) and low conductivity enhancement (σ_{14K}/σ_{rt} = 7.3) as compared to results on the single crystal ($T_{\sigma\,max} \leq$ 5 K, σ_{5K}/σ_{rt} = 20-30). Below 14 K, the conductivity of the pellet decreases slightly (σ_{4K}/σ_{14K} = 0.91). Based on these facts, the intrinsic conductivity of the powdered sample should remain metallic down to at least $T_{\sigma\,max}$ observed on the pellet. Similarly for 25, metallic property is degraded on the compressed pellet compared with the single crystal (compare $T_{\sigma\,max}$ and σ_{max}/σ_{rt} in Table 3-1). Including the results on single crystal, 25 complexes are essentially metallic to the low temperature (< 20 K), which indicates BEDO-TTF is an excellent source for stable metals. For the other TTF-based conductors, stable metallic states are realized by enhancing the interstack

interactions with the aid of heavier Se atoms and/or by extending π-conjugation system with further introduced sulfur atoms, as exemplified by the complexes of BEDT-TSF[43] and BDT-TTP.[44] The BEDO-TTF molecule, however, yields stable metals without these chemical modifications.

Semiconducting behavior was observed for 8 DA-type complexes, 2 radical salts, and 2 dication salts. Complexes 10, 13 and 37 show relatively high σ_{rt} and small Ea ($\leq$ 0.10 eV). Compared with metallic 12, σ_{rt} is 8 times decreased for 13 with its further bulky alkyl chain, which seems to inhibit metallic conduction. Highly resistive F_4TCNQ complex (2) (σ_{rt} = 7.9×10^{-8} $S\cdot cm^{-1}$, Ea = 0.40 eV) was obtained from acetonitrile as a 1:1 stoichiometry, which differs from that of metallic 3 (9:5:4THF). Other highly resistive semiconductors were neutral CT complexes with 5 weak acceptor molecules ($E_{1/2}{}^{1}(A) \leq -0.14$ V, 26-30), and the complexes of monovalent or divalent BEDO-TTF (42-44).

We should also note that BEDO-TTF DA-type complexes exhibit the following unique stoichiometry characteristics: (i) 1:1 complexes are less conducting and mainly obtained as neutral complexes (26, 28-30); (ii) only 27 shows 1:2, having a strong hydrogen-bond network among the acceptor molecules (see below); (iii) the highly conductive complexes contain the donor in excess, with donor/acceptor (D/A) ratios ranging from 1.6 (5) to 2.5 (12); (iv) about one-half of the metallic (3-5, 12, 16, and 20-22) and highly conducting (13) complexes are non-stoichiometric, and most of these contain solvent molecules. Therefore, disorder can be expected in their crystals.

It is important to emphasize that, unlike BEDT-TTF, BEDO-TTF easily provides stable molecular metals with D/A > 1 and a wide variety of acceptor molecules of different size, shape, and strength. In the following we will examine the electronic states of those complexes to clarify their conducting properties.

3–5 Thermoelectric Power

3–5–1 Metallic Complexes

Thermoelectric power (S) was measured for single crystals of metallic 25, 31, 32, 34, 39, and 40, and for a single crystal of semiconducting 37 and a compressed pellet of semiconducting 10.

Figure 3–3 shows the temperature dependent thermoelectric powers of the metallic 25, 31, 34, 39, and 40. The S values at room temperature are small positive (3–8 μV/K), and the positive sign is consistent with hole-like character of the calculated band structures presented in Chap. 5. These complexes are similar to one another in temperature dependence of S. With lowering temperature, the thermoelectric power reaches a minimum value of negative or nearly zero around 150 K, below which it gradually increases. Very similar temperature dependence is also reported for (BEDO–TTF)$_{2.4}$I$_3$ (41).[26a] It should also be noted that the S of 41 shows little in-plane anisotropy ($//a$ and $//b$). Chap. 5 will provide the discussion of the temperature dependent thermoelectric power on the basis of the band electronic structures.

3–5–2 Semiconducting Complexes

Figure 3–4 shows the temperature dependent thermoelectric power of highly conducting semiconductors 10 and 37 ($//c$ direction). The absolute values at room temperature are very large (–50, +40 μV/K, respectively), compared with those of above metallic BEDO–TTF complexes. With lowering temperature, S decreases in a divergent way. For an intrinsic semiconductor with an energy gap (E_g) at Fermi level, the thermoelectric power is

$$S = -\frac{k_B}{e}\left[\frac{b-1}{b+1}\frac{E_g}{2k_BT} + \frac{3}{4}\ln\frac{m_e}{m_h}\right] + \text{const} \qquad (3.4)$$

$$b = \mu_e/\mu_h \qquad (3.5)$$

where k_B is the Boltzmann constant, and $\mu_{e,h}$ and $m_{e,h}$ are the mobilities and effective masses of the electrons and holes, respectively.[45] Accordingly, the thermoelectric powers of these complexes are plotted against $1/T$ in Figure 3-4b. The T^{-1} dependence of 10 and 37 is characteristic of band semiconductors, although the slope of each curve is changed around 180 and 150 K, respectively. The conductivity of the complex 10 shows constant activation energy (105–290 K), which cannot account for the change of the slope. Below 180 K, 10 shows the slope of −0.0185 V. By using $E_g = 2Ea$ = 0.13 eV obtained from the conductivity, the mobility ratio b is estimated as 1.8 on the basis of eq(3.4), indicating that electrons are dominant carrier. In the case of 37, the slope of S (measured along the c axis) vs $1/T$ curve is −0.035 V for 115–150 K, and −0.014 V for 160–295 K. With Ea of 0.10 eV (//c, 90–200 K) from conductivity data, b values are estimated as 2.1 and 1.3, for respective temperature regions.

3-6 IR Spectrum and Degree of Charge Transfer

3-6-1 Vibrational Bands Derived from Acceptor Molecules

Infrared spectrum is useful for identifying the ionicity of the ground state of the CT complex;[46] degree of CT, particularly, can be estimated by utilizing those specific vibrations the frequencies of which are sensitive to the ionicity of the molecule.[47] Table 3-2 lists the frequencies of the CN stretching modes of the counter components and the $b_{1u}\nu_{31}$ mode of BEDO-TTF. First, we estimate the degree of CT (γ) for some BEDO-TTF complexes, based on the vibrations of the acceptors.

Two (BEDO-TTF)-F_4TCNQ complexes show contrastive features in their optical spectra: the vibrational bands are distinct for the insulator 2, whereas those

for metallic 3 are obscured by the CT electronic band. It has been previously reported that the two C=C stretching vibrational bands (1551 cm^{-1} ($b_{1u}\nu_{19}$) and 1598 cm^{-1} ($b_{2u}\nu_{33}$) for F_4TCNQ^0 marked by asterisks in Figure 3-5a) show red shifts by 51 and 62 cm^{-1}, respectively, on ionization to $(F_4TCNQ)^{-1}$ (Figure 3-5b).[48] The spectrum of 2 shows absorption at 1500 and 1536 cm^{-1}, corresponding to $(F_4TCNQ)^{-1}$, but shows no bands ascribable to the F_4TCNQ species in the partial or neutral CT around 1540-1600 cm^{-1} (Figure 3-5c). 2 is thus regarded as completely ionic since D/A = 1. The CN stretching frequencies (2228 cm^{-1} ($b_{1u}\nu_{18}$) and 2214 cm^{-1} ($b_{2u}\nu_{32}$) for F_4TCNQ^0, which shift by 34 and 42 cm^{-1} upon ionization, respectively) correspond to $(F_4TCNQ)^{-1}$ for 3 (2198, 2177 cm^{-1}) as well as for 2 (2195, 2170 cm^{-1}).

For other BEDO-TTF complexes with strong acceptors, such as HCBD (1) and DDQ (4), CN stretching frequencies are characteristic according to their completely ionized acceptor molecules.[49,50] An analogous conclusion can be made for 5 (ν_{CN} = 2216 cm^{-1}), based on comparison with $DBDQ^0$ (2230 cm^{-1}) and (TEA)DBDQ (2214 cm^{-1}).[51] The monoanionic acceptor molecules in 1, 3, 4, and 5 demand the partially-oxidized BEDO-TTF molecule because D/A > 1. Accordingly, in this text we define the γ of BEDO-TTF complexes as the charge on the donor molecules. The respective γ of 1, 2, 3, 4, and 5 are deduced from their D/A ratios to be 0.5, 1, 0.56, 0.60 and 0.64.

Among the BEDO-TTF radical salts, 37 has an HCP anion with charge of -2, judging from the CN stretching frequencies (2185, 2165 cm^{-1}), which are in good agreement with the reported values for HCP^{2-} (2183-2184, 2165-2168 cm^{-1}).[52] This is also confirmed by a skeletal vibrational band observed in the frequency region expected for the dianion (~ 1400 cm^{-1}) rather than for the monoanion (~ 1490 cm^{-1}). The charges on other anions are assigned as -2 in 31 and 32, and -1 in 33, 35 and 36, because these anions have too high potentials ($\geq$ 0.96 V vs. SCE, Table 3-1) to be oxidized by a $BEDO\text{-}TTF^+$

molecule ($E_{1/2}^{1}$(D) = 0.43 V). The γ values are 0.40 for 31, 33, and 37, and 0.50 for 32, 35 and 36, respectively, based simply on the stoichiometry. Since the charge on SQA is generally −2, and since SQA^{-} is detected only in solution,[53] the γ of 34 is expected to be 0.5 based on the ratio BEDO–TTF/SQA = 4.

3–6–2 Vibrational Bands Derived from Donor Molecules

It becomes rather complicated to estimate γ values for other complexes in Table 3–2 (6–25). Hence, more quantitative analysis of the ionicity of the complexes was tried based on vibration frequencies of the BEDO–TTF molecules. In order to show the spectrum change on the ionization of the donor, IR spectra of the neutral BEDO–TTF and the (BEDO–TTF)–I system with various oxidation state (41–44) are given in Figure 3–6 for the region 1700–400 cm^{-1}. All the bands in the figure solely come from the vibrations of the donor molecule. The ionization from neutral to dication (43) brings about the considerable change in the overall spectra, particularly large red shift of the ring C=C stretching band (indicated by arrows in the figure); 1646 (neutral BEDO–TTF), 1596 (41, +0.42 state), 1527 (42, +1), 1456 cm^{-1} (43, +2). These spectra thus enable the rough estimation of the oxidation states in other BEDO–TTF complexes. For example, the IR spectra of the insulating 44 is almost the same as that of a dication salt 43, indicating the divalent state of BEDO–TTF in 44, the crystal of which is unknown at present. The spectrum of monocation salt 42 shows some difference from that of (BEDO–TTF^{+})(F_4TCNQ^{-}) (2) (thin solid curve f in the figure), in spite of the same γ. Since the complex 42 contains strongly dimerized BEDO–TTF^{+} molecules in the crystal (see Chap. 4), totally symmetric (a_g) modes are expected to be IR active. Although the complete assignment of these bands require further study, the different spectra between 2 and 42 suggest the different molecular packing.

For the DA-type complexes, intense C=C and C=O vibrational bands of acceptor molecules usually superimposed on the C=C vibrational bands of BEDO-TTF, making indistinguishable from each other. Therefore, their discrimination is rather carefully required for estimation of γ from the C=C stretching mode of the donor in spite of large ionization frequency shift. Instead, Moldenhauer et al. have reported that other four absorption bands of BEDO-TTF^0 (864 (band a), 963 (b), 1011 (c), and 1082 cm^{-1} (d)) display ionization frequency shifts on the CT complex formation.[54] The vibrational bands of 31 in the region 1200-800 cm^{-1} (Figure 3-7a) are derived solely from those observed in BEDO-TTF^0; three prominent bands at 861 (a), 1006 (c), and 1179 cm^{-1} (e) and weaker two bands at 957 (b) and 1080 cm^{-1} (d). The band e is ascribed to that of BEDO-TTF^0 at 1159 cm^{-1}. Very similar spectra are observed for all other metallic BEDO-TTF complexes and for highly conducting semiconductors 13 and 37.

According to the normal coordinate analysis for neutral BEDO-TTF, the above five bands involve vibrations of C-O bonds.[55] Bands a, d, and e include the vibration between the terminal ethylene carbon and the oxygen atom. Therefore, these vibrations may be affected not only by the electronic structure, but also by the structural interactions with the counter components in the vicinity of the terminal ethylene groups. Band b shows too weak an intensity for determination of accurate frequencies for some BEDO-TTF complexes. On the other hand, the intense band c ($b_{1u}\nu_{31}$ mode), which is dominated by C_{in}-O and C_{in}-S stretches (C_{in}; the carbon atoms of the vinyl ether), is expected to be relatively insensitive to structural interactions with counter components. Consequently, we have examined whether this vibrational frequency (ω) is useful for estimating γ of the complexes.

Figure 3-7b plots the ω values obtained from the measurements with higher resolution (0.5 cm^{-1}) against the γ for neutral BEDO-TTF[55,56] and its

complexes of unambiguously known γ (1–4, 31–33, 35–37, 43, 44), as well as the reported γ values.[54] Although the band c tends to show red shift upon ionization, the correlation is not good enough for the accurate estimation of unknown γ of the complexes; the ω values are scattered by 5 cm^{-1} at γ = 0.5 and by 8 cm^{-1} at γ = 2.

Even with fully-ionic acceptor molecules, partial γ values are deduced for all the metallic BEDO-TTF complexes containing excess donor molecules. Based on the stoichiometry, γ values of 12 and 20 are at most 0.40 and 0.46, respectively. The superconducting $(BEDO\text{-}TTF)_3Cu_2(NCS)_3$ has an even further lowered γ (0.33).[27a] It has been previously established that in most DA-type complexes of $\gamma < 0.5$, the alternating stack is stable rather than the segregated one, resulting in an insulating ground state. As far as we know, metals which feature both uniformly segregated stacks and low γ (< 0.5) have been obtained only from molecules much larger than BEDO-TTF, as exemplified by $(DTEDT)_3Au(CN)_2$ (γ = 0.33) and nickel phthalocyanine triiodide (γ = 0.33).[57]

For the insulating 26–30, each IR spectrum is approximated by the superposition of the spectra of the neutral components, confirming that they are neutral complexes.

3-6-3 Vibrational Spectrum and Electronic State of Complex 10

The electronic state is somewhat complicated in the semiconducting (BEDO-TTF)(TCNQ) (10). The IR spectrum shows three CN stretching bands around 2210–2150 cm^{-1}. The highest frequency band ($b_{1u}\nu_{19}$ mode), which is often used to determine the charge on the TCNQ molecules ($-\zeta$) in its CT complexes,[47] is observed at 2194 cm^{-1} with a shoulder at 2201 cm^{-1}. Their frequency shifts ($\Delta\omega$) from neutral TCNQ (2225 cm^{-1}) suggest the fractional charge (ζ = 0.55–0.70) using the proposed formula $\Delta\omega/\zeta$ = 44 cm^{-1}.[48] Such

a splitting of $b_{1u}\,\nu_{19}$ mode is observed, not in the metallic temperature region of TTF-TCNQ, but below 55 K, where CDW drives the distortion on TCNQ stacks.[58] The crystal structure of **10**, though unknown at present, likely contains distorted TCNQ stacks. Through comparison with the spectra of (BEDO-TTF$^+$)(F_4TCNQ$^-$) (**2**) (Figure 3-5c) and TCNQ^n (n = 0, -1),[59] most of the vibrational bands of **10** can be assigned to those of BEDO-TTF$^+$ (designated by open circles in Figure 3-5d) and TCNQ$^{-\delta}$. There remain three unassigned bands at 1010, 1159, and 1635 cm^{-1}, which are in turn ascribable to those of neutral BEDO-TTF (filled triangles in Figure 3-5d are those ascribable to neutral BEDO-TTF (Figure 3-5e)). These facts suggest a charge separation among BEDO-TTF molecules.[60] Partially charged TCNQ stacks are therefore considered to afford relatively high conductivity to **10** although their distortion seems to prevent metallic conduction. This is also consistent with the thermoelectric power dominated by electrons.

3-6-4 Summary

The CT complexes with neutral (**26-30**), monovalent (**2**, **42**), divalent (**43**, **44**) or inhomogeneous charge-distributed ground states (**10**) resulted in semiconducting electronic properties, whereas all the others, which were in the partial CT ground state of the donor, resulted in metals, with the exception of only two complexes with C_{14}TCNQ (**13**) and HCP (**37**). It should be emphasized that BEDO-TTF has peculiar ability to afford metals of small γ among the TTF-based donors.

3-7 Electronic Spectrum

3-7-1 Neutral BEDO-TTF

Neutral BEDO-TTF in solution exhibits strong absorption bands at 29.9×10^3

and 31.8×10^3 cm^{-1} and much weaker one at 19.5×10^3 cm^{-1} (Figure 3-8a). These bands also appear at almost the same energy in the solid state, but the lowest one (19.9×10^3 cm^{-1}) increases in relative intensity. In addition, the higher energy bands [$(25-35) \times 10^3$ cm^{-1}] are poorly resolved compared to the solution spectrum. These features correspond well with those observed for BEDT-TTF.[61]

3-7-2 Metallic BEDO-TTF Complexes

Table 3-2 summarizes the energies of the lowest transitions ascribable to CT ($h\nu_{CT}$) and high-energy transitions (UV-VIS) for all of the BEDO-TTF complexes investigated in this work. First, we describe the absorption spectra of $(BEDO\text{-}TTF)_2Br(H_2O)_3$ (**39**) as a typical example of the metals. Since the Br^- ion and water molecule do not absorb the light in the range of (5-45) $\times 10^3$ cm^{-1}, both solution and solid spectra shown in Figure 3-8b are unambiguously related to the electronic transitions of BEDO-TTF molecules. The solution spectrum of **39** exhibits some absorption bands, which are labeled as C, D, E, and F in the figure.

The powder spectrum of **39** (Figure 3-8c) shows an additional band (band A) around 2.2×10^3 cm^{-1}. This low-lying absorption arises from the CT transition: $(BEDO\text{-}TTF)^0 + (BEDO\text{-}TTF)^+ \rightarrow (BEDO\text{-}TTF)^+ + (BEDO\text{-}TTF)^0$. The powder spectra of all other metals and of highly conducting **10**, **13**, and **37** also show the A band extending throughout the whole infrared region. With few exceptions,[62] the low-lying absorption band below 5×10^3 cm^{-1} appears as the intraband transition in metals or the intramolecular CT transition among the self-aggregated component molecules in mixed valence state. Therefore, its appearance indicates both the partial CT or mixed-valence state and segregated or self-assembling state of the component molecule,[16b,63] and hence, is reasonable for metallic complexes.

The peak C in the solid spectrum is broadened and shows a blue-shift of about 2×10^3 cm^{-1} vs that in solution. The C band is observable in the powder spectra of all the metallic BEDO-TTF complexes (Table 3-2). In the solution spectra of TTF^+, while the lowest transition is situated at 17×10^3 cm^{-1} for the monomer,[64] its dimer gives rise to an additional band at the lowered energy (14×10^3 cm^{-1}),[65] which corresponds to the CT process, $(TTF)^+ + (TTF)^+ \rightarrow (TTF)^0 + (TTF)^{2+}$. The latter transition energy is a rough measure of the effective on-site Coulomb repulsion (U_{eff}) on TTF. In the present case, however, the band C can be related to the lowest intramolecular excitation rather than this CT process for the following reasons. (i) The band C is clearly observed even for complexes of small γ (for example, 0.5 for **39**). This contradicts what has been theoretically[66] and experimentally[64,67] observed for the CT process among TTF^+ radicals; intensity of band C is greatly diminished with decrease of γ, and vanishes where γ = 0.5. (ii) On the other hand, for the monovalent (BEDO-TTF)I_3 (**42**), which contains $(BEDO\text{-}TTF^+)_2$ dimers in its crystals, the solid spectrum reveals low-energy bands [$(7\text{-}9)\times10^3$ cm^{-1}] (band B in Figure 3-8d) in addition to the band C; hence these new bands are assigned to the CT between $BEDO\text{-}TTF^+$ molecules. (iii) The equilibrium between cation monomer and its dimer in solution gives rise to a concentration dependence of the absorbance. However, the absorbance of band C of ε = 4.0×10^3 (per one mol of $BEDO\text{-}TTF^+$) is independent of the concentration of $BEDO\text{-}TTF^+$ (1×10^{-6} to 4×10^{-5} $mol\cdot l^{-1}$). (iv) BEDT-TTF radical salts reveal their absorption band at about 10×10^3 cm^{-1} in the spectra polarized along the long axis of the donor molecule; this spectrum is assigned to their lowest intramolecular excitation.[68] This transition was explained by an electronic one from the second highest occupied molecular orbital (SHOMO) to the HOMO, which accommodates an unpaired electron in the ground state.[64] According to the PES measurement,[39] the differences between the first and second

ionization potentials for BEDO–TTF (1.01 eV) and BEDT–TTF (~1.2 eV) are much smaller than that for TTF (1.88 eV). The decrease of the energy difference between HOMO and SHOMO for BEDO–TTF is in good agreement with the magnitude of the red shift of the band C (17×10^3 cm^{-1} (TTF^+) $\rightarrow$ 10.7×10^3 cm^{-1} (BEDO–TTF^+), decrease by 0.8 eV). Based on the items i–iv, the band C in solution can be assigned to the lowest intramolecular excitation. C band in the solid is also assignable to this transition. However, because the BEDO–TTF molecules are not strictly perpendicular to the stack in the crystal, the CT processes creating the doubly–occupied states may be mixed in this band, as has previously been proposed for β-(BEDT–TTF)$_2I_3$.[69]

By analogy with TTF salts,[64,65] bands D, E and F observed in the solution of 39 are attributable to the intramolecular transition of BEDO–TTF^+. From comparison with solution spectrum of neutral BEDO–TTF, bands G and H in 39 are ascribable to the absorption of the neutral BEDO–TTF. In the powder spectrum, the bands D–H are broadened, poorly resolved, and in some cases, observed only as shoulders due to a solid state effect. The metallic BEDO–TTF complexes of DA–type yield further complicated solid spectra due to the superimposed absorptions of ionized acceptors.

Among the acceptor molecules for the metallic complexes, H_2CHA and H_2BRA are strong dibasic acids (pKa1 = 0.45, pKa2 = 2.50 for H_2CHA).[70] The cyclic voltammetry of these molecules shows only cathodic peak in acetonitrile which was used for preparations of these complexes. Therefore, the radical anions of these acceptors are regarded as unstable due to the succeeding irreversible process. In the complexes 24 and 25 where the donor molecules are partially oxidized, the acceptor molecules are negatively charged. Furthermore, the structural analysis of 25 (see Chap. 5) suggests that the H_2CHA molecule is partly or completely deprotonated. Figure 3–9a,b shows the solid and solution (in CH_3CN) spectra of 25, respectively. Both spectra are

similar to each other except the existence of the low-lying CT band A (2 $\times 10^3$ cm^{-1}) and poor resolution in the solid. The solution spectrum of 25 shows bands at 10.7×10^3 cm^{-1} (C), 16.2×10^3 cm^{-1} (D), 20.3×10^3 cm^{-1} (E), 21.6×10^3 cm^{-1} (F), and 29.7×10^3 cm^{-1} (G), which are unambiguously related to the absorptions of the BEDO-$TTF^{+\gamma}$ molecule (γ = 0, 1) from comparison with the solution spectra of 39. Curve d in the figure shows the absorptions of the anions obtained by subtraction of the spectra of 39 (curve c) from that of 25. This spectrum well agrees with the electronic spectra of $HCHA^-$ (19.4×10^3 cm^{-1}, 33.4×10^3 cm^{-1}, curve e)[71] rather than CHA^{2-} (20.5×10^3 cm^{-1}, 30.5×10^3 cm^{-1}, 31.4×10^3 cm^{-1}, curve f) or H_2CHA (23.2×10^3 cm^{-1}, 33.3×10^3 cm^{-1}, curve g). The ESR spectrum of this solution gave a single signal (g = 2.0072) originated from the BEDO-TTF^+ radical (g = 2.0073 in CH_3CN solution of 39), indicating the absence of radical species of the acceptor. Therefore, the complex 25 is regarded as the radical salt with formula of (BEDO-$TTF)_2^+(HCHA^-)$, the same situation of which may be expected for the complex (24) with the bromine analogue H_2BRA. The partial deprotonation is also reported for the cyanilic acid (H_2CNAL) which combines with TMTTF to yield $(TMTTF)_2^+(HCNAL^-)$ complex.[72]

3-7-3 Semiconducting BEDO-TTF Complexes

The monocation and dication salts of BEDO-TTF exhibit different spectra from those of metallic BEDO-TTF complexes. Figure 3-8d,e,f shows the spectra of the complexes 42-44 measured on the KBr disk. There are no A bands in the IR region, confirming the absence of the self-assembled BEDO-TTF molecules in the partial CT ground state. These three complexes commonly reveal the band C around (12-13)$\times10^3$ cm^{-1}, as is observed for other complexes of partially oxidized BEDO-TTF. This observation is not surprising, because the above discussed intramolecular excitation is possible also for dication salts; an

electronic transition from the SHOMO to the HOMO, which is half-filled for BEDO-TTF^{+} and vacant for BEDO-TTF^{2+}. As mentioned before, monocation salt 42 exhibited additional bands B at 7.3×10^{3} and 9.4×10^{3} cm^{-1}. Considering that $(BEDO\text{-}TTF^{+})_2$ dimers have large intradimer and interdimer interactions (see Chap. 5), these two bands can be related to the intradimer and interdimer CT transitions. These CT transition energies are considerably small in comparison to TTF (14×10^{3} cm^{-1}),[65] indicating the reduction of U_{eff} for the BEDO-TTF molecule. The complex 44 gave almost the same spectra as that of 43, not only for IR region but also for higher energy region, confirming the similar electronic states between these salts.

The CT band of the alternating stacking type is related to the transition from $D^{+\gamma}A^{-\gamma}$ to $D^{+(1-\gamma)}A^{-(1-\gamma)}$. This band's transition energies for neutral ($h\nu_{CT}^{N}$) and ionic complexes ($h\nu_{CT}^{I}$) are represented differently[12a,41] as

$$h\nu_{CT}^{N} = I_P(D) - E_A(A) - C' + X \quad (\gamma < 0.5), \tag{3.6}$$

$$h\nu_{CT}^{I} = -I_P(D) + E_A(A) + (2\alpha - 1)C' + X' \quad (\gamma > 0.5) \tag{3.7}$$

Here α is the Madelung constant, C' is the averaged electrostatic attraction energy of a D-A pair (defined as positive), and X, X' are mainly the resonance stabilization energies. Since the $E_A(A)$ data are not available for all the acceptors used, the $\Delta E^{o,r}$ ($= E_{1/2}^{1}(D) - E_{1/2}^{1}(A)$) value, which is originally related to the adiabatic values, $I_P^{ad}(D)$ and $E_A^{ad}(A)$ as previously described, is often used instead of the $I_P(D) - E_A(A)$.

Figure 3-10 shows a plot of $h\nu_{CT}$ versus $\Delta E^{o,r}$ for all the BEDO-TTF complexes of DA-type. The Eqs.(3.6) and (3.7) are portrayed in the figure as a V-shaped line (Torrance's diagram).[12a] This diagram helps us to predict the stacking manner and ionicity of a CT complex[12a,73] with some care.[74] The open and filled squares in the figure represent metallic and semiconducting

complexes, respectively. The neutral BEDO–TTF complexes, 26, 28, and 30 locate along the V–shape line, which corresponds to the CT transition from donor to acceptor molecule. The CT transitions in 27 and 29 can also be related to the same type in consideration of their crystal structures (see below). The irreversible reduction processes of these acceptor molecules prevent the accurate determination of $\Delta E^{o,r}$ values, which may be responsible for the deviation from the V–shaped line.

If the complexes of mixed stacking type located near the neutral–ionic boundary (the bottom of V–shaped line), they may exhibit neutral–ionic transition under cooling and/or pressure.[12] However, this transition is hardly expected for BEDO–TTF complexes, which easily fall into segregated stacking or layered structure rather than the mixed stacking near this boundary.

The metallic complexes and highly conducting semiconductors 10 and 13 yield CT bands (band A) at much lower energy (below the dotted line in Figure 3–10 drawn as the approximate upper border of A band at 5×10^3 cm^{-1}). In the case of (BEDO–TTF)(TCNQ) (10), our previous discussion of the IR spectrum suggests both the charge separation among BEDO–TTF molecules and the partial CT ground state of TCNQ molecules. Therefore, the TCNQ stack is likely to dominate the conductivity and contribute to the A band (4.5×10^3 cm^{-1}).

The overall spectrum of the fully ionic (BEDO–TTF)(F_4TCNQ) (2) is complicated and similar to that for (BEDT–TTF)(F_4TCNQ) of mixed stacking type;[23,24b] the absorption bands appear at 6.7×10^3, 9.3×10^3, 12×10^3, 13×10^3, and 26×10^3 cm^{-1} for the former complex, and at 6.1×10^3, 9.3×10^3, 14×10^3, and 26×10^3 cm^{-1} for the latter. The high CT transition energy of 2 (6.7×10^3 cm^{-1}) corresponds to the insulating nature. Considering that this energy is also close to the CT transition energy among F_4TCNQ^- molecules (6.3×10^3 cm^{-1} for K(F_4TCNQ)), it is currently difficult to predict stacking type in 2.

3–7–4 Brief Summary

The spectra of all BEDO–TTF complexes except the divalent salts 43 and 44 show the lowest absorption band ascribable to that CT process, in addition to the intramolecular excitations of neutral and/or ionized BEDO–TTF and of counter component molecules. Their CT transition energy was consistently correlated to the conducting property.

3–8 Magnetic Properties

3–8–1 Neutral BEDO–TTF

The static magnetic susceptibility of neutral BEDO–TTF exhibited a temperature independent value of $(-1.4 \pm 0.1)\times10^{-4}$ emu·mol^{-1} (2–300 K), which is in agreement with that calculated from the Pascal's constants (1.51×10^{-4} emu·mol^{-1}) within an experimental error.

3–8–2 g–Tensor of BEDO–TTF^{+} Radical

Although the ESR measurements have been done on some BEDO–TTF radical salts, its *g* tensor has not been reported yet in the literature. In order to determine the *g* tensor of the BEDO–TTF^{+} radical, angular dependent ESR spectra were collected on a $(BEDO–TTF)_5HCTMM(PhCN)_2$ (31) crystal, the structure of which consists of the donor molecules aligned in parallel and the diamagnetic counter component molecules. The ESR spectrum exhibited a Dysonian line shape when the microwave electric field is applied parallel to the BEDO–TTF conducting layer (i.e. the *ac* plane), and otherwise a Lorentzian line shape. The angular dependence of the *g* value is indicated in Figure 3–11a, where the squares, circles, and triangles represent the data obtained by rotations of the magnetic field (B) from the *a* to the b^* axis, from the *c'* (*c'* ≡

$a \times b^*$) to the b^* axis, and from the c' to the a axis, respectively. The g value is well described by the equation,

$$g^2 = \sum_{i,j=1}^{3} g_{ij}^2 l_i l_j \qquad (3.8)$$

where l_i and l_j are the direction cosines of the principal axes. The solid curves represent the least squares fitting of the g values. Table 3-3 lists the obtained principal values (g_1, g_2, g_3) and direct cosines of the g tensor. The directions of the largest (g_1 = 2.0132), middle (g_2 = 2.0051), and smallest principal values (g_3 = 2.0005) are parallel to the molecular long axis, the short axis, and the normal axis of the BEDO-TTF molecule, respectively. This orientation as well as the principal g values are in good agreement with those observed for the BEDT-TTF salts (g_1 = 2.014, g_2 = 2.006, g_3 = 2.001).[75] The averaged g value, $\bar{g}$ [$\equiv (g_1 + g_2 + g_3)/3$] of BEDO-TTF$^+$ radical (2.0063) is almost the same as the value observed in the acetonitrile solution of (BEDO-TTF)$_2$Br(H$_2$O)$_3$ salt (39) (g = 2.0073).

As fitted by solid curves in Figure 3-11b, the linewidths of 31 vary from 27 G to 43 G, and is well described by the equation

$$\Delta H = \sum_{i,j=1}^{3} \Delta H_{ij} m_i m_j \qquad (3.9)$$

where m_i and m_j are the direction cosines of the principal axes. According to the mechanism proposed by Elliott,[76] the spin-lattice relaxation of the conduction-electron spins in metals is dominated by spin-orbit coupling modulated by lattice vibrations. In this case, ΔH is proportional to the $\tau/(\Delta g)^2$ where $\Delta g = g - 2.0023$ and τ is the relaxation time of carriers, and hence the principal directions of linewidth and g tensors agree with each other. In the complex 31, the g value and linewidth show similar angular dependence, but the phase of the linewidth curve for the a-b^* rotation is somewhat different from that of the g value, indicating that the disagreement

of the principal directions between these tensors. Therefore, Elliott mechanism fails to elucidate the angular dependent ESR linewidth, as is pointed out also in the β-(BEDT-TTF)$_2$I$_3$.[75]

3-8-3 Metallic BEDO-TTF Complexes and Highly Conducting Complex 13

Table 3-4 summarizes the results of the magnetic susceptibility measurements performed on 10 metallic BEDO-TTF complexes and highly conducting 13.

The spin susceptibility (χ_s) of the metallic complexes 17, 25, 31 shows the small temperature dependence (Figure 12). The room temperature value of 25 is (2.3 ± 0.2)x10^{-4} emu·(mol of BEDO-TTF)$^{-1}$. The complex 31 shows χ_s of (2.2 ± 0.2)x10^{-4} emu·(mol of BEDO-TTF)$^{-1}$, which is close to the value deduced from the ESR measurements [1.8x10^{-4} emu·(mol of BEDO-TTF)$^{-1}$].[75] The χ_s of the radical salt 31 is unambiguously ascribable to the spin on the BEDO-TTF$^+$ radical, considering that the counterion HCTMM^{2-} has a closed shell electronic structure. In the case of metals with no electron-electron interactions (U_{eff} = 0), the susceptibility at T = 0 K can be simply described by the Pauli paramagnetism as,

$$\chi_{Pauli} = \mu_B^2 \cdot N(E_F) \qquad (1.10)$$

where μ_B is the Bohr magneton, and $N(E_F)$ the density of states at Fermi level including the spin degeneracy. The χ_s of 31 is 4-5 times larger than the χ_{Pauli} value estimated by tight-binding band calculation [$N(E_F)$ = 1.36 states(total)/(eV·molecule of BEDO-TTF) (see Chap. 5)]. The enhanced Pauli susceptibility is usually observed for molecular metals, because the effective on-site Coulomb energy cannot be negligible as compared to the transfer integrals. It is emphasized that Pauli paramagnetism for these complexes retains down to very low temperatures (> 2 K), which is consistent with the observations of no metal-insulator transitions in conductivity.

Some metallic complexes reveal the Curie paramagnetism in addition to the Pauli paramagnetism at low temperatures. Figure 3-13a plots the χ_S as a function of $1/T$, which demonstrates that χ_S of 4, 15, and 18 at low temperatures (< 50 K) is well described by the equation,

$$\chi_S = \chi_O + C/T \tag{3.11}$$

where χ_O is the temperature independent part of the susceptibility and C the constant. Based on the slope C, concentration of the defects with spin S = 1/2 is estimated by

$$N = \frac{Ck_B}{\mu_B{}^2 N_A} \tag{3.12}$$

where N_A is the Avogadro number. The similar temperature dependence is observed for the complex 19. The spin susceptibility after subtracted this Curie paramagnetism, is nearly constant for all the temperature region (Figure 13b).

The metallic 12 and 23, and highly conducting semiconductive 13 also exhibit the nearly constant susceptibility above 100 K. Below this temperature, their susceptibility reveals much rapid upturn, compared with those of above 4, 15, 18, and 19. This temperature dependence is similar to a Curie tail, but shows the deviation from the linear dependence on $1/T$, as exemplified by the χ_S of 12 deviated from the linear dotted line in Figure 3-13a. Instead, a linear relation was found in the plot of log χ_S vs log T (Figure 3-13c): the χ_S increases according to the power law,

$$\chi_S = C'T^{-\alpha} \tag{3.13}$$

where C' and α are constants. The least squares fit to the data below 20 K gives α = 0.88 for 12 and 23, and 0.82 for 13 (solid line in Figure 3-13c).

For these three complexes, the constant C', which corresponds to the above C if $\alpha = 1$, is much larger than C of 4, 15, 18, 19, indicating the larger concentration of the disorder. The concentration of the disorder is estimated as 3–4 % per donor molecules, assuming the eq(3.12). Such a $T^{-\alpha}$ ($\alpha < 1$) dependence has been observed for some organic conductors containing the asymmetric component molecules or disorders introduced by chemical doping or irradiation. This behavior has been interpreted in terms of a random exchange Heisenberg antiferromagnetic chain (REHAC) with $S = 1/2$ spins,[77] which arises from the random exchange coupling between the localized electronic states produced by disorder. The disorder in the complexes 12, 13, and 23 are attributed to the nonstoichiometric character, inclusion of solvent molecules and/or the asymmetric shape of the acceptor molecules. Then, why does the complex 31 show no Curie–like upturn in the susceptibility in spite of the solvent inclusion and the presence of disorder in the crystal? The crystal structure (see below) of 31 contains the disordered counter component molecules, all of which are considered to be nonmagnetic species, however. The lack of the Curie tail indicates very little amount of defects in the layers of cation radicals. On the other hand for the DA–type complexes 12, 13, and 23 as well as 4, 15, 18, and 19, the disorder in the crystal is inevitably located on radical ions of donor and/or acceptor, leading to the Curie–like upturn in the susceptibility. It should be noted that the complex 23 is metallic even down to 8 K, in spite of rather high concentration of defects. The concentration is further high for the poorly metallic 12 and semiconducting 13.

The χ_s of metallic (BEDO–TTF)$_2$Br[MnBr$_2$(H$_2$O)$_4$](H$_2$O) (40) is very large at room temperature [1.3×10^{-2} emu·(mol of BEDO–TTF)$^{-1}$] compared with the Pauli paramagnetism for other BEDO–TTF complexes. The χ_s vs $1/T$ curve shown in the inset of Figure 3–14 exhibits the Curie–Weiss law,

$$\chi_S = \frac{C}{T - \theta} \qquad (3.14)$$

where θ = −0.5 K. Figure 3–14b plots the temperature dependent effective moment, μ_{eff} [$\equiv (3k_B T\chi_S/N_A)^{1/2}$]. The μ_{eff} value at room temperature (5.5 μ_B) is close to that expected for high spin state of Mn(II) ions (5.92 μ_B, S = 5/2). Therefore, the dominant component of the χ_S in this molecular metal can be related to the $MnBr_2(H_2O)_4$ molecule, which is a neutral spacer with a localized magnetic moment.

Summarizing the magnetic properties of the above metallic complexes, it is emphasized that the metallic conduction is little affected by the disorder and/or the localized spins on the counter component molecules.

3–8–4 Semiconducting BEDO–TTF Complexes

The semiconducting (BEDO–TTF)(TCNQ) (**10**) exhibited a paramagnetism (Figure 3–15a) with the room temperature value of 9.0×10^{-4} emu·mol^{-1}. The χ_S above 100 K can be well expressed by the Curie–Weiss law (eq.3.14) with C = 0.334 emu·K·mol^{-1} and θ = −80 K as shown by T vs $1/\chi_S$ curve in Figure 3–15b. The μ_{eff} (1.46 μ_B at room temperature) shows gradual decrease on lowering temperature (Figure 3–15c), indicating an antiferromagnetic coupling between the spins. The Curie constant C corresponds to 0.89 spins of S = 1/2 per formula unit, which is much smaller than that expected from all the ionized radical species on the basis of the above estimated degree of CT (0.55–0.70). ESR spectrum of the randomly oriented polycrystalline sample at room temperature (Figure 3–16) shows the axial anisotropy of g values ($g_{//}$ = 2.0097 and $g_{\perp}$ = 2.0048). The averaged g value [$\equiv (g_{//} + 2g_{\perp})/3$] of 2.0064 is very close to that of BEDO–TTF^+ radicals (2.006–2.007) rather than $TCNQ^-$ radicals (2.0025),[78] indicating the dominant contribution of the former species to the spin susceptibility. On the basis of the above discussion of the optical

spectra, the following explanation can be proposed for these magnetic behavior: (i) Curie–Weiss behavior arise from the spins localized on the BEDO–TTF^+ molecules which coexist with the neutral species in the donor stack of inhomogeneous charge distribution; (ii) the distortion on the stack of partially charged TCNQ molecules, if Peierls type, will lead to nonmagnetic ground state of the acceptor stack. Below 100 K, χ_S does not obey the Curie–Weiss law.

The insulating (BEDO–TTF)(F_4TCNQ) (2) shows a paramagnetism with the room temperature value of 2.3×10^{-3} emu·mol^{-1}. The $1/\chi_S$ vs T curve in Figure 3–15b indicates the antiferromagnetic exchange, although the susceptibility does not obey the Curie–Weiss expression for all the temperature region measured. The μ_{eff} at room temperature (2.33 μ_B) corresponds to 1.8 spins of S = 1/2 per formula unit, and below the temperature it gradually decreases, showing anomaly at 50 K (Figure 3–15c). Therefore, both component molecules are regarded as radicals, which is in agreement with the IR spectra that indicates the fully ionic state of this complex. The χ_S below 50 K can be well fitted to the theoretical susceptibility proposed by Bonner and Fischer[79] for the Heisenberg antiferromagnetic chains of alternately coupled S = 1/2 spins,

$$\chi_{BF} = \frac{Ng^2\mu_B{}^2}{k_BT}\,\frac{A + Bx + Cx^2}{1 + Dx + Ex^2 + Fx^3} \tag{3.15}$$

where $x = |J|/k_BT$, and the value for parameters A through F are

$$\begin{aligned} A &= 0.25 \\ B &= -0.12587 + 0.22752a \\ C &= 0.019111 - 0.13307a + 0.509a^2 - 1.3167a^3 + 1.0081a^4 \\ D &= 0.10772 + 1.4192a \\ E &= 0.0028521 - 0.423462a + 2.1953a^2 - 0.82412a^3 \\ F &= 0.37754 - 0.067022a + 5.9805a^2 - 2.1678a^3 + 15.838a^4 \end{aligned} \tag{3.16}$$

In order to see the g value, preliminary ESR measurement was performed on

the randomly oriented polycrystalline sample at room temperature. Figure 3-16 shows the ESR spectrum, which has a peak-to-peak line width of 5.1 G, and gives g value of 2.004 assuming a Lorentzian line shape, although its fitting curve slightly deviates from the spectrum. This value, which is intermediate between the g value of BEDO-TTF$^+$ (2.006) and that of F_4TCNQ^- (2.0029),[80] was used for the fitting procedure. The exchange integral J is related to the temperature at maximum susceptibility T_{max}:

$$k_B T_{max}/|J| = 1.282 \qquad (3.17)$$

From the experimental data (T_{max} = 5.4 K), J is deduced as -4.2 K. The best fitting represented by a solid curve in Figure 3-15a was obtained for a = 0.15 with one spin per formula unit, which is only half amount of spins at room temperature. Above 50 K, the observed χ_S rapidly deviate from the theoretical curve of χ_{BF}. The $\chi_S - \chi_{BF}$ plotted in Figure 3-15d exhibits a nearly constant value of 1×10^{-3} emu·mol^{-1} above 60 K. Its rapid drop around 50 K implies the loss of additional spins by phase transition at this temperature. Although the crystal structure of 2 is unknown at present, the magnetic susceptibility suggests the presence of two kinds of chains: the alternating antiferromagnetic chains with small J, and the additional antiferromagnetic chains of strongly coupled.

In contrast with 2, the monocation salt 42 is diamagnetic for all the temperature region measured (2-350 K). As shown later, this complex contains strongly dimerized (BEDO-TTF$^+$)$_2$ units in the crystal. The resultant electronic band has a gap at Fermi level, which should provide the insulating and nonmagnetic ground state. In this case, singlet-triplet thermal excitation gives rise to the temperature dependent magnetic susceptibility as

$$\chi = \chi_d + \frac{2Ng^2\mu_B{}^2}{k_B T} \frac{1}{3 + \exp(-2J/k_B T)} \qquad (3.18)$$

where the first term is the Pascal diamagnetism. Taking the experimental error ($|\chi - \chi_d| < 2\times10^{-4}$ emu·mol^{-1}) at 350 K into consideration, the energy gap between the singlet and triplet states ($-2J$) is deduced to be larger than 0.11 eV.

The diamagnetism is observed also for the complex **44** for entire temperature region measured (2–300 K). This is consistent with the divalent state of BEDO–TTF with closed-shell electronic structure.

3–9 Features of Acceptors in Metallic Complexes.

One of the peculiar features of the BEDO–TTF complexes is that the metals are fertile with regard to shape and size of the acceptor molecules. Ten metals are obtained from acceptors with the TCNQ skeleton, traditional one of the superior building blocks of molecular metals. Even THBTCNQ and DHBTCNQ possessing bulky substituents which tend to prohibit uniform stacking, provided good metals (σ_{rt} = 110 and 33 S·cm^{-1}, respectively) of very low $T_{\sigma max}$. Although the bulky substituents without delocalized π-electrons in their acceptors are regarded as disadvantageous for the highly conducting metals, BEDO–TTF can yield a metal **12**, and a highly conducting complex **13**. It is noteworthy that we have found also the metallic nature of **12** and **18** on the LB films.[81] Metallic complexes are also derived from nine out of ten *p*-benzoquinone derivatives, which have been known to form alternating stack, preferably in CT complexes. The percyano-olefins (HCBD and TCNE) are no exception, despite the fact their component molecules are inferior for producing usual molecular metals. Furthermore, this donor allows metals with two fluorene derivatives for the first time. These facts indicate that BEDO–TTF molecules construct the metallic columns or layers preferably, and that counter molecules serve the functions of charge-compensating and/or space

filling.

Another interesting feature is the strength of acceptor molecules for producing metallic BEDO–TTF complexes. In the 1:1 TTF–TCNQ system the following condition is required for molecular metals: $-0.02 \leq \Delta E^{o,r} \leq 0.34$ V,[17] the boundaries of which are shown by vertical lines in Figure 3–10. BEDO–TTF ($E_{1/2}{}^{1}$(D) = +0.43 V) meets this criterion for twelve acceptors used, ten of which actually gave metals.

In general, 1:1 CT complexes are fully ionic insulators in the region $\Delta E^{o,r} <$ −0.02 V, and (BEDO–TTF)(F_4TCNQ) (2) is just such a case ($\Delta E^{o,r}$ = −0.17 V). Although other acceptors in the same region (for 1, 3–5) are also fully ionized, non 1:1 stoichiometries will allow partial oxidation of the donor and resultant metallic state.

Segregated stacking is rarely found in complexes beyond the other boundary of $\Delta E^{o,r}$ = 0.34 V, which has been regarded as corresponding to γ = 0.5. Nevertheless, this region involves eight metallic BEDO–TTF complexes. The $\Delta E^{o,r}$ values of 24 and 25 are highest among these, but still somewhat uncertain due to the irreversible reduction of acceptors. At present it seems evident that the upper boundary of $\Delta E^{o,r}$ for metallic BEDO–TTF complexes locates between +0.41 V (23) and +0.57 V (26), considerably higher than conventional TTF–TCNQ–based molecular metals.

The above results lead to the conclusion that BEDO–TTF molecules can construct the self-aggregated (segregated columnar or layered) structure so easily that the acceptor molecules of a wide variety of shapes, sizes and strengths are allowed to yield molecular metals.

3–10 Summary

This work has produced 45 BEDO–TTF complexes, 33 of which are metals.

The physical properties of these metals can be summarized as the following features. (i) All the metallic complexes of DA-type show large D/A ratios (1.6-2.5, typically 2), which realize the partial γ even in the complexes of fully ionized acceptors. (ii) The acceptor molecules of a wide variety of shapes, sizes and strengths are allowed to produce molecular metals. (iii) The metallic state is little affected by localized magnetic moment or severe disorder as is characterized by the large $C'T^{-\delta}$ component in the susceptibility, non-stoichiometric character, and/or solvent inclusion. (iv) The metallic state is stable down to very low temperatures. The items i-iii indicate that oxidized BEDO-TTF molecules are self-aggregated very easily in excess proportion so as to form metallic segregated stacks or layers. The following structural properties will clarify the origin of the stable metallic states and the strong self-aggregating ability. Also from items iii and iv, these metals are expected to have higher dimensional electronic structures than 1D, because 1D metals are usually unstable at low temperatures and their carrier transport is very susceptible to disorders.[82] These novel properties of BEDO-TTF molecules have led to our successful improvement on the metallic nature of complexes in LB films[81] and reticulate-doped polymer composites,[83] both of which inevitably contain considerable structural defects and disorders. Chap. 5 will demonstrate the dimensionality of electronic band structures of BEDO-TTF complexes.

This chapter has also discussed the physical properties and electronic states of semiconducting BEDO-TTF complexes. In most cases, their semiconducting nature was accounted by the neutral, inhomogeneous charge-distributed, monovalent, or divalent ground state of BEDO-TTF molecules. Besides, too bulky substituents without delocalized π-electrons in the acceptors degrade the metallic conduction among the partially oxidized donor molecules, as discussed for the complex 13. On the other hand, only 37 remains unsettled

in its semiconducting behavior in spite of the partial CT ground state of BEDO–TTF molecules. The following chapters will also explore the crystal and electronic structures of the semiconducting BEDO–TTF complexes including this complex, for deeper understanding of the physical properties.

Table 3-1. Conducting Properties of BEDO-TTF Complexes and Redox Potentials of Their Counter Components

	complex[a]	$E_{1/2}^{1}$(A),[b] V vs SCE	conductivity σ_{rt},[c] S·cm^{-1}		$T_{\sigma max}$,[d] K	σ_{max}/σ_{rt}	Ea, eV
			DA-type$_2$Complexes				
1.	D_2(HCBD)	+0.72	1.0×10^{2}	(M)	13	5.9	
2.	D(F_4TCNQ)	+0.60	7.9×10^{-8}	(S)*			0.48
3.	$D_9(F_4TCNQ)_5(THF)_4$	+0.60	1.4x10	(M)	100	1.8	
4.	$D_5(DDQ)_3(CH_3CN)$	+0.56	4.7x10	(M)	15	4.0	
5.	$D_{11}(DBDQ)_7(CH_3CN)$	+0.54	$3.6\times10_{}$	(M)	72	2.2	
6.	$D_2(F_2TCNQ)$	+0.41	1.0×10^{2}	(M)	11	12	
7.	$D_4(FTCNQ)_2(CH_3CN)$	+0.32	6.5x10	(M)	5	19	
8.	D_2(TCNE)	+0.29	6.9x10	(M)	13	7.9	
9.	D_2(DTENF)	+0.23	1.8x10	(M)	94	1.8	
10.	D(TCNQ)	+0.22	8.1×10^{-2}	(S)			0.066
11.	D_2(DCNQ)	+0.21	1.1x10	(M)	48	5.3	
12.	$D_{10}(C_{10}TCNQ)_4(H_2O)$	+0.21	7.3	(M)	136	1.4	
13.	$D_9(C_{14}TCNQ)_4(H_2O)_2$	+0.21	9.9×10^{-1}	(S)			0.026 (90-200K)
14.	D_2(DHBTCNQ)	+0.18	1.1×10^{2}	(M)	13	5.2	
15.	D_2(THBTCNQ)	+0.16	3.3x10	(M)	18	3.6	
16.	$D_9(Me_2TCNQ)_5(CH_3CN)$	+0.15	$3.6\times10_{}$	(M)	18	4.5	
17.	$D_2(Et_2TCNQ)$	+0.15	1.4×10^{2}	(M)	9	4.9	
18.	$D_2[(MeO)_2TCNQ]$	+0.05	4.7x10	(M)	5**	15	
19.	$D_2(QCl_4)$	+0.05	7.6x10	(M)	16	8.1	
20.	$D_{11}(QF_4)_5(H_2O)_6$	+0.04	6.8x10	(M)	20	4.2	
21.	$D_9(QBr_4)_5(H_2O)$	+0.04	3.6x10	(M)	77	2.0	
22.	D_7(BTDA-TCNQ)$_4$	+0.03	6.1x10	(M)	164	1.1	
23.	$D_2(DTNF)(CH_3CN)$	+0.02	6.5x10	(M)	8	6.0	
24.	$D_2(H_xBRA)$	-0.12[1]	1.4×10^{2}	(M)	16	5.7	
25.	D_2(HCHA)	-0.13[1]	$(1\text{-}2)\times10^{2}$ (//c)	(M)+	1.3**		
			1.7×10^{2}	(M)	11	4.2	
26.	D(TENF)	-0.14	5.6×10^{-10}	(S)*			0.45
27.	D[Q(OH)$_2$]$_2$	-0.38[1]	10^{-7}	(S)*,+			0.35
28.	D(TNF)	-0.43	2.5×10^{-10}	(S)*			0.50
29.	D(TNBP)	-0.56[1]	3.5×10^{-8}	(S)*,+			0.35
30.	D(DNBP)	-0.98	4.5×10^{-10}	(S)*			0.47
			Radical Salts				
31.	$D_5(HCTMM)(PhCN)_2$	+0.96[2,3]	2.8x10 (//a+2c)	(M)+	5**	40	
			7.0x10 (//2a-c)	(M)+	5**	30	
			1.4×10^{2}	(M)	14	7.3	
32.	$D_4(HCTMM)(TCE)_2$	+0.96[2,3]	1.1×10^{2} (//c)	(M)+	235	1.1	
33.	$D_{10}(CF)_4(H_2O)_3$	+1.32[2,5]	1.1×10^{2} (//c)	(M)+	1.3**	19	
34.	$D_4(SQA)(H_2O)_6$		1.7×10^{2} (//c)	(M)+	1.4**	46	
35.	$D_6(PIC)_3(TCE)$	>1.4 [4]	2 $\times10^{2}$	(M)+	1.4**	49	
36.	$D_8(PCA)_4(H_2O)$	>1.4 [4]	3.3x10	(M)+	16	5.2	
37.	$D_5(HCP)(PhCN)_{0.2}$	+0.42[3]	1.8x10 (//c)	(S)+			0.10
		+1.21[4]	4.1×10^{-1} (//b)	(S)+			0.05
38a.	$D_2Cl(H_2O)_3$ (plate)		4×10^{2}	(M)+	1.4**	43	
38b.	$D_2Cl(H_2O)_3$ (needle)		8 x10	(M)+	1.3**	13	
39.	$D_2Br(H_2O)_3$		7 x10 (//c)	(M)+	4**	7	
40.	$D_2Br[MnBr_2(H_2O)_4](H_2O)$		200-300 (//c)	(M)+			
			40-160 (//a-c)	(M)+	1.5**	240	
41.	$D_{2.4}I_3$		3 x10 (//b)	(M)+	1.3**	105	
42.	D(I_3)		1 $\times10^{-6}$	(S)*			0.43
			Dication$_9$Salts				
43.	$D(I_3)_2$		$< 10^{-9}$	(S)*,+			
44.	$D(I_5)_2$		8 $\times10^{-7}$	(S)*,+			

[a] D = BEDO-TTF. [b] First half-wave reduction potential, 1) irreversible (cathodic peak potential), 2) irreversible (anodic peak potential), 3) TBA salt (X^{2-}/X^{-}), 4) TBA salt (X^{-}/X), 5) K salt (X^{-}/X) [c] (M), metal; (S), semiconductor; rt, room temperature (285 K); (+), measured on single crystal (otherwise, on compressed pellet); (*), 2 probe. [d] (**) Lowest temperature we measured.

Table 3-2. Optical Properties of BEDO-TTF and Its Complexes

complex[a]	vibrational spectra,[b] cm^{-1}		electronic spectra,[b] $10^3 cm^{-1}$		average charge[d] on BEDO-TTF, γ
	$b_{1u}\nu_{31}$[c]	ν_{CN}	$h\nu_{CT}$	UV-vis	
BEDO-TTF	1015.4			20, 26*, 29*, 32	0.00
DA-type complexes					
1. $D_2(HCBD)$	1004.0	2220, 2188, 2170	2.6	14, 16*, 22, 30*	0.50
2. $D(F_4TCNQ)$	1000.2	2195, 2170	6.7*	9, 3*, 12, 13, 20*, 26	1.0
3. $D_9(F_4TCNQ)_5(THF)_4$	1005.7	2198, 2177	1.8	8*, 11, 13*, 14*, 26	0.56
4. $D_5(DDQ)_3(CH_3CN)$	1002.3	2215	2.0	12, 20, 31*	0.60
5. $D_{11}(DBDQ)_7(CH_3CN)$	1001.9	2216	2.0	12, 19	0.64
6. $D_2(F_2TCNQ)$	1006	2194, 2172	2.5	7, 12*, 14, 25, 27	
7. $D_4(FTCNQ)_2(CH_3CN)$	1004	2188	2.9	12, 13, 16, 27	
8. $D_2(TCNE)$	1003	2144	2.0	13, 32	
9. $D_2(DTENF)$	1006	2183*, 2158	2.4	8*, 12, 17, 32*	
10. D(TCNQ)	1011.0	2201*, 2194, 2179	4.5	10, 12*, 16*, 20, 28	**
	1003.3	2160			
11. $D_2(DCNQ)$	1002	2193	3.0	13, 20, 32*	
12. $D_{10}(C_{10}TCNQ)_4(H_2O)$	1006	2178	2.5	12, 13, 16, 28	
13. $D_9(C_{14}TCNQ)_4(H_2O)_2$	1005	2176, 2159	4.0	12, 13, 15*, 27	
14. $D_2(DHBTCNQ)$	1007	2172	2.2	12, 13, 16*, 29	
15. $D_2(THBTCNQ)$	1007	2158	2.0	12, 13, 17, 29	
16. $D_9(Me_2TCNQ)_5(CH_3CN)$	1007	2188	2.4	12, 13*, 17, 27	
17. $D_2(Et_2TCNQ)$	1006	2183	2.0	12*, 13*, 17, 26	
18. $D_2[(MeO)_2TCNQ]$	1008	2188	2.5	12*, 14, 17, 26, 30*	
19. $D_2(QCl_4)$	1006		3.5	13, 24, 34	
20. $D_{11}(QF_4)_5(H_2O)_6$	1006		2.2	12, 32	
21. $D_9(QBr_4)_5(H_2O)$	1006		3.5	14, 23, 33	
22. $D_7(BTDA\text{-}TCNQ)_4$	1006	2191	2.5	9, 13, 16*, 22*, 32	
23. $D_2(DTNF)(CH_3CN)$	1007	2179	1.8	8*, 13, 32	
24. $D_2(H_xBRA)$	1003		2.1	13, 20*, 32	
25. $D_2(HCHA)$	1003		2.5	12, 18*, 31	0.5
26. D(TENF)	1010		7.4*	12, 19	
27. $D[Q(OH)_2]_2$	1010		8*	11, 18, 35	
28. D(TNF)	1014		10.3	13, 19*, 35	
29. D(TNBP)	1012		15*	19*, 38	
30. D(DNBP)	1012		14*	17, 32	
Radical salts					
31. $D_5(HCTMM)(PhCN)_2$	1006.2	2229, 2176, 2162	2.2	13, 29	0.40
32. $D_4(HCTMM)(TCE)_2$	1004.0	2189, 2177, 2163*	2.3	13, 30	0.50
33. $D_{10}(CF)_4(H_2O)_3$	1005.2	2158	2.5	12, 28*, 32	0.40
34. $D_4(SQA)(H_2O)_6$	1006.2		2.1	13	0.50
35. $D_6(PIC)_3(TCE)$	1001.4		3.0	13, 23*, 27	0.50
36. $D_8(PCA)_4(H_2O)$	1003.8	2198	3.0	13, 26	0.50
37. $D_5(HCP)(PhCN)_{0.2}$	1006.0	2185,2165	3.0	12, 31	0.40
38a. $D_2Cl(H_2O)_3$ (plate)	1003		2.1	13, 20*, 32	0.50
38b. $D_2Cl(H_2O)_3$ (needle)	1004		2.2	12, 20*, 32	0.50
39. $D_2Br(H_2O)_3$	1003		2.2	13, 20*, 31	0.50
40. $D_2Br[MnBr_2(H_2O)_4](H_2O)$	1003		1.9	12, 20*, 32	0.50
41. $D_{2.4}I_3$	1005.2		2.2	12*, 20, 24*, 32	0.42
42. $D(I_3)$	1007.4#		7.3*, 9.4	13, 27, 33	1.0
Dication Salts					
43. $D(I_3)_2$	1002.6			14, 27, 35	2.0
44. $D(I_5)_2$	994.6			13, 25, 35	2.0

[a] D = BEDO-TTF. [b] On KBr disk; (*) shoulder. [c] The results on the higher resolution (0.5 cm^{-1}) measurements are represented by larger fingers than the usual ones (4 cm^{-1}). (#) $a_g\nu_7$ mode activated by strongly dimerized donor molecule. [d] Determined from the charge on the counter component and stoichiometry; (**) charge separation (see text).

Table 3–3. Principal values and direction cosines of g tensor.

	a	b^*	c'
g_1 = 2.0132	-0.24	0.97	0.01
g_2 = 2.0051	0.92	0.23	0.30
g_3 = 2.0005	-0.29	-0.08	0.95
$\bar{g}$ = 2.0063			
BEDO-TTF			
long axis	-0.28	0.96	0.05
short axis	0.92	0.26	0.29
normal to plane	-0.27	-0.12	0.96

$\bar{g} = (g_1 + g_2 + g_3)/3$

Table 3–4. Magnetic Properties of BEDO–TTF Complexes

complex[a]		χ_s(rt)[b]	Curie component C	REHAC parameter C'	a	estimated concentration of defects, % per donor
$D_5(DDQ)_3(CH_3CN)$	(4)	1.8 ±0.3	5.2×10^{-3}			1.4
$D_{10}(C_{10}TCNQ)_4(H_2O)$	(12)	2.1 ±0.2		1.3×10^{-2}	0.88	3.5
$D_9(C_{14}TCNQ)_4(H_2O)_2$	(13)	2.1 ±0.3		1.2×10^{-2}	0.82	3.2
D_2(THBTCNQ)	(15)	1.7 ±0.3	2.8×10^{-3}			0.75
$D_2(Et_2TCNQ)$	(16)	1.5 ±0.1	9.5×10^{-5}			0.03
$D_2[(MeO)_2TCNQ]$	(18)	3.4 ±0.2	1.1×10^{-3}			0.29
$D_2(QCl_4)$	(19)	2.0 ±0.2	3.8×10^{-3}			1.0
$D_2(DTNF)(CH_3CN)$	(23)	2.1 ±0.3		9.9×10^{-3}	0.88	2.6
D_2(HCHA)	(25)	2.3 ±0.2	7.7×10^{-5}			0.02
$D_5(HCTMM)(PhCN)_2$	(31)	2.2 ±0.2				0
$D_2Br[MnBr_2(H_2O)](H_2O)$	(40)	130	***			

[a] D = BEDO-TTF

[b] Spin susceptibility at room temperature; unit, 10^{-4}emu·(mol of donor molecule)$^{-1}$

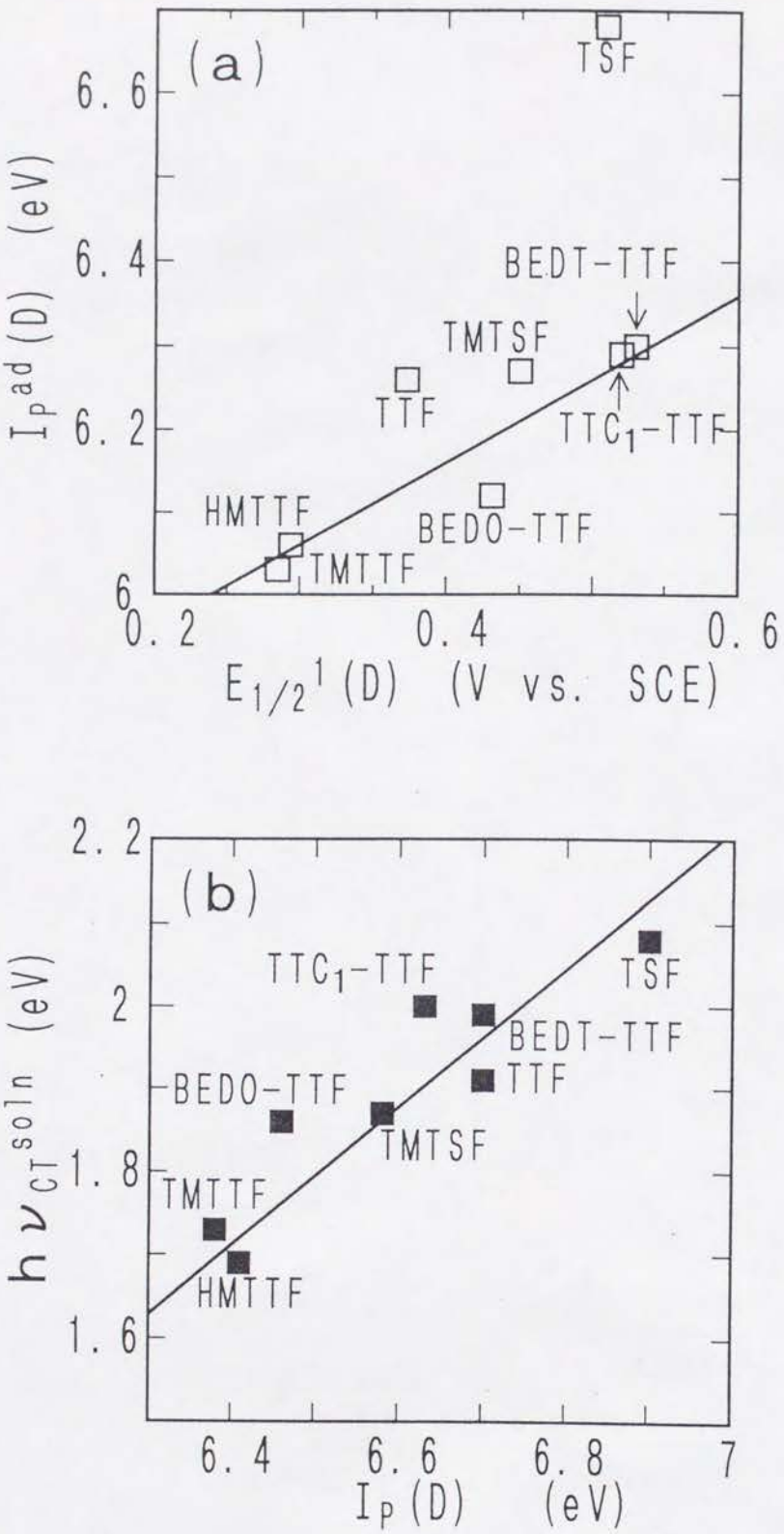

Figure 3-1. (a) Correlation between the adiabatic ionization potential ($I_p^{ad}(D)$)[39,40] and the first oxidation potential ($E_{1/2}^{1}(D)$) for the TTF derivatives. The solid line represents Eq(3.1). (b) Correlation between the CT transition energy of the *s*-trinitrobenzene complexes in chloroform ($h\nu_{CT}^{soln}$) and the first vertical ionization potential ($I_p(D)$)[39,40] of the TTF derivatives. The solid line is the least squares fit (Eq(3.3)).

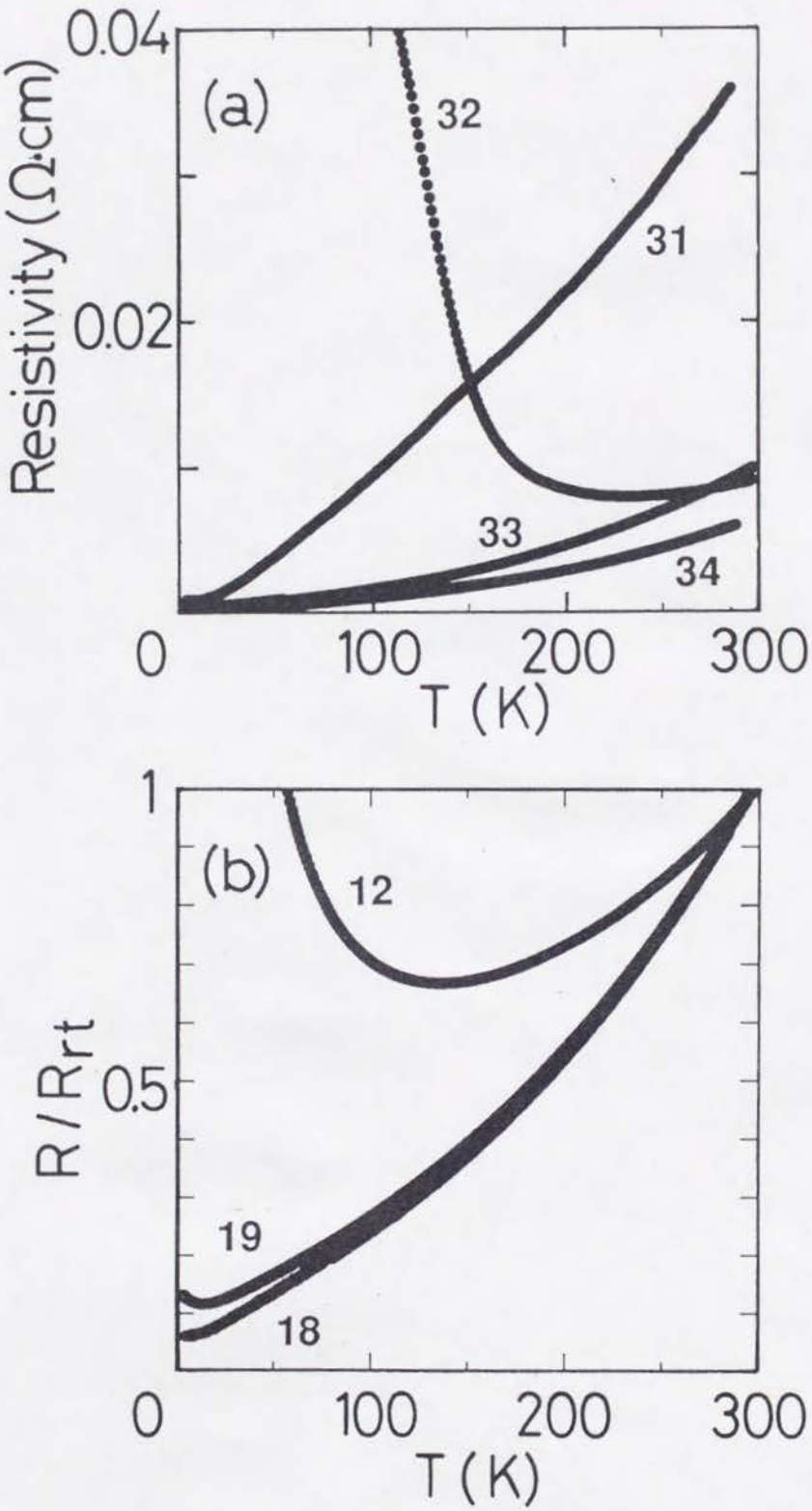

Figure 3-2. Temperature dependence of the resistivity. (a) On single crystals for $(BEDO\text{-}TTF)_5(HCTMM)(PhCN)_2$ (31) (*//a*+2*c*), $(BEDO\text{-}TTF)_4(HCTMM)(TCE)_2$ (32), $(BEDO\text{-}TTF)_{10}(CF)_4(H_2O)_3$ (33) (*//c*), and $(BEDO\text{-}TTF)_4(SQA)(H_2O)_6$ (34) (*//c*). (b) On the compressed pellets for $(BEDO\text{-}TTF)_{10}(C_{10}TCNQ)_4(H_2O)$ (12), $(BEDO\text{-}TTF)_2[(MeO)_2TCNQ]$ (18), and $(BEDO\text{-}TTF)_2(QCl_4)$ (19).

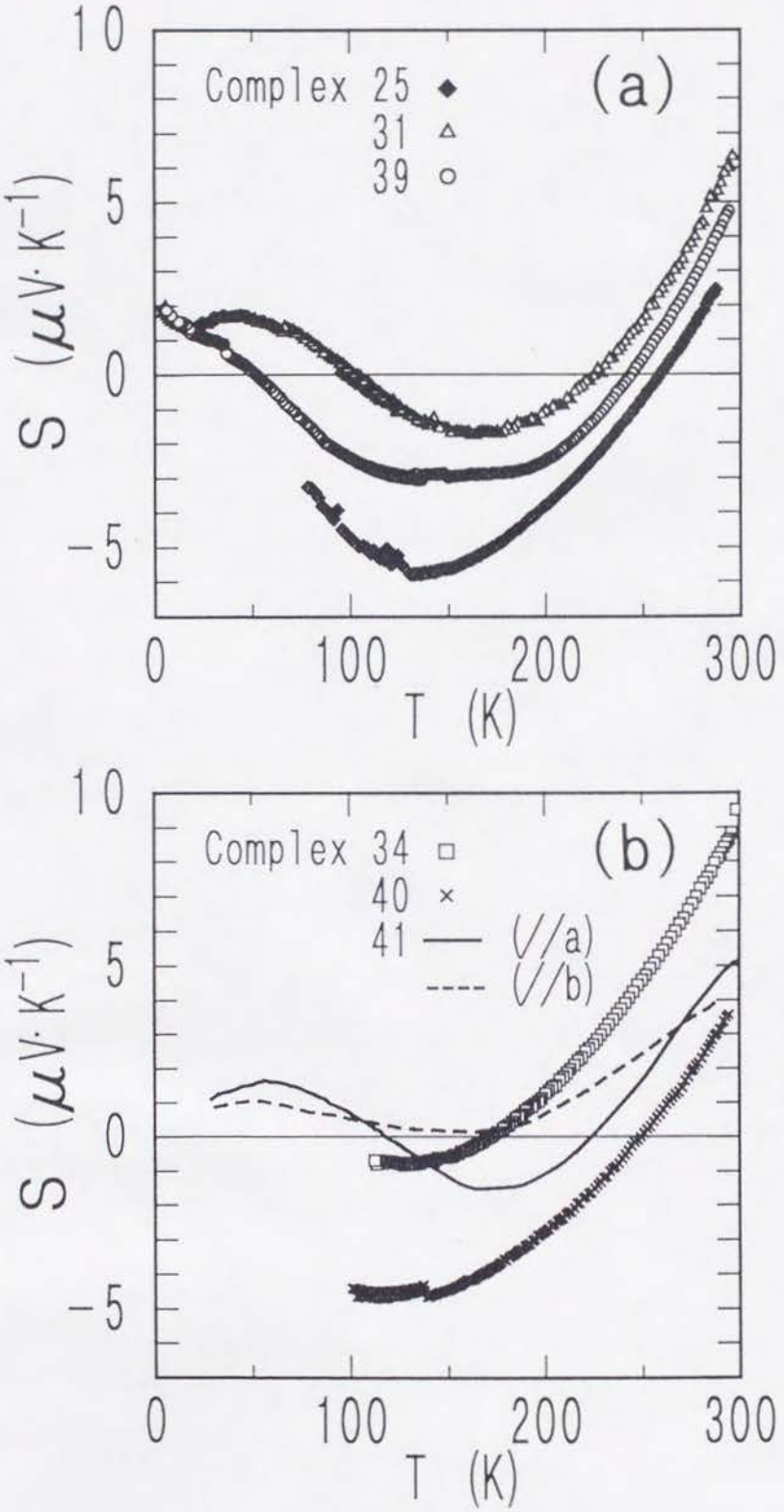

Figure 3-3. Temperature dependent thermoelectric power (S) of (a) (BEDO-TTF)$_2$(HCHA) (25, //c, filled squares), (BEDO-TTF)$_5$(HCTMM)(PhCN)$_2$ (31, open triangles), (BEDO-TTF)$_2$Br(H_2O)$_3$ (39, //c, open circles), (b) (BEDO-TTF)$_4$(SQA)(H_2O)$_4$ (34, //c, open squares), (BEDO-TTF)$_2$Br[$MnBr_2$(H_2O)$_4$](H_2O) (40, //c, cross), and (BEDO-TTF)$_{2.4}I_3$ (41, solid line for //a, dotted line for //b, taken from ref.25b).

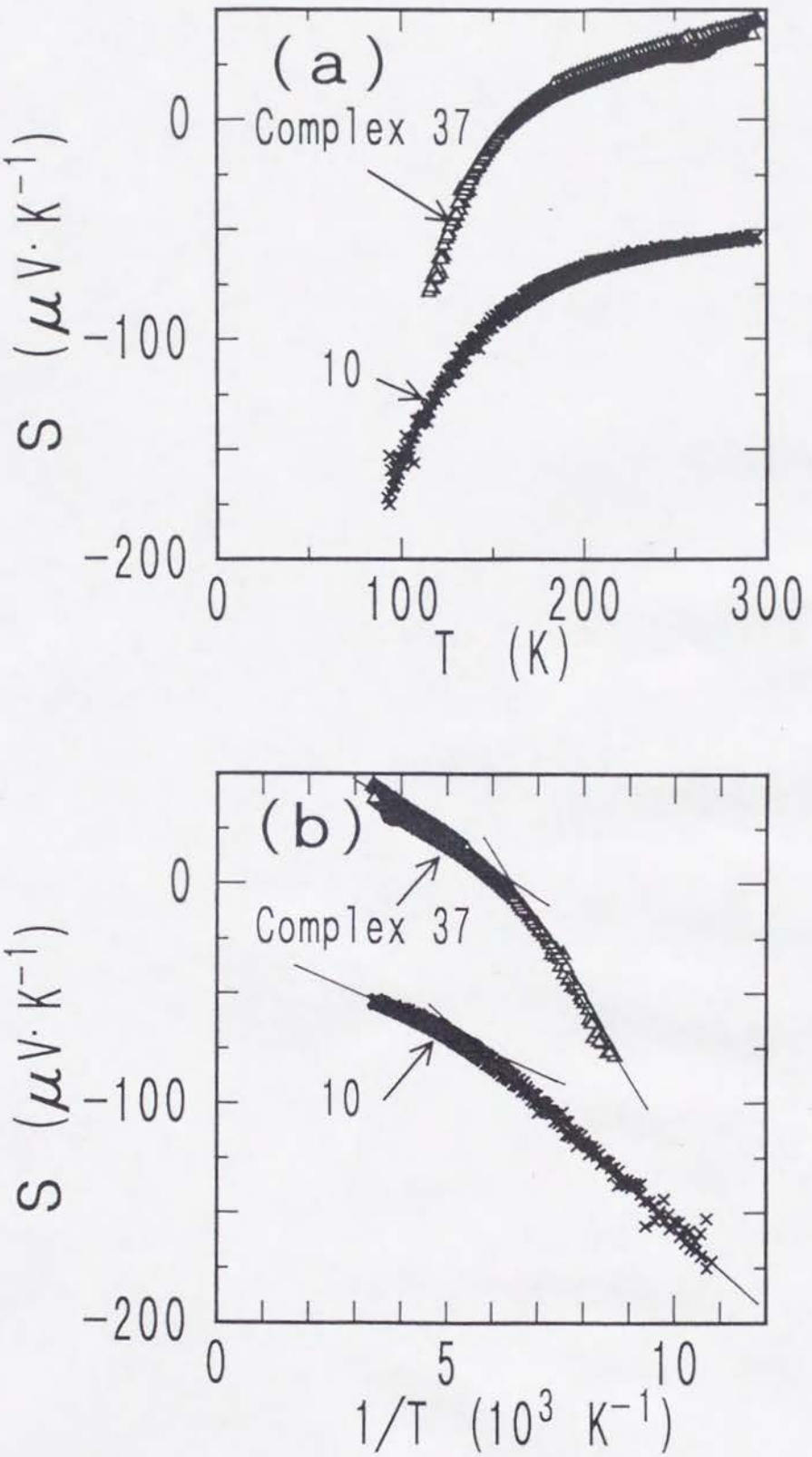

Figure 3-4. Thermoelectric power (S) of (BEDO-TTF)(TCNQ) (10, compressed pellet, crosses) and $(BEDO\text{-}TTF)_5(HCP)(PhCN)_{0.2}$ (37, //c, open triangles) plotted as a function of temperature (a) and reciprocal temperature (b).

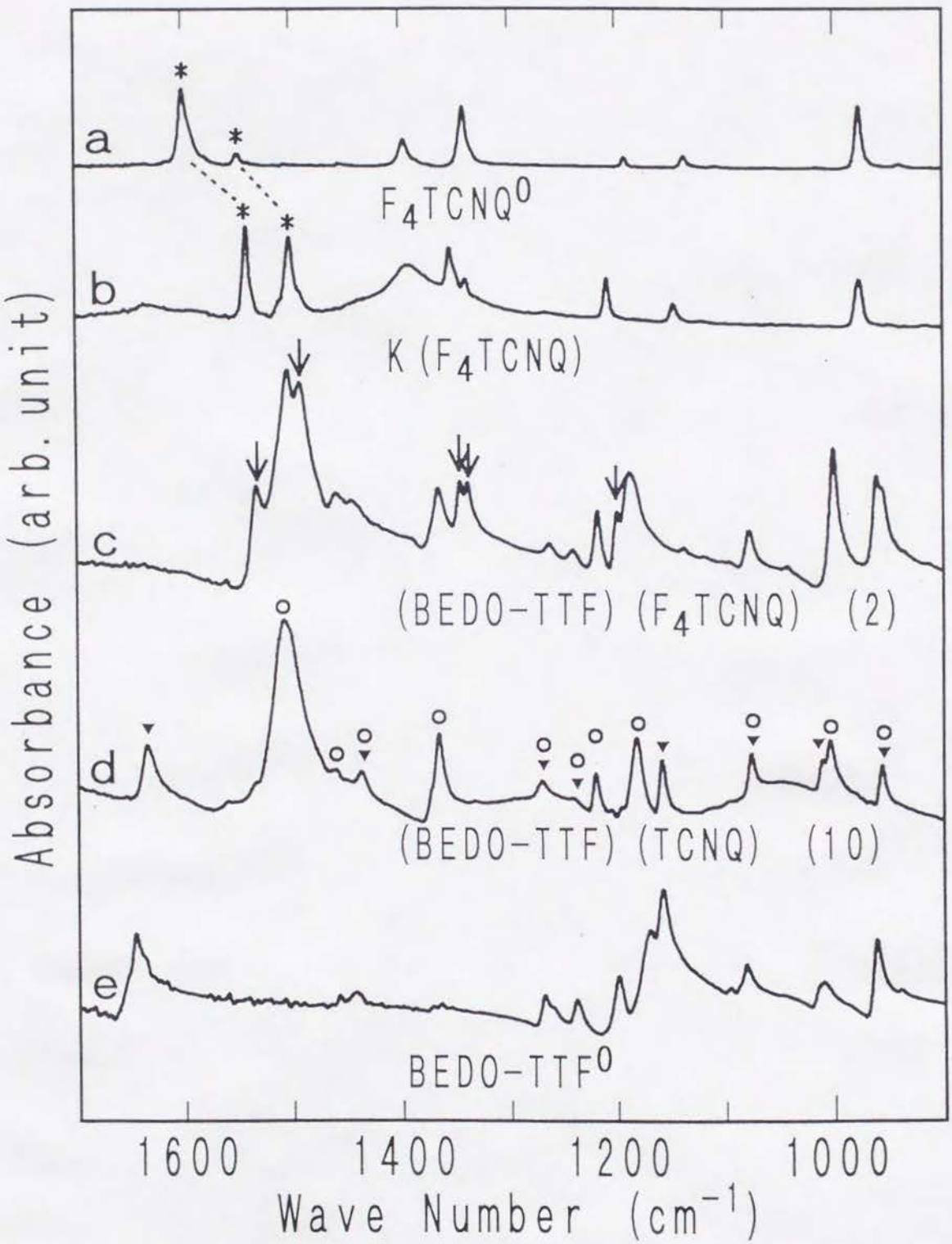

Figure 3-5. IR spectra of (a) neutral F_4TCNQ, (b) K(F_4TCNQ), (c) (BEDO-TTF)(F_4TCNQ) (2), (d) (BEDO-TTF)(TCNQ) (10), and (e) neutral BEDO-TTF on KBr pellet. Vibrational bands of F_4TCNQ^- are represented by arrows for complex 2. Vibrational bands designated by open circles and filled triangles are ascribed to those of ionized and neutral BEDO-TTF molecules, respectively.

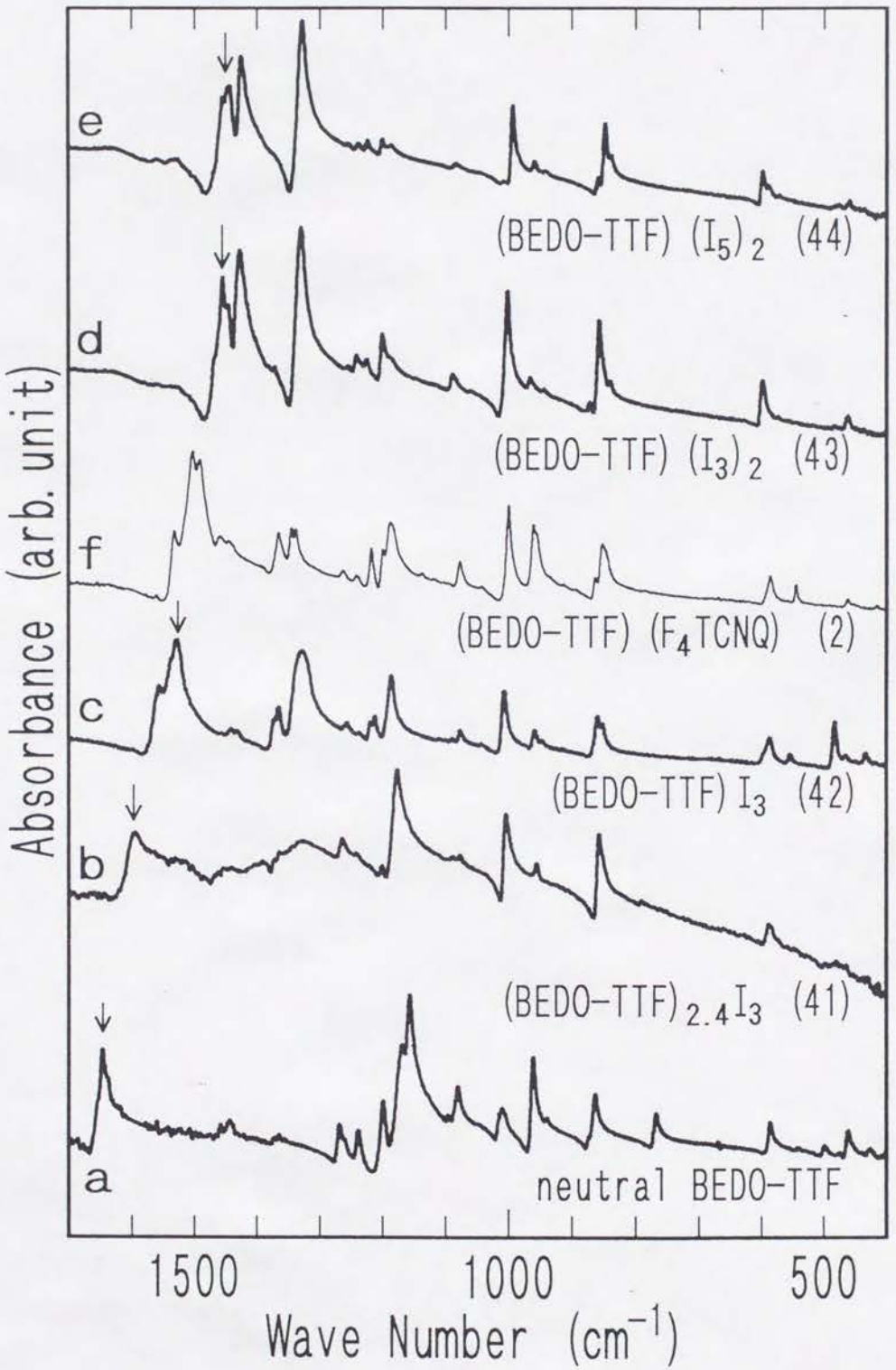

Figure 3-6. IR spectra of (a) neutral BEDO-TTF, (b) $(BEDO\text{-}TTF)_{2.4}I_3$ (41), (c) $(BEDO\text{-}TTF)I_3$ (42), (d) $(BEDO\text{-}TTF)(I_3)_2$ (43), and (e) $(BEDO\text{-}TTF)(I_5)_2$ (44) on KBr pellet. Spectra of the complex 2 is shown by the dotted curve (f). Vibrational bands designated by arrows are ascribed to those of C=C stretching mode.

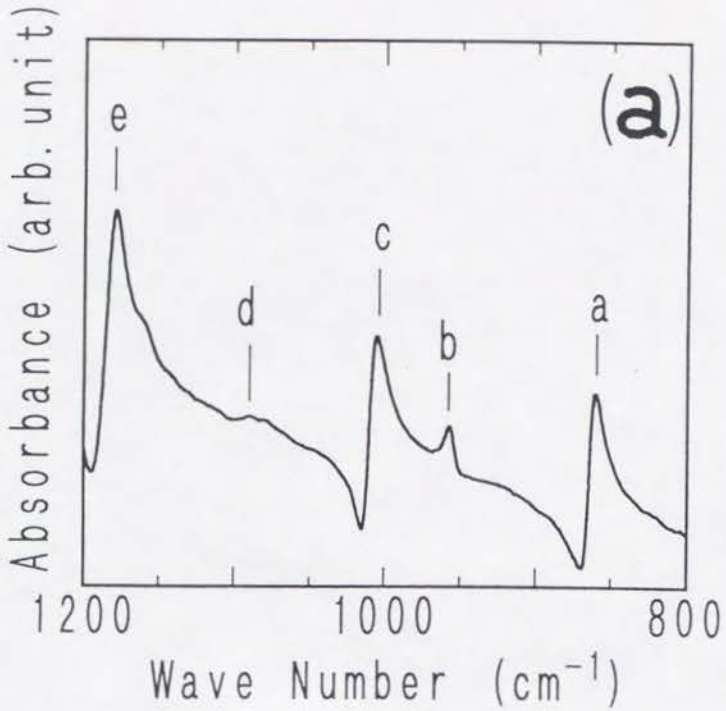

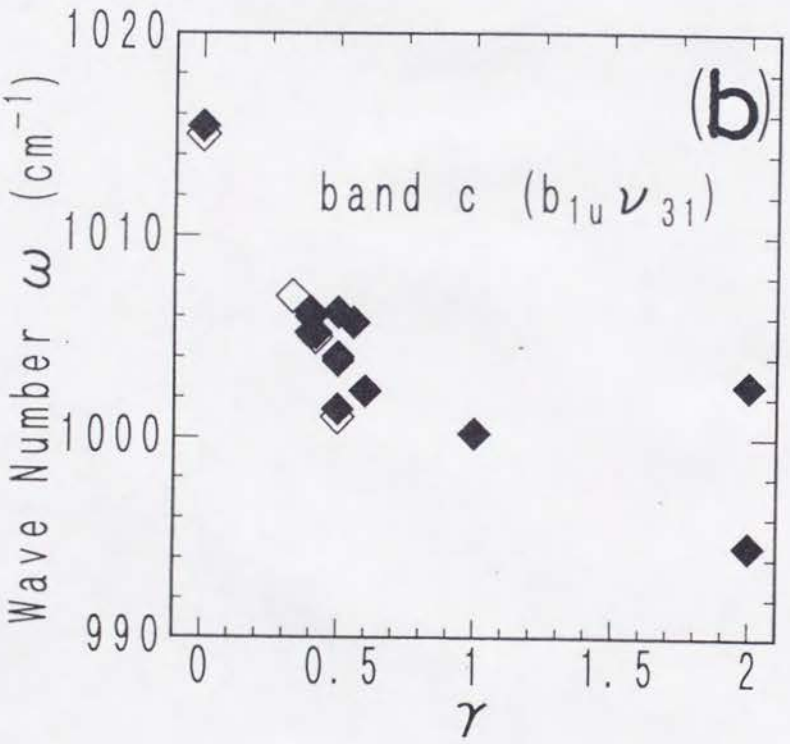

Figure 3-7. (a) IR spectra of $(BEDO\text{-}TTF)_5(HCTMM)(PhCN)_2$ (31) in the KBr disk. See text for the assignment of a-e. (b) Dependence of the frequency (ω) of $b_{1u}\nu_{31}$ mode on the average charge on the donor, γ. The results of this work are represented by filled squares for neutral BEDO-TTF and its CT complexes of known γ (1-5, 31-37, 43, 44). Open squares represent the reported data for neutral BEDO-TTF [55] and its radical salts[54] with $Cu_2(NCS)_3^-$ (γ = 0.33), I_3^- (0.42, complex 41) and ReO_4^- (0.50).

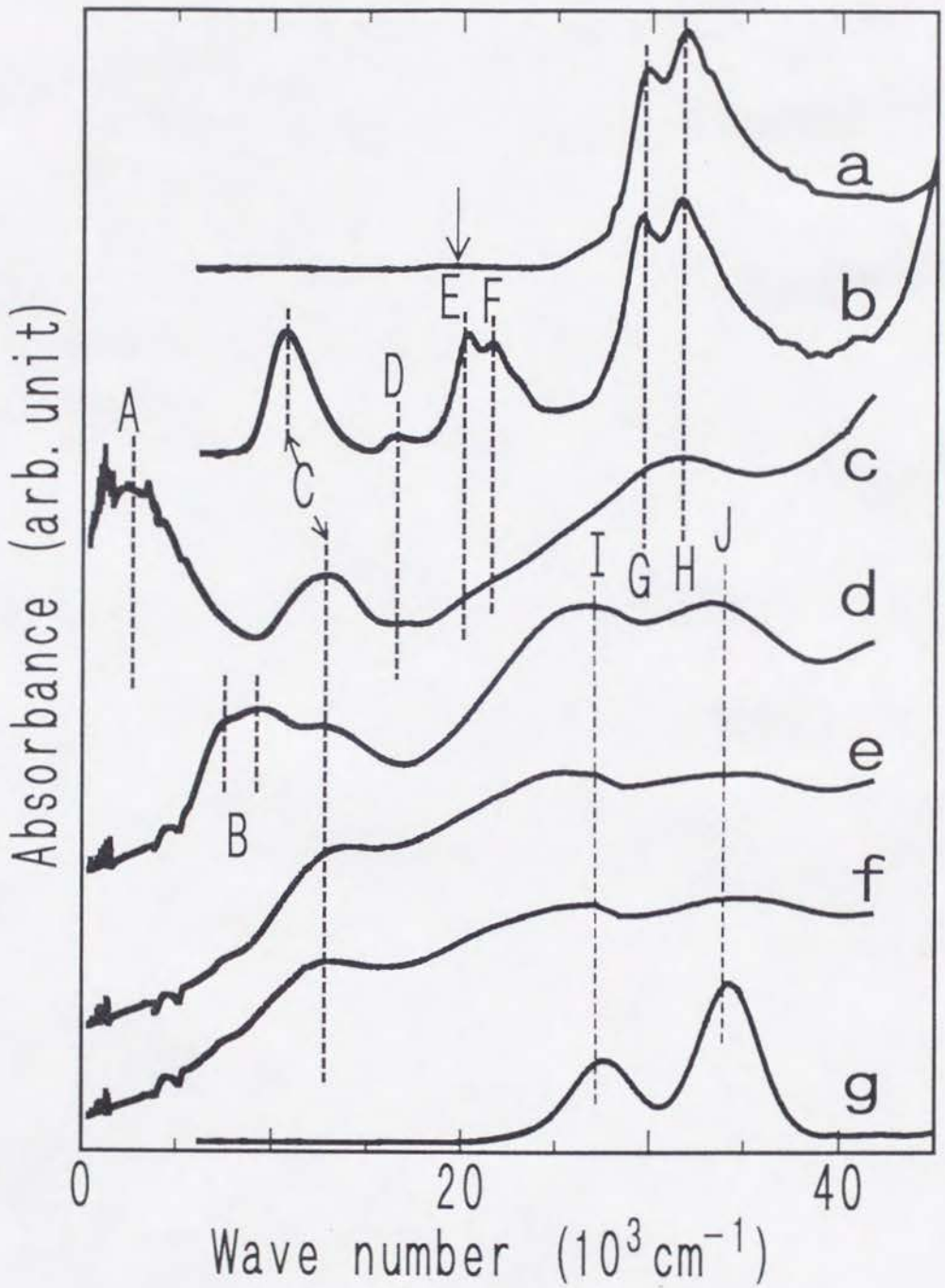

Figure 3-8. Optical absorption spectra of (a) neutral BEDO-TTF in CH_3CN solution, (b) $(BEDO\text{-}TTF)_2Br(H_2O)_3$ (39) in CH_3CN solution, (c) 39 on KBr pellet, (d) $(BEDO\text{-}TTF)I_3$ (42) on KBr pellet, (e) $(BEDO\text{-}TTF)(I_3)_2$ (43) on KBr pellet, (f) $(BEDO\text{-}TTF)(I_5)_2$ (44) on KBr pellet, and (g) $(TBA)I_3$ in CH_3CN solution. The arrow in curve a indicates the weak absorption at 19.5×10^3 cm^{-1}. See text for assignment of A-J.

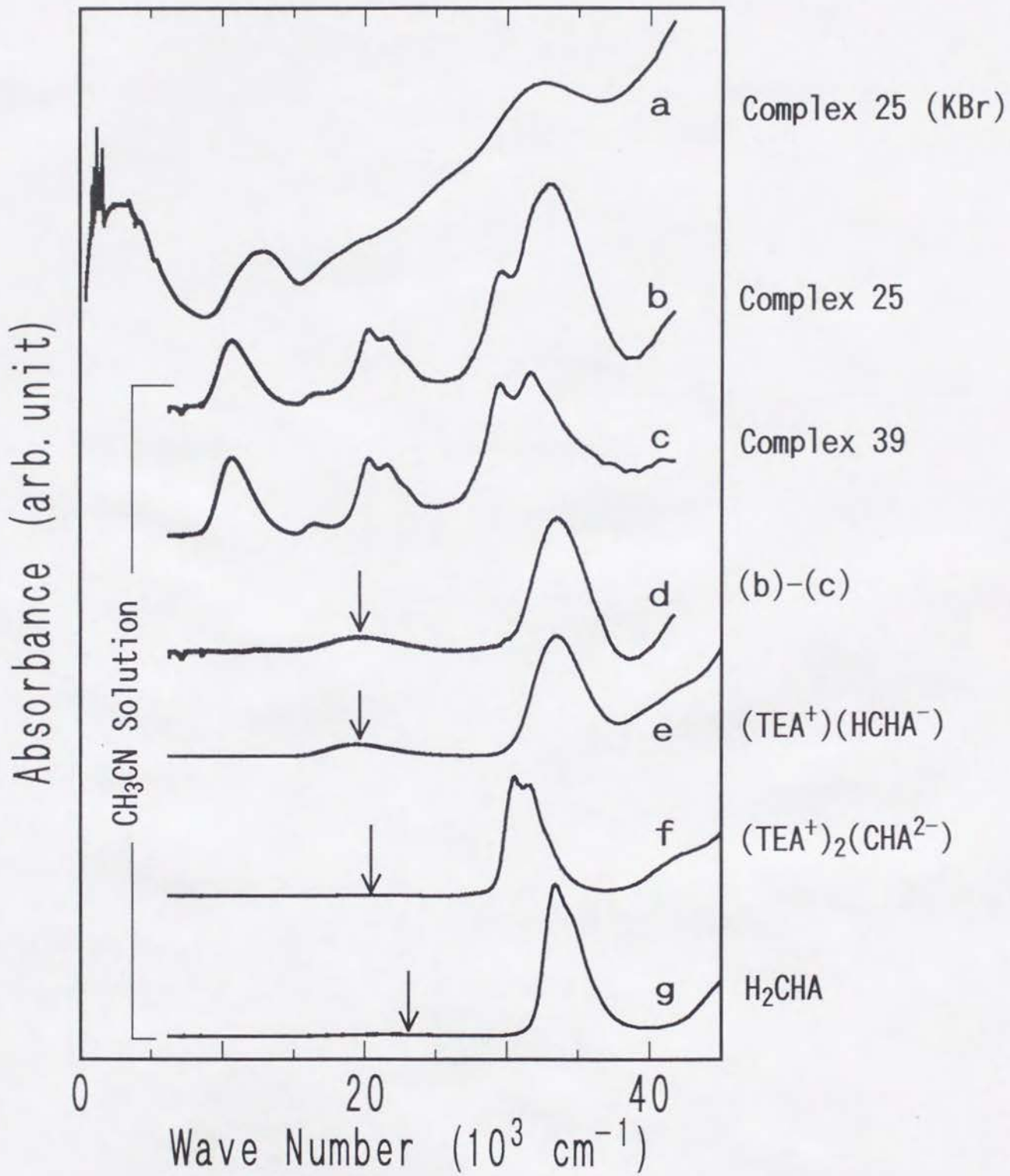

Figure 3-9. Optical absorption spectra. On a KBr pellet of $(BEDO\text{-}TTF)_2(HCHA)$ (25) (a). Solution spectra of 25 (b), $(BEDO\text{-}TTF)_2Br(H_2O)_3$ (39) (c), differenece between 25 and 39 (d), (TEA)(HCHA) (e), $(TEA)_2CHA$ (f), and H_2CHA in CH_3CN (g). Arrows indicate the peak positions of the lowest electronic absorption bands.

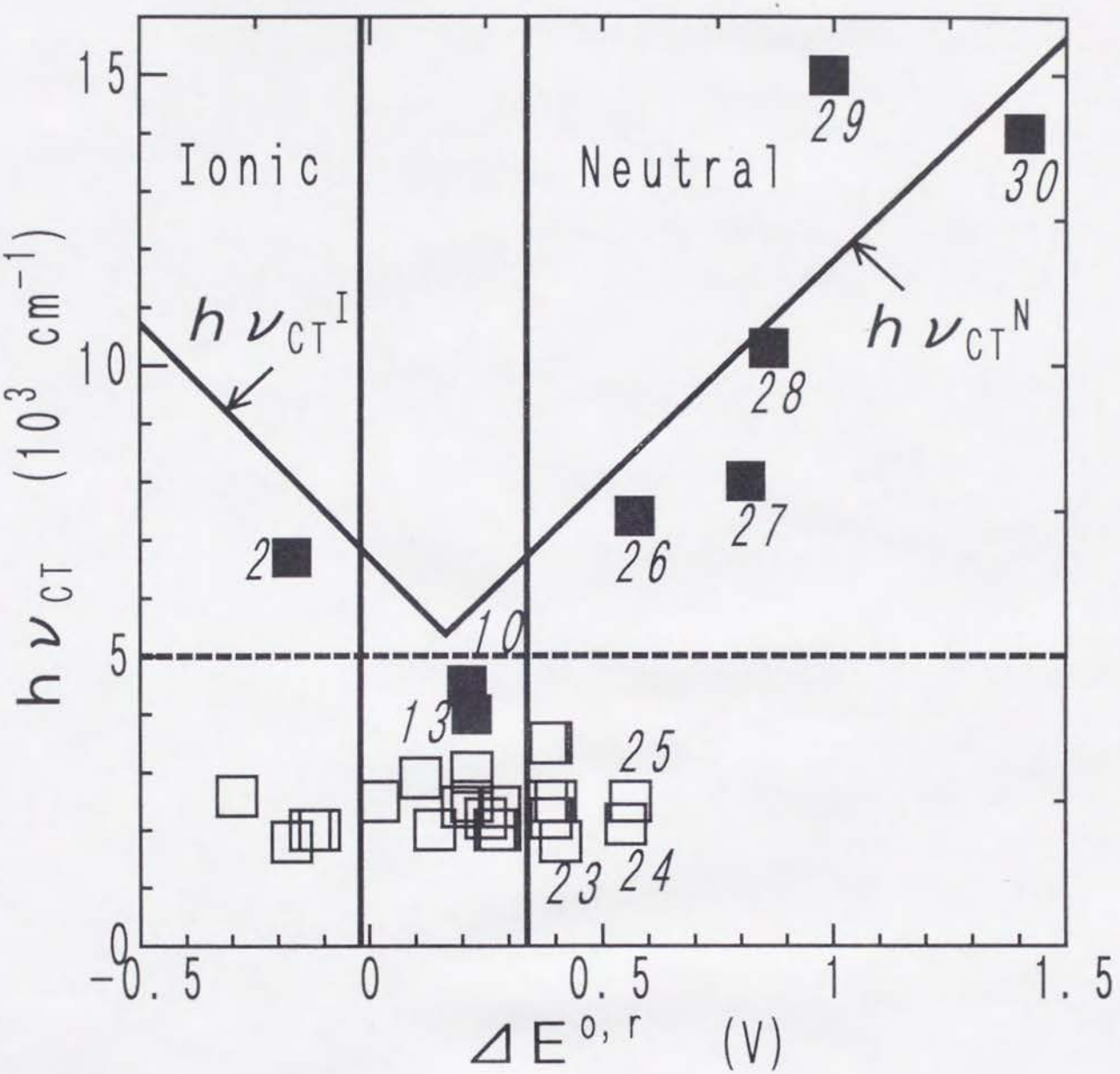

Figure 3-10. Comparison of CT bands of BEDO-TTF complexes of DA-type on KBr pellet ($h\nu_{CT}$) and $\Delta E^{o,r}$ (= $E_{1/2}{}^{1}$(D) - $E_{1/2}{}^{1}$(A)). Semiconducting and metallic complexes are represented by filled and open squares, respectively. For the V-shaped, vertical, and horizontal dotted lines, see text. Numbers represent the entry numbers of the complexes.

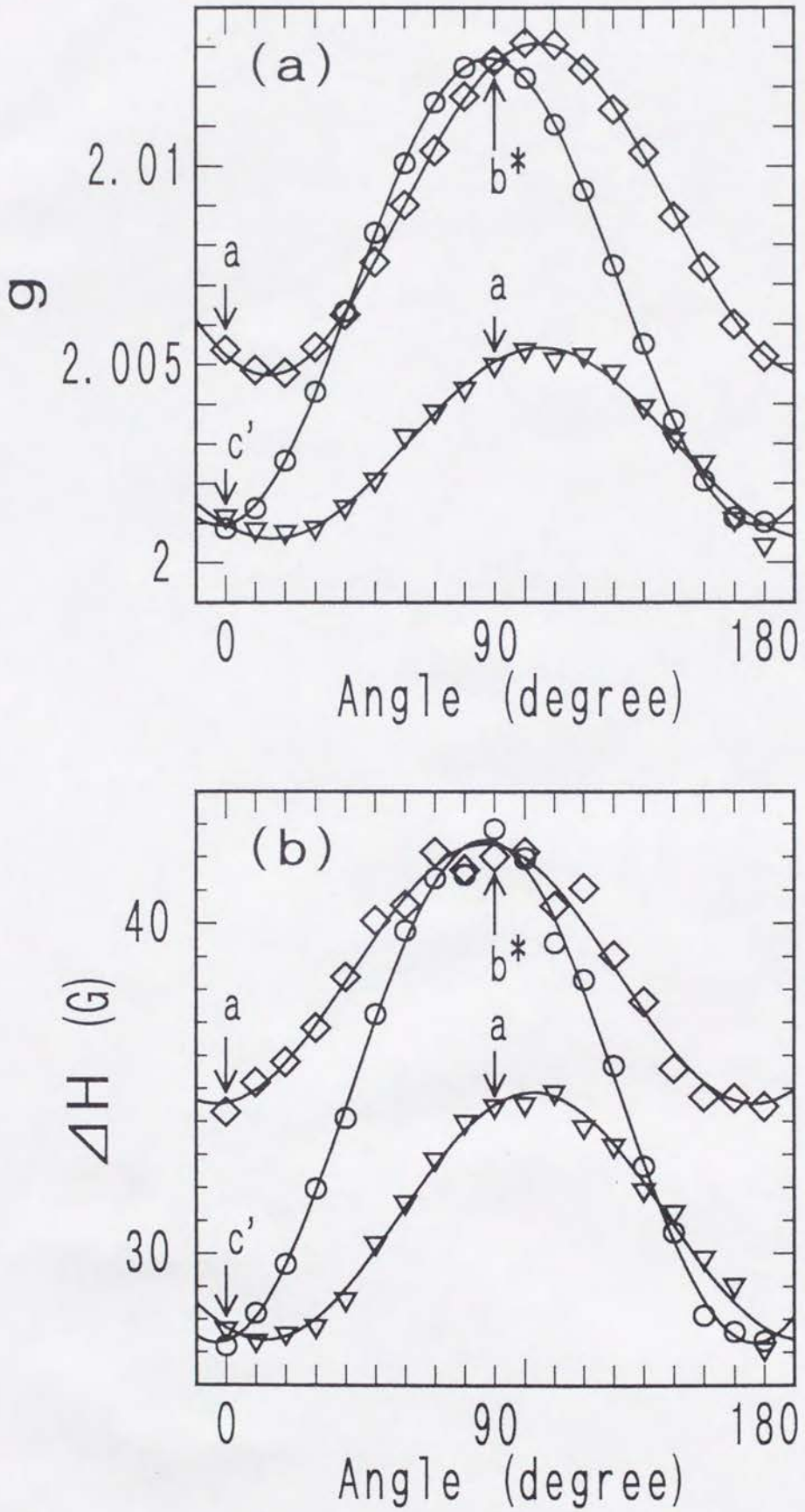

Figure 3-11. Angular dependence of the (a) g value and (b) peak-to-peak linewidth ΔH for $(BEDO\text{-}TTF)_5(HCTMM)(PhCN)_2$ (31) crystal; open squares, circles, and triangles represent the data obtained at room temperature by rotations of field in the a-b^*, c'-b^*, and c'-a planes, respectively. Solid curves are least squares fits (eqs 3.8, 3.9).

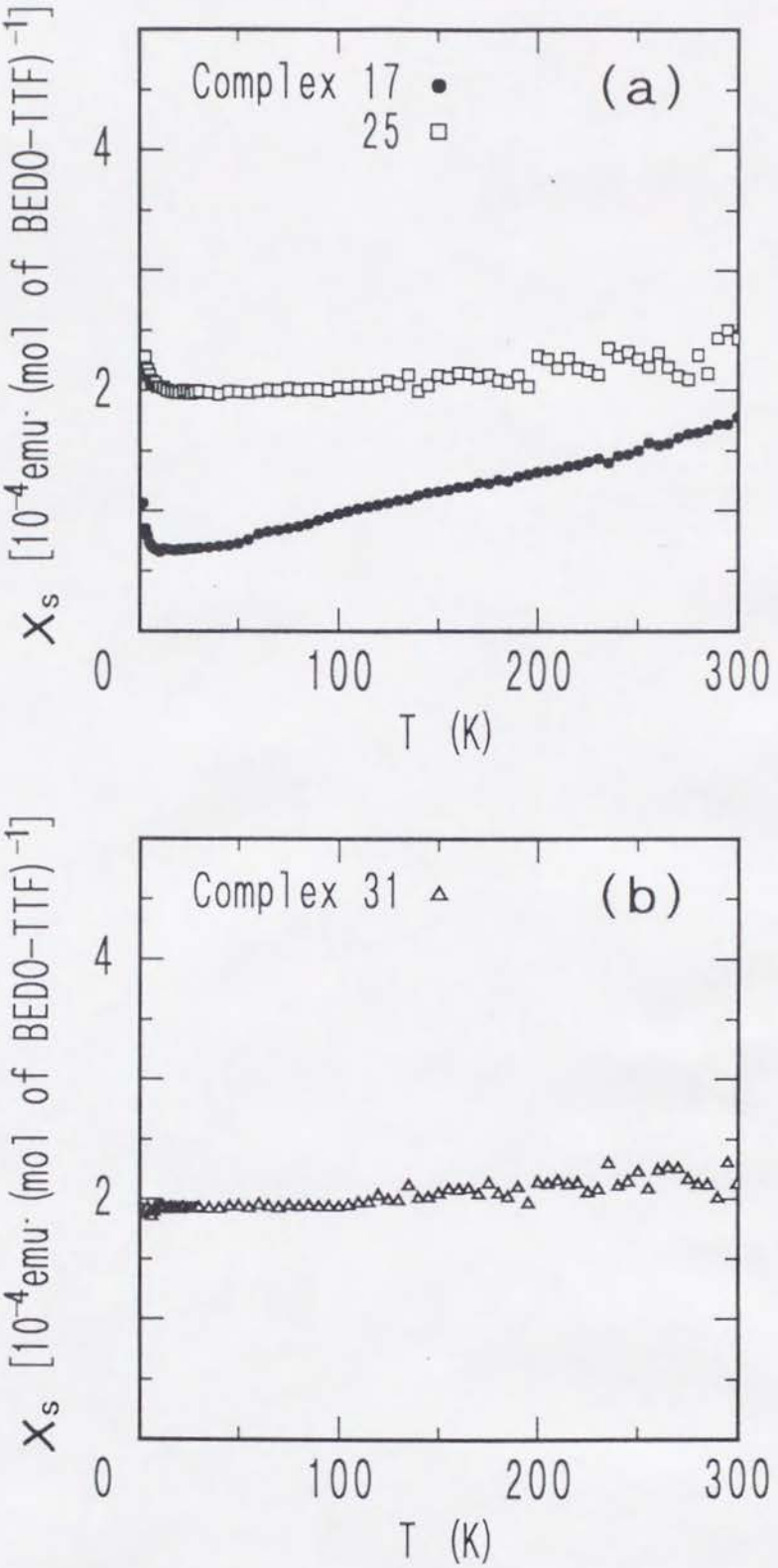

Figure 3-12. Temperature dependent spin susceptibility (χ_s) of the metallic (a) (BEDO-TTF)$_2$(Et_2TCNQ) (17) (filled circle), (BEDO-TTF)$_2$(HCHA) (25) (open square), and (b) (BEDO-TTF)$_5$(HCTMM)(PhCN)$_2$ (31) (filled triangle).

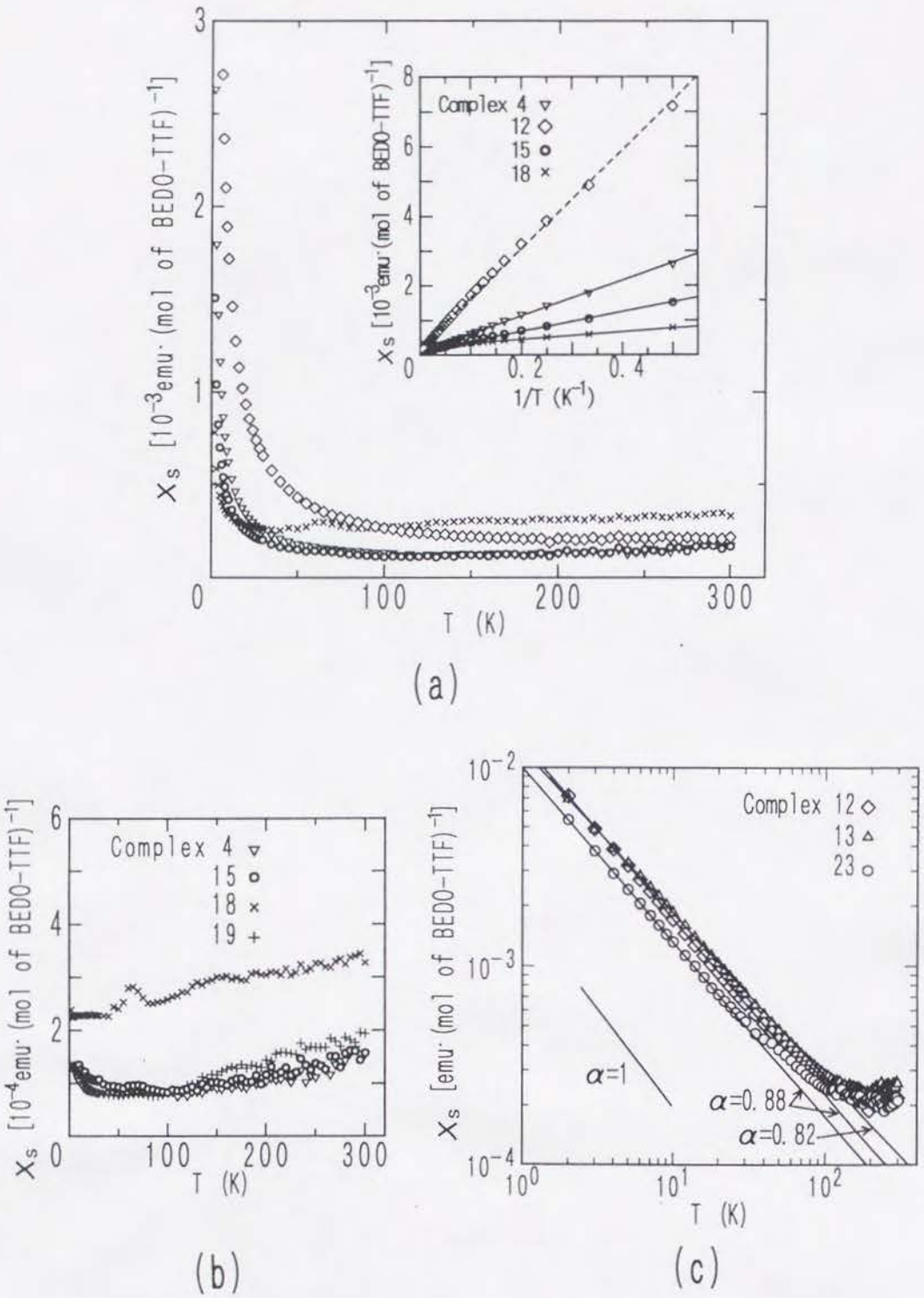

Figure 3-13. (a) Temperature dependent spin susceptibility (χ_s) of the metallic $(BEDO\text{-}TTF)_5(DDQ)_3(CH_3CN)$ (4, open triangle), $(BEDO\text{-}TTF)_{10}(C_{10}TCNQ)_4(H_2O)$ (12, open square), $(BEDO\text{-}TTF)_2(THBTCNQ)$ (15, open circle), and $(BEDO\text{-}TTF)_2[(MeO)_2TCNQ]$ (18, cross). The inset depicts the χ_s vs $1/T$ plot. Solid and dotted lines are least squares fit to Curie law for the data below 50 K. (b) Spin susceptibility of 4 (open triangle), 15 (open circle), 18 (cross), and $(BEDO\text{-}TTF)_2(QCl_4)$ (19, plus) obtained by subtracting the Curie paramagnetism. (c) Log-log plot of temperature dependent spin susceptibility of 12 (open square), $(BEDO\text{-}TTF)_9(C_{14}TCNQ)_4(H_2O)_2$ (13, open triangles), and $(BEDO\text{-}TTF)_2(DTNF)(CH_3CN)$ (23, open circle). Solid lines are least squares fit to the $C''T^{-\alpha}$ law for the data below 20 K.

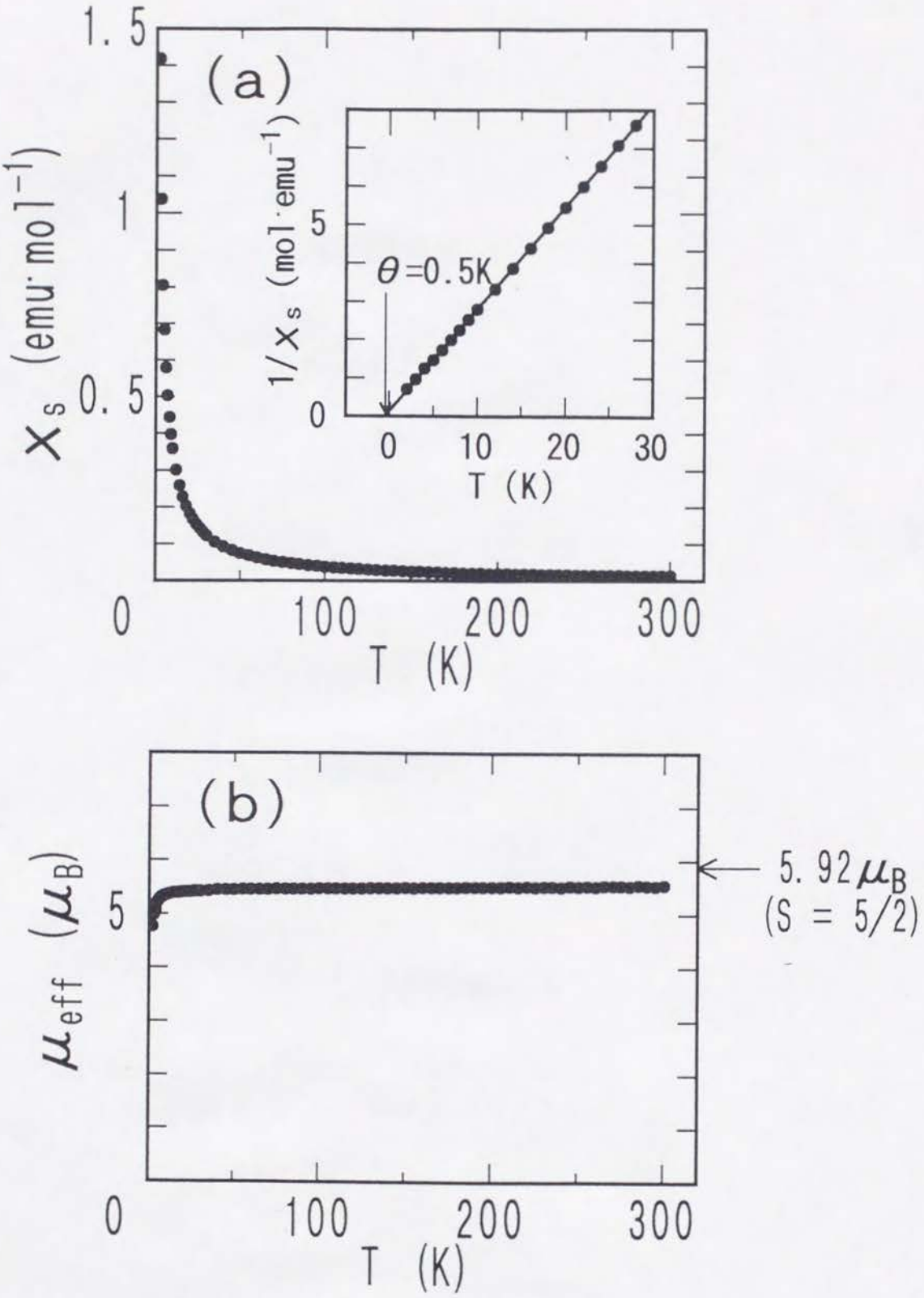

Figure 3-14. (a) Temperature dependent spin susceptibility (χ_s) of (BEDO-TTF)$_2$Br[MnBr$_2$(H$_2$O)$_4$](H$_2$O) (40). The inset depicts the reciprocal spin susceptibility ($1/\chi_s$) as a function of temperature. The solid line is a least squares fit to the Curie-Weiss law. (b) Temperature dependence of the effective moment (μ_{eff}).

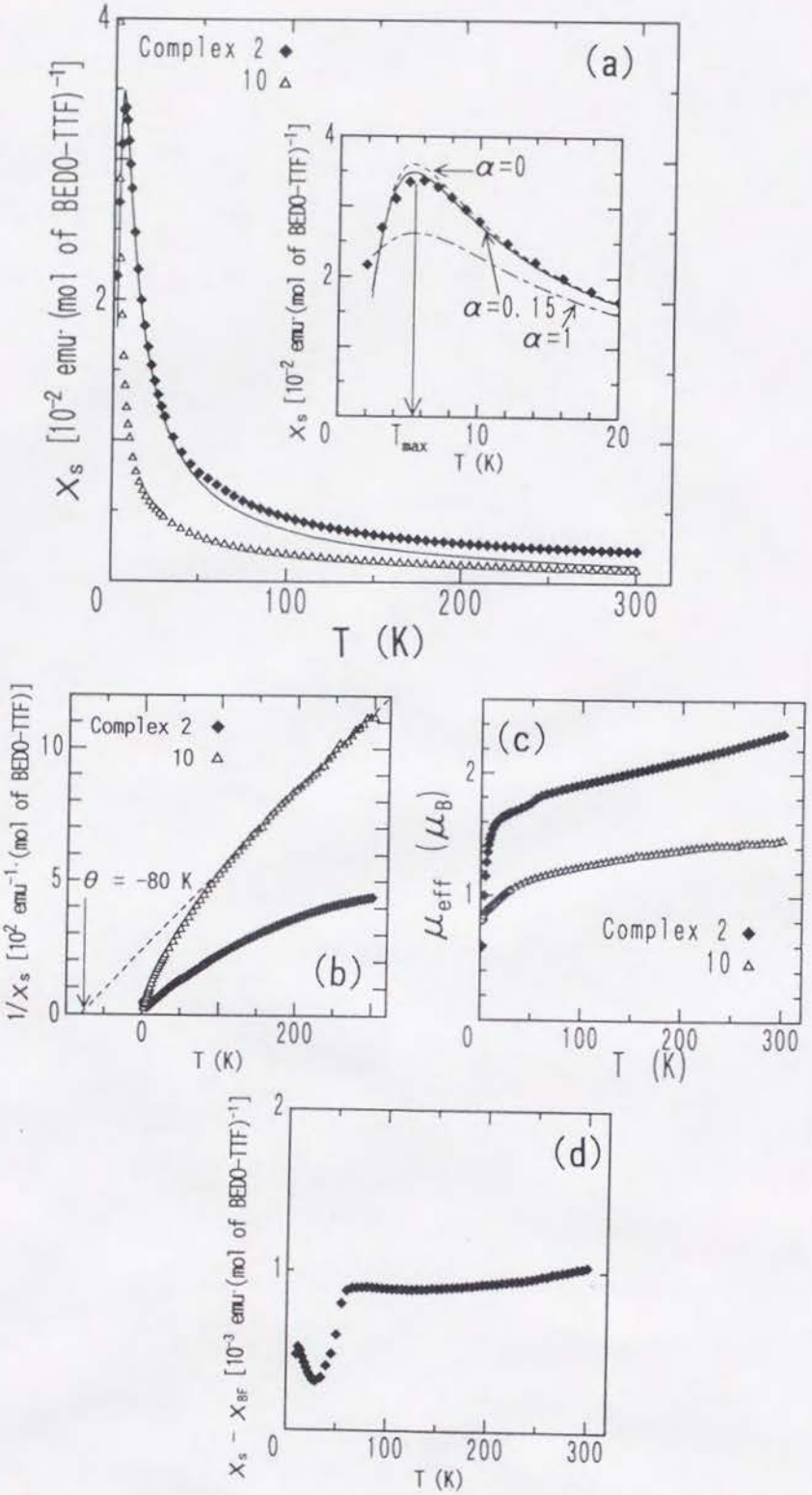

Figure 3-15. (a) Temperature dependent spin susceptibility (χ_s) of the complexes (BEDO-TTF)(F_4TCNQ) (2) (filled square), and (BEDO-TTF)(TCNQ) (10) (open triangle). The curves represent the theoretical susceptibility for the Heisenberg antiferromagnetic chains of alternately coupled S = 1/2 spins (χ_{BF}). The inset expands the low temperature region. (b) Reciprocal spin susceptibility ($1/\chi_s$) as a function of temperature. The dotted line is the least squares fit (eq 3.14) to the data of 10 above 100 K. (c) Temperature dependence of the effective moment (μ_{eff}). (d) Spin susceptibility of 2 obtained by subtracting χ_{BF}.

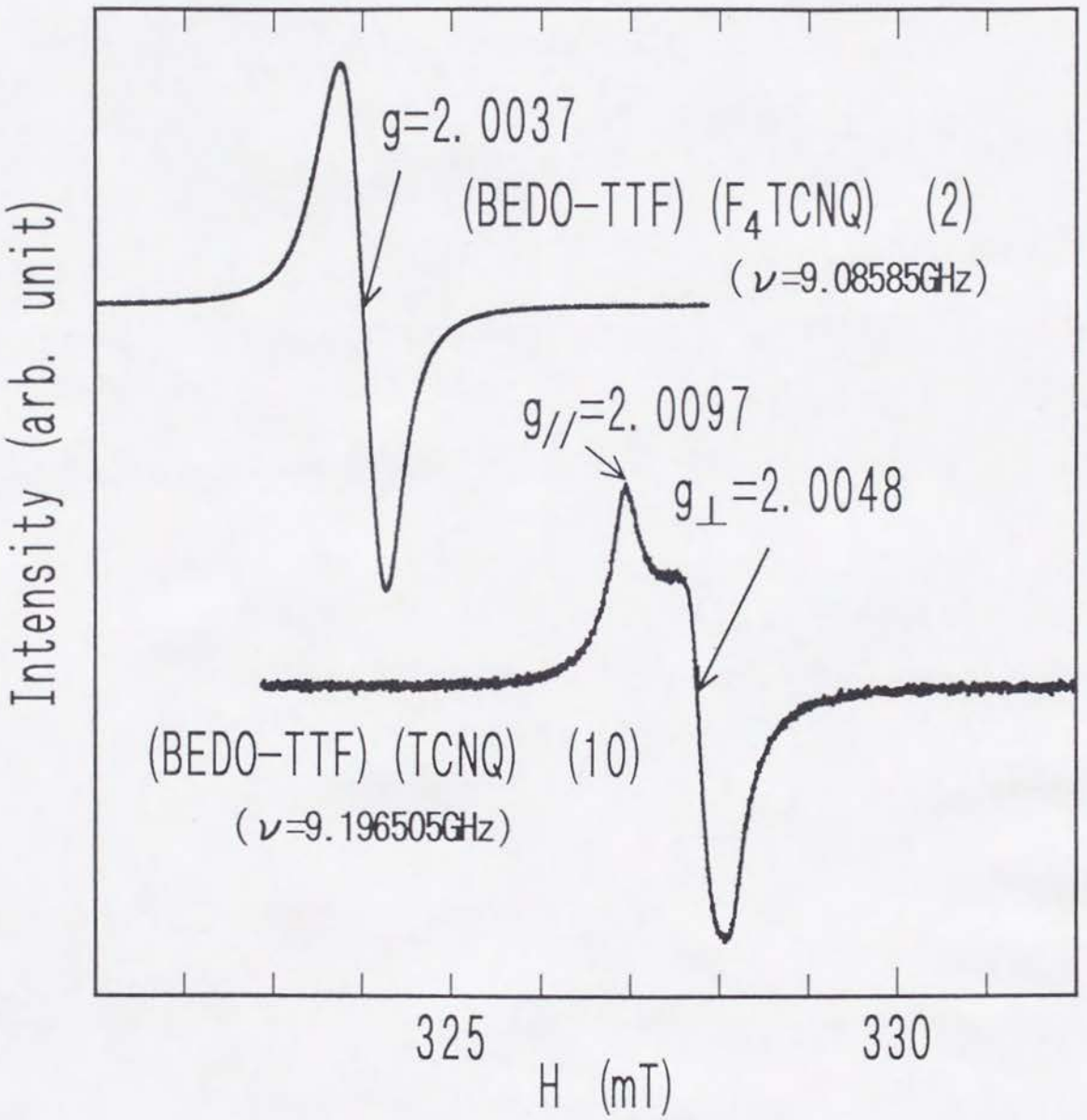

Figure 3-16. ESR spectra of randomly oriented polycrystalline samples of (BEDO-TTF)(F_4TCNQ) (2) and (BEDO-TTF)(TCNQ) (10) at room temperature.

Chapter 4 Structural Properties

4-1 Introduction

Crystal structure determination is indispensable for understanding of the above unusual properties of the BEDO-TTF complexes. Before this work, however, available structural data were limited to only 4 BEDO-TTF salts with inorganic anions,[26a,c,e] and during the present study, 5 crystal structures were presented by other groups.[26e,38,84] Here is presented the crystal structures of metallic 25, 31, 33, 34, 39, 40, and semiconducting 37, which are partially oxidized BEDO-TTF complexes containing counter components of various shapes and sizes. This chapter will demonstrate these structural properties at first. The expanded structural data on BEDO-TTF complexes serve to clarify the origin of strong self-aggregation of the donor molecules in the complexes.

This chapter also examines the relation between the structural properties and electronic states on the basis of the neutral, monovalent, and divalent BEDO-TTF complexes. The crystal structures of neutral CT complexes are exhibited for 27 and 29, both of which reveal characteristic hydrogen bondings. As the monovalent and divalent states of the donor molecule, the crystal structures will be discussed for 42 and 43, which are complexes of I_3^- with distinct stoichiometry. These structural data establish the relation between the geometry and oxidation state of the BEDO-TTF molecule. Finally, this relation will be applied to estimation of γ for the complex 25.

Tables of final atomic parameters for the complexes 25, 27, 29, 31, 33, 34, 37, 39, 40, 42, and 43, and their respective bond distances and angles in the molecules are summarized in Appendix.

4-2 Crystal Structures of Complexes of Partially Oxidized BEDO-TTF

4-2-1 $(BEDO\text{-}TTF)_5(HCTMM)(PhCN)_2$ (31) and $(BEDO\text{-}TTF)_{10}(CF)_4(H_2O)_3$ (33)

These two salts crystallize in the triclinic $P\bar{1}$ space group (Table 2-4), and show common structural features, which are discussed together here. The crystals are elongated along the a+2c and c directions for 31 and 33, respectively, developing the (010) plane. The unit cells contain five and one donor molecules for 31 and 33, respectively. As distinct from the tub-shape in the neutral crystal,[25a] BEDO-TTF molecules are almost planar, except for the terminal ethylene groups of the eclipsed conformation. This molecular structure can be commonly seen in most of the BEDO-TTF salts. The rigidity of the ethylene groups makes a striking contrast with the BEDT-TTF salts, in which various conformations are allowed and in some cases are related to the salt's physical properties.[85]

The donor molecules form layers along the *ac* planes (Figure 4-1a), where they stack along the a+2c and c directions for 31 and 33, respectively. Their layered arrangements are similar to those of $(BEDO\text{-}TTF)_{2.4}I_3$ salt,[26a] and will be designated as the I_3 type donor packing in this paper.

To compare the stacking manner of the BEDO-TTF salts, we defined the three structural parameters, D, δ, and ε (Figure 4-1b, c). D is the intermolecular separation along the stack obtained by averaging the atomic displacement of the $C_6O_4S_4$ moiety (excluding the ethylene groups) from the neighboring molecular plane. δ and ε are the tilted (acute) angles of the stacking direction with the molecular plane and with the central C=C bond, respectively (Table 4-1). The stacking axis in 33 tilts by 60.6° to the molecular plane with D of 3.51 Å and ε is 90.0°, indicating slipped stacking only along their transverse directions. In the case of 31, little variation in the crystallographically-independent D (3.48-3.59 Å), δ (59.0-62.3°), and ε

(87.5–89.5°) indicates the almost uniform stacking. Furthermore, these values are very close to those of 33.

The donor molecules in 31 and 33 show short intermolecular C–H··O contacts (H··O distance < 2.72 Å, dotted lines in Figure 4–1b for 31), though no S··S and S··O contacts shorter than the van der Waals radii (vdW) sums exist along the stack.[86]

Each donor molecule is linked by three S··S (3.40–3.49 Å) and two S··O (3.27–3.28 Å) short atomic contacts with coplanar neighboring ones (side–by–side contact) along the $3a+c$ and $a+c$ directions in 31 and 33, respectively (see Figure 4–1d for 31).

In neither salts could we determine the position of the counter components due to the components' severe disorder. This may indicate that the periodicities of the counter molecules are disregarded during formation of the uniform donor array. Also for the next complex, counter component molecules are disordered, but their averaged distribution can be recognized.

4–2–2 (BEDO–TTF)$_2$Br(H$_2$O)$_3$ (39)

The complex 39 crystallizes in the triclinic $P\bar{1}$ space group (Table 2–4). The crystal is elongated along the *c* direction developing the (010) plane. Since the obtained cell includes only half of the formula unit, the structural analysis assumed the averaged packing of Br^- anion and water molecules. The donor molecule lies on an inversion center, and shows the same geometry as that observed in 31 and 33. All donor molecules are self–aggregated in parallel, forming layers along the *ac* plane (Figure 4–2). Each layer is separated by Br^- ions and H_2O molecules. The long molecular axes are approximately perpendicular to the layer. The *c* direction corresponds to the stacking of donor molecules, which are connected by short C–H··O contacts (dotted lines in Figure 4–2b). The side–by–side array shows characteristic S··S and S··O

atomic contacts. Such intralayer array is the same as that of 31 and 33, and hence, is regarded as the I_3 type. The water molecules and Br^- ions are disordered and distributed along the *a* axis. The next crystal shows also averaged but more definite packing of the counter component molecules.

4-2-3 $(BEDO\text{-}TTF)_4(SQA)(H_2O)_6$ (34)

The complex 34 crystallizes in the triclinic $P\bar{1}$ space group with about twice *c* and *V* of 33 or 39 (Table 2-4). The crystal is elongated along the *c* direction developing the (010) plane. The BEDO-TTF molecules locate on two nonequivalent inversion centers and reveal the same molecular structure as those in 31, 33, and 39. The planar squarate and a pair of water molecules occupy the corner of the unit cell alternately along the *c* direction.

The donor molecules form a layer along the *ac* plane (Figure 4-3a) with *c* as the stacking axis. The donor packing shares most of the features of that in 31, 33, and 39 (the I_3 type).

However, the interstack array is slightly modified; the molecules adjacent along the *a*-2*c* direction are nearly coplanar (dihedral angle of 4.6°) but the numbers of short atomic contacts is decreased; two S··S (3.39-3.54 Å) and one S··O (3.09 Å) distances are shorter than the vdW sums.

The squarate molecules are packed parallel to the *ac* plane, forming a sheet with water molecules (Figure 4-3b). The oxygen atoms construct a 2D network of the intermolecular hydrogen bonds (O··O distance ~ 2.8 Å; dotted lines in the figure).

The interactions between donor and counter components are dominated by a number of C-H··O contacts (H··O distance < 2.72 Å), which are the likely origin of the slightly modified interstack array of the donor.

The I_3 type donor packing is also found for the next radical salt 40, which is a complex of four components including a magnetic ion.

4-2-4 $(BEDO\text{-}TTF)_2Br[cis\text{-}MnBr_2(H_2O)_4](H_2O)$ (40)

The complex 40 crystallizes in the triclinic $P\bar{1}$ space group (Table 2-4). The platelet crystal develops the (010) plane. The asymmetric unit contains a BEDO-TTF molecule at a general position, and two half BEDO-TTF molecules on different inversion centers, (1/2, 1, 0) and (0, 1, 1/2). The Br^-, $MnBr_2(H_2O)_4$, and water molecules are located at general positions. Therefore, this salt comprises four kinds of molecules (or ion). All the donor molecules show the same molecular structure as those in the above salts. The manganese atom is coordinated to two bromides and four water molecules in octahedral geometry of *cis*-type.

All the donor molecules are packed in parallel, forming a layers along the *ac* plane with *a*-*c* as the stacking direction (Figures 4-4a,b). The donor stack is characterized by a number of short C-H··O contacts, almost uniform separation (D = 3.51-3.53 Å), and slipped overlapping along the transverse molecular axis. Along the *c* direction, the donor molecules are coplanarly linked with short S··S (3.39-3.51 Å) and S··O distances (3.24-3.27 Å). The packing motif is quite the same as the above I_3 type.

In the anion layer, Br^-, H_2O, and $MnBr_2(H_2O)_4$ are tightly connected with one another by a number of intermolecular Br··O and O··O contacts (dotted lines in Figure 4-4c). These atomic distances are shorter than sum of the van der Waals and/or ion radii (Table 4-2), and are characteristic to the hydrogen bonds.* It should be noted that each of these oxygen atoms participates in two intermolecular hydrogen bonds.

Final example of the I_3 type array is the next complex 25, which is the only metallic DA-type complex of the determined crystal structure, revealing the acceptor stacks.

4-2-5 (BEDO-TTF)$_2$(HCHA) (25)

The complex 25 crystallizes in the monoclinic $P2_1/a$ space group (Table 2-4). The crystal is elongated along the *c* direction developing the (010) plane. The asymmetric unit comprises a BEDO-TTF molecule on a general position, and half of the acceptor molecule on an inversion center. The molecular structure of the donor is the same as that observed in the above salts.

The acceptor molecule is planar, and its geometry is different from the quinoid geometry observed in the neutral H_2CHA[87] and its dihydrate crystals[88] as shown in Table 4-3. The four C-O bonds are of nearly equal length, which is intermediate between that of C=O (1.222 Å) and of C-OH (1.322 Å). The C-C bonds parallel to the C-Cl bonds are significantly longer than the other four C-C bonds, which are of nearly identical length. This molecular structure is very similar to that of the completely deprotonated dianion in the $(NH_4^+)_2CHA^{2-}(H_2O)$[89] and $(NH_4^+)(H_5O_2^+)CHA^{2-}$ (Table 4-3).[90,91] We could not find the hydrogen atoms for the acceptor molecule by differential Fourier analysis. These facts suggest the deprotonation from the acceptor molecule in 25, in agreement with the optical spectra that suggests the formula of $(BEDO\text{-}TTF)_2^+(HCHA^-)$ as discussed in the Chap. 3. It is difficult to see the degree of deprotonation from the present structural analysis, which assumes only one crystallographically independent proton site of the acceptor molecule.

The donor molecules form layers along the *ac* plane with *c* as the stacking direction (Figure 4-5a, b). The molecules stack in the slipped manner along their lateral direction with uniform separation of D = 3.47 Å, and are connected by a number of short C-H··O contacts (Figure 4-5c). Along the $a+2c$ direction, the donor molecules are coplanarly linked with short S··S (3.31-3.50 Å) and S··O distances (3.04 Å). The packing motif quite resembles to those in the above complexes of the I_3 type.

The acceptor molecules form uniform stacks along the *c* direction, which is

also parallel to the donor stacks. They overlap in a slipped manner along a C–O bond with intermolecular separation of 3.47 Å (Figure 4–5d). The dihedral angle between the donor and acceptor molecules is about 32°. All the intermolecular O··O distances are longer than 3.2 Å, indicating the absence of strong intermolecular hydrogen bonding. There are C–H··O contacts between the donor and acceptor molecules. The next complex 37 is found to be a new type with respect to the donor packing.

4–2–6 (BEDO–TTF)$_5$(HCP)(PhCN)$_{0.2}$ (37)

The complex 37 crystallizes in the monoclinic $P2_1/c$ space group (Table 2–4). The crystal is elongated along the *c* direction developing the (100) plane. One BEDO–TTF molecule is crystallographically independent, and its geometry is the same as in the above salts. The donor packing in the accurate cell (*a*, 5*b*, *c*) must be unchanged from this averaged one, because the thermal parameters are normal for any atoms of the donor molecule. This is also supported by the fact that the superlattice gives few and weak reflections.

The donor molecules form a layer along the *bc* plane with *b* as the stacking axis. The anion molecules alternate with donor layers (the *bc* plane). The donor packing pattern is somewhat different from the I_3 type, so it will be designated as HCP type. Each donor layer consists of a repetition of four stacks (Figure 4–6a). The stacks A (or B) and A' (or B') are related to each other by the inversion centers; hence, the molecular planes are parallel. On the other hand, the stack B' is related to the stack A by the 2-fold screw axis (x = 1/2, z = 1/4) with the dihedral angle of 60.2°. Consequently, the molecular planes alternate every two stacks to form an AA'BB' stack array. Such a packing motif resembles that in α''-(BEDT–TTF)$_2$CsHg(SCN)$_4$.[92]

Donor packing in the stack pairs AA' or BB' shows the same pattern as the I_3 type, as is evident from both the similar values of D, δ, and ε and the

existence of the intermolecular short C–H··O contacts. The molecules A1 and A'1 in Figure 4–6a are coplanarly linked side–by–side with each other by three S··S (3.41–3.51 Å) and two S··O (3.26 Å) short atomic contacts like those of 31 and 33.

However, the molecules A1 and B'1, which are inclined to each other, have only one short S··S contact (3.53 Å) (Figure 4–6c).

The planar HCP anions, the molecular planes of which tilt by 76° to the long axis of the donor molecule, form the periodicity of 5*b* (Figure 4–6b) along the 2–fold screw axis (x = 0, z = 1/4 or 3/4).

The donor hydrogen atoms closest to the anions orient toward the large cavities surrounded by nitrile groups with the (CN)··H distances of 2.3–2.9 Å, which indicates the presence of donor–anion interaction. Since the molecular orientation of the donor is alternated at z = 1/4 and 3/4 planes which cross near the center of the anions, this interaction seems to modify the I_3–type arrangement. However, most of the structural features of the I_3 type are still preserved for this HCP type, which can be regarded as a minor modification of the I_3 type.

4–2–7 Donor Packing Pattern in the BEDO–TTF Radical Salts

Including the above structural data, crystal structures have been determined for 16 BEDO–TTF radical salts, which are listed in Table 4–1. This table also includes the complex 32, the structure of which is still preliminary due to the poor crystal quality. Its cell parameter β is almost the same and *a* and *c* are twice (Table 2–5) as compared with those corresponding values for 33 (Table 2–4). This parameter suggests the I_3 type packing, which is actually found by solving the structure. All of these 17 complexes feature a donor layer with long molecular axes aligned nearly in parallel.

The donor packing patterns in the layer can be classified into five (the I_3,

HCP, Cl, κ, and $Pt(CN)_4$) types (Table 4-1), the former two of which have already been mentioned. The donor packing is shown for the Cl, κ, and $Pt(CN)_4$ types in Figure 4-7. The most simple array is the I_3 type, which is composed of uniformly packed molecules with their planes parallel to each other. This packing is the major type found in 13 salts. For the HCP (37) and $Pt(CN)_4$ types,[84] the molecular planes are alternated by two stacks to form AA'BB' type array. Although the recently reported (BEDO-TTF)$_4$Pt(CN)$_4$(H_2O) salt shows a distinct stacking pattern from the HCP type (compare Figures 4-6a and 4-7a), further discussion is impossible here due to no available atomic parameters in the literature. For the Cl salt (**38a**), the BEDO-TTF molecules are alternated by stack to form herringbone-type arrangement (Figure 4-7b). (BEDO-TTF)$_2CF_3SO_3$ is the only example of the κ type array among BEDO-TTF complexes, and reveals self-assembled orthogonal $(BEDO\text{-}TTF)_2^+$ dimers instead of the donor stacks (Figure 4-7c).

The donor stacking is strictly or almost uniform for the I_3, HCP, and Cl types, as evidenced by the marginal variation in crystallographically independent D, δ and ε values (Table 4-1). The former two types share almost the same stacking parameters ($D \simeq 3.5$ Å, $\delta \simeq 60°$, $\varepsilon \simeq 90°$). The Cl type shows slipped stacking along the transverse axis ($\varepsilon = 92.7°$), having a much smaller δ (43.8°) than other salts.

The short intrastack C-H··O contacts, which have been pointed out to stabilize the stacks in the ClO_4, $AuBr_2$, and $Cu_2(NCS)_3$ salts,[93] are observed in all the BEDO-TTF salts except the Cl salt (Table 4-1). Some BEDO-TTF salts also show interstack C-H··O contacts.

The interstack arrays in the I_3 and HCP types reveal coplanar linkage of the molecules with two or three S··S and one or two S··O short atomic contacts. Only the Cl type has no pairs of coplanar molecules.

The above features indicate the strong self-aggregation of BEDO-TTF

molecules into the I_3 type array almost regardless of the counter components. This nature is explicitly observed as a severe disorder of the counter components in the two I_3 type salts (31, 33, 39) and a misfit of periodicity between the donor layer and the anion in $(BEDO-TTF)_{2.4}I_3$.[26a]

In the case of BEDT-TTF salts, the donor packing is determined mainly by the donor-anion interactions,[94,95] which allow the flexible conformation of terminal ethylene groups and various packing patterns depending on the anions. On the other hand, the BEDO-TTF molecule has rigidly fixed terminal ethylene groups and is frequently compelled to stack monotonously. Such contrastive structural features can be attributed to the different electronegativity of the outer heteroatoms (oxygen (3.5) vs. sulfur (2.5)). As exemplified by the O-H··O bonds in the complex 29, strong hydrogen bonding is allowed for the BEDO-TTF, but impossible for the BEDT-TTF. The oxygen atoms in the BEDO-TTF salts afford 2-4 intermolecular C-H··O contacts on the average per molecule (Table 4-1). The C-H··O contact is often seen in organic crystals and has been known, as the weak hydrogen bond, to play an important role in determining molecular array.[96] Upon oxidation to BEDO-TTF^+, the oxygen atom is considered to remain electronegative because of its little HOMO coefficient (see below). Therefore, the C-H··O contacts in the cation salts are also expected to be electrostatic so as to stabilize the donor packing. The geometry of the contacts is a typical one among the known C-H··O hydrogen bonds. For example, 33 shows the intrastack H··O distances of 2.63-2.72 Å, and its C-H··O angles (148-151°) are very close to the mean values of C-H··O angle (152.7°).[96] The sp^3 lone-pairs of the oxygen atoms direct approximately towards the hydrogen atoms; the angles of C_{in}-O··H (125-127°) and C_{out}-O··H (91-94°) are close to the idealized lone-pair direction (109.5°) (see Figure 5-1 for definition of C_{in} and C_{out}). Although the individual energy of the C-H··O bond is small (estimated at 0.6-1.8 kcal/mol),[97,98] this

interaction seems to stabilize particularly the I_3 type array due to the numerousness of the contacts. The importance of intermolecular C–H··O interactions among the terminal ethylenedioxy groups is further confirmed by the recent characterization of the neutral BEDO–DBTTF crystal: the donor molecules stack in almost the same manner as that in the I_3 type, having a number of C–H··O contacts.[63] It should be noted that a sufficiently large number of weak hydrogen bonds between the donor and counter molecules can more or less modify the donor packing. A most typical example is the **38a**, in which a number of short C–H··O and C–H··Cl contacts with counter components can be regarded as the origin of the different array of the donor.

Finally notice should be paid to the difference between BEDO–TTF and BEDT–TTF in the side–by–side atomic contacts. For the clarity, S_{in} and S_{out} are defined as the sulfur atoms in TTF moiety and in the six–membered rings of BEDT–TTF, respectively. In the BEDT–TTF salts, the six–membered rings are larger than those of BEDO–TTF so as to prevent the short S_{in}··S_{in} contacts observed in BEDO–TTF complexes. In turn, BEDT–TTF molecules make short S_{in}··S_{out} and S_{out}··S_{out} contacts. As discussed later, S_{in}··S_{in} contacts are highly effective for the increment of the intermolecular overlap integrals, and hence, the pattern of S··S atomic contacts reflects the magnitude of the interstack interactions.

4–3 Crystal Structure of Neutral BEDO–TTF Complexes

4–3–1 (BEDO–TTF)[Q(OH)$_2$]$_2$ (27)

The complex **27** crystallizes in the triclinic $P\bar{1}$ space group (Table 2–4), and its unit cell comprises one BEDO–TTF molecule on the center of inversion and two $Q(OH)_2$ ones in the general position. The crystal is elongated along the $a+b$ or c direction developing the $(1\bar{1}0)$ plane. The bond lengths and angles

of these molecules are almost identical to those of their respective neutral crystals (see Table 4-3).[25a,99] Two hydrogen atoms are bonded to the hydroxylic oxygen atoms of the acceptor molecule, indicating no deprotonation. The formation of this neutral CT complex accompanies the conformational change of the donor molecule from deformed to planar (except the terminal ethylene groups), as is similarly observed in the formation of several complexes of tetrakis(alkylchalcogeno)-TTF.[101]

The complex 27 consists of DAA-type alternating stack along the *a*+*b* direction (Figure 4-8a). This molecular packing is quite different from that observed for 25, the complex of a chlorine analog molecule of $Q(OH)_2$. The interplanar separations are 3.4 Å for D-A and 3.2 Å for A-A, accompanied by many intermolecular atomic contacts shorter than the vdW sums. The dihedral angle between molecules is 7.1° for D-A and 0° for A-A.

The (120) plane contains the $Q(OH)_2$ molecules, which are uniformly arranged along the *c* axis (Figure 4-8b). They are connected by hydrogen bonding between carbonyl and hydroxy groups with the O··O distances of 2.80 Å.

The intermolecular S··S and S··O contacts (dotted lines in the figure) uniformly link donor molecules with each other along the *c* axis. This side-by-side array is similar to that in the neutral BEDO-TTF crystal but different from the arrangement in radical salts. The S··S distance of 3.20 Å is quite short compared with usual > 3.3 Å, as well as with the distance for the neutral BEDO-TTF crystal (3.5 Å).

The BEDO-TTF molecule has a number of short C-H··O contacts with $Q(OH)_2$ molecules on the same and neighboring (120) planes. The $Q(OH)_2$ molecules tightly-linked by hydrogen bonds seem to induce the markedly short intermolecular S··S contacts indirectly through these C-H··O contacts.

4-3-2 (BEDO-TTF)(TNBP) (29)

The complex **29** crystallizes in the monoclinic *C*2/c space group (Table 2–4). The rhombic crystal develops the (001) plane with *a* as its long diagonal. The half of the respective molecules are crystallographically independent. The 2-fold axis crosses the BEDO–TTF molecule along the normal of molecular plane, while the TNBP molecule locates on the center of inversion.

The terminal ethylene groups of the planar donor molecule are disordered, in contrast to the usual eclipsed conformation in the crystals. This difference can be attributed to the absence of short C–H··O contacts between the donor molecules in this crystal. Of the two crystallographically independent nitro groups of TNBP, one is disordered into two conformations by respective weight of 1/2. Only the oxygen atoms of this disordered nitro group deviate from the molecular plane.

The ORTEP drawing and the schematic representation of this crystal structure are illustrated in Figure 4–9a. Both component molecules, which tilt their longitudinal directions by 80° and their planes by 16° with respect to each other, fail to construct columnar structures.

TNBP molecules link to each other at the disordered nitro groups along the *c* axis by short N··O contacts (3.03 Å) with the dihedral angle of 32°. In the light of the steric problem, the disordered nitro group should contact with a differently conformed group of the neighboring molecule.

The most characteristic feature in this crystal is the hydrogen bonds. The hydroxy groups of TNBP form not only intramolecular O–H··O bonds, but also intermolecular bonds using the oxygen of BEDO–TTF (the dotted lines in Figure 4–9). This suggests that the oxygen atom of this donor possesses a high ability to form intermolecular hydrogen bonds with hydroxy-groups of an organic acid.

4–4 Crystal Structure of Monocation Salt (BEDO–TTF)I_3 (42)

The complex 42 crystallizes in the triclinic $P\bar{1}$ space group (Table 2-4). The rhombic crystal develops the (001) plane. The BEDO-TTF molecule is located on a general position, while each of two I_3^- anions occupies a center of inversion. The BEDO-TTF molecule is slightly bent into a tub-shape (Figure 4-10a). Both I_3^- molecules are strictly linear and have I-I bond lengths of 2.92(2) Å.

The crystal packing contains mixed layers consisting of both donor and I_3^- anion molecules (Figure 4-10b). These mixed layers are separated from each other by layers of another crystallographically independent I_3^- anions as is observed in γ-$(ET)_3(I_3)_{2.5}$ and δ-$(ET)I_3(TCE)_{0.333}$.[102] Within the mixed layer, the donor molecules form a dimer by overlapping in almost eclipsed face-to-face manner (Figure 4-10c), in contrast with the usual slipped stacking along the transverse molecular axis. The dimer has an intermolecular separation of 3.54 Å accompanied with very short S··S distances (3.306-3.313 Å) (Figure 4-10a). The dimerized BEDO-TTF molecules and I_3^- anions alternate along the *a*+*b* direction to construct the mixed (BEDO-TTF)-I_3 layers. The $(BEDO\text{-}TTF)_2$ dimers are connected by another short S··S contacts (3.433-3.472 Å), forming two-dimensional network. On the other hand, the distances of atomic contacts between the I_3^- and BEDO-TTF molecules are longer than the vdW sums, indicating that the I_3^- molecules are loosely packed within the mixed layer. All the intermolecular I-I distances are longer than the vdW sums in this crystal.

4-5 Crystal Structure of Dication Salt (BEDO-TTF)$(I_3)_2$ (43).

The complex 43 crystallizes in the triclinic $P\bar{1}$ space group. The rhombic crystal develops the (010) plane. The BEDO-TTF molecule and I_3^- anion are

located on an inversion center and on a general position, respectively. BEDO-TTF molecules are almost planar except for the terminal ethylene groups of the eclipsed conformation. This conformation is the same as those observed in the above metallic BEDO-TTF complexes. The I_3^- molecule is almost linear (I-I-I angle of 178.01°) and has I-I bond lengths of 2.887(2) and 2.959(2) Å. As shown in Figure 4-11, all molecules are oriented almost parallel to each other, and form DAA type stack along the *a*-*c* direction. The donor molecules are completely isolated from each other by the surrounding I_3^- anions, having a number of short S··I distances (3.60-3.78 Å). Short I··I distance (3.739(3) Å) is found between the I_3^- molecules neighboring along the long molecular axis with each other. It is interesting to compare the structures of the donor-anion mixed layer in 42 (Figure 4-10d) and of a layer of 43 (Figure 4-11b). Replacing the donor molecules and the I_3^- anions in the former salt with each other gives the packing pattern of the latter one.

4-6 Bond Distances of BEDO-TTF Molecule

Now, a number of BEDO-TTF complexes are available for investigation of the relation between the geometry and a wide range of oxidation state of the donor molecule (γ = 0-2). Table 4-4 summarizes the averaged bond lengths of BEDO-TTF molecules in the neutral crystal and the complexes. Oxidation of the molecule results in an increase in lengths of two C-S and C_{in}-O bonds and a decrease in C=C bond lengths. This qualitatively agrees with the MO calculation that the HOMO is antibonding for the C-S and C-O bonds and bonding for the C=C bonds (see Chap.6). Similar results are reported for the correlation between bond lengths and oxidation state (0-2) of ET molecule.[103,104] In order to establish the reliable correlation, the plotted data are restricted for the complexes with small *R* factor (< 9 %) and enough

number of independent reflections (N_{ref}) for the number of refined parameters (N_p); $N_{ref}/N_p \geq 8$. Figure 4-12a plots the bond distances as a function of γ on BEDO-TTF molecules. The smallest standard deviations of bond distances are usually obtained for the C_{cen}-S bonds (d_{Ccen-S}), the distances of which also give the best correlation with the γ (Figure 4-12b). The least squares fit provided the relation,

$$d_{Ccen-S} = 1.7592 - 0.0300\,\gamma \qquad (4.1).$$

This relationship is useful for rough estimation of unknown γ of the BEDO-TTF complexes. For example, the d_{Ccen-S} values of 27 (1.755 Å) and 29 (1.758 Å) correspond to γ = 0.14 and 0.04, respectively, consistent with the optical spectra that indicated the neutral ionicity of these complexes. For the complex 25, γ is deduced as $+0.56\pm0.1$. Therefore, the stoichiometry demands about -1 charge on the acceptor molecules, which agrees well with the formula of $(BEDO\text{-}TTF)_2^+(HCHA^-)$ based on the solution spectra.

4-7 Summary

The partially charged donor molecules form layered structures in all the complexes characterized in this chapter. Their unusually strong self-aggregation suggested in the previous chapter is now appeared as the I_3 type packing. Then, how can this packing pattern stabilize the metallic state down to low temperatures regardlessly to the nature of the counter component molecules? The answer can be found through the band calculations in next chapter.

On the other hand in the neutral, monovalent, and divalent complexes, the BEDO-TTF molecules overlap with acceptor molecules or counter ions in alternating manner, which is consistent with the insulating nature. The

present structural studies have also presented very useful relations for estimating charge on the BEDO-TTF molecules (γ) which is a critical parameter in the complexes' physical properties.

Table 4–1. Comparison of Donor Packing in BEDO–TTF Complexes

complex		packing type	D,[a,b] Å	δ,[a] deg	ε,[a] deg	no. of C-H··O contacts: intrastack	no. of C-H··O contacts: interstack	ref.
$(BEDO\text{-}TTF)_2(HCHA)$	(25)	I_3	3.47	59.1	87.8	3.0	0.0	
$(BEDO\text{-}TTF)_5(HCTMM)(PhCN)_2$	(31)	I_3	3.48-3.59	59.0-62.3	87.5-89.5	3.2	0.4	
$(BEDO\text{-}TTF)_{10}(CF)_4(H_2O)_3$	(33)	I_3	3.51	60.6	90.0	4.0	0.0	
$(BEDO\text{-}TTF)_4(SQA)(H_2O)_6$	(34)	I_3	3.54-3.58	59.8-60.8	86.6-88.5	2.0	0.0	
$(BEDO\text{-}TTF)_2Br(H_2O)_3$	(39)	I_3	3.50	60.6	89.0	4.0	0.0	
$(BEDO\text{-}TTF)_2Br[MnBr_2(H_2O)_4](H_2O)$	(40)	I_3	3.51-3.53	59.8-60.0	89.1-89.7	2.5	0.5	
$(BEDO\text{-}TTF)_{2.4}I_3$	(41)	I_3	3.50	60.4	89.2	4.0	0.0	26a
$(BEDO\text{-}TTF)_2ClO_4$		I_3	3.50	60.3	89.5	4.0	0.0	26c
$(BEDO\text{-}TTF)_2AuBr_2$		I_3	3.45-3.59	57.7-61.4	88.9-89.0	2.0	1.0	26c
$(BEDO\text{-}TTF)_3Cu_2(NCS)_3$		I_3	3.60-3.67	56.4-59.4	88.3-88.9	1.3	0.7	27a
$(BEDO\text{-}TTF)_2ReO_4(H_2O)$		I_3	3.44-3.49	58.7-59.4	88.1-89.9	3.0	0.5	27e
$(BEDO\text{-}TTF)_2CF_3SO_3(THF)_{0.5}$		I_3	(*)					38
$(BEDO\text{-}TTF)_4(HCTMM)(TCE)_2$	(32)	I_3	(**)					
$(BEDO\text{-}TTF)_5(HCP)(PhCN)_{0.2}$	(37)	HCP	3.52	59.4	88.6	3.0	0.0	
$(BEDO\text{-}TTF)_2Cl(H_2O)_3$	(38a)	Cl	3.54	43.8	87.3	0.0	2.0	27e
$(BEDO\text{-}TTF)_2CF_3SO_3$		κ	3.64 (+)	65.1	66.8			38
$(BEDO\text{-}TTF)_2Pt(CN)_4(H_2O)$		$Pt(CN)_4$	(*)					81

[a] See text for definitions of D, δ, and ε. [b] (*) No atomic parameters are given in the literature; (**) preliminary structural analysis; (+) no stacks in donor layers; D, δ, and ε are defined within a dimer.

Table 4–2. Intermolecular Hydrogen Bonding with Short Br··O (< 3.4 Å) and O··O (< 3.0 Å) Distances (Å) in $(BEDO\text{-}TTF)_2Br[MnBr_2(H_2O)_4](H_2O)$ (40).

Br1 ·· O32 [a]	3.319(9)	Br3 ·· O35 [d]	3.300(10)
Br1 ·· O34 [b]	3.369(9)	Br3 ·· O33	3.316(10)
Br2 ·· O31 [a]	3.323(9)	Br3 ·· O31 [a]	3.319(9)
Br2 ·· O34 [b]	3.335(9)	O35 ·· O32 [a]	2.741(14)
Br3 ·· O33 [c]	3.301(10)		

[a] $x, y, z + 1$; [b] $1 - x, 1 - y, 1 - z$; [c] $-x, 1 - y, 1 - z$; [d] $-x, 1 - y, 2 - z$

Table 4–3. Comparison of Bond Length (Å) of H_xCHA and $Q(OH)_2$ Molecules

compound	C-X	C-O		C-C			ref.
	a	b	c	d	e	f	
X=Cl							
H_2CHA	1.717	1.222	1.322	1.346	1.445	1.501	87
$H_2CHA \cdot 2H_2O$	1.720	1.229	1.317	1.345	1.446	1.512	88
$(NH_4^+)_2(CHA^{2-}) \cdot H_2O$	1.741	1.243	1.253	1.401	1.407	1.535	89
$(C_6H_5NH_3^+)_2(CHA^{2-})$	1.744	1.241	1.284	1.361	1.437	1.517	90
$(NH_4^+)(H_5O_2^+)(CHA^{2-})$	1.740	1.258	1.263	1.385	1.375	1.522	90
$(BEDO\text{-}TTF)_2(HCHA)$ (25)	1.730	1.264	1.252	1.409	1.392	1.533	
X=H							
$Q(OH)_2$ *	0.94	1.235	1.327	1.355	1.442	1.506	99
2K salt of $Q(OH)_2$		1.27	1.28	1.40	1.38	1.53	100
$(BEDO\text{-}TTF)[Q(OH)_2]_2$ (27)	0.96	1.231	1.332	1.348	1.440	1.502	

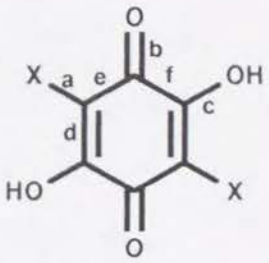

H_2CHA (X=Cl)
$Q(OH)_2$ (X=H)

[a] Averaged values of crystallographically independent bond lengths.
[b] At room temperature; (*) at -162 °C

Table 4–4. Correlation Between Bond Distances and Charge of BEDO–TTF Molecule

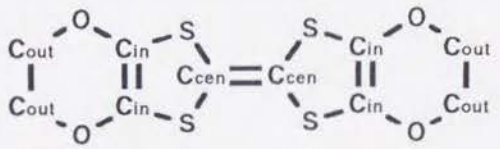

compound		γ known	γ calcd	bond distance (Å) C_{cen}=C_{cen}	C_{cen}-S	C_{in}-S	C_{in}=C_{in}	C_{in}-O	*R*, %	*Nref/Np*	ref.
D = BEDO-TTF		0.00		1.357	1.762	1.754	1.333	1.368	4.8	10	25a
D(TNBP)	(29)		0.04	1.339	1.758	1.754	1.309	1.370	7.4	13	
$D[Q(OH)_2]_2$	(27)		0.14	1.353	1.755	1.749	1.331	1.366	3.7	13	
$D_3Cu_2(NCS)_3$		0.33		1.353	1.751	1.747	1.319	1.369	3.0	12	27a
$D_5HCTMM(PhCN)_2$	(31)	0.40		1.336	1.759	1.751	1.342	1.352	12.7	10	
$D_{10}(CF)_4(H_2O)_3$	(33)	0.40		1.35	1.75	1.72	1.36	1.36	10	12	
$D_5HCP(PhCN)_{0.2}$	(37)	0.40		1.355	1.750	1.740	1.335	1.373	8.4	9	
$D_{2.4}I_3$	(41)	0.42		1.347	1.742	1.737	1.299	1.361	5.5	24	102
$D_4(SQA)(H_2O)_6$	(34)	0.50		1.361	1.743	1.739	1.341	1.356	5.0	17	
$D_2Cl(H_2O)_3$	(38a)	0.50		1.357	1.749	1.748	1.328	1.362	4.3	15	27e
$D_2Br(H_2O)_3$	(39)	0.50		1.357	1.745	1.739	1.348	1.352	7.0	14	
$D_2Br[MnBr_2(H_2O)_4](H_2O)$	(40)	0.50		1.355	1.747	1.739	1.357	1.348	7.9	13	
$D_2ReO_4(H_2O)$		0.50		1.37	1.741	1.737	1.351	1.344	4.9	9	27e
D_2ClO_4		0.50		1.369	1.740	1.734	1.343	1.361	6.6	17	
D_2AuBr_2		0.50		1.336	1.750	1.731	1.334	1.357	15	9	
$D_2CF_3SO_3$		0.50		1.39	1.733	1.750	1.325	1.353	9	4	38
$D_2(HCHA)$	(25)		0.57	1.372	1.742	1.739	1.353	1.351	5.1	8	
$D_2Ni(dto)_2$		1.0		1.39	1.728	1.735	1.325	1.367	6.2	7	26g
$D_2Pd(dto)_2$		1.0		1.390	1.730	1.736	1.342	1.356	4.0	20	26g
DI_3	(42)	1.0		1.398	1.723	1.727	1.350	1.352	4.0	15	
$D(I_3)_2$	(43)	2.0		1.427	1.702	1.702	1.420	1.309	7.1	22	

Bond distances are averaged assuming D_{2h} symmetry for the $C_6O_4S_4$ moiety excluding the terminal ethylene groups. *Nref* is a number of independent reflections used in the refinement of *Np* parameters in structural analyses.

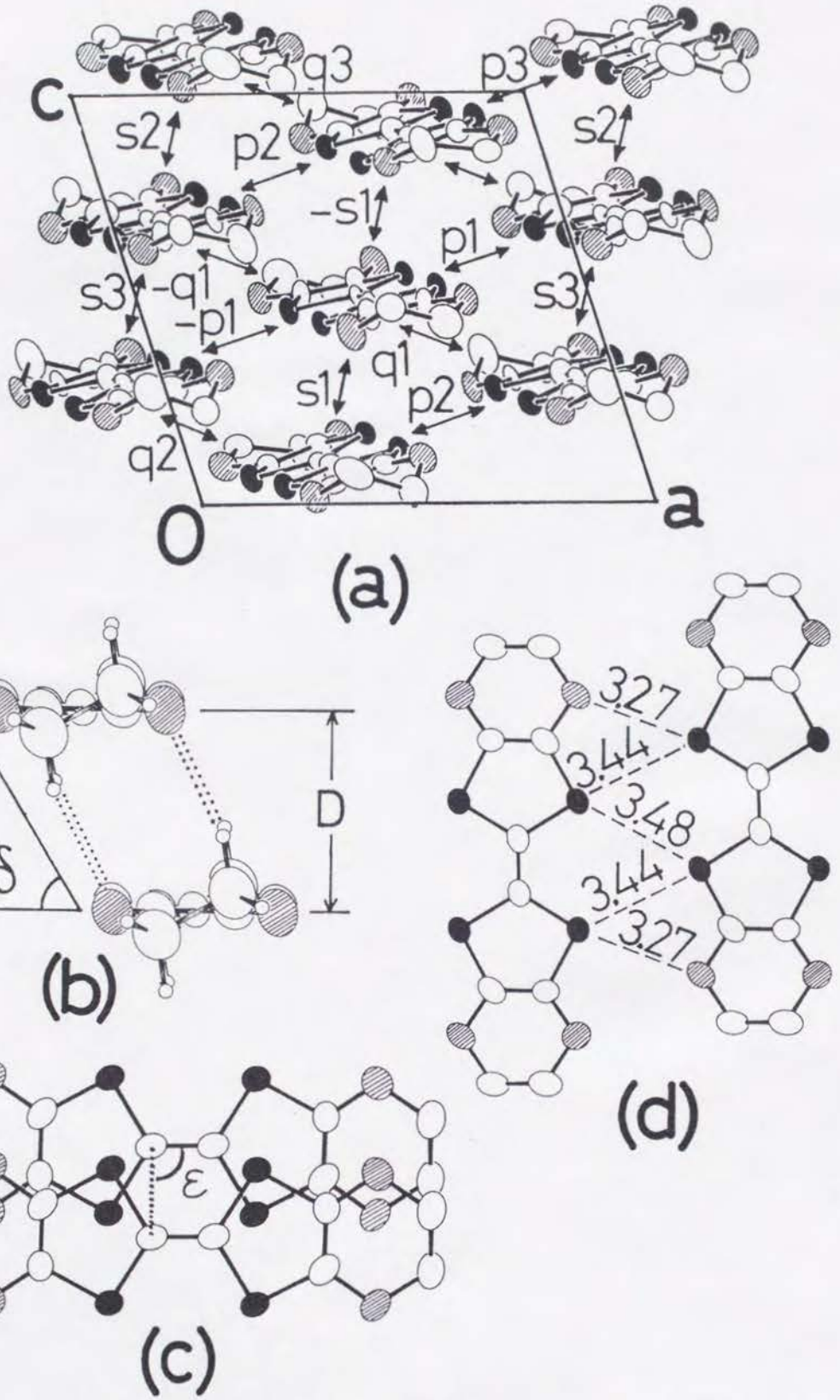

Figure 4-1. Crystal structures of $(BEDO\text{-}TTF)_5(HCTMM)(PhCN)_2$ (31). (a) The molecular arrangement in a donor layer viewed along the *b* axis with scheme of the intermolecular overlap integrals. (b) Stacking motif of the donor molecules projected along the long direction of the molecule. Intermolecular short C-H··O contacts (H··O < 2.72 Å) are shown by dotted lines. (c) Stacking motif of the donor molecule viewed on the molecule. (d) Side-by-side arrangement of the donor molecules. The averaged distances are shown in angstrom. Hydrogen atoms are omitted for clarity in the (a), (c) and (d). For s_i, p_i, q_i (i = 1-3), D, δ and ε, see text.

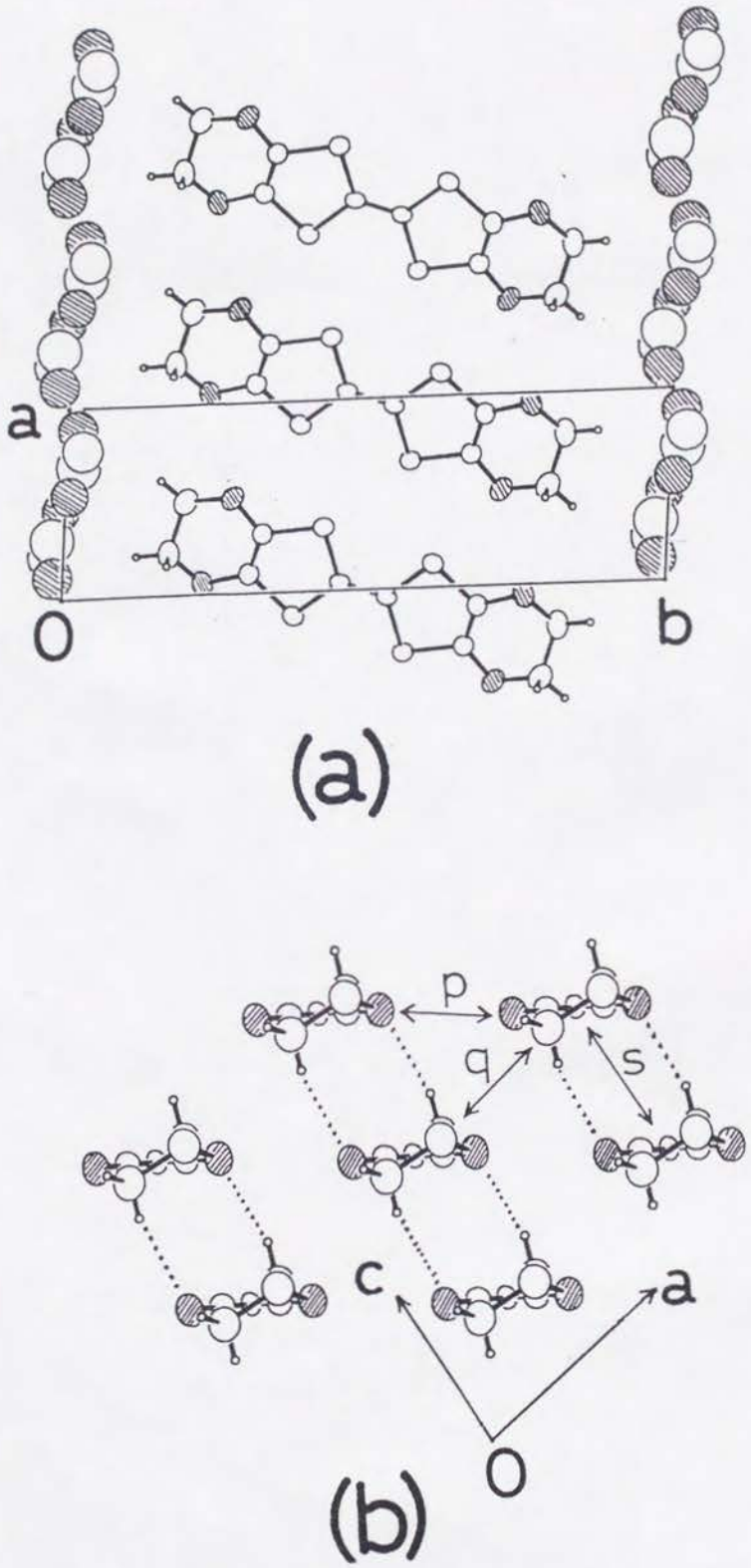

Figure 4-2. Crystal structures of $(BEDO\text{-}TTF)_2Br(H_2O)_3$ (39). (a) Crystal structure projected on the *c* axis. (b) Donor arrangement viewed along the long molecular axis with scheme of the intermolecular overlap integrals. Intermolecular short C-H··O contacts (H··O < 2.72 Å) are shown by dotted lines. Oxygen atoms are shaded.

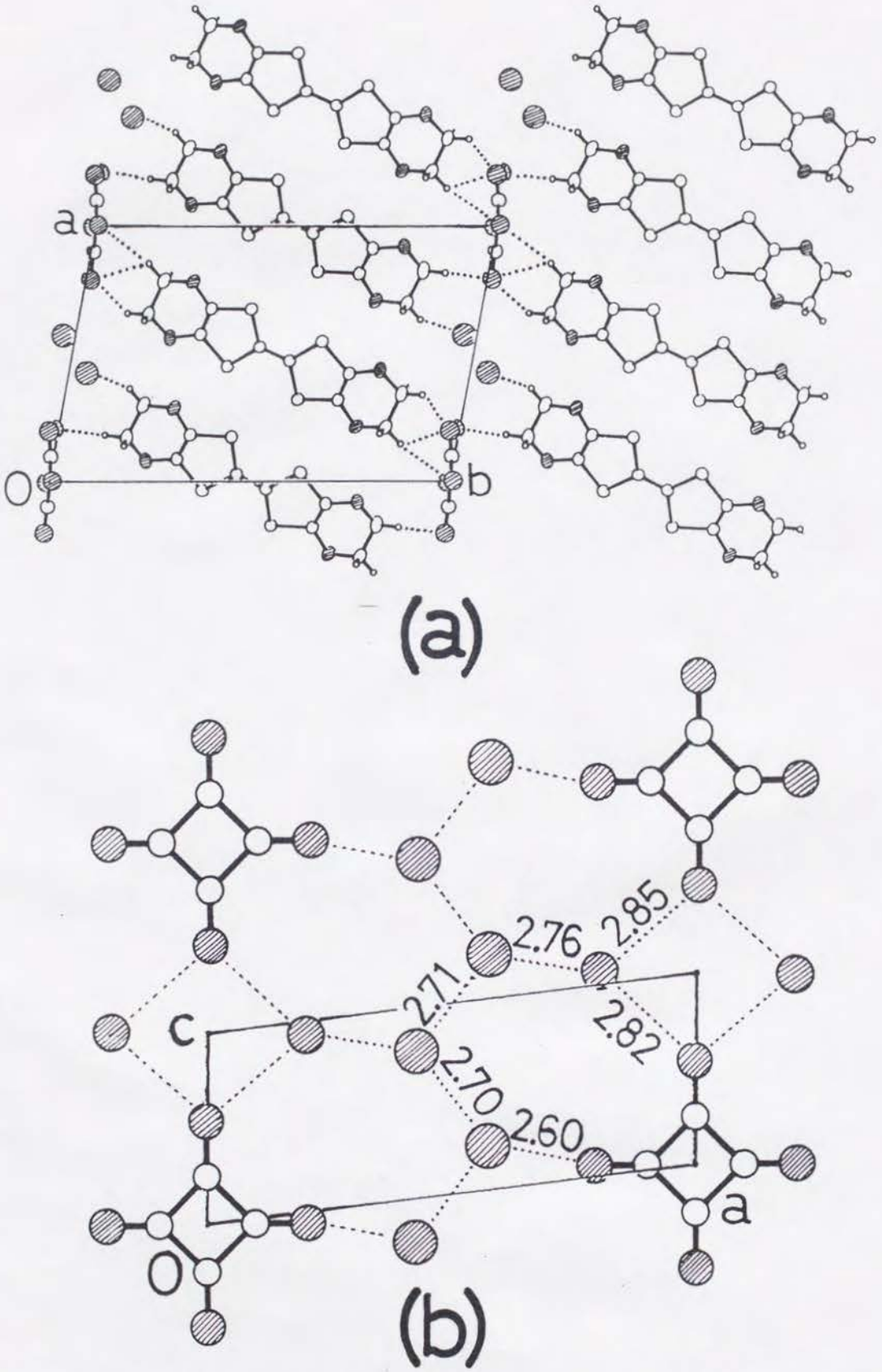

Figure 4-3. Crystal structures of $(BEDO\text{-}TTF)_4(SQA)(H_2O)_6$ (34). (a) Crystal structure projected on the *c* axis. Intermolecular short C-H··O contacts (H··O < 2.72 Å) between the donor and counter component molecules are shown by dotted lines. (b) Arrangement of the squarate ions and water molecules projected on the *b* axis. Intermolecular hydrogen bonds (OH··O, Å) are shown by dotted lines (hydrogen atoms are not depicted).

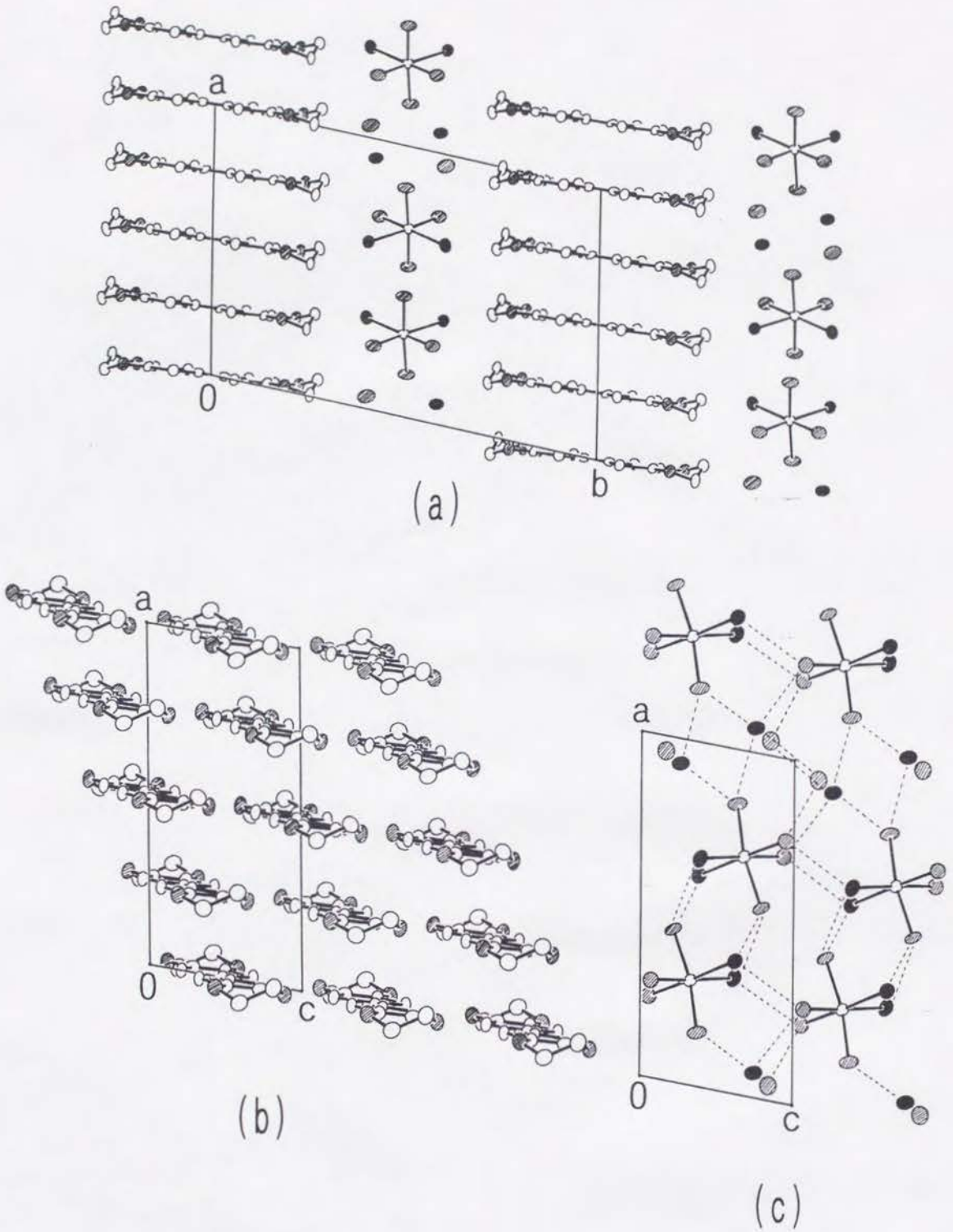

Figure 4-4. Crystal structures of $(BEDO\text{-}TTF)_2Br[MnBr_2(H_2O)_4](H_2O)$ (40). (a) Crystal structure projected on the *c* axis. Oxygen and bromine atoms are shaded and filled, respectively. (b) Layer of BEDO-TTF molecules projected along the *b* axis. (c) Arrangement in the anion layer (y = 1/2) viewed on the *b* axis. Intermolecular hydrogen bonds are shown by dotted lines (hydrogen atoms are not depicted).

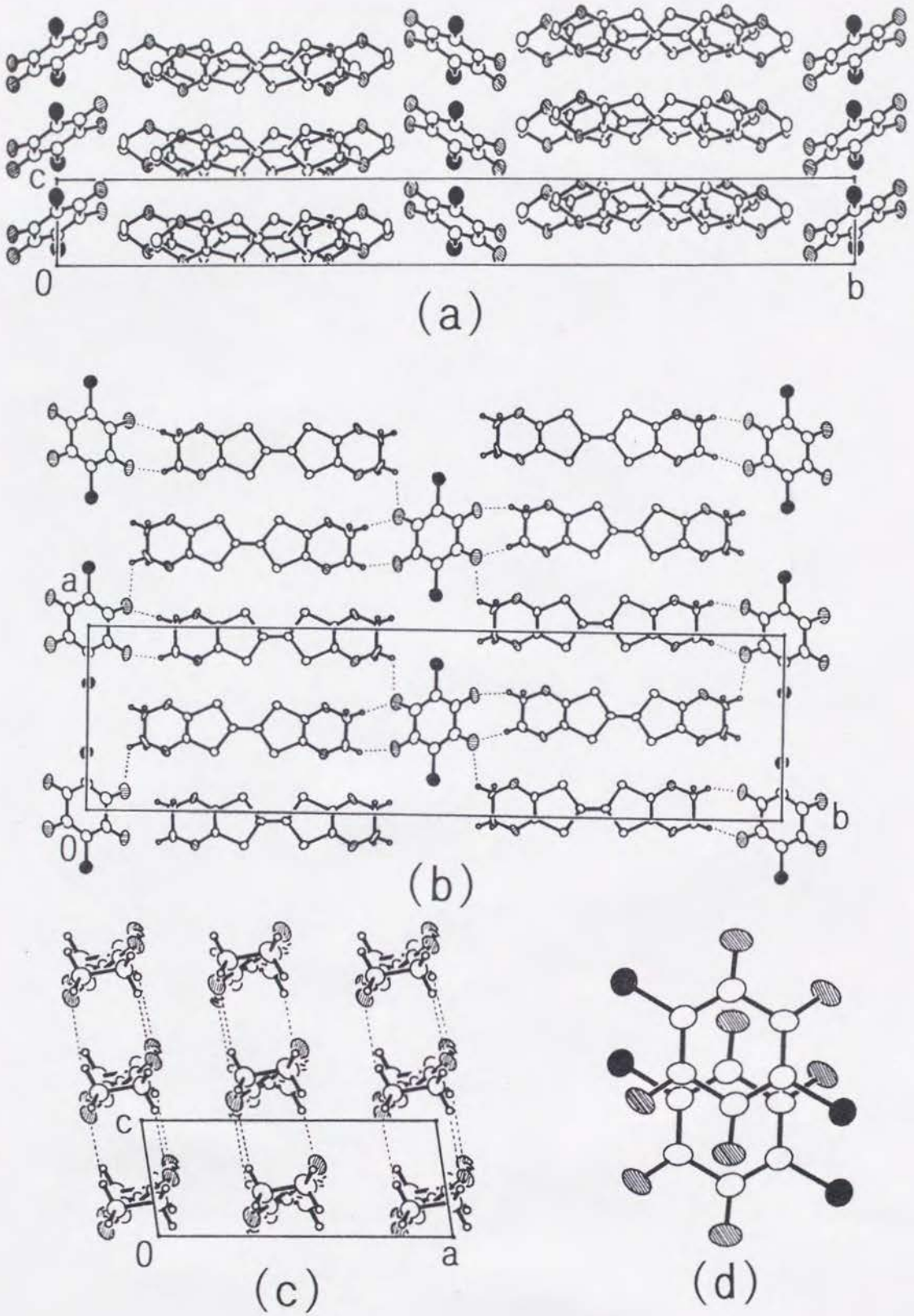

Figure 4-5. Crystal structures of $(BEDO\text{-}TTF)_2(HCHA)$ (25). (a) Crystal structure projected on the *c* axis. Oxygen and chlorine atoms are shaded and filled, respectively. (b) Layer of BEDO-TTF molecules projected along the *b* axis. (c) Arrangement in the anion layer ($y = 1/2$) viewed on the *b* axis. (d) Stacking motif of acceptor molecules viewed on the molecule.

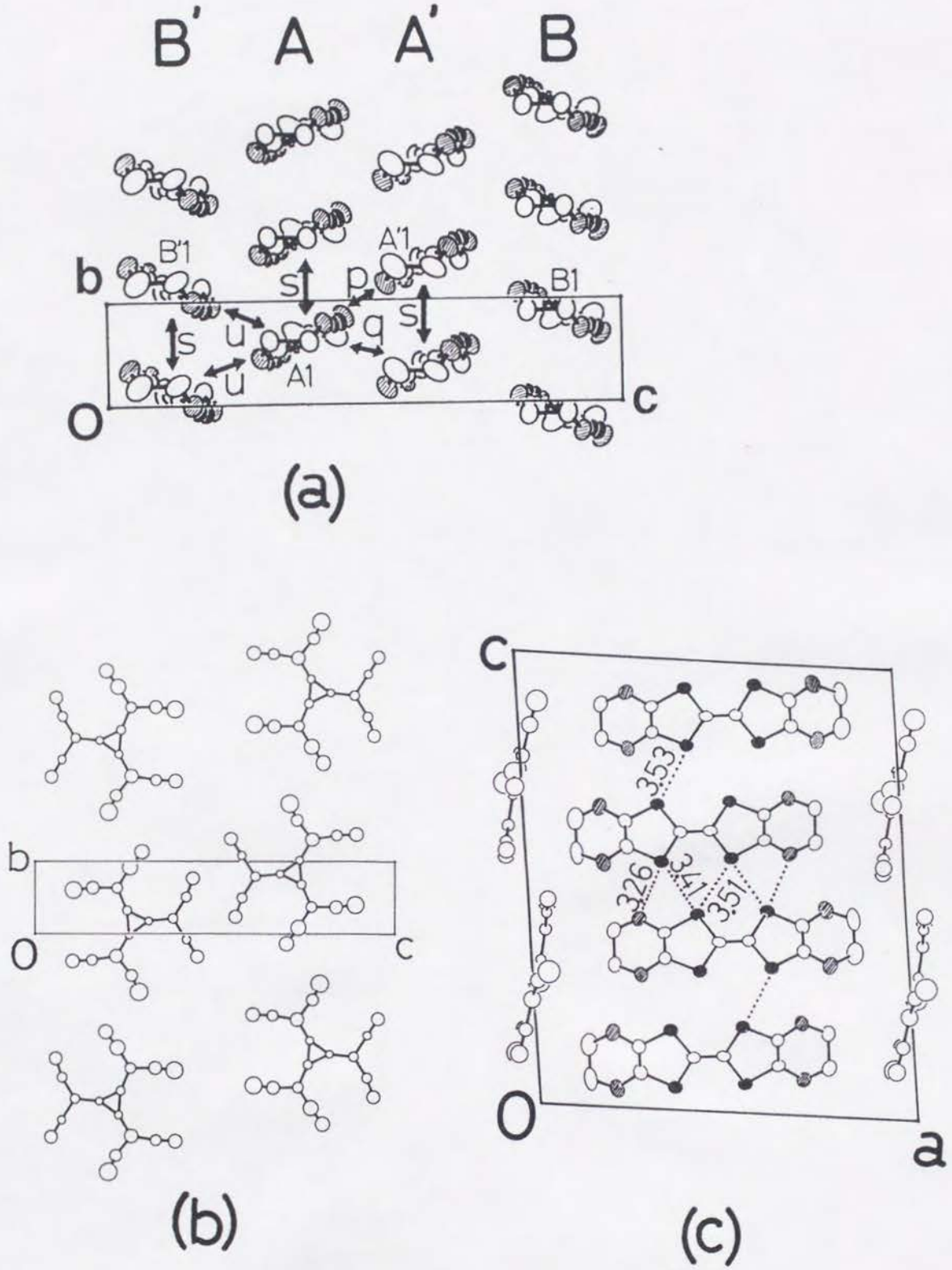

Figure 4-6. Crystal structures of $(BEDO\text{-}TTF)_5(HCP)(PhCN)_{0.2}$ (37). (a) Layer of BEDO-TTF molecules viewed along the *a* axis with scheme of the intermolecular overlap integrals (*s*, *p*, *q*, *u*). Regarding A, A', B, B', A1, A'1, and B1, B'1, see text. (b) Arrangement of HCP^{2-} molecules viewed along the *a* axis. (c) Crystal structure viewed along the *b* axis. The dotted lines show atomic S··S and S··O contacts among the molecules A1, A'1, B1 and B'1 with the distances (Å).

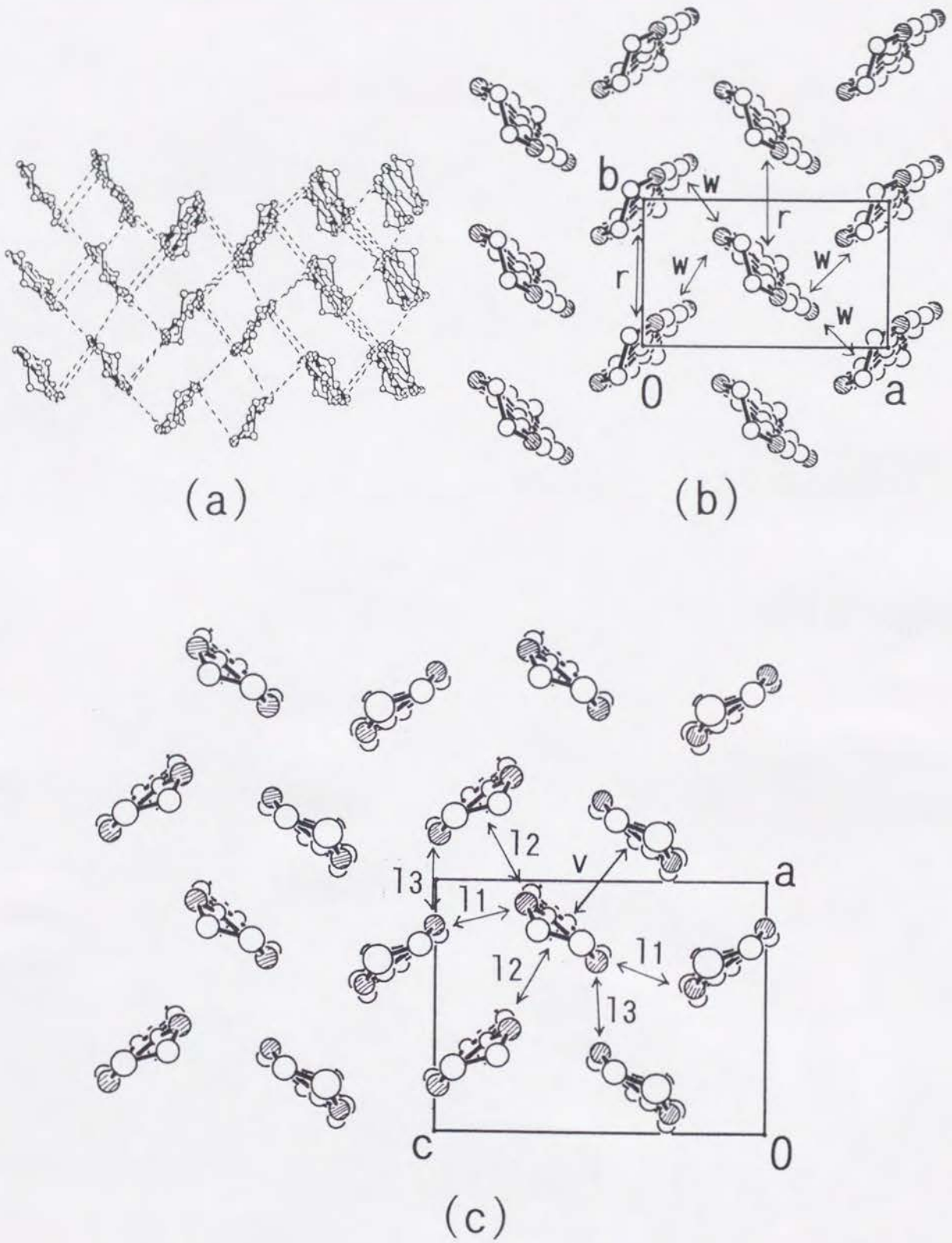

Figure 4-7. Layer of BEDO-TTF molecules with scheme of intermolecular overlap integrals (r, w, v, l_i (i = 1-3). (a) $(BEDO\text{-}TTF)_4Pt(CN)_4(H_2O)$ viewed along the molecular long axis (taken from ref.81). Dotted lines represent the short S··S distances (< 3.60 Å). (b) $(BEDO\text{-}TTF)_2Cl(H_2O)_3$ (38a) viewed along the c axis. (c) The molecules on y = 0 in κ-$(BEDO\text{-}TTF)_2CF_3SO_3$ viewed along the b axis. Oxygen atoms are shaded.

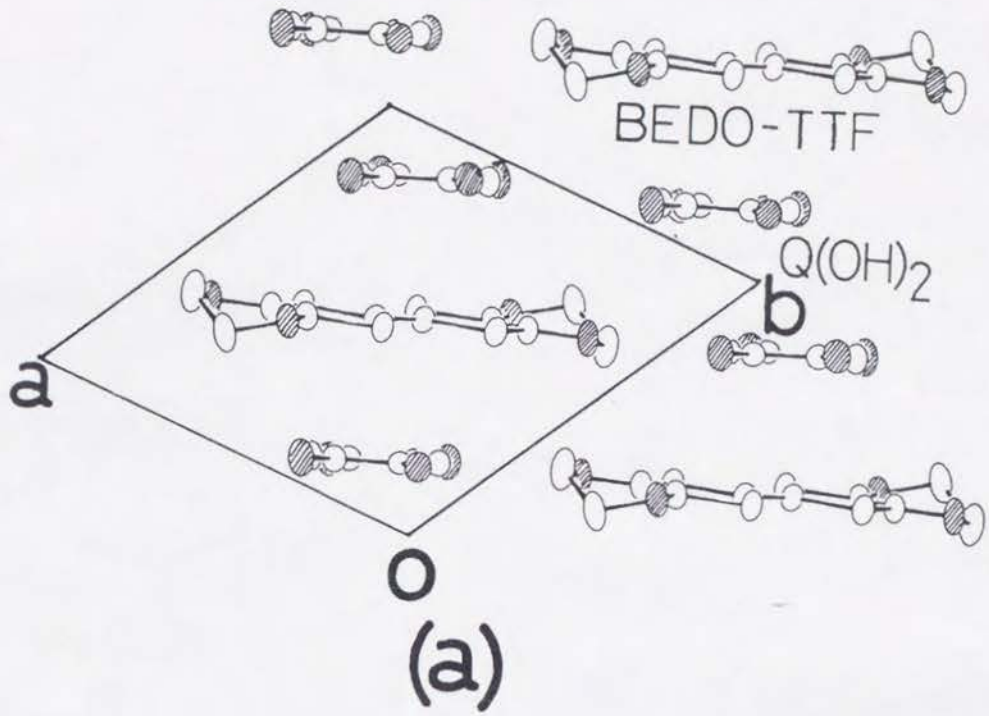

(a)

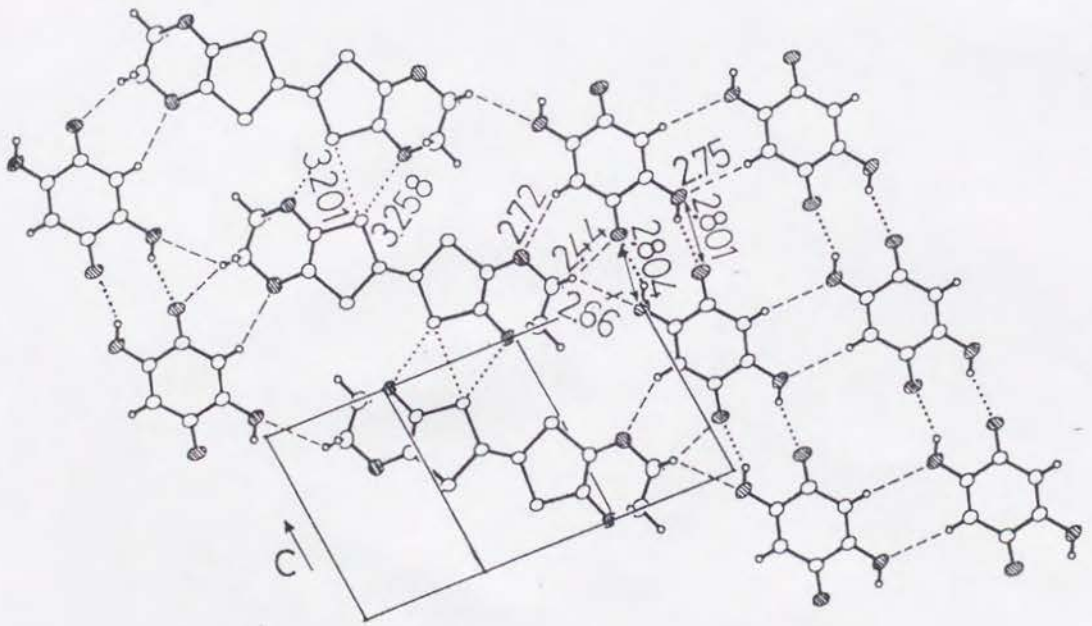

(b)

Figure 4-8. Crystal structures of (BEDO-TTF)$[Q(OH)_2]_2$ (27). (a) Crystal structure viewed along the *c* axis. (b) Nearly coplanar arrangement of molecules viewed onto the (120) plane. Short O-H··O hydrogen bonds and S··S and S··O contacts are shown by dotted lines. Short C-H··O contacts are shown by broken lines. The distances are shown in angstrom for crystallographically-independent contacts.

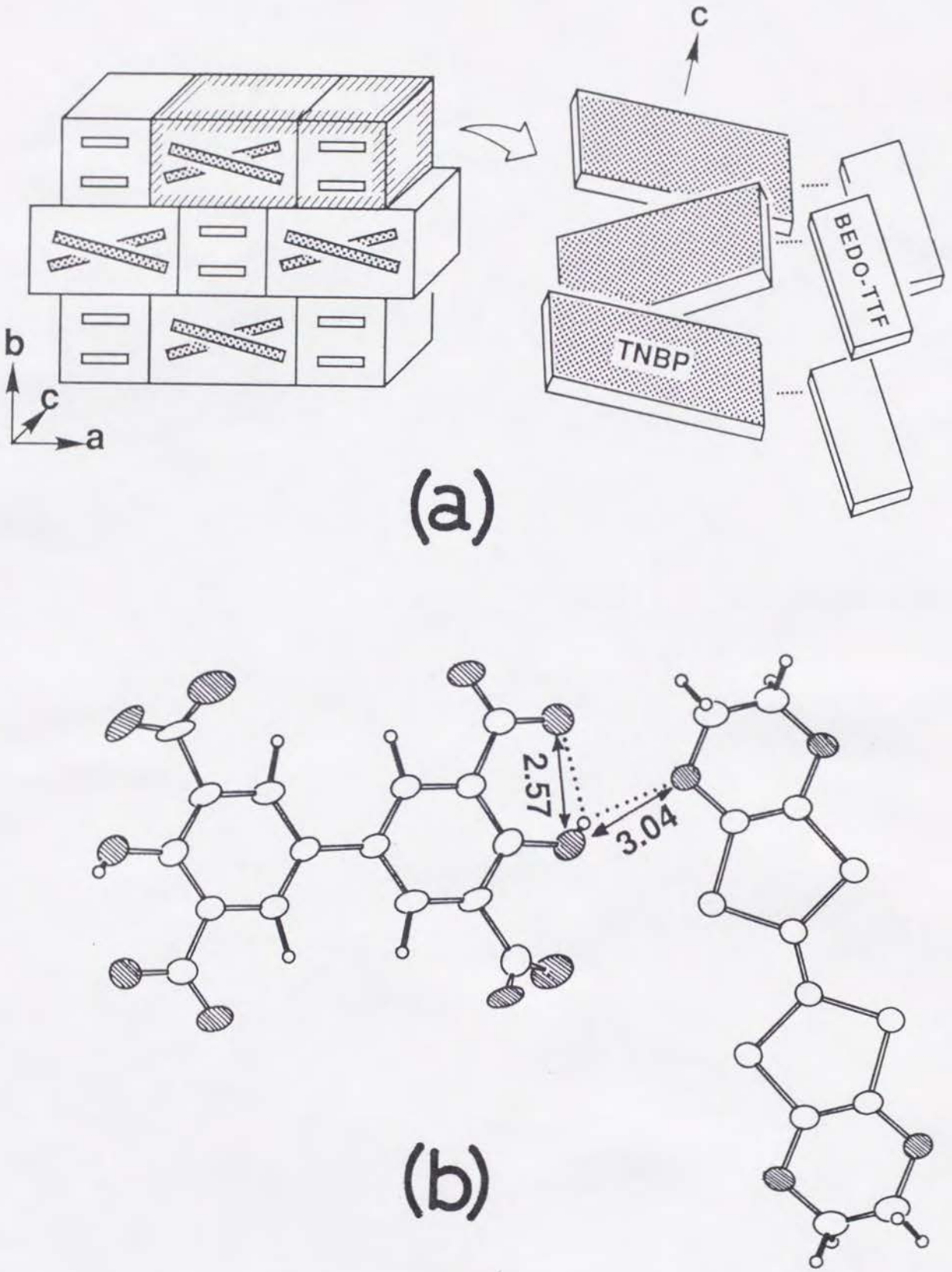

Figure 4-9. Crystal structures of (BEDO-TTF)(TNBP) (29). (a) Schematic representation of molecular packing. The left figure indicates projection approximately along the *c* axis (almost parallel to the molecular plane). A portion is magnified on the right as the projection from the direction oblique to the molecular planes. BEDO-TTF and TNBP molecules are depicted by unshaded and shaded plates, respectively. Intermolecular O-H··O hydrogen bonds are shown by dotted lines. (b) Inter- and intramolecular hydrogen bonds (Å) between donor and acceptor molecules. Oxygen atoms are shaded.

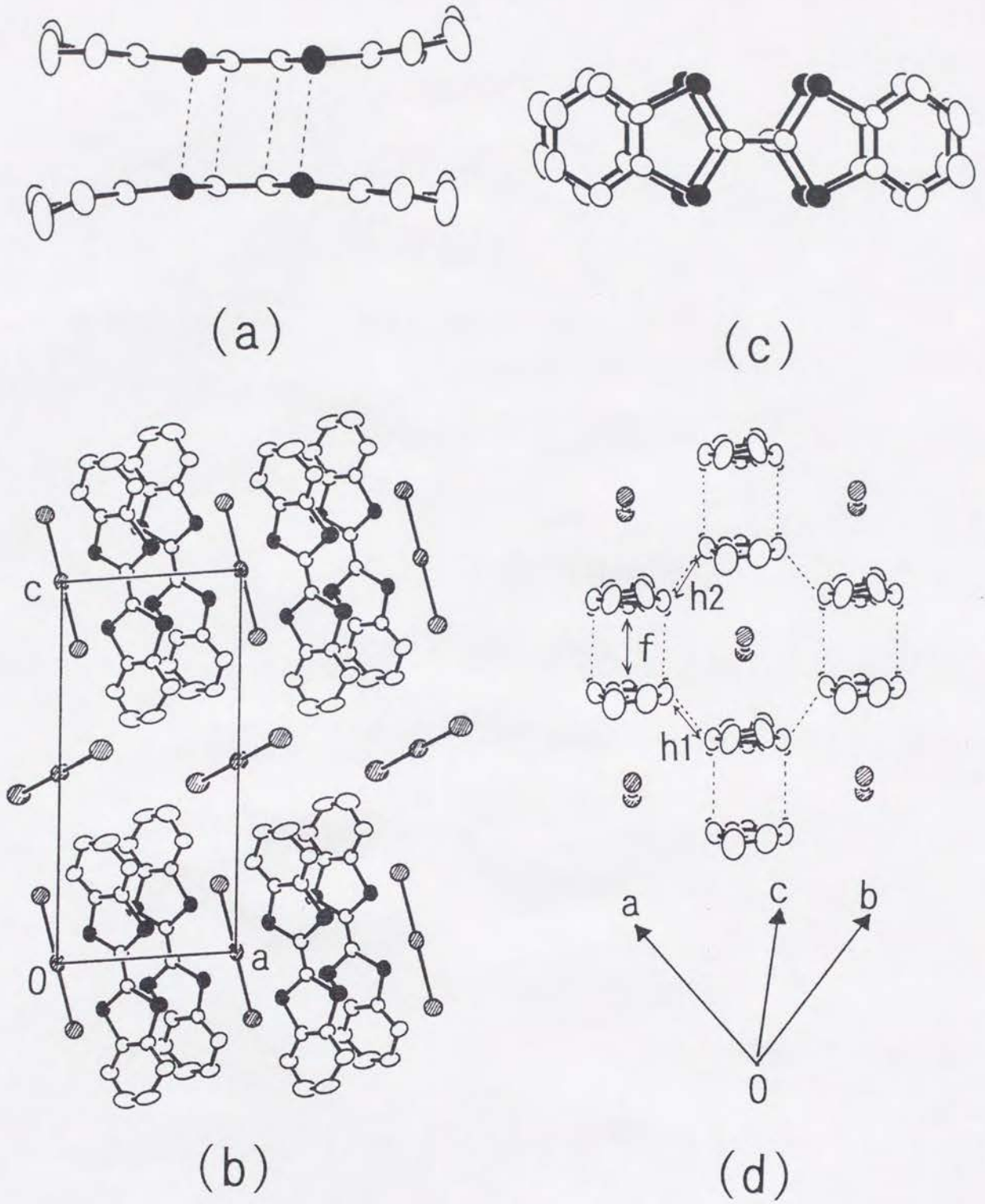

Figure 4-10. Crystal structures of (BEDO-TTF)I_3 (42). (a) (BEDO-TTF^+)$_2$ dimer viewed on the short molecular axis. Short S··S (3.31 Å) and C··C distances (3.31 Å) are shown by dotted lines. Sulfur atoms are filled. (b) Crystal structure viewed along the *b* axis. Sulfur and iodine atoms are filled and shaded, respectively. (c) (BEDO-TTF^+)$_2$ dimer projected on the molecule. (d) Molecular packing in the (BEDO-TTF)-I_3 mixed layer (z = 0) projected along the longitudinal axis of BEDO-TTF molecule. Dotted lines represent short S··S distances (< 3.6 Å).

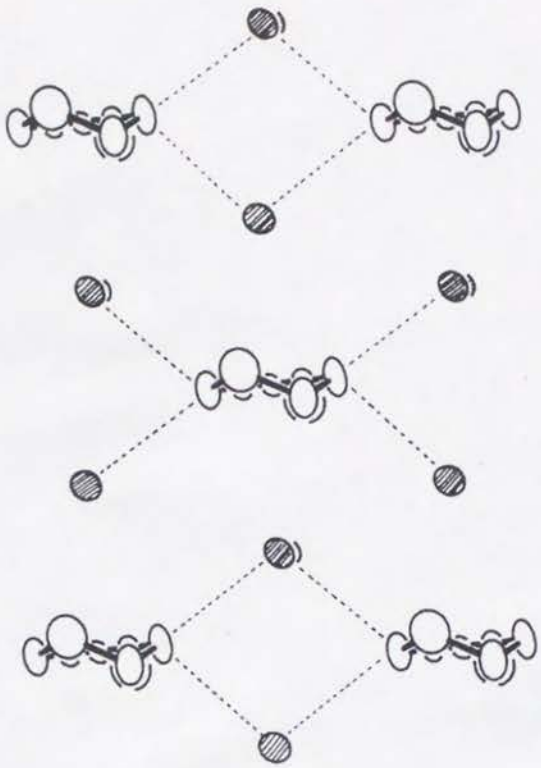

(a)

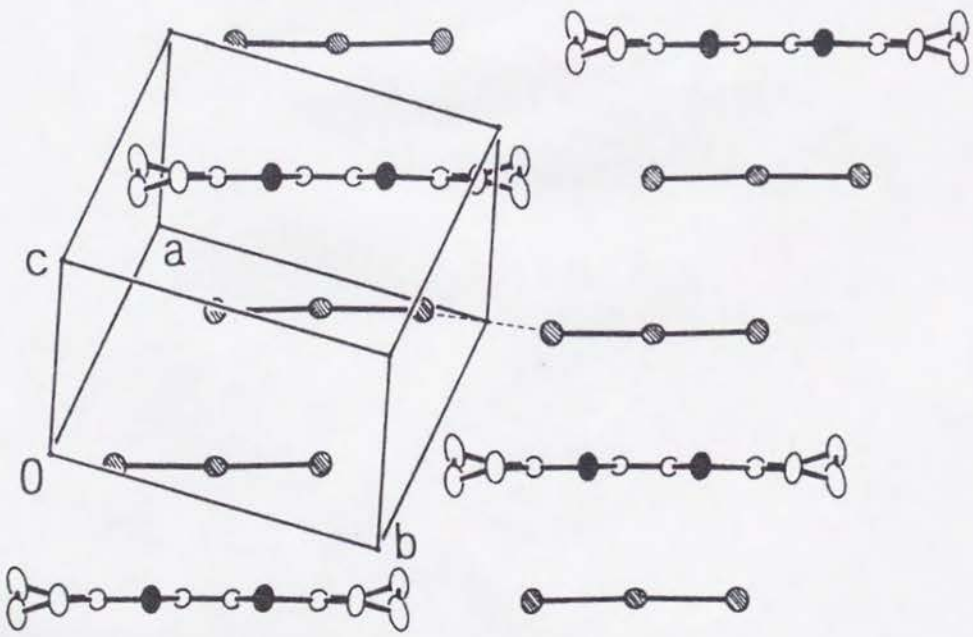

(b)

Figure 4-11. Crystal structure of (BEDO-TTF)$(I_3)_2$ (43) projected along (a) the longitudinal and (b) transverse axes of BEDO-TTF molecule. Iodine and sulfur atoms are shaded and filled, respectively. Short I··I (3.74 Å) and S··I distances (3.60-3.78 Å) are shown by the dotted lines.

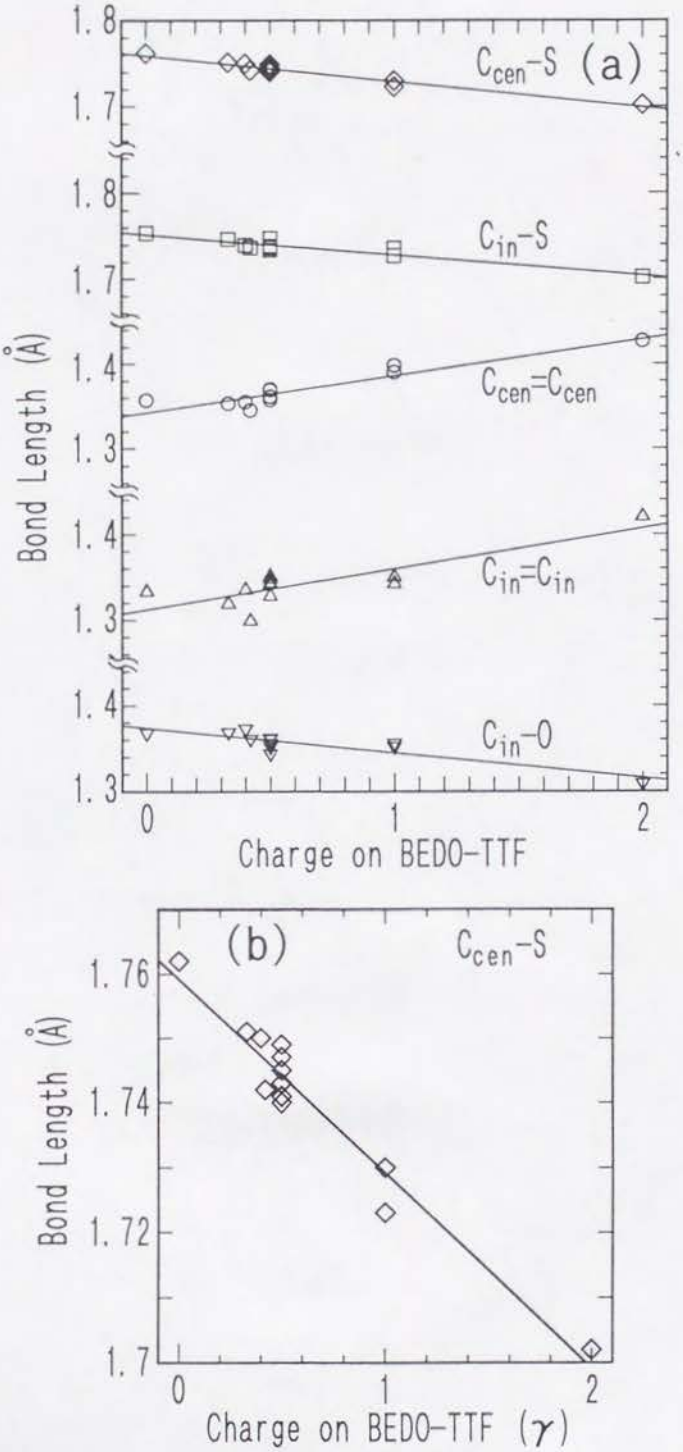

Figure 4-12. Averaged bond distances (Å) of BEDO-TTF molecules as a function of averaged charge on the molecule (γ) (a). The best correlation found for C_{cen}-S is expanded in (b). The solid lines represent the respective least squares fit.

Chapter 5 Electronic States of BEDO–TTF Complexes

5–1 Introduction

The band electronic structure of molecular metals has been of considerable interest, because it has been possible to rationalize many experimental observations even by the simple calculations.[105] Also, to understand the correlation between the crystal and electronic structures has been an essential step for the search and design of materials with interesting and novel properties. The calculated band structures have already been reported for 7 BEDO–TTF complexes.[26c,27a,38,106,107] Including these, this chapter will demonstrate the band structures of 15 BEDO–TTF complexes with known structures, in order to examine the relation between the packing types and band structures. The present calculations, which differ in parameters used from the refs. 26c, 27a, 38, and 102, have reproduced qualitatively the same energy dispersions and Fermi surfaces as the reported ones. The present results emphasize that 2D bands are realized particularly for the typical packing (i.e. the I_3) type of this donor molecule. The origin of 2D intermolecular overlap will be discussed from the molecular point of view based on the comparison of BEDO–TTF and BEDT–TTF conductors.

5–2 Molecular Orbital Calculations

Figure 5–1 shows the HOMO, second HOMO (SHOMO), and LUMO of BEDO–TTF calculated by extended Hückel method based on the molecular structure in 34. It also exhibits the calculated HOMO of BEDT–TTF in the $(BEDT\text{–}TTF)_2ClO_4(TCE)_{0.5}$.[36] Each HOMO has the same symmetry (b_{1u}) and the maximum coefficients on S_{in} atoms. It should be noted that the coefficients on the oxygen atoms in BEDO–TTF are much smaller than those on the S_{out} atoms

in BEDT-TTF. The calculated HOMO is bonding on the C=C bonds and antibonding on the C-S and C_{in}-O bonds, which was qualitatively proved by the change of bond distances with increasing γ as discussed above.

5-3 Intermolecular Overlap Integral.

The intermolecular overlap integrals in the I_3, HCP and Cl types are classified into six types (p, q, r, s, u, w) according to their packing motives as follows. The I_3 type exhibits three kinds of interactions within a stack (s_i: i = 1-3), and between stacks along the transverse (p_i: i = 1-3) and oblique (q_i: i = 1-3) directions (for example see Figure 4-1a). For the HCP salt (37), s, p, q are defined in the same way for the interactions in the stacking pairs AA' and BB' whose packing motif is closely related to the I_3 type. An additional interaction in the pairs A'B and B'A is denoted by u (Figure 4-6a). The intra- and interstack interactions of the Cl type are labeled differently (r and w, respectively) from those in the other two types because of the distinct donor packing. The donor layer in κ type complex, $(BEDO\text{-}TTF)_2CF_3SO_3$,[38] which is made up of the orthogonal $(BEDO\text{-}TTF)_2^+$ dimers instead of stacks, consists of one intradimer (v) and three interdimer (l_i, i = 1-3) interactions (Figure 4-7c).

Table 5-1 summarizes the calculated overlap integrals. The I_3 and HCP types show the same trend in the magnitude of s, p and q; the intrastack interactions are the smallest ($3\times10^{-3} < s < 6\times10^{-3}$) while the side-by-side ones (p) are larger than 10^{-2}, reflecting the multi heteroatom contacts. The oblique interstack interactions (q) are as large as the value of p, despite the absence of S$\cdots$S vdW contacts. The 2D semimetal $(BEDT\text{-}TTF)_2(ClO_4)(TCE)_{0.5}$ has been shown to be an example of intrastack interaction being smaller than the interstack ones.[36a] In the HCP salt, the interstack interaction between the

non-parallel molecules (u) is small compared with those between parallel molecules (p, q). The Cl type shows intrastack interaction (r) comparable to the interstack one (w), though the former is much larger than s_i in other salts. The intradimer interaction v (24.4×10^{-3}) in κ type complex, (BEDO-TTF)$_2$CF$_3$SO$_3$, which exceeds the interdimer interactions ($l_1 = -4.7\times10^{-3}$, $l_2 = 6.8\times10^{-3}$, $l_3 = 16.6\times10^{-3}$), is the largest among these BEDO-TTF complexes.

In the I_3, HCP, and Cl types, the interstack interactions are found to be significant. The hint to the origin of these interactions was found by the following examination of the relation between of interaction magnitude and the side-by-side atomic contacts. In the radical salts, there are two or three short S$\cdots$S ($\leq$ 3.60 Å) and one or two S$\cdots$O ($\leq$ 3.32 Å) contacts (Figure 5-2a), which combination results in the large p. For our comparison, we calculated the interactions in the neutral BEDO-TTF and the neutral complexes, (BEDO-TTF)[Q(OH)$_2$]$_2$ (**27**) and (BEDO-TTF)(TNBP) (**29**). The former two crystals are very similar in side-by-side array, which includes only one short S$\cdots$S and two S$\cdots$O contacts (Figure 5-2b). Compared with neutral BEDO-TTF (-1.8×10^{-3}), the very short S$\cdots$S distance (3.20 Å) in **27** enhances the overlap integral (3.8×10^{-3}), which is, however, much smaller than those in the radical salts ($p > 10\times10^{-3}$). The interaction between the donor molecules linked by only two S$\cdots$O contacts in **29** (Figure 5-2c) is even smaller (0.2×10^{-3}). These facts indicate that the number of the $S_{in}\cdots S_{in}$ rather than the $S_{in}\cdots O$ contacts is critical for the increment of the side-by-side interactions.

To examine how the heteroatoms of BEDO-TTF contribute to the intermolecular interactions, we calculated the overlap integrals assuming zero coefficients of the HOMO for all the orbitals on the outer ethylenedioxy groups. For example, in (BEDO-TTF)$_{2.4}$I$_3$, the magnitude of the overlap integrals ($\times10^{-3}$) decreases slightly; s, 5.5 → 5.3 (−3.1 %); p, 15.2 → 15.0 (−1.9 %); and q, 13.0 → 12.6 (−3.4 %). Therefore, contribution of the oxygen atoms to

the interactions is slight. For comparison, we performed an analogous calculation on β''-(BEDT-TTF)$_2$AuBr$_2$, because of the similar donor arrangement to the I_3 type,[108] and obtained contrastive results with those for BEDO-TTF as follows. Eliminating the HOMO coefficients on the ethylenedithio groups results in a considerable decrease in overlap integrals: ($\times 10^{-3}$) intrastack, 1.5 → 0.2 (-83 %), 6.6 → 3.9 (-41 %); side-by-side, 8.7 → 5.9 (-32 %), 9.6 → 4.4 (-54 %); oblique, 15.0 → 11.3 (-25 %). This indicates the importance of the S_{out} atoms in the intermolecular interactions of BEDT-TTF.

To account for such a difference between two analogous donors, one must compare their HOMOs (Figure 5-1). Their features can be summarized as follows: i) the coefficients on the carbon atoms show little difference between the donors; ii) larger coefficients are found on the S_{in} atoms (0.44, 0.41) than on the outer heteroatoms (0.06 (O), 0.17 (S_{out})) for BEDO-TTF and BEDT-TTF, respectively; iii) the coefficients on the oxygen atoms (0.06) are very small compared to those of on the S_{out} atoms (0.17); iv) the C_{out} atoms have coefficients of almost zero. From ii), the inner sulfur atoms can be regarded as the most effective for increasing interactions for both donors. Due to iii), the contribution of the oxygen atoms is much smaller than that of the S_{out} atoms of BEDT-TTF, which represents the clear distinction between the two donors.

In addition to the character of the HOMOs, the steric factors must be considered, particularly in the case of the side-by-side interactions. As discussed in the previous section, the smaller six-membered ring enables the closer $S_{in}\cdots S_{in}$ contacts among BEDO-TTF molecules as compared to the BEDT-TTF molecules. Reflecting this, the side-by-side interaction p in the (BEDO-TTF)$_{2.4}I_3$ (15.2×10^{-3}) is much larger than the corresponding ones in β''-(BEDT-TTF)$_2$AuBr$_2$ (8.7×10^{-3}, 9.6×10^{-3}).

To summarize the above discussion, the large intermolecular interactions in

the BEDO-TTF salts are realized by the sterically-allowed close contacts among the inner sulfur atoms having maximum HOMO coefficients.

5-4 Band Electronic Structure

5-4-1 Band Structure of I_3-Type Complexes

The calculated Fermi surfaces, energy dispersions, and densities of states (DOS) are shown in Figure 5-3. The complexes 33, 39, and 41 contain only one donor molecule in the respective unit cell to form one HOMO band. The resulting Fermi surfaces are ellipses elongated approximately along the stacking direction where the intermolecular interactions are the weakest (Figure 5-3a,b,c).

For other I_3 type salts containing a large number of donor molecules in the unit cell, the first Brillioun zones (BZs) are folded according to the respective periodicity. While a closed Fermi surface remains unfolded in 25 and (BEDO-TTF)$_3$Cu$_2$(NCS)$_3$ (Figure 5-3d,e), the respective BZs fold the original closed ones, producing closed pockets and/or open Fermi surfaces for the 31, 34, 40, (BEDO-TTF)$_2$X (X = ClO_4, $AuBr_2$) and (BEDO-TTF)$_2$ReO$_4$(H$_2$O). For example, the Fermi surfaces of 31 consist of closed ones centered around the B point and open ones along the k_c direction (Figure 5-3f). In the case of 34 (Figure 5-3g), two electron-like and one hole-like pockets are centered around B, Z and X points, respectively. The hole-like pocket at B point and two pairs of open orbits for 40 are unambiguously recognized as a result of superposition of original ellipse-like Fermi surfaces centered at B point. Table 5-1 summarizes the respective area ratios of the closed Fermi surfaces to the BZ (S_{FS}/S_{BZ}), the density of states at the Fermi level $N(E_F)$, and band width W.

With the exception of (BEDO-TTF)$_2$AuBr$_2$ with 1D character, all I_3 type salts show 2D Fermi surfaces. The 2D nature is supported by the nearly isotropic

conductivities in the layer for 31 ($\sigma_{a+2c}/\sigma_{2a-c}$ = 0.4), 40 (σ_{a-c}/σ_{c} ~ 0.4), and (BEDO–TTF)$_2$ReO$_4$(H$_2$O) (σ_a^*/σ_c = 1/3)[106b]. Also, for (BEDO–TTF)$_2$ReO$_4$(H$_2$O), the recent observations of the Shubnikov–de Haas effect[106b] confirm the existence of the closed pockets. It is thus concluded that BEDO–TTF tends to form a 2D electronic structure due to the large interstack interactions, *p* and *q*.

5–4–2 Band Structure of Other Packing Types

The Fermi surface of metallic (BEDO–TTF)$_2$Cl(H$_2$O)$_3$ (38a) is close to a circle, which phenomenon arises from almost the isotropic intermolecular overlap (*w*) within a donor layer (Figure 5–31).[109] Recently, Mori *et al.* reported the Shubnikov–de Haas and de Haas–van Alphen effects,[107] confirming the existence of the closed Fermi surfaces with S_{FS}/S_{BZ} of 50 %.

2D nature is also calculated for κ–(BEDO–TTF)$_2$CF$_3$SO$_3$ (Figure 5–3n). The closed Fermi surface is folded at the ZM zone boundary where the energy dispersion is degenerate. This band structure is very similar to those of κ'–(BEDT–TTF)$_2$Cu$_2$(CN)$_3$ and κ–(BEDT–TTF)$_2$I$_3$ rather than κ–(BEDT–TTF)$_2$X (X = Cu(NCS)$_2$, Cu(CN)[N(CN)$_2$]) which show an energy gap on the zone boundary. κ–(BEDO–TTF)$_2$CF$_3$SO$_3$ is a semiconductor, which contradicts with the calculation. Electron localization induced by the strong dipole moment of $CF_3SO_3^-$ ion is proposed for the origin of the semiconducting behavior.

(BEDO–TTF)$_5$(HCP)(PhCN)$_{0.2}$ (37) shows four HOMO bands, which are much more dispersive along the b^* than along the c^* axis (Figure 5–3m). The energy band at the ZM zone boundary is degenerate due to the existence of the *c* glide plane. The Fermi level determined by γ = 0.40 cuts the upper two bands along the b^* direction. The resulted Fermi surfaces are open and very similar to those of α"–(BEDT–TTF)$_2$CsHg(SCN)$_4$, as is the donor packing.[92] The two Fermi surfaces are well superposed to each other by

translation vector Q (= $3/5b^*$) (arrows in Figure 5-3m). The nesting of the Fermi surfaces, which is often seen in the quasi-1D materials, typically causes the CDW or SDW-associated metal-insulator transition. As mentioned above, the anion arrangement in 37 is considered to give the superlattice of (a, $5b$, c), which corresponds to the vector Q. Although the structural analysis assumes a uniform donor stack, the periodicity of the anions should distort the stack more or less through the electrostatic interaction in the actual crystal. With a little periodic potentials on the stack, the electronic system can gain large stabilization energy due to the almost perfect nesting and the larger $N(E_F)$ as compared to other BEDO-TTF salts (Table 5-1). This is the most plausible reason for the semiconducting nature of 37.

5-4-3 Density of State

Next we will see the density of states (DOS) in the metallic BEDO-TTF salts. The shapes of Fermi surfaces and band fillings vary with salts, but, following common features can be seen in the DOSs of the HOMO bands. i) Their total bands have no energy gaps, owing to the nearly uniform donor packing. ii) Their widths (0.9-1.2 eV) are little dependent on the salts. iii) The DOS's are almost independent on the energy in their upper region where the Fermi level lies, and the maximum peaks appear in the lower region. These similarities can be attributed to the similar donor arrangements and intermolecular interactions. It should also be noted that the $N(E_F)$ values are almost independent on the salts (Table 5-1).

Finally, we will discuss the relation between the conducting properties and the DOS of BEDO-TTF salts. The higher superconducting transition temperature (Tc) is often found to be originated from the larger $N(E_F)$. In the case of BEDT-TTF based superconductors, Tc values have been found to be proportional to the volume of the space of the delocalized carriers, which

should be related to the $N(E_F)$.[91] On the other hand, the narrower band width enhances the effective mass of conduction electrons. Therefore, poor conductivity is generally expected in the salts having large $N(E_F)$, assuming equivalent relaxation time and concentrations of carriers. It is interesting to note that the $N(E_F)$ values of the superconducting $Cu_2(NCS)_3$ and ReO_4 salts (Tc ~ 1 K) are the largest (1.46 states(total)/(eV·molecule)) among the metallic BEDO–TTF salts. These values are, however, much smaller than those of κ–$(BEDT\text{–}TTF)_2X$ salts (X = $Cu(NCS)_2$, $Cu[N(CN)_2]Br$, $Cu(CN)[N(CN)_2]$) with high Tc (10–13 K) ($N(E_F)$ = 1.8–2.1 states(total)/(eV·molecule)).[94,110] Such low $N(E_F)$ may be one of the reasons why the Tc of the BEDO–TTF salts are very low. Conversely, concerning the σ_{rt} values, BEDO–TTF (70–200 $S\cdot cm^{-1}$) is superior to the above κ–$(BEDT\text{–}TTF)_2X$ salts (40–50 $S\cdot cm^{-1}$), which concurs with the above expectation. Therefore, one should increase $N(E_F)$ to obtain the BEDO–TTF salts of higher Tc. To meet this requirement, two methods can be proposed; one is the reduction of the intermolecular overlap integrals by modification of the molecular array, and the other is the control of the γ value. However, the former seems rather difficult since BEDO–TTF tends to form the same (I_3 type) array independently on the anions. Considering the energy-dependence of the DOS of the above BEDO–TTF salts, increasing γ and hence lowering the Fermi level will raise the $N(E_F)$; γ = 1.1–1.3 corresponds to the maximal $N(E_F)$. To put it another way, further oxidation is needed for higher Tc.

5–4–4 Calculations of Thermoelectric Power

Tight-binding band calculation is also useful for the analysis of thermoelectric power.[111] The Boltzmann equation[112] represents the thermoelectric power tensor (S) of metals as

$$S_{ij} = \frac{1}{eT} \sum_{k=1}^{3} (L_0^{-1})_{ik} (L_1)_{kj} \qquad (5.1)$$

$$(L_0)_{ij} = e^2 \int \left(\frac{dk}{4\pi^3}\right) \left(-\frac{\partial f^0}{\partial \varepsilon}\right) \tau v_i(k) v_j(k) \qquad (5.2)$$

$$(L_1)_{ij} = e^2 \int \left(\frac{dk}{4\pi^3}\right) \left(-\frac{\partial f^0}{\partial \varepsilon}\right) \tau v_i(k) v_j(k) (\varepsilon(k) - \mu) \qquad (5.3)$$

where $(L_0)_{ij}$ and $(L_1)_{ij}$ are tensors, f^0 is the Fermi distribution function, τ is the relaxation time of the carriers, and μ is the chemical potential. The velocity $v = (\partial \varepsilon(k)/\partial k)/h$ at wave vector k was obtained from the tight-binding band structures. The most simple example is (BEDO-TTF)$_{2.4}$I$_3$ (41), which shows only one HOMO band represented as

$$\varepsilon(k) = 2t_q \cos(k \cdot a) + 2t_p \cos[k \cdot (a-b)] + 2t_s \cos(k \cdot b) \qquad (5.4)$$

The thermoelectric powers along the *a* (oblique interstack) and *b* (stacking) directions were obtained by numerical calculations using the above calculated transfer integrals. The thermoelectric powers at room temperature (S_{rt}) are plotted in Figure 5-4 as a function of charge on the donor molecule (γ). The plotted curves for both directions are very similar to each other for $0 < \gamma < 1$, and this small in-plane anisotropy is in good agreement with the experimental results (4 and 5 μV/K for *a* and *b* directions, respectively).[25b] Also these small positive values are comparable to that calculated from $\gamma = 0.42$ (12 and 13 μV/K, respectively).

The S_{rt} values, which show large positive, decrease with increasing γ, and turn to be negative at around $\gamma = 0.8$. As already noted, the metallic complexes 25, 31, 34, 39, and 40 as well as (BEDO-TTF)$_3$Cu$_2$(NCS)$_3$[26e] and (BEDO-TTF)$_2$ReO$_4$(H$_2$O)[27b] exhibited almost the same donor packing patterns and intermolecular interactions as those in 41. Therefore, their band electronic structures can be regarded as essentially unchanged, and consequently S_{rt} values are expected to show this γ dependence. The observed S_{rt} values for these BEDO-TTF complexes plotted by open squares in

Figure 5-4 are roughly distributed along the calculated curves, confirming the above expectation.

On the other hand, the calculated S is simply proportional to the temperature, and hence, it alone cannot elucidate the minimum peak observed in the actual temperature dependence. The complicated temperature dependence may be originated by the scattering mechanism, which has been proposed for the 2D β-(BEDT-TTF)$_2$I$_3$ having a similar ellipse-like Fermi surface.[113]

5-5 (BEDO-TTF)I_3 (42)

The donor molecules in the complex 42 form dimers, which alternate with I_3^- anion to show layers of (BEDO-TTF$^+$)$_2I_3^-$ (see Figure 4-10d). In this mixed layer, three kinds of interactions are found among BEDO-TTF$^+$ molecules. One is the intradimer interaction with very large overlap integral (57.1×10^{-3}, denoted by *f* in the figure), due to the eclipsed face-to-face overlap with considerably short four S$\cdots$S distances (3.31 Å). The others are interdimer interactions labeled by *h1* (25.2×10^{-3}) and *h2* (23.8×10^{-3}) in Figure 4-10d. These interdimer interactions are stronger than those observed for metallic complexes ($\leq 15\times10^{-3}$), but much weaker than *f*. Therefore, the calculated HOMO band has an energy gap (0.1 eV) between the two dispersions (Figure 5-5). Almost isotropic interdimer interactions within the mixed layer lead to 2D dispersions in both upper and lower bands. With monovalent state of the donor molecule, the lower band is completely filled, which qualitatively agrees with the insulating and diamagnetic ground state of this salt as shown in Chap. 3.

5-6 Origin of Stable Metallic States of BEDO-TTF Complexes.

Here we discuss the origin of the metallic behavior of BEDO–TTF complexes from a molecular point of view. One of the important features of the BEDO–TTF radical salts is the self-assembled layered structure of the donor molecule. Such a layered structure is essential, but alone is not sufficient for the 2D electronic structure which will suppress the Peierls transition and stabilize the metallic state to the low temperature. In the I_3 type, two kinds of large interstack interactions (p, q) of almost the same magnitude are crucial for 2D. Although BEDO–TTF is analogous to BEDT–TTF, their 2D nature is realized in different ways. The outer heteroatoms directly contribute to the increment of the interstack interactions in the BEDT–TTF compounds, but not in the BEDO–TTF. Instead, the oxygen atoms of a BEDO–TTF molecule play two kinds of indirect roles in fabricating the 2D electronic structure. The first role is that the small oxygen atoms allow close contacts among the inner sulfur atoms sterically, and consequently enhance the intermolecular overlap. The second is that the electronegative oxygen atoms drive the molecules to assemble into the I_3 type array via the C–H··O interactions, so that a higher-dimensional electronic structure is achieved. Chart 5–1 schematizes these roles of heteroatoms in stabilizing metallic state.

Another important characteristic of the BEDO–TTF complexes is their wide band width, which is also the stabilizing factor of the metallic state. In the case of molecular metals of TTF–TCNQ system, most are 1D so that the band width is described simply by $4t$ where t is the transfer integral. The overlap integral of the TTF derivatives (excluding Se derivatives) maximizes when the molecules stack in a face-to-face eclipsed manner.[36a] In this case, overlap integral is at most 25×10^{-3}, and thus the band width is narrower than 1 eV using $t = -ES$ where $E = -10$ eV. Although the individual overlap integrals are much smaller than 25×10^{-3} in the BEDO–TTF complexes, the calculated total

bands in the I_3 and Cl types have as large widths as 0.9–1.2 eV, owing to 2D interactions. In the case of BEDT–TTF salts, strong dimerization of the donor molecules frequently splits the HOMO bands and sometimes leads to the Mott insulator.[114] For BEDO–TTF salts, on the other hand, the almost uniform array of the donor molecules prevents an opening of the energy gap in the HOMO bands.

Table 5-1. Results of Band Calculations of BEDO-TTF Complexes of I_3, HCP, and Cl types

complex		type	intrastack				interstack								$N(E_F)$[a]	W,[b] eV	S_{FS}/S_{BZ}[c] (center)
			s1	*s2*	*s3*	*r*	*p1*	*p2*	*p3*	*q1*	*q2*	*q3*	*u*	*w*			
$(BEDO\text{-}TTF)_{2.4}I_3$	(41)	I_3	5.5				15.2			-13.0					1.30	1.13	42(Y)
$(BEDO\text{-}TTF)_{10}(CF)_4(H_2O)_3$	(33)	I_3	5.9				14.9			-13.3					1.26	1.13	40(Z)
$(BEDO\text{-}TTF)_2Br(H_2O)_3$	(39)	I_3	5.6				14.6			-13.4					1.30	1.12	50(Z)
$(BEDO\text{-}TTF)_2(HCHA)$	(25)	I_3	6.6				14.9			-12.8					1.36	1.11	50(Z)
$(BEDO\text{-}TTF)_5HCTMM(PhCN)_2$	(31)	I_3	-5.6	3.8	-3.7		-12.9	-13.2	-14.6	-15.6	14.4	9.8			1.36	1.10	25(B)
$(BEDO\text{-}TTF)_4SQA(H_2O)_6$	(34)	I_3	5.3	6.2			12.3			-13.5					1.46	1.03	8.0(X), 2.8(B), 5.1(Z)
$(BEDO\text{-}TTF)_2Br[MnBr_2(H_2O)_4](H_2O)$	(40)	I_3	5.9	5.7			14.8	14.5	14.6	-13.7	-12.1				1.46	1.10	5.2(B)
$(BEDO\text{-}TTF)_2ClO_4$		I_3	5.9				14.1			-13.6					1.40	1.11	1.7(Z)
$(BEDO\text{-}TTF)_2AuBr_2$		I_3	-5.2				-14.6			-9.3	-14.4				1.30	1.07	
$(BEDO\text{-}TTF)_3Cu_2(NCS)_3$		I_3	5.3	-4.3			-13.2	-10.2		-10.0	12.6				1.46	0.92	50(Z)
$(BEDO\text{-}TTF)_2ReO_4(H_2O)$		I_3	3.3	4.8			11.7	12.8		-13.3	-14.7				1.46	1.05	8.4(X), 6.5(B), 2.0(Z)
$(BEDO\text{-}TTF)_5HCP(PhCN)_{0.2}$	(37)	HCP	5.6				-13.8			13.3			-7.8		1.93	0.73	
$(BEDO\text{-}TTF)_2Cl(H_2O)_3$	(38a)	Cl				-11.4								-14.6	1.20	1.22	50(r)

[a] Fermi-level DOS including spin degeneracy; units, states(total)/(eV molecule of BEDO-TTF). [b] Total band width.

[c] Area ratio (%) of closed Fermi surface to the Brillioun zone.

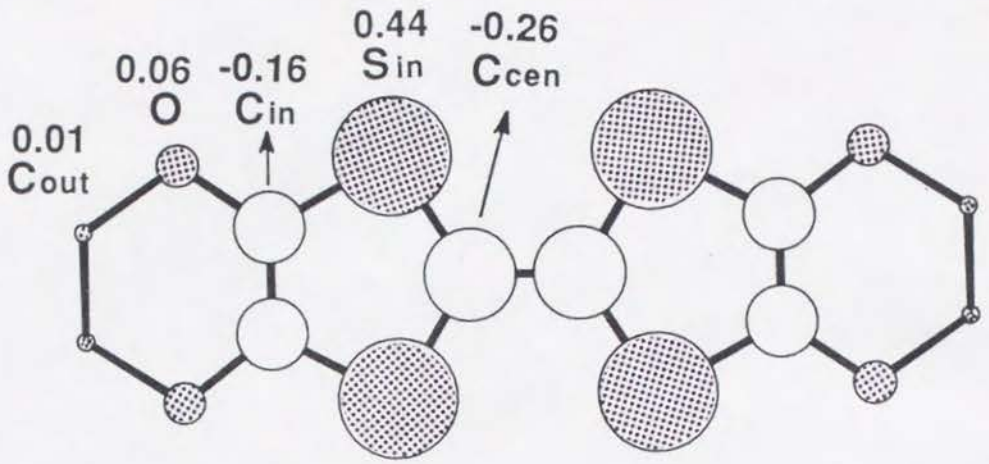

BEDO-TTF

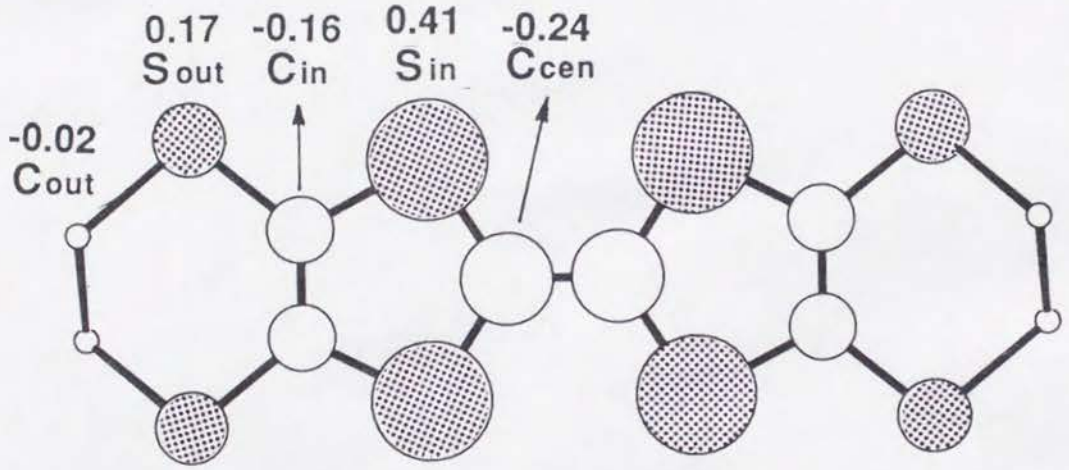

BEDT-TTF

Figure 5-1. Calculated HOMO coefficients of BEDO-TTF and BEDT-TTF. The magnitude of the coefficient is shown by the radius of the circle.

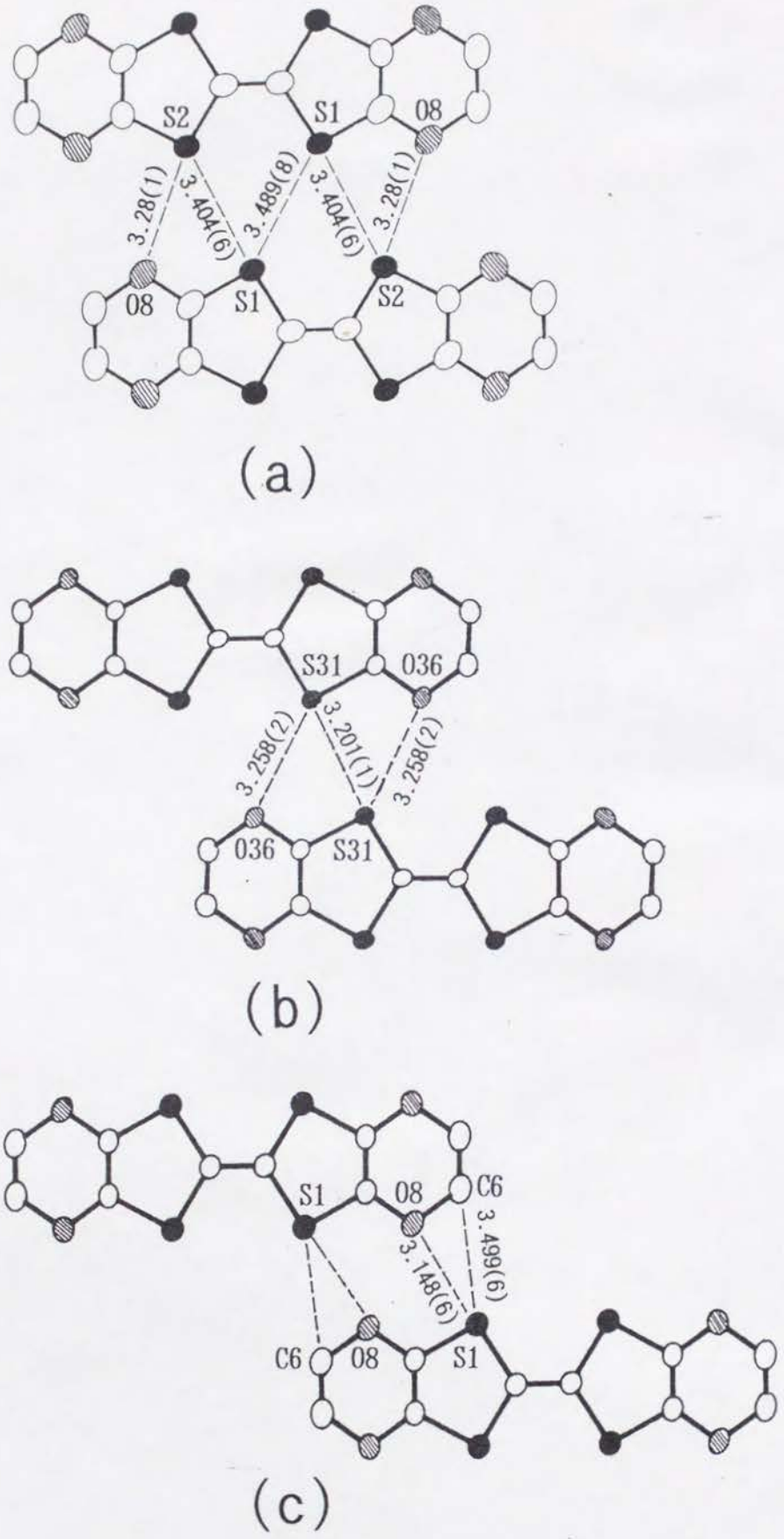

Figure 5-2. Comparison of side-by-side heteroatom contacts in (a) the metallic BEDO-TTF complexes (e.g. 33), (b) (BEDO-TTF)[Q(OH)$_2$]$_2$ (27), and (c) (BEDO-TTF)(TNBP) (29). Sulfur and oxygen atoms are filled and shaded, respectively. The distances of heteroatom contacts are given in angstrom.

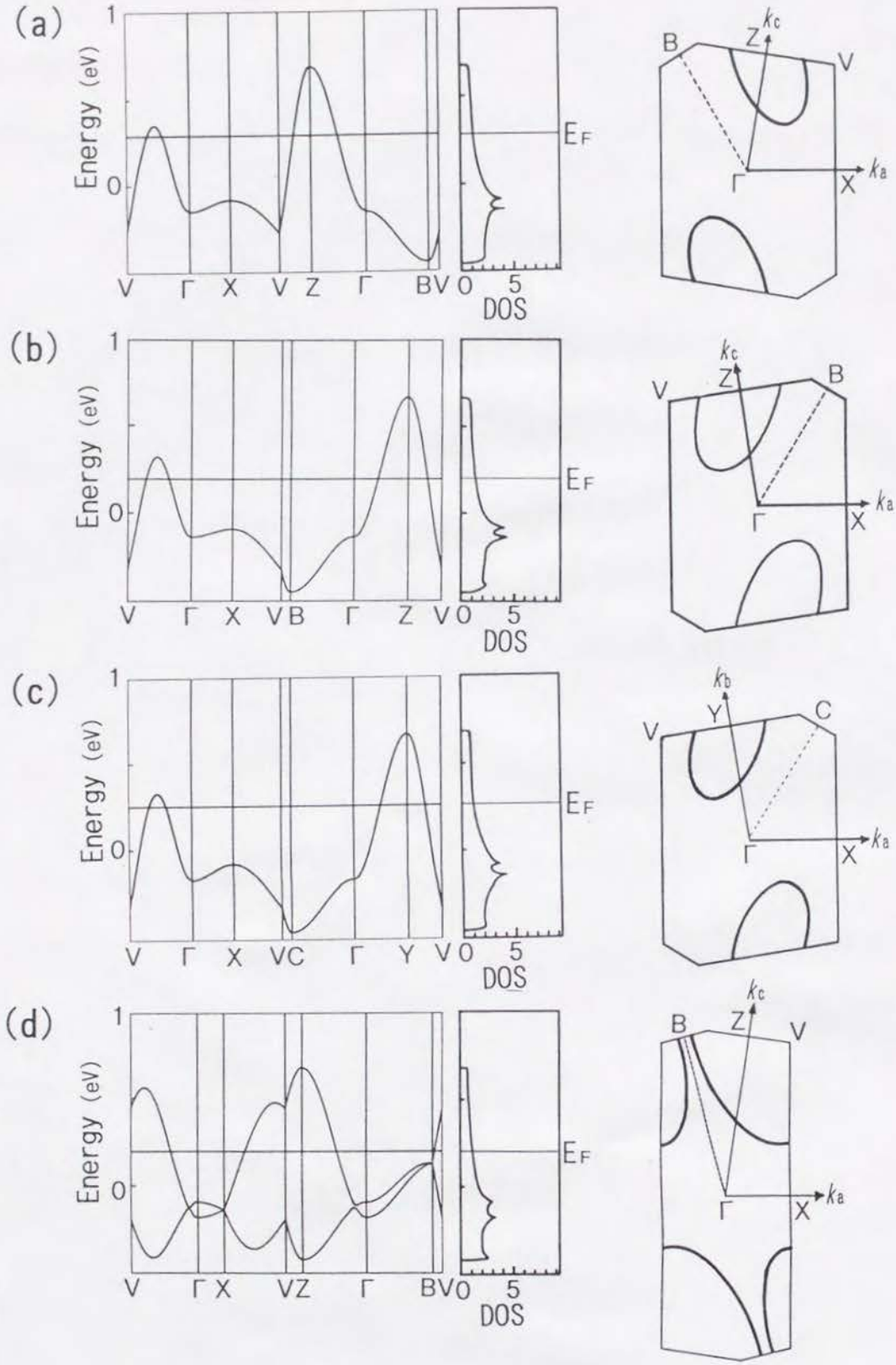

Figure 5-3. Calculated band structures, densities of states (DOSs), and Fermi surfaces of (a) $(BEDO\text{-}TTF)_{10}(CF)_4(H_2O)_3$ (33), (b) $(BEDO\text{-}TTF)_2Br(H_2O)_3$ (39), (c) $(BEDO\text{-}TTF)_{2.4}I_3$ (41), (d) $(BEDO\text{-}TTF)_2(HCHA)$ (25), (e) $(BEDO\text{-}TTF)_3Cu_2(NCS)_3$, (f) $(BEDO\text{-}TTF)_5(HCTMM)(PhCN)_2$ (31), (g) $(BEDO\text{-}TTF)_4(SQA)(H_2O)_6$ (34), (h) $(BEDO\text{-}TTF)_2Br[MnBr_4(H_2O)_2](H_2O)$ (40), (i) $(BEDO\text{-}TTF)_2ClO_4$, (j) $(BEDO\text{-}TTF)_2AuBr_2$, (k) $(BEDO\text{-}TTF)_2ReO_4(H_2O)$, (l) $(BEDO\text{-}TTF)_2Cl(H_2O)_3$ (39a), (m) $(BEDO\text{-}TTF)_5(HCP)(PhCN)_{0.2}$ (37), and (n) κ-$(BEDO\text{-}TTF)_2CF_3SO_3$. The DOSs are given in states(total)/(eV·molecule of BEDO-TTF). The nesting vector Q is represented by arrows in (m) (continued to next three pages).

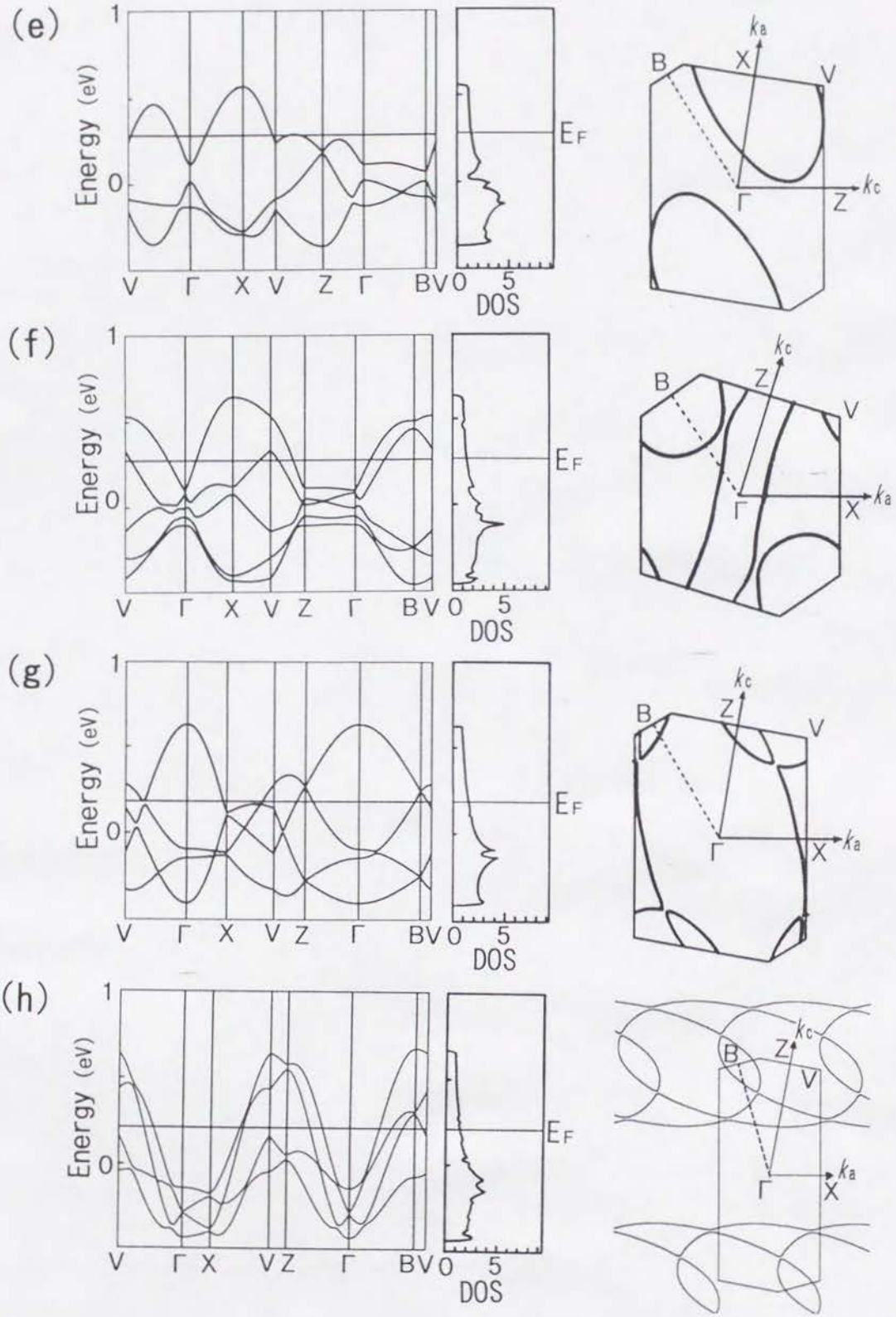

Figure 5-3. (Continued)

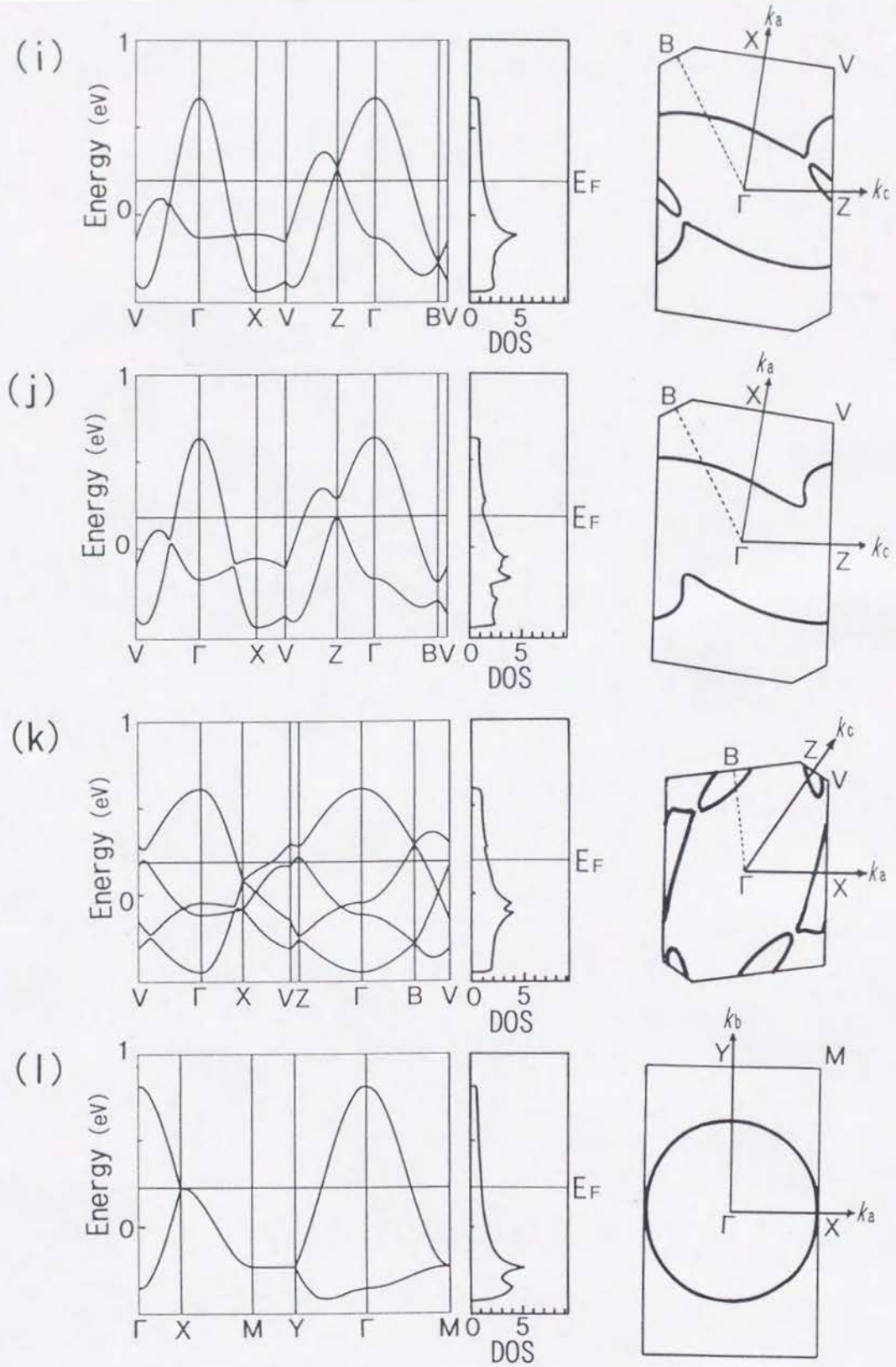

Figure 5-3. (Continued)

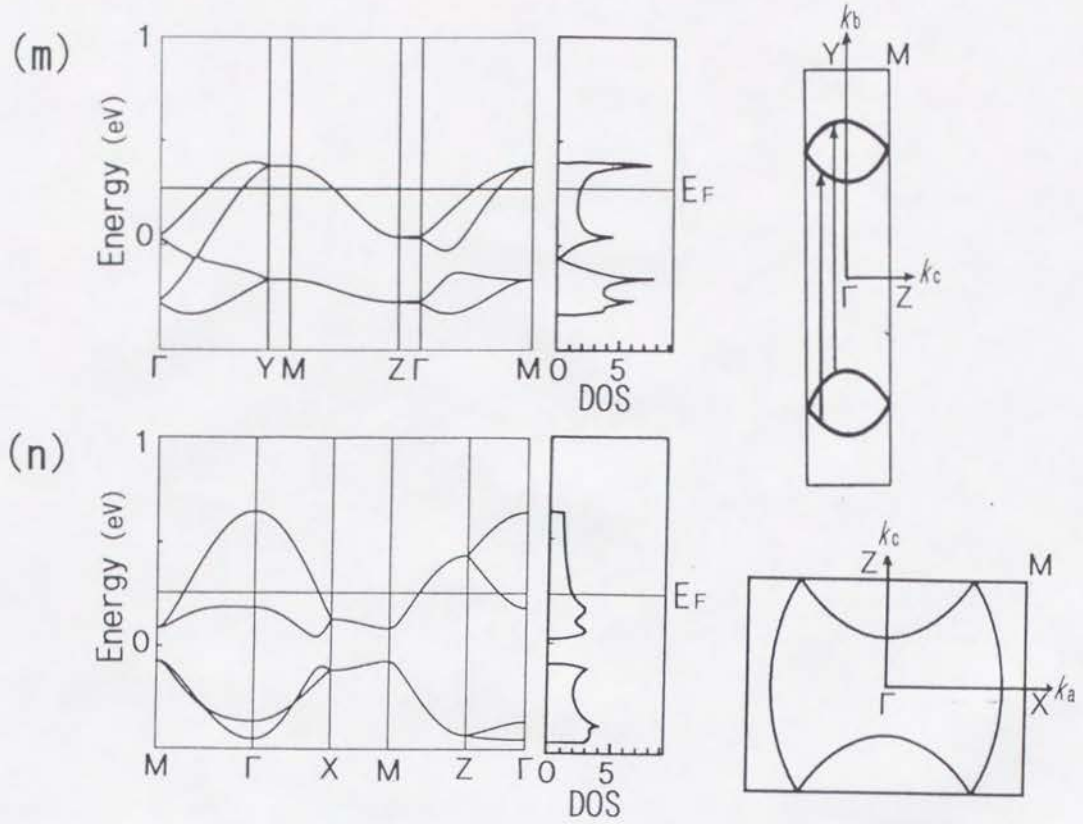

Figure 5-3. (Continued)

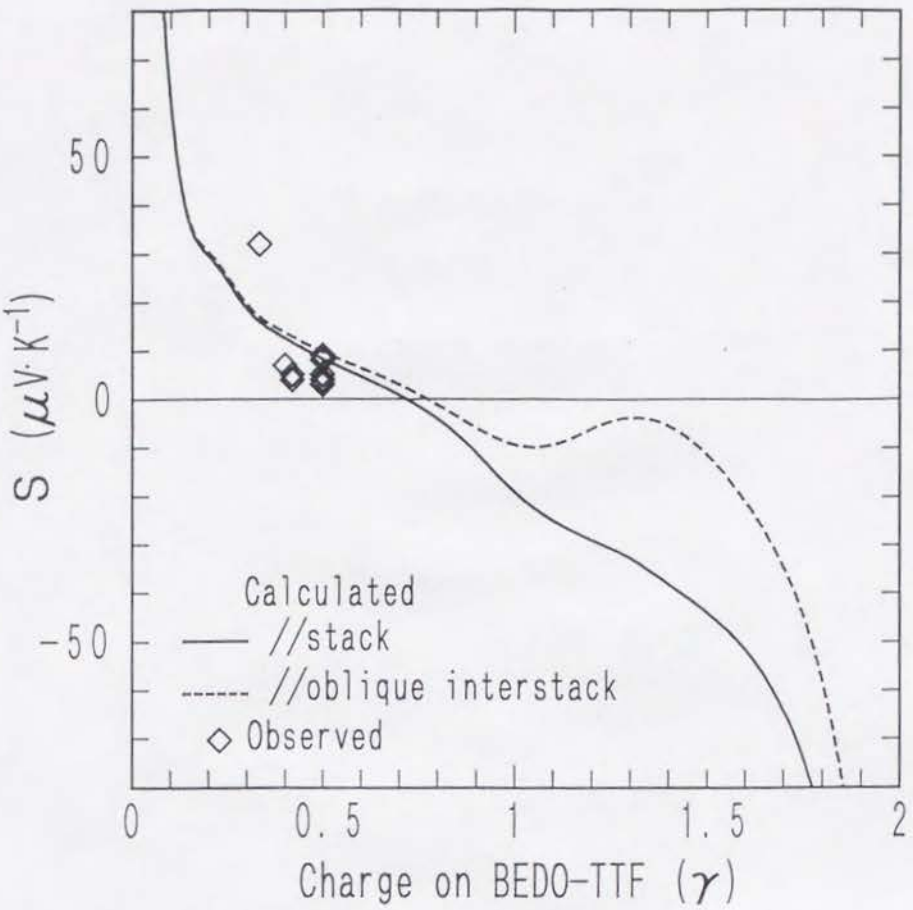

Figure 5-4. Correlation between the average charge on the donor (γ) and thermoelectric power at room temperature for I_3-type BEDO-TTF complexes. The solid and dotted curves represent the calculated ones along the stacking and oblique interstack directions, respectively. The observed data are plotted by open squares.

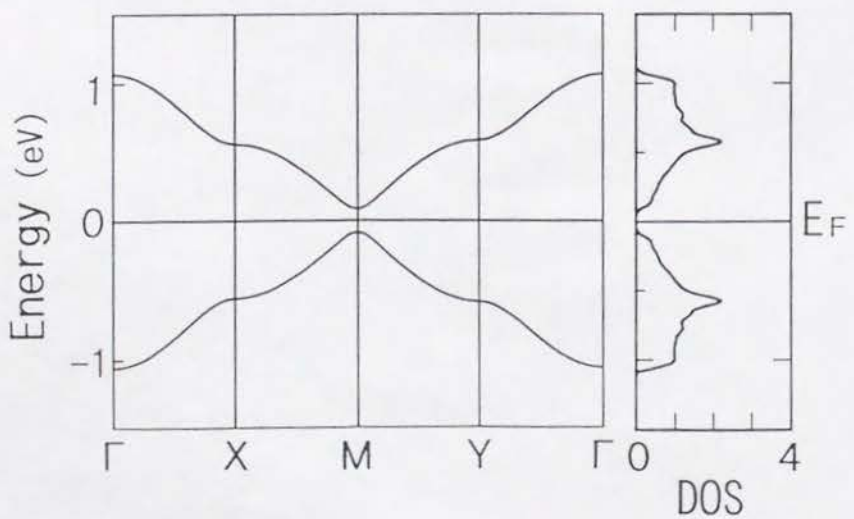

Figure 5-5. Calculated band structures and density of states (DOS) for (BEDO-TTF)I_3 (42). The DOSs are given in states(total)/(eV·molecule of BEDO-TTF).

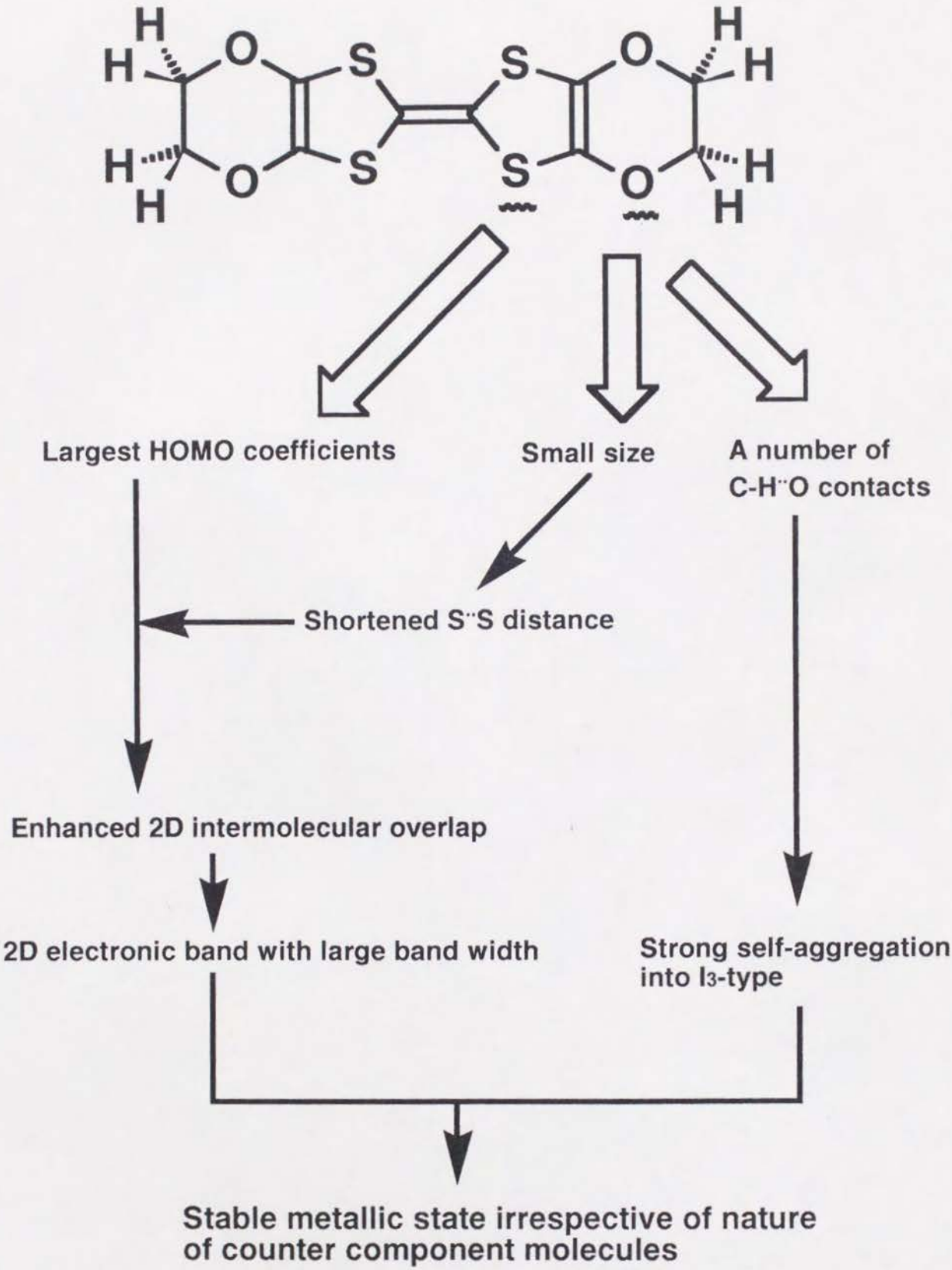

Chart 5-1. Schematized roles in stabilizing metallic state in BEDO-TTF complexes.

Chapter 6. Conclusion

This work has demonstrated the peculiar ability of BEDO–TTF to produce wide variety of molecular metals independent of the size, shape and electronic structures of their counter components. Furthermore, the metallic state of these BEDO–TTF complexes is often stable to low temperatures (< 20 K). This donor provides a number of molecular metals with smaller degree of CT ($\gamma \geq 0.3$) and from combination with much weaker acceptors ($\Delta E^{o,r} \leq 0.57$ V) than expected with conventional metals of TTF–TCNQ system ($\gamma \geq 0.5$, -0.02 V $\leq \Delta E^{o,r} \leq 0.34$ V). Another unique characteristic of the metallic complexes is their excess content of BEDO–TTF, which allows the partial CT ground state in the complexes with strong acceptor molecules. Also the metallic properties are not degraded in spite of the considerable amount of defects, disordered counterparts and/or localized spins.

Besides the metals, this donor yielded some semiconductors, although not so many, which have also served useful and basic data for understanding the properties and electronic states of the complexes.

In the crystals of metallic BEDO–TTF complexes, donor molecules aggregate to form a layered structure and usually construct uniform (I_3 type) array connected by intrastack C–H···O and side–by–side heteroatom short contacts. Most metallic BEDO–TTF complexes show 2D band electronic structures and relatively wide band width due to two kinds of strong interstack interactions. The unusually easy access to molecular metals is attributable to strong trend in the structural properties of BEDO–TTF. We also noted that the $N(E_F)$ of these metallic salts are much lower than in the superconducting BEDT–TTF salts having higher *T*c. With the same donor packing, higher γ will be needed to produce a higher *T*c BEDO–TTF superconductor. We actually found a BEDO–TTF complex of high γ, 41, which unfortunately experienced the

structural modification, resulted in an insulator.

The sulfur atoms (S_{in}) are dominant for intermolecular orbital overlap, while the smaller oxygen atoms not only enhance side-by-side $S_{in}\cdots S_{in}$ contacts, but also stabilize the self-aggregated structure of BEDO-TTF molecules through weak hydrogen bonding. From these facts we can conclude that the shape and electronic state of BEDO-TTF are very suitable for 2D band structure, resulting in a stable metallic state.

The above features clearly tell that various counter component molecules can be introduced without changing the structure of metallic 2D layers of BEDO-TTF. Particularly successful applications of these novel properties are the recent developments of metallic LB films and highly transparent films of metallic reticulate-doped polymer composites. Although such example is very few at present, this donor molecule have a great possibility in further fabricating materials with various functions.

References

1) Cowan, D. O.; Fortkort, J. A.; Metzger, R. M. In *Low-Dimensional Systems and Molecular Electronics*, Metzger, R. M.; Day, P.; Papavassiliou, G. C. Eds.; Plenum Press: New York, 1991; p.1.

2) (a) Inokuchi, H.; Saito, G.; Wu, P.; Seki, K. *Chem. Lett.* **1986**, 1263. (b) Rovira, M. C.; Novoa, J. J.; Terres, J.; Rovira, C.; Veciana, J.; Yang, S.; Cowan, D. O.; Canadell, E. *Adv. Mater.* **1995**, *7*, 1023. (c) Oakley, R. T. *Can. J. Chem.* **1993**, *71*, 1775.

3) (a) Mulliken, R. S. *J. Am. Chem. Soc.* **1952**, *74*, 811. (b) Mulliken, R. S. *J. Phys. Chem.* **1954**, *56*, 801.

4) Akamatu, H.; Inokuchi, H.; Matsunaga, Y. *Nature* **1954**, *173*, 168.

5) (a) Acker, R. J.; Hertler, W. R. *J. Am. Chem. Soc.* **1962**, *84*, 3372. (b) Melby, L. R.; Harder, R. J.; Hertler, W. R.; Mahler, W.; Benson, R. E.; Mochel, W. E. *J. Am. Chem. Soc.* **1962**, *84*, 3374.

6) (a) Wudl, F.; Smith, G. M.; Hufnagel, E. J. *J. Chem. Soc. Chem. Commun.* **1970**, 1453. (b) Hünig, S.; Kiesslich, G.; Scheutzow, D.; Zahradnik, R.; Carsky, P. *Int. J. Sulfur Chem. Part C* **1971**, 109. (c) Ferraris, J. P.; Cowan, D. O.; Walatka, V. V; Perlstein, J. H. *J. Am. Chem. Soc.* **1973**, *95*, 948.

7) Jerome, D.; Schulz, H. J. *Adv. Phys.* **1982**, *31*, 299.

8) Saito, G.; Enoki, T.; Toriumi, K.; Inokuchi, H. *Solid State Commun.* **1982**, *42*, 557.

9) (a) Urayama, H.; Yamochi, H.; Saito, G.; Nozawa, K.; Sugano, T.; Kinoshita, M.; Sato, S.; Oshima, K.; Kawamoto, A.; Tanaka, J. *Chem. Lett.*, 1988, 55. (b) Kini, A. M.; Geiser, U.; Wang, H. H.; Carlson, K. D.; Williams, J. M.; Kwok, W. K.; Vandervoort, K. G.; Thompson, J. E.; Stupka, D. L.; Jung, D.; Whangbo, M. -H.; *Inorg. Chem.* **1990**, *29*, 2555. (c) Williams, J. M.; Kini, A. M.; Wang, H. H.; Carlson, K. D.; Geiser, U.; Montgomery, L. K.; Pyrka, G. J.; Watkins, D. M.; Kommers, J. M.; Boryschuk, S. J.; Crouch, A. V. S.; Kwok, W. K.; Schirber, J. E.; Overmyer, D. L.; Jung, D.; Whangbo, M. -H. *Inorg. Chem.* **1990**, *29*, 3272. (d) Komatsu, T.; Nakamura, T.; Matsukawa, N.; Yamochi, H.; Saito, G.; Ito, H.; Ishiguro, T.; Kusunoki, M.; Sakaguchi, K. *Solid State Commun.*, **1991**, *80*, 843.

10) Hebart, A. F.; Rosseinsky, M. J.; Haddon, R. C.; Murphy, D. W.; Glarum, S. H.; Palstra, T. T. M.; Ramirez, A. P.; Kortan, A. R. *Nature*, **1991**, *350*, 600.

11) *Molecular Magnetism*, Coronado, E.; Delhaes, P.; Gatteschi, D.; Miller, J. S. Eds.; NATO ASI Series; Kluwer Academic Publishers, Dordrecht, 1996.

12) (a) Torrance, J. B.; Vazquez, J. E.; Mayerle, J. J.; Lee, V. Y. *Phys. Rev. Lett.* **1981**, *46*, 253. (b) Torrance, J. B.; Girlando, A.; Mayerle, J. J.; Crowey, J. I.; Lee, V. Y.; Batail, P.; LePlace, S. J. *Phys. Rev. Lett.* **1981**, *47*, 1747.

13) Iwasa, Y.; Koda, T.; Tokura, Y.; Koshihara, S.; Iwasawa, N.; Saito, G. *Appl. Phys. Lett.* **1989**, *55*, 2111.

14) Iwasa, Y.; Koda, T.; Koshihara, S.; Tokura, Y.; Iwasawa, N.; Saito, G. *Phys. Rev. B.* **1989**, *39*, 10441.

15) Bray, J. W.; Hart, H. R.; Interrante, L. V.; Jacobs, I. S.; Kasper, J. S.; Watkins, G. D.; Wee, S. H.; Bonner, J. C. *Phys. Rev. Lett.* **1975**, *35*, 744.

16) (a) Garito, A. F.; Heeger, A. J. *Acc. Chem. Res.* **1974**, *7*, 232. (b) Torrance, J. B. *Acc. Chem. Res.* **1979**, *12*, 79.

17) Saito, G.; Ferraris, J. P. *Bull. Chem. Soc. Jpn.* **1980** *53*, 2141, and the references cited therein.

18) (a) *Semiconductors and Semimetals Vol. 27: Highly Conducting Quasi-One-Dimensional Organic Crystals* Conwell, E. Ed.; Academic Press: New York, 1988. (b) *Extended Linear Chain Compounds, Vol. 1-3*, Miller, J. S. Ed.; Plenum Press: New York, 1982.

19) (a) Bloch, A. N.; Cowan, D. O.; Bechgaard, K.; Pyle, R. E.; Banks, R. H. Poehler, T. O. *Phys. Rev. Lett.* **1975**, *34*, 1561. (b) Mays, M. D.; McCullough, R. D.; Cowan, D. O.; Poehler, T. O.; Bryden, W. A.; Kistenmacher, T. J. *Solid State Commun.* **1988**, *65*, 1089.

20) (a) Ishiguro, T.; Yamaji, K. *Organic Superconductors*, Springer Ser. Solid State Sci. *88*, Springer, Berlin, 1990. (b) Williams, J. M.; Ferraro, J. R.; Thorn, R. J.; Carlson, K. D; Geiser, U.; Wang, H. H.; Kini, A. M.; Whangbo, M. -H. *Organic Superconductors (including Fullerenes): Synthesis, Structure, Properties, and Theory*; Prentice Hall, Englewoods Cliffs, NJ, 1992. (c) Saito, G. *Phosphorus, Sulfur and Silicon and the Related Elements* **1992**, *67*, 345. (d) Saito, G. In *New Materials*, Joshi, S. K., Tsuruta, T., Rao, C. N. R., Nagakura, S., Eds.; Narosa Publishing House: New Delhi, India, 1992, p127.

21) Saito, G. In *Metal-Insulator Transition Revisited*, Edwards P. P.; Rao, C. N. R. Eds.; Taylor & Francis: London, UK, 1995; p.231.

22) Mori, T.; Inokuchi, H. *Solid State Commun.* **1986**, *59*, 355.

23) Hasegawa, T.; Itoh, N.; Inukai, K. Kagoshima, S.; Mochida, T.; Izuoka, A.; Sugawara, T.; Iwasa, Y.; Sugiura, S. private communication.

24) (a) Mizuno, M.; Garito, A. F.; Cava, M. P. *J. Chem. Soc. Chem. Commun.* **1978**, 18. (b) Saito, G.; Hayashi, H.; Enoki, T.; Inokuchi, H. *Mol. Cryst. Liq. Cryst.* **1985**, *120*, 341. (c) Yamashita, Y.; Suzuki, T.; Saito, G.; Mukai, T. *J. Chem. Soc. Chem. Commun.* **1986**, 1489. (d) Mori, T.; Inokuchi, H. *Bull. Chem. Soc. Jpn.* **1987**, *60*, 402. (e) Yui, K.; Aso, Y.; Otsubo, T.; Ogura, F. *ibid.* **1989**, *62*, 1539. (f) Yui, K.; Ishida, H.; Aso, Y.; Otsubo, T.; Ogura, F.; Kawamoto, A.; Tanaka, J. *ibid.* **1989**, *62*, 1547. (g) Suzuki, T.; Yamashita, Y.; Kabuto, C.; Miyashi, T. *J. Chem. Soc. Chem. Commun.* **1989**, 1102. (h) Izuoka, A.; Tachikawa, T.; Sugawara, T.; Suzuki, Y.; Konno, M.; Saito, Y.; Shinohara, H. *ibid.* **1992**, 1472. (i) Günther, E.; Hünig, S.; Schütz, J. -U.; Langohr, U.; Rieder, H.; Söderholm, S.; Werner, H. -P.; Peters, K.; Schnering, H. G.; Lindner, H. J. *Chem. Ber.*, **1992**, *125*, 1919.

25) (a) Suzuki, T.; Yamochi, H.; Srdanov, G.; Hinkelmann, K.; Wudl, F. *J. Am. Chem. Soc.* **1989**, *111*, 3108. (b) Suzuki, T.; Yamochi, H.; Isotalo, H.; Fite, C.; Kasmai, H.; Liou, K.; Srdanov, G.; Wudl, F.; Coppens, P.; Maly, K.; Frost-Jensen, A. *Synth. Met.* **1991**, *41-43*, 2225.

26) (a) Wudl, F.; Yamochi, H.; Suzuki, T.; Isotalo, H.; Fite, C.; Kasmai, H.; Liou, K.; Srdanov, G.; Coppens, P.; Maly, K.; Frost-Jensen, A. *J. Am. Chem. Soc.* **1990**, *112*, 2461. (b) Wudl, F.; Yamochi, H.; Suzuki, T.; Isotalo, H.; Fite, C.; Liou, K.; Kasmai, H.; Srdanov, G. in *The Physics and Chemistry of Organic Superconductors* Springer Proceeding in Physics, Vol.51, Saito, G.; Kagoshima, S. Eds.; Springer-Verlag: Berlin, 1990, p358. (c) Beno, M. A.; Wang, H. H.; Carlson, K. D.; Kini, A. M.; Frankenbach, G. M.; Ferraro, J. R.; Larson, N.; McCabe, G. D.; Thompson, J. E.; Purnama, C.; Vashion, M.; Williams, J. M. *Mol. Cryst. Liq. Cryst.* **1990**, *181*, 145. (d) Yamochi, H.; Nakamura, T.; Saito, G.; Kikuchi, T.; Sato, S.; Nozawa, K.; Kinoshita, M.; Sugano, T.; Wudl, F. *Synth. Met.* **1991**, *41-43*, 1741. (e) Schweitzer, D.; Kahlich, S.; Heinen, I.; Lan, S. E.; Nuber, B.; Keller, H. J.; Winzer, K.; Helberg, H. W. *Synth. Met.* **1993**, *55-57*, 2827. (f) Saito, G.; Yoshida, K.;

Shibata, M.; Yamochi, H.; Kojima, N.; Kusunoki, M.; Sakaguchi, K. *Synth. Met.*, **1995**, *70*, 1205. (g) Yoshida, K. Master Thesis, Kyoto University, 1994; in Japanese.

27) (a) Beno, M. A.; Wang, H. H.; Kini, A. M.; Carlson, K. D.; Geiser, U.; Kwok, W. K.; Thompson, J. E.; Williams, J. M.; Ren, J.; Whangbo, M. -H. *Inorg. Chem.* **1990**, *29*, 1599. (b) Kahlich, S.; Schweitzer, D.; Heinen, I.; Lan, S. E.; Nuber, B.; Keller, H. J.; Winzer, K.; Helberg, H. W. *Solid State Commun.* **1991**, *80*, 191.

28) Kucera, J. J.; Carpenter, D. C. *J. Am. Chem. Soc.* **1935**, *57*, 2346.

29) (a) Webster, O. W. *J. Am. Chem. Soc.* **1964**, *86*, 2898. (b) Wheland, R. C.; Martin, E. L. *J. Org. Chem.* **1975**, *40*, 3101. (c) Thiele, J.; Günther, F. *Ann.* **1906**, *349*, 45. (d) Hutzinger, O.; Haecock, R. A.; Macneil, J. D.; Frei, R. W. *J. Chromatogr.* **1972**, *68*, 173. (e) Reynolds, G. A.; Vanallen, J. A. *J. Org. Chem.* **1964**, *29*, 3591. (f) Uno, M.; Seto, K.; Masuda, M.; Ueda, W.; Takahashi, S. *Tetrahedron Lett.* **1985**, *26* 1553. (g) Torrey, H. A.; Hunter, W. H. *J. Am. Chem. Soc.* **1912**, *34*, 702. (h) Yamashita, Y.; Suzuki, T.; Mukai, T.; Saito, G. *J. Chem. Soc. Chem. Commun.* **1985**, 1044. (i) Mukherjee, T. K.; Levasseuer, L. A. *J. Org. Chem.* **1965**, *30*, 644. (j) Ray, F. E.; Francis, W. C. *J. Org. Chem.* **1943**, *8*, 52. (k) Kunze, E. *Chem. Ber.* **1888**, *21*, 3331. (l) Gull, H. C.; Turner, E. E. *J. Chem. Soc.* **1929**, 491. (m) Middelton, W. J.; Little, E. L.; Coffman, D. D.; Engelhardt, V. A. *J. Am. Chem. Soc.* **1958**, *80*, 2795. (n) Park, J. D.; Cohen, S.; Lacher, J. R. *J. Am. Chem. Soc.* **1962**, *84*, 2919. (o) Birr, W. *Z. Physik. Chem.* **1931**, *153*, 1. (p) Yamochi, H.; Tsuji, T.; Saito, G.; Suzuki, T.; Miyashi, T.; Kabuto, C. *Synth. Met.* **1988**, *27*, A479. and ref. cited therein. (q) Fukunaga, T. *J. Am. Chem. Soc.* **1976**, *98*, 610. (r) *Inorg. Synth. Vol. IX*, 137. (s) *Inorg. Synth. Vol. IX*, 139.

30) *Chemistry Handbook*, 3rd ed. ed. by The Chemical Society of Japan; Maruzen: Tokyo, 1984; in Japanese.

31) Mackay, S.; Edwards, C.; Stewart, N. *Crystan-GM A Computer Program for the Solution and Refinement of Crystal Structures from X-Ray Diffraction Data*; University of Glasgow, Scottland.

32) Sheldrick, G. M. "SHELXS-86, Program for Crystal Structure Determination" and "SHELX-76, Program for Crystal Structure Determination", Univ. of Göttingen, Federal Republic of Germany.

33) Ashida, T. "HBLS-V (UNICS)" **1967**.

34) The sp^3 configuration with the C-H bond length of 1.0 Å is assumed for ethylene groups in the donor molecules.

35) Miller, J. S.; Ward, M. D.; Zhang, J. H.; Reiff, W. M. *Inorg. Chem.* **1990**, *29*, 4063.

36) Mori, T.; Kobayashi, A.; Sasaki, Y.; Kobayashi, H.; Saito, G.; Inokuchi, H. *Bull. Chem. Soc. Jpn.* **1984**, *57*, 627.

37) (a) Summerville R. H.; Hoffmann, R. *J. Am. Chem. Soc.* **1976**, *98*, 7240. (b) Berlinsky, A.J.; Carolan, J. F.; Weiler, L. *Solid State Commun.* **1974**, *15*, 795.

38) Fettouhi, M.; Ouahab, L.; Serhani, D.; Fabre, J. M.; Ducasse, L.; Amiell, J.; Canet, R.; Delhaés, P. *J. Mater. Chem.* **1993**, *3*, 1101.

39) Lichtenberger, D. L.; Johnston, R. L.; Hinkelmann, K.; Suzuki, T.; Wudl, F. *J. Am. Chem. Soc.* **1990**, *112*, 3302.

40) Sato, N.; Saito, G.; Inokuchi, H. *Chem. Phys.* **1983**, *76*, 79, and references cited therein.

41) Foster, R. *Organic Charge Transfer Complexes*, Academic Press, London, 1969.

42) Coleman, L. B. *Rev. Sci. Instrum.* **1978**, *49*, 58.

43) (a) Kato, R.; Kobayashi, H.; Kobayashi, A. *Synth. Met.* **1991**, *41*, 2093. (b) Kobayashi, A.; Kato, R.; Naito, T.; Kobayashi, H. *ibid.* **1993**, *56*, 2078. (c) Montgomery, L. K.; Burgin, T.; Huffman, J. C.; Carlson, K. D.; Dudek, J. D.; Yaconi, G. A.; Megna, L. A.; Mobley, P. R.; Kwok, W. K.; Williams, J. M.; Schirber, J. E.; Overmyer, D. L.; Ren, J.; Rovira, C.; Whangbo, M. -H. *ibid.* **1993**, *56*, 2090.

44) Misaki, Y.; Fujiwara, H.; Yamabe, T.; Mori, T.; Mori, H.; Tanaka, S. *Chem. Lett.* **1994**, 1653.

45) Harman, T. C.; Honig, J. M. *Thermoelectric and Thermomagnetic Effects and Applications*; McGraw-Hill, New York, 1967; eq.(3.13.10).

46) Matsunaga, Y. *Nature* **1965**, *205*, 72.

47) Chappell, J. S.; Bloch, A. N.; Bryden, W. A.; Maxfield, M.; Poehler, T. O.; Cowan, D. O. *J. Am. Chem. Soc.* **1981**, *103*, 2442.

48) Meneghetti, M.; Pecile, C. *J. Chem. Phys.* **1986**, *84*, 4149.

49) (a) Miller, J. S.; Zhang, J. H.; Reiff, W. M. *J. Am. Chem. Soc.* **1987**, *109*, 4584. (b) Miller, J. S.; Calabrese, J. C.; Dixon, D. A. *J. Phys. Chem.* **1991**, *95*, 3139.

50) Miller, J. S.; Krusic, P. J.; Dixon, D. A.; Reiff, W. M.; Zhang, J. H.; Anderson, E. C.; Epstein, A. J. *J. Am. Chem. Soc.* **1986**, *108*, 4459.

51) (TEA)DBDQ was prepared by mixing DBDQ and (TEA)I in analogous way of the preparation of (TEA)DDQ.[50]

52) LePage, T. J.; Breslow, R. *J. Am. Chem. Soc.* **1987**, *109*, 6412.

53) Patton, E. V.; West, R. *J. Phys. Chem.* **1973**, *77*, 2652.

54) Moldenhauer, J.; Pokhodnia, K. I.; Schweitzer, D.; Heinen, I.; Keller, H. J. *Synth. Met.* **1993**, *55-57*, 2548.

55) Pokhodnia, K. I.; Kozlov, M. E.; Onischenko, V. G.; Schweitzer, D.; Moldenhauer, J.; Zamboni, R. *Synth. Met.* **1993**, *55-57*, 2364.

56) The neutral BEDO-TTF shows two bands at 1011 and 1015 cm^{-1}. The former is assigned to the totally-symmetric ($a_g \nu_7$) mode,[55] which becomes infrared active due to the deformed molecular structure (tub-shape) from the D_{2h} symmetry. The authors in Ref.54 show the frequency shifts based from 1011 cm^{-1}. However, this a_g mode should be infrared inactive in the CT complexes, where the flat donor molecules with almost D_{2h} symmetry tend to stack regularly (see later text). Even the ReO_4 salt, where slightly dimerized donor molecules construct the layers, shows no corresponding vibronic bands around 1000 cm^{-1} in the reflectance spectra along the donor layer. Swietlik, R.; Kushch, N. D. *Phys. Stat. Sol. (a)* **1994**, *142*, 515. Thus, we utilize the normal active $b_{1u} \nu_{31}$ mode at 1015 cm^{-1} in Figure 4b.

57) (a) Misaki, Y.; Higuchi, N.; Fujiwara, H.; Yamabe, T.; Mori, T.; Mori, H.; Tanaka, S. *Angew. Chem.* **1995**, *34*, 1222. The stoichiometry was corrected later. Misaki, Y.; Higuchi, N.; Ohta, T.; Fujiwara, H.; Yamabe, T.; Mori, H.; Tanaka, S. *Mol. Cryst. Liq. Cryst.* **1996**, *284*, 27. (b) Schramm, C. J.; Scaringe, R. P.; Stojakovic, D. R.; Hoffman, B. M.; Ibers, J. A.; Marks, T. J. *J. Am. Chem. Soc.* **1980**, *102*, 6702.

58) Etemad, S. *Phys. Rev. B.* **1981**, *24*, 4959.

59) Bozio, R.; Zanon, I.; Girlando, A.; Pecile, C. *J. Chem. Soc. Faraday Trans. 2* **1978**, *74*, 235.

60) The complex **10** is regarded as a single phase because the appearances and the IR spectra are unchanged under the different preparation conditions.

61) Kozlov, M. E.; Tanaka, Y.; Tokumoto, M.; Tani, T. *Chem. Phys. Lett.* **1994**, *223*, 318.

62) A band below $5x10^3$ cm^{-1} appears in a system of a Mott insulator of an extremely small on-site Coulomb repulsion (ex. (BDNT)PF_6, BDNT = 4,9-bis(benzo-1,3-dithiol-2-ylidene)-4,9-dihydronaphtho[2,3-c][1,2,5]thiadiazole) Dong, J.; Yakushi, K.; Yamashita, Y. *J. Mater. Chem.* **1995**, *5*, 1735.

63) Senga, T.; Kamoshida, K.; Kushch, L. A.; Saito, G.; Inayoshi, T.; Ono, I. *Mol. Cryst. Liq. Cryst.* in press.

64) Sugano, T.; Yakushi, K.; Kuroda, H. *Bull. Chem. Soc. Jpn.* **1978**, *51*, 1041.

65) Torrance, J. B.; Scott, B. A.; Welber, B.; Kaufman, F. B.; Seiden, P. E. *Phys. Rev. B.* **1979**, *19*, 730.

66) Maldague, P. F. *Phys. Rev. B.* **1977**, *16*, 2437.

67) Jacobsen, C. S.; Tanner, D. B.; Bechgaard, K. *Phys. Rev. B.* **1983**, *28*, 7019.

68) Sugano, T.; Hayashi, H.; Kinoshita, M.; Nishikida, K. *Phys. Rev. B.* **1989**, *39*, 11387.

69) Jacobsen, C. S.; Tanner, D. B.; Williams, J. M.; Geiser, U.; Wang, H. H. *Phys. Rev. B.* **1987**, *35*, 9605.

70) Verchere, J. -F. *J. Chem. Res. (M)* **1978**, 2216-2240.

71) The solution spectrum of TEA(HCHA) was obtained by mixing the acetonitrile solutions of H_2CHA and $(TEA)_2CHA$ with 1:1 ratio.

72) Zaman, M. B., Ph. D. Thesis, Graduate University for Advanced Studies, 1995.

73) Nakasuji, K. *Pure & Appl. Chem.* **1990**, *62*, 477.

74) Some fully ionic complexes with alternating stacking show the absorptions of CT process among D^+ (or A^-) molecules instead of the back CT absorption (from A^- to D^+) (e.g. (BEDT-TTF)(F_4TCNQ)[23]). Therefore, strictly speaking, the stacking types are not determined solely from the analysis of Torrance's diagram, although such exceptions are few.

75) Sugano, T.; Saito, G.; Kinoshita, M. *Phys. Rev. B* **1987**, *35*, 6554.

76) Elliott, R. J. *Phys. Rev.* **1954**, *96*, 266.

77) Bulaevskii, L. N.; Zvarykina, A. V.; Karimov, Y. S.; Lyubovskii, R. B.; Shchegolev, I. F. *Sov. Phys. JETP* **1972**, *35*, 384.

78) Kinoshita, M.; Akamatu, H. *Nature* **1965**, *207*, 291.

79) (a) Bonner, J. C.; Fischer, M. E. *Phys. Rev. A* **1964**, *135*, 640. (b) Bonner, J. C., Ph. D. Dissertation, University of London, 1968. (c) Hall, J. W.; Marsh, W. E.; Weller, R. R.; Hatfield, W. E. *Inorg. Chem.* **1981**, *20*, 1033.

80) Rataiczak, R. D.; Jones, M. T.; Reeder, J. R. *Mol. Phys.* **1985**, *56*, 65.

81) (a) Nakamura, T.; Yunome, G.; Azumi, R.; Tanaka, M.; Tachibana, H.; Matsumoto, M.; Horiuchi, S.; Yamochi, H.; Saito, G. *J. Phys. Chem.* **1994**, *98*, 1882. (b) Nakamura, T.; Isotalo, H.; Akutagawa, T.; Tachibana, H.; Azumi, R.; Matsumoto, M.; Horiuchi, S.; Yamochi, H.; Saito, G. *Mol. Cryst. Liq. Cryst.*, **1996** *284*, 235. (c) Ogasawara, K.; Ishiguro, T.; Horiuchi, S.; Yamochi, H.; Saito, G. *Jpn. J. Appl. Phys.*, **1996**, *35*, L571.

82) Zuppiroli, L.; Przybylski, M.; Pukacki W. *J. Physique.* **1985**, *45*, 1925.

83) (a) Tracz, A.; Jeszka, J. K.; Sroczynska, A.; Ulański, J.; Plocharski, J.; Yamochi, H.; Horiuchi, S.; Saito, G. *Synth. Met.*, in press. (b) Horiuchi, S.; Yamochi, H.; Saito, G.; Jeszka, J. K.; Tracz, A.; Sroczynska, A.; Ulański, J. *Mol. Cryst. Liq. Cryst.*, in press.

84) Zhilyaeva, E. I.; Lyubovskaya, R. N.; Torunava, S. A.; Konovalikhin, S. V.; Dyachenko, O. A.; Lyubovskii, R. B. *Synth. Met.* **1996**, *80*, 91.

85) Leung, P. C.; Emge, T. J.; Beno, M. A.; Wang, H. H.; Williams, J. M.; Petricek, V.; Coppens, P. *J. Am. Chem. Soc.* **1985**, *107*, 6184.

86) The van der Waals radii (vdW) and ion radii employed in this paper are as follows; C 1.70 Å, H 1.20 Å, N 1.55 Å, O 1.52 Å, S 1.80 Å, Cl 1.75 Å, Br 1.85 Å, I 1.98 Å. Bondi, A. *J. Phys. Chem.* **1964**, *68*, 441.

87) Andersen, E. K. *Acta Cryst.* **1967**, *22*, 188.

88) Andersen, E. K. *Acta Cryst.* **1967**, *22*, 191.

89) Andersen, E. K. *Acta Cryst.* **1967**, *22*, 196.

90) Aliev, Z. G.; Kondrat'ev, S. I.; Atovmyan, L. O.; Khidekel', M. L.; Karpov V. V. *Bull. Acad. Sci. USSR*, **1981**, *30*, 339.

91) Kulpe, S.; Dähne, S. *Acta Cryst.* **1978**, *B34*, 3616.

92) Mori, H.; Tanaka, S.; Mori, T.; Maruyama, Y.; Inokuchi, H.; Saito, G. *Solid State Commun.* **1991**, *78*, 49.

93) (a) Whangbo, M. -H.; Jung, D.; Ren, J.; Evain, M.; Novoa, J. J.; Mota, F.; Alvarez, S.; Williams, J. M.; Beno, M. A.; Kini, A. M.; Wang, H. H.; Ferraro, J. R. in *The Physics and Chemistry of Organic Superconductors* Springer Proceeding in Physics, Vol.51, Saito, G.; Kagoshima, S. Eds.; Springer-Verlag: Berlin, 1990; p262. (b) Whangbo, M. -H.; Novoa, J. J.; Jung, D.; Williams, J. M.; Kini, A. M.; Wang, H. H.; Geiser, U.; Beno, M. A.; Carlson, K. D. in *Organic Superconductivity* Kresin, V. Z.; Little, A. W. Eds.; Prenum Press: New York, 1990; p243.

94) Yamochi, H.; Komatsu, T.; Matsukawa, N.; Saito, G.; Mori, T.; Kusunoki, M.; Sakaguchi, K. *J. Am. Chem. Soc.* **1993**, *115*, 11319.

95) Whangbo, M. -H.; Williams, J. M.; Schultz, A. J.; Emge, T. J.; Beno, M. A. *J. Am. Chem. Soc.* **1987**, *109*, 90.

96) Desiraju, G. R. *Acc. Chem. Res.* **1991**, *24*, 290.

97) Novoa, J. J.; Tarron, B.; Whangbo, M. -H.; Williams, J. M. *J. Chem. Phys.* **1991**, *95*, 5179.

98) Seiler, P.; Dunitz, D. D. *Helv. Chim. Acta* **1989**, *72*, 1125.

99) Semmingsen, D. *Acta Chem. Scand.* **1977**, *B31*, 11.

100) Kulpe, S.; Dähne *Tetrahedron Lett.* **1968**, *21*, 2591.

101) Saito, G.; Kumagai, H.; Katayama, C.; Tanaka, C.; Tanaka, J.; Wu, P.; Mori, T.; Imaeda, K.; Enoki, T.; Inokuchi, H.; Higuchi, Y.; Yasuoka, N. *Israel J. Chem.* **1986**, *27*, 319.

102) Shibaeva, R. P. ; Kaminskii, V. F. ; Yagubskii, E. B. *Mol. Cryst. Liq. Cryst.* **1985**, *119*, 361 .

103) Chou, L. K.; Quijada, M. A.; Clevenger, M. B.; de Oliveira, G. F.; Abboud, K. A.; Tanner, D. B.; Talham, D. R. *Chem. Mater.* **1995**, *7*, 530.

104) Guionneau, P.; Kepert, C. J.; Chasseau, D.; Truter, M. R.; Day, P. *Synth. Met.* in press.

105) Wosnitza, J. *Int. J. Mod. Phys. B* **1993**, *15*, 2707.

106) (a) Cisarova, I.; Maly, K.; Bu, X.; Frost-Jensen, A.; Sommer-Larsen, P.; Coppens, P. *Chem. Mater.* **1991**, *3*, 647. (b) Kahlich, S.; Schweitzer, D.; Rovira, C.; Paradis, J. A.; Whangbo, M. -H.; Heinen, I.; Keller, H. J.; Nuber, B.; Bele, P.; Brunner, H.; Schibaeva, R. P. *Z. Phys. B Condense Matter* **1994**, *94*, 39.

107) Mori, T.; Oshima, K.; Okuno, H.; Kato, K.; Mori, H.; Tanaka, S. *Phys. Rev. B.* **1995**, *51*, 11110.

108) Mori, T.; Sakai, F.; Saito, G.; Inokuchi, H. *Chem. Lett.* **1986**, 1037.

109) The authors in ref.14e described the stoichiometry of **38a** as (BEDO-TTF)Cl(H_2O). However, Mori *et al.*

showed the stoichiometry as (BEDO-TTF)$_2$Cl(H$_2$O)$_3$ based on the Shubnikov-de Haas and de Haas-van Alphen effects.[107] Our elemental analysis (Table 2-3) and measurement of the crystal density also confirm the latter result ($\rho_{obs} = \rho_{calc} = 1.73$ vs. $\rho_{calc} = 1.77$ for 1:1:1 stoichiometry).

110) The $N(E_F)$ values of the κ-(BEDT-TTF)$_2$X salts were calculated based on the same parameters as in this work. $N(E_F)$ = 1.90 states(total)/(eV·molecule) was obtained for the X = Cu[N(CN)$_2$]Br salt by utilizing its structural data.[9b]

111) Mori, T.; Inokuchi, H. *J. Phys. Soc. Jpn.* **1988**, *57*, 3674.

112) Ashcroft, N. W.; Mermin, N. D. *Solid State Physics*; Saunders College, Philadelphia, 1976; eqs.(13.46) and (13.61).

113) Mortensen, K.; Williams, J. M.; Wang, H. H. *Solid State Commun.* **1985**, *56*, 105.

114) (a) Beno, M. A.; Firestone, M. A.; Leung, P. C. W.; Sowa, L. M.; Wang, H. H.; Williams, J. M.; Whangbo, M. -H. *Solid State Commun.* **1986**, *57*, 735. (b) Obertelli, S. D.; Friend, R. H.; Talham, D. R.; Kurmoo, M.; Day, P. *J. Phys. Condense. Matter.* **1989**, *1*, 5671. (c) Parker, I. D.; Friend, R. H.; Kurmoo, M.; Day, P. *ibid.* **1989**, *1*, 5681. (d) Kinoshita, N.; Tokumoto, M.; Anzai, H.; Saito, G. *Synth. Met.* **1987**, *19*, 203. (e) Tokumoto, M.; Anzai, H.; Ishiguro, T.; Saito, G.; Kobayashi, H.; Kato, R.; Kobayashi, A. *ibid.*, **1987**, *19*, 215. (f) Iwasa, Y.; Mizuhashi, K.; Koda, T.; Tokura, Y.; Saito, G. *Phys. Rev. B* **1994**, *49*, 3580. (g) Komatsu, T.; Matsukawa, N.; Inoue, T.; Saito, G. *J. Phys. Soc. Jpn.* **1996**, *65*, 1340.

Abbreviations for Chemicals in Text

TTF, tetrathiafulvalene; BEDO-TTF, bis(ethylenedioxy)-TTF; BEDT-TTF, bis(ethylenedithio)-TTF; TMTSF, tetramethyltetraselenafulvalene; TSF, tetraselenafulvalene; HMTTF, hexamethylene-TTF; TMTTF, tetramethyl-TTF; TTC_1-TTF, tetra(methylthio)-TTF; BEDO-DBTTF, bis(ethylenedioxy)-dibenzotetrathiafulvalene; BEDT-TSF, bis(ethylenedithio)-TSF; BDT-TTP, 2,5-bis(1',3'-dithiol-2'-ylidene)-1,3,4,6-tetrathiapentalene; DTEDT, 2-(1,3-dithiol-2-ylidene)-5-(2-ethanediylidene-1,3-dithiole)-1,3,4,6-tetrathiapentalene; TCNQ, 7,7,8,8-tetracyano-*p*-quinodimethane; F_4TCNQ, tetrafluoro-TCNQ; F_2TCNQ, 2,5-difluoro-TCNQ; FTCNQ, 2-fluoro-TCNQ; Me_2TCNQ, 2,5-dimethyl-TCNQ; Et_2TCNQ, 2,5-diethyl-TCNQ; $(MeO)_2$TCNQ, 2,5-dimethoxy-TCNQ; C_{10}TCNQ, 2-decyl-TCNQ; C_{14}TCNQ, 2-tetradecyl-TCNQ; DHBTCNQ, dihydrobarreleno-TCNQ; THBTCNQ, tetrahydrobarreleno-TCNQ; BTDA-TCNQ, bis-1,2,5-thiadiazolo-TCNQ; DDQ, 2,3-dichloro-5,6-dicyano-*p*-benzoquinone; DBDQ, 2,3-dibromo-5,6-dicyano-*p*-benzoquinone; QF_4, 2,3,5,6-tetrafluoro-*p*-benzoquinone; QCl_4, 2,3,5,6-tetrachloro-*p*-benzoquinone; QBr_4, 2,3,5,6-tetrabromo-*p*-benzoquinone; H_2CHA, 2,5-dichloro-3,6-dihydroxy-*p*-benzoquinone; H_2BRA, 2,5-dibromo-3,6-dihydroxy-*p*-benzoquinone; $Q(OH)_2$, 2,5-dihydroxy-*p*-benzoquinone; DCNQ, 2,3-dicyano-1,4-naphthoquinone; HCBD, hexacyano-1,3-butadiene; TCNE, tetracyanoethylene; DTENF, 9-dicyanomethylene-2,4,5,7-tetranitrofluorene; DTNF, 9-dicyanomethylene-2,4,7-trinitrofluorene; TENF, 2,4,5,7-tetranitrofluorene-9-one; TNF, 2,4,7-trinitrofluorene-9-one; TNBP, 3,3',5,5'-tetranitrobiphenyl-4,4'-diol; DNBP, 4,4'-dinitrobiphenyl; CF^-, cyanoform anion; HCP^{2-}, hexacyanotrimethlenecyclopropandiide; SQA^{2-}, squarate, PCA^-, 1,1,2,3,3-pentacyanopropenide; PIC^-, picrate; $HCTMM^{2-}$, hexacyanotrimethylenemethanediide; TBA^+, tetra(*n*-butyl)ammonium; TPA^+, tetra(*n*-propyl)ammonium; TEA^+, tetraethylammonium; THF, tetrahydrofuran; PhCN, benzonitrile; TCE, 1,1,2-trichloroethane.

Acknowledgements

The author would like to express his sincere gratitude to Prof. Gunzi Saito at Kyoto University for his guidance, supervision and continuous encouragements throughout the present study. The author feels deeply grateful to Prof. Hideki Yamochi (Kyoto University) for valuable discussions as well as his kind technical instructions in various experiments.

The present study has been also supported by a number of corporations of other laboratories. The author wishes to thank Prof. Masami Kusunoki and Mr. Ken-ichi Sakaguchi at Osaka University for X-ray diffraction measurements, crystal structure analyses, and discussion in the crystal structures. The author is very grateful to Prof. Jacek Ulański (Polish Academy of Science), Dr. Jeremiasz K. Jeszka, Dr. Adam Tracz, and Dr. Agnieszka Sroczyńska (University of Lodz, Poland) for significant discussions through the collaboration in the development of new metallic reticulate-doped polymer composites of BEDO-TTF complexes. The author feels grateful to Prof. Kiyoshi Matsumoto (Kyoto University) for collaboration in the X-ray diffraction measurements. The author wishes to express appreciation to Prof. Takayoshi Nakamura (Hokkaido University) and Prof. Mutsuyoshi Matsumoto (National Institute of Materials and Chemical Research), who offered some acceptors and greatly encouraged the present work through the collaboration in the development of metallic LB films of BEDO-TTF complexes. The author is much indebted to Prof. Takamasa Momose and Prof. Tadamasa Shida at Kyoto University for the IR measurements with high resolution. The author is also indebted to Prof. Takehiko Ishiguro (Kyoto University) and Dr. Kazuyoshi Ogasawara (Kyoto University), who have stimulated the present study through the discussion and collaboration in the study of LB films of metallic BEDO-TTF complexes. The author is grateful to Ms. Akiko Nakao (MAC Science Co. Ltd.) for the X-ray measurements. The

author is also grateful to Prof. Kazuhiro Nakasuji (Osaka University) for providing some acceptors, and Dr. Tatsuo Hasegawa (Tokyo University) for his kind advice for the synthesis of F_2TCNQ and FTCNQ. The author feels thankful to Prof. Takehiko Mori (Tokyo Institute of Technology) for providing his calculating program used in the band structure calculations.

The author acknowledges the encouragements, helpful advises and discussions by Prof. Norimichi Kojima (Tokyo University), Dr. Akihiro Otsuka (Kyoto University), Dr. Hiroshi Kitagawa (JAIST), Dr. Toshikazu Nakamura (Gakushuin University), Dr. Taichi Terashima (NRIM), Dr. Tomoyuki Akutagawa (Hokkaido University), Dr. Tokutaro Komatsu (Tokyo University), Dr. Tetsuo Kondo (Kyoto University), and all the members at Saito laboratory. The author would like to express thanks to Mr. Hirotsugu Nishishita (Kyoto University) for the assistance in the low-temperature experiments, and also to Kyoto University which has been educated the author.

The author would like to conclude the thesis with emphasizing the thanks to my parents for continuous encouragements and precious support.

Appendix

Atomic coordinates and equivalent isotropic thermal parameters in 11 BEDO-TTF complexes are given below Tables X1-11. Equivalent isotropic thermal parameters are defined as

$$B_{eq} = (8\pi^2/3)\Sigma_i U_{ii}.$$

Table X1. Atomic Coordinates and Equivalent Isotropic Thermal Parameters in $(BEDO\text{-}TTF)_2[HCHA]$ (25)

Atom	x	y	z	B_{eq}
S1	0.32616(17)	0.18499(5)	0.1038(5)	1.94
S2	0.58244(17)	0.18749(5)	0.5697(5)	1.90
S3	0.32084(18)	0.27041(4)	0.0732(5)	1.88
S4	0.57798(17)	0.27344(5)	0.5361(5)	1.85
O1	0.3261(6)	0.11465(15)	0.1619(15)	2.71
O2	0.5758(5)	0.11629(14)	0.6153(15)	2.64
O3	0.3199(5)	0.34138(14)	0.0476(14)	2.31
O4	0.5699(5)	0.34405(13)	0.5055(14)	2.15
C1	0.4528(6)	0.2107(2)	0.3284(17)	1.77
C2	0.3948(7)	0.14447(19)	0.2625(19)	2.04
C3	0.5108(7)	0.1456(2)	0.4770(19)	2.09
C4	0.3755(9)	0.0845(2)	0.371(2)	3.23
C5	0.5256(9)	0.0845(2)	0.440(2)	3.21
C6	0.4505(6)	0.2473(2)	0.3144(17)	1.80
C7	0.3886(7)	0.31200(18)	0.1793(18)	1.84
C8	0.5048(7)	0.3139(2)	0.3966(17)	1.82
C9	0.3666(8)	0.37314(19)	0.234(2)	2.51
C10	0.5173(8)	0.3744(2)	0.296(2)	2.77
CL	0.6893(3)	0.00109(7)	0.1998(7)	4.29
O5	0.8507(8)	0.05648(17)	0.6317(19)	4.26
O6	1.1040(8)	0.05539(18)	0.881(2)	4.53
C11	0.8579(10)	0.0002(3)	0.364(2)	3.33
C12	0.9130(10)	0.0291(2)	0.563(2)	3.17
C13	1.0629(9)	0.0285(3)	0.705(2)	3.43
H4A	0.34396	0.06177	0.25567	
H4B	0.33898	0.08603	0.58784	
H5A	0.55669	0.06309	0.57728	
H5B	0.56200	0.08322	0.22255	
H9A	0.33158	0.37308	0.45292	
H9B	0.33182	0.39482	0.10428	
H10A	0.55278	0.37338	0.07812	
H10B	0.54717	0.39730	0.41205	

Table X2. Atomic Coordinates and Equivalent Isotropic Thermal Parameters in (BEDO–TTF)$[Q(OH)_2]_2$ (27)

Atom	x	y	z	B_{eq}
S31	0.4917(5)	0.5392(5)	0.7934(4)	2.65
S32	0.3138(5)	0.5785(6)	0.4527(4)	2.67
C33	0.4594(18)	0.526(2)	0.5518(15)	2.29
C34	0.344(2)	0.600(2)	0.8183(16)	2.59
C35	0.266(2)	0.618(2)	0.6661(17)	2.70
O36	0.3245(15)	0.6336(15)	0.9949(12)	3.38
O37	0.1506(16)	0.6683(17)	0.6624(13)	3.93
C38	0.248(3)	0.733(3)	0.994(2)	4.47
C39	0.103(3)	0.670(3)	0.842(2)	4.99
C101	0.2686(19)	0.1113(19)	0.7898(16)	2.28
C102	0.1551(19)	0.1803(19)	0.7506(16)	2.22
C103	0.1105(19)	0.202(2)	0.5786(16)	2.39
C104	0.1735(18)	0.1583(18)	0.4278(16)	2.03
C105	0.291(2)	0.094(2)	0.4676(16)	2.38
C106	0.336(2)	0.072(2)	0.6395(17)	2.87
O107	0.2974(16)	0.0886(16)	0.9486(12)	3.47
O108	0.0984(16)	0.2154(17)	0.8952(12)	3.67
O109	0.1352(15)	0.1694(15)	0.2654(12)	2.89
O110	0.3467(17)	0.0575(17)	0.3227(13)	3.92
H21	0.03(3)	0.24(3)	0.56(2)	1.89
H22	0.14(3)	0.20(3)	0.99(3)	3.50
H23	0.40(2)	0.02(2)	0.66(2)	1.15
H24	0.32(3)	0.09(3)	0.23(3)	2.85
H41	0.22(3)	0.73(3)	1.13(3)	3.51
H42	0.33(3)	0.84(3)	0.98(2)	2.37
H43	0.03(3)	0.57(3)	0.85(3)	3.76
H44	0.05(3)	0.73(3)	0.84(2)	2.12

Table X3. Atomic Coordinates and Equivalent Isotropic Thermal Parameters in (BEDO-TTF)(TNBP) (29)

Atom	x	y	z	B_{eq}
S1	0.36991(7)	0.70326(16)	0.63943(6)	4.93
S2	0.57025(6)	0.69807(13)	0.65369(5)	3.75
C3	0.4877(2)	0.6965(4)	0.7068(2)	2.86
C4	0.3966(2)	0.6858(4)	0.5449(2)	3.43
C5	0.4843(2)	0.6840(4)	0.5501(2)	2.91
C6	0.3541(3)	0.6803(8)	0.3984(3)	9.04
C7	0.4393(3)	0.6530(7)	0.4042(3)	7.98
O8	0.3220(2)	0.6775(4)	0.4691(2)	4.94
O9	0.5158(2)	0.6730(3)	0.4819(2)	3.93
C11	0.0451(2)	0.4835(4)	0.4947(2)	2.81
C12	0.0528(3)	0.4730(5)	0.4130(2)	4.48
C13	0.1344(3)	0.4385(5)	0.4027(2)	4.43
C14	0.2156(3)	0.4114(4)	0.4711(2)	3.50
C15	0.2075(3)	0.4263(4)	0.5529(2)	3.05
C16	0.1251(2)	0.4601(4)	0.5647(2)	2.78
N17A	0.1276(6)	0.4050(8)	0.3122(4)	5.53
N17B	0.1427(5)	0.4570(7)	0.3134(5)	4.33
N18	0.2886(2)	0.4027(4)	0.6307(2)	4.14
O19A	0.0513(5)	0.3490(8)	0.2633(4)	8.76
O19B	0.1041(4)	0.5349(5)	0.2675(3)	3.98
O20A	0.1870(6)	0.4170(8)	0.2915(5)	7.81
O20B	0.1806(6)	0.3596(7)	0.2914(5)	5.78
O21	0.3627(2)	0.3732(4)	0.6214(2)	5.82
O22	0.2796(2)	0.4147(4)	0.7002(2)	6.19
O23	0.2912(2)	0.3757(4)	0.4553(2)	5.33
H31	0.3426	0.7711	0.3736	7.16
H32	0.3095	0.6193	0.3509	5.96
H33	0.4393	0.5581	0.3902	7.38
H34	0.4539	0.7036	0.3542	5.68
H35	0.0049	0.4861	0.3478	5.45
H36	0.1413	0.4613	0.6341	4.89
H37	0.3243	0.3691	0.4806	4.89

Table X4. Atomic Coordinates and Equivalent Isotropic Thermal Parameters in $(BEDO\text{-}TTF)_5(HCTMM)(PhCN)_2$ (31)

Atom	x	y	z	B_{eq}
S11	0.59096	0.40129	0.82885	2.25
S12	0.87318	0.43814	0.93654	2.76
O13	0.65002	0.26783	0.83023	3.05
O14	0.92523	0.30609	0.90556	3.77
C15	0.71422	0.46182	0.89539	1.73
C16	0.70032	0.33658	0.85343	2.21
C17	0.82700	0.35807	0.90476	2.18
C18	0.74155	0.21735	0.87322	3.48
C19	0.87782	0.24223	0.85575	2.85
S21	0.19461	0.39576	0.04368	2.58
S22	0.47274	0.43589	0.13224	2.19
O23	0.25296	0.26826	0.01786	3.13
O24	0.51886	0.31099	0.11064	3.47
C25	0.31297	0.46477	0.09138	2.59
C26	0.30248	0.33130	0.04600	2.78
C27	0.43030	0.35089	0.09462	2.22
C28	0.35541	0.22072	0.07357	4.05
C29	0.47383	0.24377	0.02925	3.66
S31	0.79236	0.40018	0.24207	2.67
S32	1.07325	0.44126	0.33382	2.44
O33	0.85336	0.27118	0.22216	3.74
O34	1.13131	0.30713	0.31812	3.77
C35	0.91470	0.46665	0.30265	1.64
C36	0.89458	0.33101	0.25730	2.26
C37	1.01361	0.34676	0.28468	3.98
C38	0.96677	0.21971	0.28061	5.94
C39	1.07422	0.24117	0.23221	3.72
S41	0.39067	0.40371	0.44034	1.99
S42	0.67204	0.44300	0.52842	2.25
O43	0.45052	0.26753	0.41905	3.83
O44	0.72671	0.30577	0.49627	3.18
C45	0.51279	0.46697	0.49220	1.50
C46	0.50275	0.32917	0.46188	3.78
C47	0.63330	0.35188	0.48903	2.64
C48	0.55533	0.22019	0.47771	3.09
C49	0.66595	0.23578	0.44278	4.22
S51	-0.00430	0.39857	0.65146	2.84
S52	0.27212	0.44133	0.72113	2.58
O53	0.05233	0.26761	0.62685	4.00
O54	0.32203	0.30483	0.71742	2.59
C55	0.11537	0.47357	0.68478	3.66
C56	0.10418	0.33746	0.65838	2.18
C57	0.22863	0.35089	0.69632	1.81
C58	0.14939	0.21842	0.67220	3.41
C59	0.27374	0.23851	0.63706	4.13
H18A	0.71034	0.17310	0.81794	
H18B	0.75275	0.20855	0.97129	
H19A	0.94268	0.20808	0.90160	
H19B	0.86869	0.24043	0.75605	
H28A	0.32622	0.17207	0.03820	
H28B	0.37831	0.22227	0.17524	
H29A	0.54205	0.20854	0.05211	
H29B	0.44923	0.25127	-0.07081	
H38A	0.93716	0.17077	0.24779	
H38B	0.99367	0.22223	0.38246	
H39A	1.13935	0.20429	0.24635	
H39B	1.04382	0.25115	0.13318	
H48A	0.52461	0.17142	0.44463	
H48B	0.57636	0.22335	0.57921	
H49A	0.72998	0.19960	0.47947	
H49B	0.64395	0.23424	0.34118	
H58A	0.11562	0.17177	0.62821	
H58B	0.17011	0.21541	0.77323	
H59A	0.33841	0.20163	0.66403	
H59B	0.25501	0.24556	0.53727	

Table X5. Atomic Coordinates and Equivalent Isotropic Thermal Parameters in $(BEDO\text{-}TTF)_{10}(CF)_4(H_2O)_3$ (33)

Atom	x	y	z	B_{eq}
S1	0.8397(7)	0.0698(2)	0.8182(10)	3.38
S2	0.3857(7)	0.1140(2)	0.4075(11)	3.49
C3	0.545(2)	0.0390(9)	0.546(3)	3.21
C4	0.821(3)	0.1679(10)	0.818(3)	3.51
C5	0.616(3)	0.1901(9)	0.634(3)	3.34
C6	1.012(3)	0.3004(10)	0.916(4)	4.91
C7	0.745(3)	0.3256(10)	0.886(4)	4.89
O8	1.0176(19)	0.2223(7)	1.010(3)	4.25
O9	0.576(2)	0.2656(7)	0.612(3)	4.51
H11	1.12690	0.34163	1.09762	
H12	1.07245	0.29619	0.69047	
H13	0.74397	0.37894	0.82634	
H14	0.68242	0.32967	1.11029	

Table X6. Atomic Coordinates and Equivalent Isotropic Thermal Parameters in $(BEDO\text{-}TTF)_4(SQA)(H_2O)_6$ (34)

Atom	x	y	z	B_{eq}
S1	0.54730(8)	0.61453(5)	0.2730(2)	2.36
S2	0.32253(8)	0.57522(5)	0.7154(2)	2.37
C3	0.4724(3)	0.5405(2)	0.4983(7)	2.04
C4	0.4221(3)	0.6947(2)	0.3842(8)	2.37
C5	0.3207(3)	0.6768(2)	0.5856(8)	2.35
C6	0.3427(4)	0.8337(2)	0.4540(9)	3.47
C7	0.2120(4)	0.8082(2)	0.4957(9)	3.44
O8	0.4357(3)	0.7711(2)	0.2647(7)	3.09
O9	0.2154(2)	0.7321(2)	0.6940(7)	3.10
S11	0.03494(8)	0.62065(5)	0.3077(2)	2.47
S12	-0.17715(8)	0.56645(5)	0.7555(2)	2.37
C13	-0.0302(3)	0.5398(2)	0.5134(7)	2.10
C14	-0.0897(3)	0.6961(2)	0.4718(8)	2.41
C15	-0.1850(3)	0.6717(2)	0.6761(8)	2.37
C16	-0.1743(4)	0.8312(2)	0.6060(9)	3.55
C17	-0.3022(4)	0.8030(2)	0.6564(9)	3.34
O18	-0.0825(3)	0.7754(2)	0.3851(7)	3.10
O19	-0.2902(3)	0.7222(2)	0.8192(7)	3.10
C21	0.0996(7)	-0.0072(4)	-0.0288(12)	2.84
C22	-0.0011(7)	-0.0045(4)	0.2518(12)	2.83
O23	0.2073(9)	-0.0108(6)	-0.0588(13)	4.67
O24	-0.0033(8)	-0.0135(5)	0.5427(13)	4.57
O25	0.2000(10)	-0.0230(6)	-0.0723(13)	5.04
O26	0.4269(5)	0.0347(3)	0.7695(10)	7.32
H31	0.36924	0.83882	0.67546	
H32	0.33872	0.88804	0.33436	
H33	0.18822	0.79923	0.27438	
H34	0.14697	0.85271	0.60801	
H35	-0.14220	0.83172	0.82346	
H36	-0.18419	0.88813	0.50751	
H37	-0.33235	0.79988	0.43793	
H38	-0.36569	0.84330	0.79551	

Table X7. Atomic Coordinates and Equivalent Isotropic Thermal Parameters in $(BEDO\text{–}TTF)_5(HCP)(PhCN)_{0.2}$ (37)

Atom	x	y	z	B_{eq}
S1	0.44786(10)	0.4087(5)	0.30927(8)	2.81
S2	0.45071(11)	0.7719(5)	0.43545(8)	2.99
S3	0.63901(11)	0.4360(5)	0.32403(8)	3.00
S4	0.63694(11)	0.7945(5)	0.45014(9)	3.15
C5	0.5035(4)	0.5974(16)	0.3760(3)	2.46
C6	0.3577(4)	0.5297(18)	0.3349(3)	2.82
C7	0.3599(4)	0.6904(18)	0.3912(3)	2.85
C8	0.2222(4)	0.619(2)	0.3150(4)	4.21
C9	0.2253(5)	0.611(2)	0.3912(4)	4.49
C10	0.5834(4)	0.6053(17)	0.3819(3)	2.60
C11	0.7276(4)	0.5729(18)	0.3637(4)	3.11
C12	0.7274(4)	0.7318(19)	0.4202(4)	3.46
C13	0.8614(5)	0.697(2)	0.3646(6)	6.11
C14	0.8628(5)	0.683(3)	0.4403(7)	6.59
O15	0.2911(3)	0.4434(14)	0.2957(2)	3.82
O16	0.2947(3)	0.7876(15)	0.4199(2)	4.08
O17	0.7947(3)	0.5011(15)	0.3351(3)	4.61
O18	0.7927(3)	0.8477(15)	0.4588(3)	4.81
C31	0.0007(17)	-0.017(3)	0.2646(8)	1.73
C32	0.0241(19)	0.174(4)	0.3189(7)	1.59
C33	0.000(2)	0.319(3)	0.2591(9)	2.14
C34	-0.006(3)	-0.308(3)	0.2290(10)	4.74
C35	0.041(2)	0.208(3)	0.3866(6)	2.40
C36	-0.007(3)	0.630(3)	0.2316(11)	2.97
C37	-0.028(3)	-0.365(4)	0.1610(10)	3.09
C38	0.013(2)	-0.578(4)	0.2718(16)	3.75
C39	0.0467(16)	-0.085(3)	0.4241(11)	1.84
C40	0.0491(18)	0.503(3)	0.4234(12)	2.60
C41	0.019(3)	0.915(4)	0.2673(17)	6.02
C42	-0.032(4)	0.635(5)	0.1629(12)	4.40
N43	-0.049(3)	-0.379(4)	0.1067(11)	4.95
N44	0.043(2)	-0.806(4)	0.292(2)	8.18
N45	0.052(2)	-0.318(4)	0.4539(13)	4.38
N46	0.050(3)	0.765(3)	0.4416(16)	4.40
N47	0.018(3)	1.137(4)	0.3004(16)	5.45
N48	-0.054(4)	0.602(5)	0.1091(12)	7.59
H21	0.22285	0.85074	0.29950	
H22	0.17273	0.51102	0.29477	
H23	0.22784	0.37880	0.40681	
H24	0.17676	0.71575	0.40484	
H25	0.91175	0.60632	0.35146	
H26	0.85546	0.92860	0.34913	
H27	0.91111	0.79553	0.46161	
H28	0.86325	0.45036	0.45529	

Table X8. Atomic coordinates and Equivalent Isotropic Thermal Parameters in $(BEDO\text{-}TTF)_2Br(H_2O)_3$ (39).

Atom	x	y	z	B_{eq}
S1	-0.1230(2)	0.38588(6)	0.7179(3)	2.67
S2	0.3342(2)	0.43068(6)	0.2593(3)	2.61
C3	0.0437(7)	0.4610(2)	0.4947(9)	2.25
C4	0.1025(8)	0.3100(3)	0.5786(10)	2.78
C5	0.3106(8)	0.3296(3)	0.3683(10)	2.72
C6	0.2174(10)	0.1759(3)	0.4754(13)	4.26
C7	0.4914(10)	0.2006(3)	0.4192(13)	4.31
O8	0.0561(7)	0.2339(2)	0.6815(9)	3.78
O9	0.5018(6)	0.2780(2)	0.2376(9)	3.60
O10	0.462(2)	-0.0067(15)	0.047(2)	8.85
O11	0.8823(16)	0.0169(9)	-0.0083(18)	10.02
Br12	0.6884(16)	0.0198(11)	-0.0538(18)	12.52
Br13	0.7731(15)	0.0260(10)	-0.0730(17)	10.52
H6A	0.21144	0.12201	0.59044	
H6B	0.15535	0.17298	0.25367	
H7A	0.60356	0.15932	0.28515	
H7B	0.55198	0.20504	0.64109	

The populations of Br12 and Br13 equal 1/8, while those of O10 and O11 are 1/4 and 1/2, respectively.

Table X9. Atomic Coordinates and Equivalent Isotropic Thermal Parameters in $(BEDO\text{-}TTF)_2Br[MnBr_2(H_2O)_4](H_2O)$ (40)

Atom	x	y	z	B_{eq}
S1	0.2335(2)	0.89332(15)	0.0789(5)	2.23
S2	0.2485(2)	0.93244(15)	0.5489(4)	2.14
S3	0.2475(2)	1.05016(14)	-0.0431(4)	2.05
S4	0.2621(2)	1.08773(15)	0.4267(4)	2.06
C1	0.2450(8)	0.9576(5)	0.2776(13)	1.93
C2	0.2299(8)	0.8287(6)	0.2657(13)	2.03
C3	0.2359(8)	0.8467(5)	0.4813(13)	2.01
C4	0.1930(9)	0.7154(6)	0.3542(15)	3.01
C5	0.2554(9)	0.7379(6)	0.5801(15)	2.98
C6	0.2514(7)	1.0238(5)	0.2276(13)	1.78
C7	0.2612(8)	1.1357(5)	0.0265(13)	1.93
C8	0.2663(8)	1.1531(6)	0.2417(14)	2.25
C9	0.2463(9)	1.2448(6)	-0.0630(14)	2.68
C10	0.3082(9)	1.2665(6)	0.1603(15)	3.02
O1	0.2203(7)	0.7649(4)	0.1888(12)	2.86
O2	0.2349(7)	0.8029(4)	0.6460(11)	2.73
O3	0.2631(6)	1.1801(4)	-0.1368(11)	2.64
O4	0.2775(6)	1.2168(4)	0.3220(11)	2.66
S11	0.4862(2)	0.90233(15)	-0.1715(4)	2.20
S12	0.5010(2)	0.94191(15)	0.2965(5)	2.16
C11	0.4968(7)	0.9668(5)	0.0238(13)	1.76
C12	0.4837(8)	0.8383(5)	0.0177(13)	1.96
C13	0.4896(8)	0.8559(5)	0.2286(13)	2.09
C14	0.4487(9)	0.7250(6)	0.1045(15)	3.09
C15	0.5122(9)	0.7486(5)	0.3269(14)	2.59
O11	0.4749(6)	0.7741(4)	-0.0607(12)	2.82
O12	0.4905(7)	0.8127(4)	0.3968(11)	2.82
S21	-0.0152(2)	0.90299(16)	0.3226(5)	2.25
S22	0.0004(2)	0.94023(15)	0.7935(5)	2.16
C21	-0.0029(7)	0.9669(6)	0.5242(13)	1.91
C22	-0.0212(8)	0.8381(5)	0.5046(13)	2.00
C23	-0.0149(8)	0.8545(6)	0.7219(14)	2.36
C24	-0.0660(9)	0.7248(6)	0.5844(15)	3.27
C25	-0.0046(10)	0.7442(6)	0.8106(15)	3.17
O21	-0.0324(7)	0.7734(4)	0.4260(12)	3.01
O22	-0.0184(7)	0.8100(4)	0.8835(11)	2.84
Br1	0.33563(11)	0.39873(7)	0.6133(2)	3.14
Br2	0.38573(10)	0.59837(7)	0.6202(2)	2.82
Br3	0.07236(11)	0.58339(8)	0.7459(3)	3.69
Mn1	0.30531(14)	0.49579(10)	0.3263(3)	2.37
O31	0.2844(7)	0.5714(5)	0.0674(12)	3.65
O32	0.2370(7)	0.4178(5)	0.0539(12)	3.71
O33	0.1574(7)	0.5041(6)	0.3728(13)	4.61
O34	0.4452(6)	0.4953(6)	0.2120(12)	3.98
O35	0.0441(8)	0.4015(6)	0.8425(13)	4.83
H1	0.12130	0.71151	0.36133	
H2	0.20405	0.67000	0.31044	
H3	0.32728	0.74315	0.57321	
H4	0.23811	0.70298	0.68961	
H5	0.26405	1.28002	-0.17093	
H6	0.17461	1.24024	-0.05459	
H7	0.29879	1.31231	0.20446	
H8	0.37977	1.26908	0.15459	
H11	0.37722	0.72090	0.11362	
H12	0.46000	0.67963	0.06130	
H13	0.58388	0.75525	0.31575	
H14	0.49767	0.71346	0.43731	
H21	-0.13722	0.72442	0.58852	
H22	-0.05948	0.67842	0.53902	
H23	0.06701	0.74665	0.80523	
H24	-0.02544	0.70912	0.91660	

Table X10. Atomic Coordinates and Equivalent Isotropic Thermal Parameters in (BEDO-TTF)I_3 (42).

Atom	x	y	z	B_{eq}
I1*	1.0000	1.0000	0.0000	3.28
I2*	1.0000	0.5000	0.5000	4.87
I3	0.9016(1)	0.8571(1)	0.17957(5)	4.38
I4	0.7710(2)	0.8570(1)	0.44930(6)	6.10
S1	0.5091(3)	0.8411(3)	-0.07400(15)	3.06
S2	0.8206(3)	0.5401(3)	-0.07034(15)	3.09
S3	0.4288(3)	0.7083(3)	0.12865(15)	3.21
S4	0.7416(3)	0.4104(4)	0.13003(15)	3.19
C1	0.6429(11)	0.6526(11)	-0.0151(6)	2.89
C2	0.6458(12)	0.8349(11)	-0.1677(6)	2.96
C3	0.7897(11)	0.6971(12)	-0.1650(5)	2.84
C4	0.734(3)	0.9580(19)	-0.3076(8)	5.98
C5	0.8617(18)	0.798(2)	-0.3100(7)	5.80
C6	0.6062(11)	0.5967(11)	0.0730(5)	2.75
C7	0.4877(12)	0.5747(13)	0.2264(6)	3.13
C8	0.6299(11)	0.4365(13)	0.2275(6)	3.03
C9	0.483(3)	0.530(3)	0.3709(8)	7.07
C10	0.608(3)	0.370(3)	0.3734(10)	7.42
O1	0.6025(9)	0.9666(10)	-0.2375(5)	3.88
O2	0.9099(10)	0.6723(11)	-0.2325(5)	3.90
O3	0.3886(11)	0.6169(12)	0.2971(5)	4.36
O4	0.6989(10)	0.3250(12)	0.2980(5)	4.23
H4A	0.79930	1.05424	-0.31123	
H4B	0.67040	0.98274	-0.35793	
H5A	0.81824	0.73114	-0.34413	
H5B	0.97104	0.83434	-0.33793	
H9A	0.39312	0.50559	0.41708	
H9B	0.54602	0.61779	0.38198	
H10A	0.69680	0.37009	0.41048	
H10B	0.54430	0.27209	0.39868	

(*)Site occupancy = 0.5.

Table X11. Atomic Coordinates and Equivalent Isotropic Thermal Parameters in (BEDO-TTF)$(I_3)_2$ (43).

Atom	x	y	z	B_{eq}
S1	0.7637(7)	0.3980(5)	0.2744(7)	2.57
S2	1.0291(7)	0.3222(5)	0.6239(7)	2.51
C3	0.957(2)	0.4369(15)	0.478(2)	2.05
C4	0.735(2)	0.2447(16)	0.316(2)	2.18
C5	0.869(2)	0.2058(17)	0.483(2)	2.28
C6	0.563(3)	0.055(2)	0.280(3)	3.68
C7	0.749(4)	-0.002(3)	0.377(4)	5.55
O8	0.597(2)	0.1673(14)	0.194(2)	3.14
O9	0.869(2)	0.0927(13)	0.535(2)	3.05
I1	0.0942(2)	0.1698(2)	0.0872(2)	3.62
I2	0.2702(2)	0.4245(1)	0.1743(2)	2.65
I3	0.4572(2)	0.6828(1)	0.2541(2)	3.22
H1	0.09415	0.16981	0.08717	
H2	0.47880	-0.01003	0.17406	
H3	0.80318	-0.02383	0.27386	
H4	0.72984	-0.08079	0.43315	

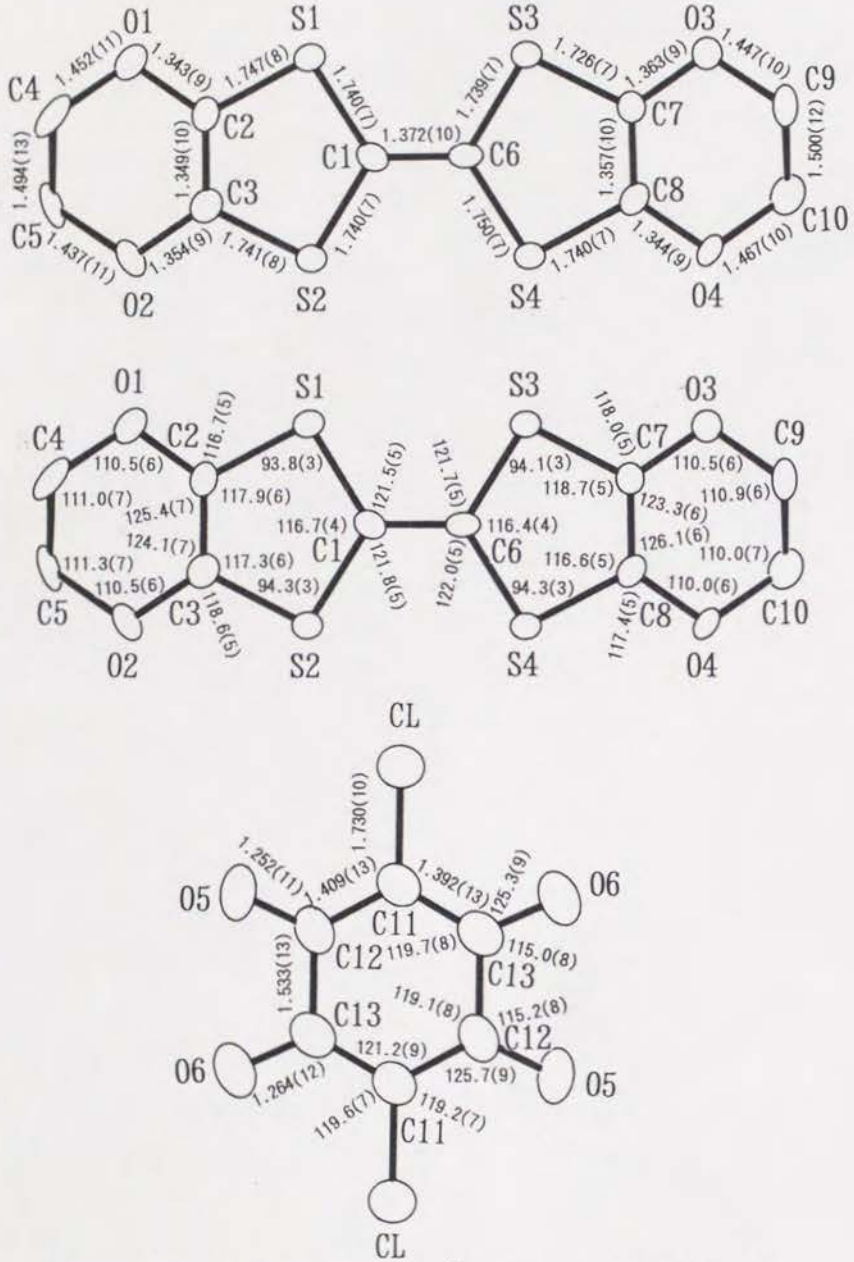

Figure A1. Bond lengths (Å) and angles (deg) in $(BEDO\text{-}TTF)_2(HCHA)$ (25)

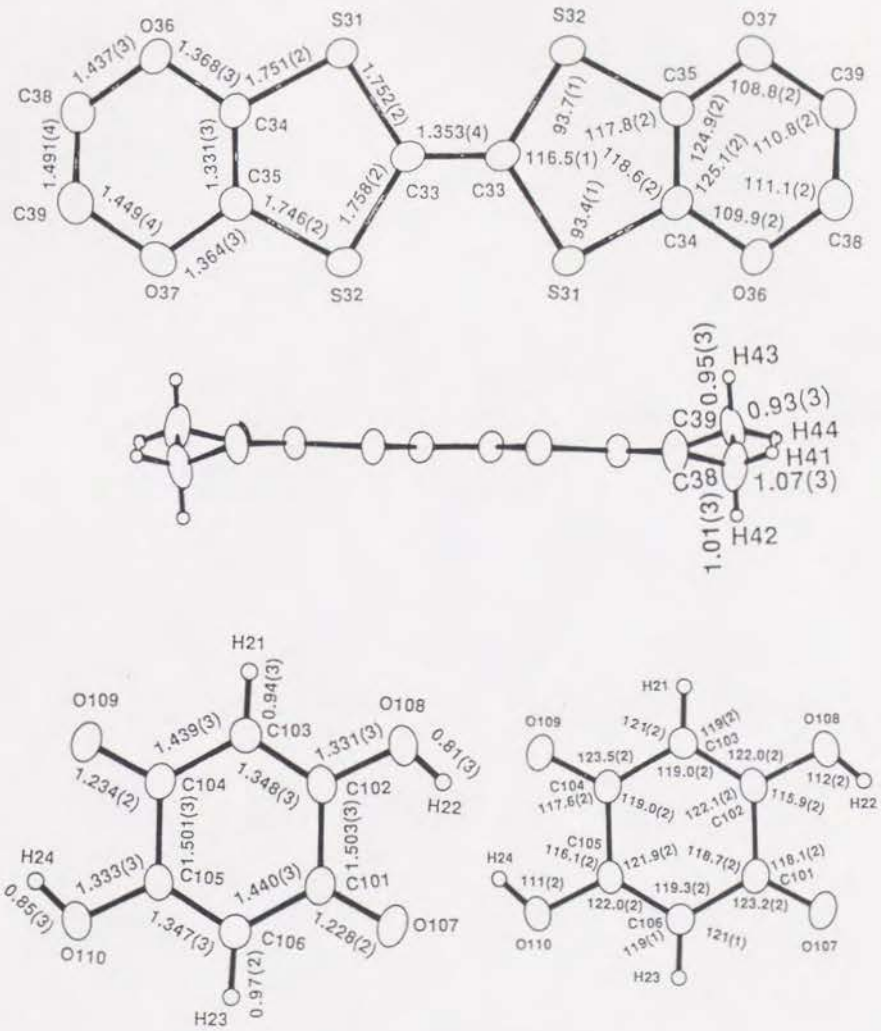

Figure A2. Bond lengths (Å) and angles (deg) in $(BEDO\text{-}TTF)[Q(OH)_2]_2$ (27)

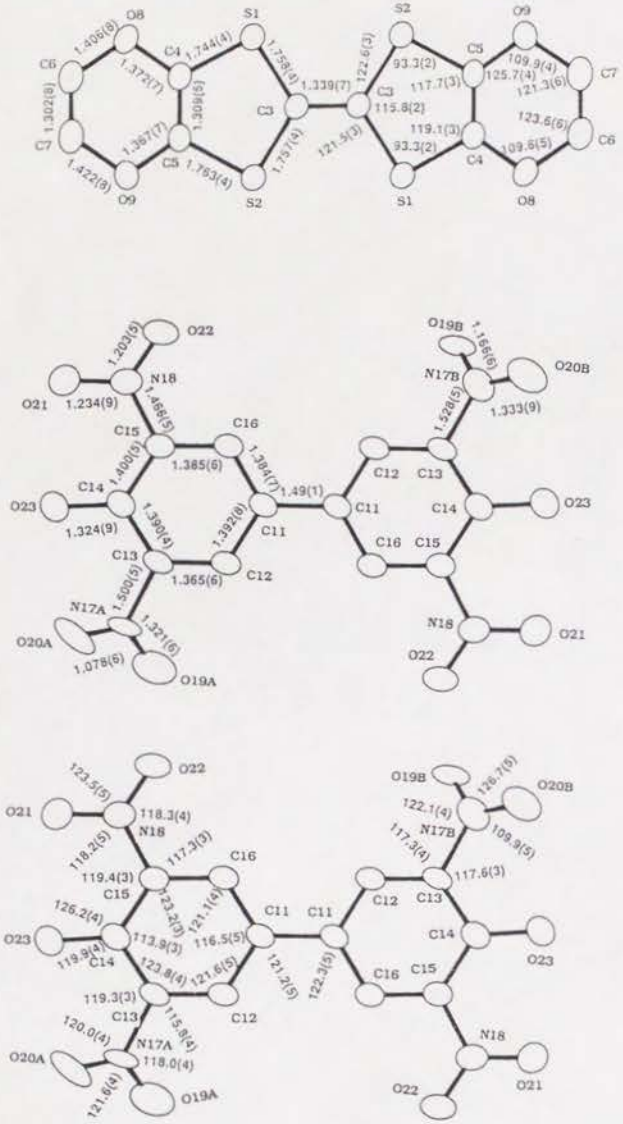

Figure A3. Bond lengths (Å) and angles (deg) in (BEDO-TTF)(TNBP) (29)

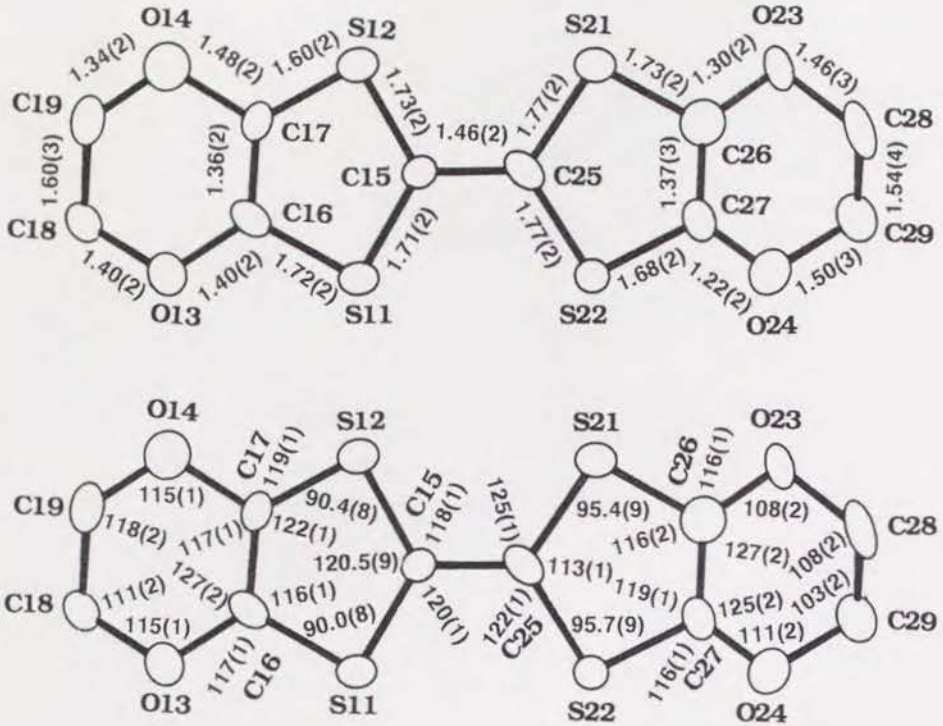

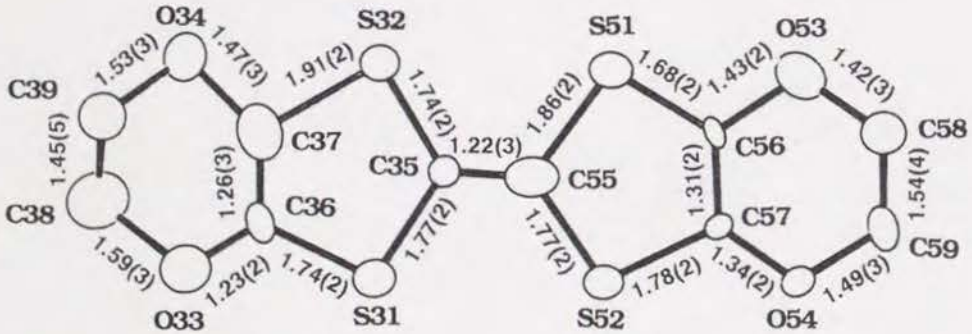

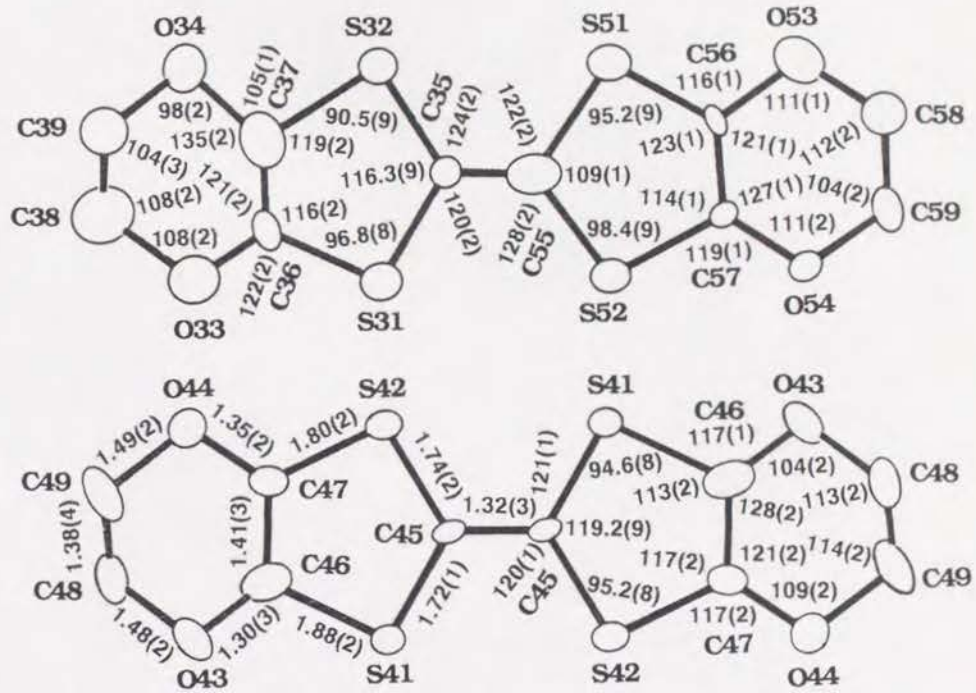

Figure A4. Bond lengths (Å) and angles (deg) in $(BEDO\text{-}TTF)_5(HCTMM)(PhCN)_2$ (31)

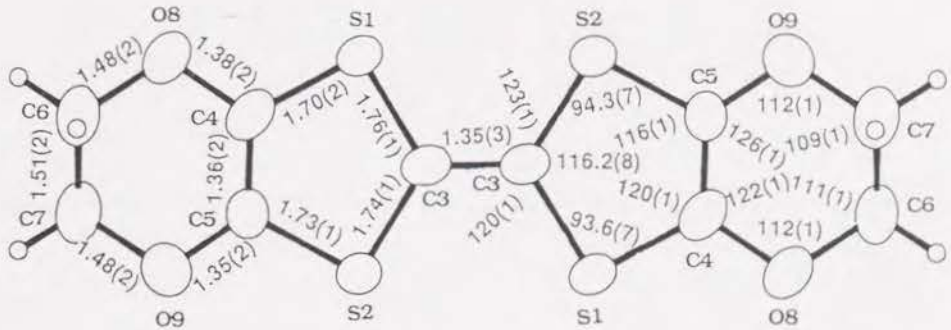

Figure A5. Bond lengths (Å) and angles (deg) in $(BEDO\text{-}TTF)_{10}(CF)_4(H_2O)_3$ (33)

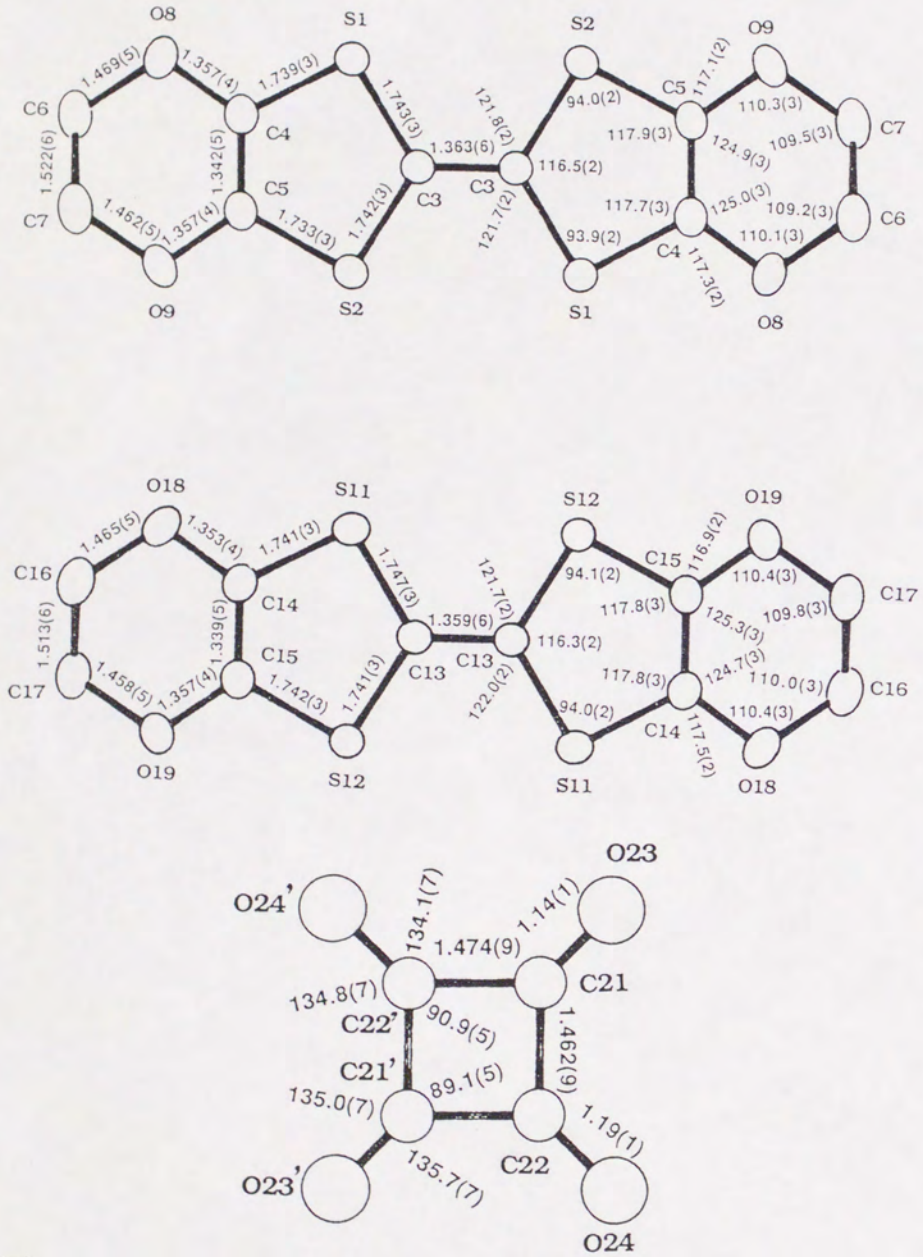

Figure A6. Bond lengths (Å) and angles (deg) in $(BEDO\text{-}TTF)_4(SQA)(H_2O)_6$ (34)

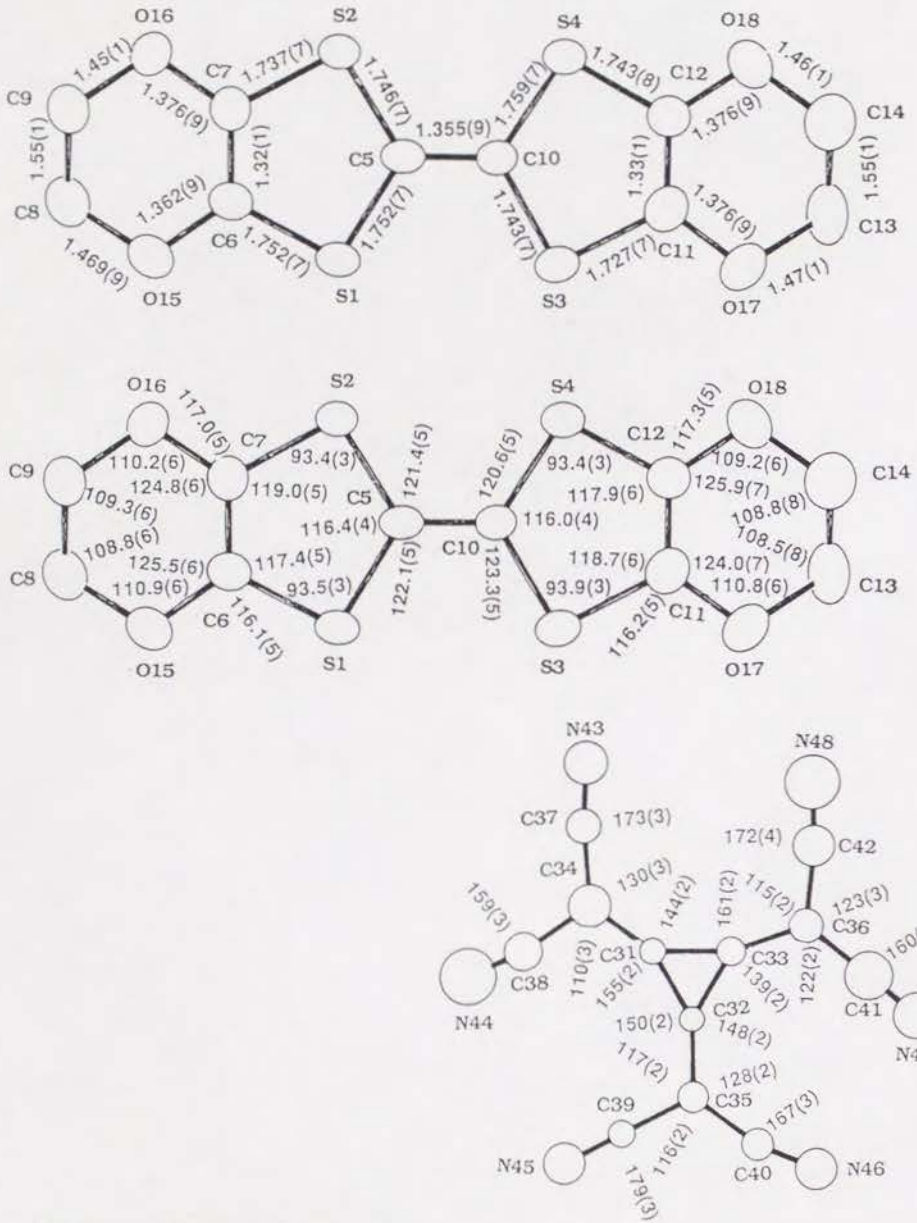

Figure A7. Bond lengths (Å) and angles (deg) in $(BEDO\text{-}TTF)_5(HCP)(PhCN)_{0.2}$ (37)

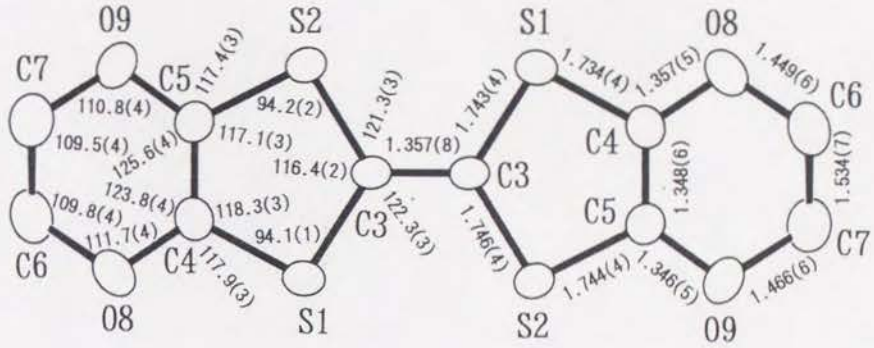

Figure A8. Bond lengths (Å) and angles (deg) in $(BEDO\text{-}TTF)_2Br(H_2O)_3$ (39)

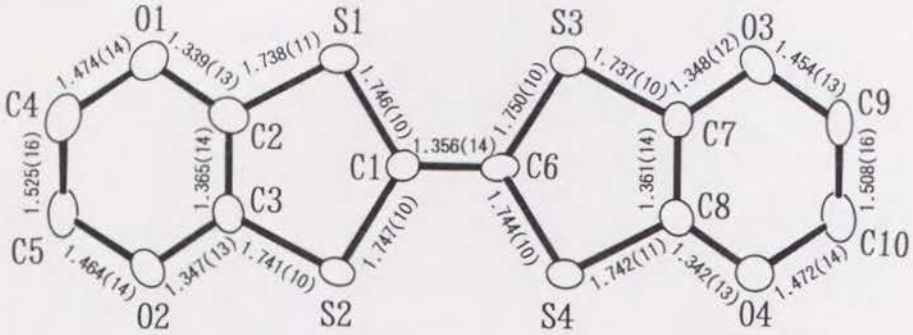

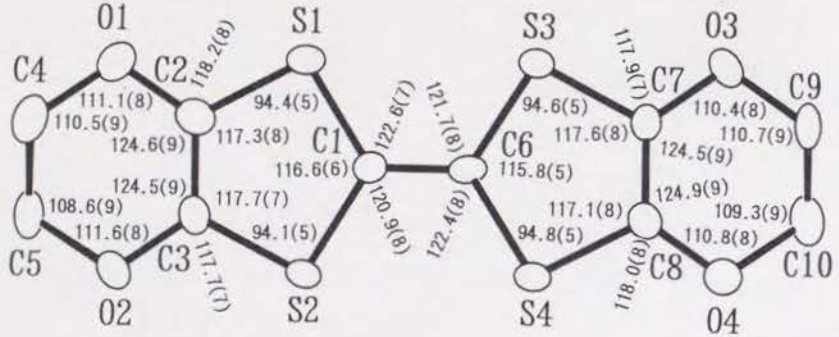

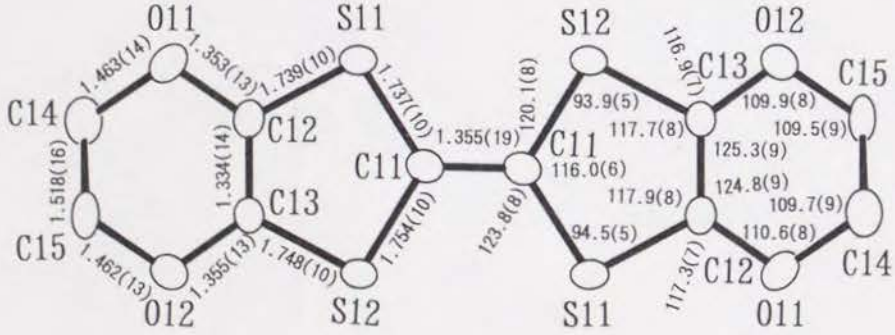

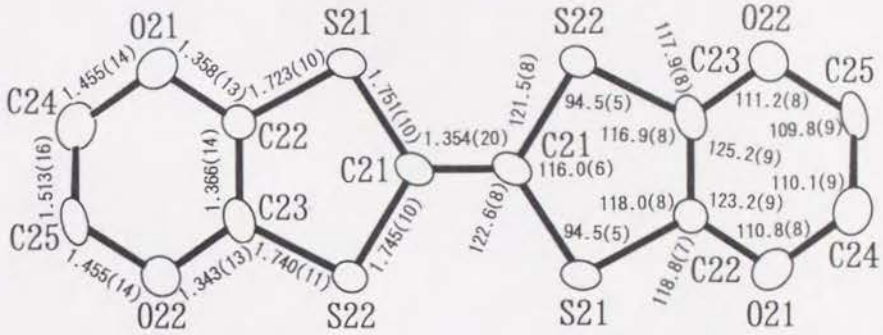

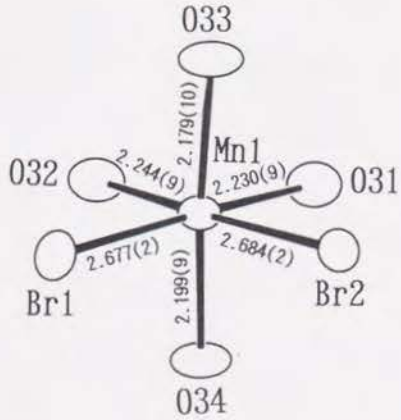

	Bond Angle (deg)		Bond Angle (deg)
Br1 -Mn1 -Br2	94.39(7)	Br2 -Mn1 -034	93.7(3)
Br1 -Mn1 -031	175.2(3)	031 -Mn1 -032	85.1(3)
Br1 -Mn1 -032	91.4(3)	031 -Mn1 -033	84.6(4)
Br1 -Mn1 -033	98.7(3)	031 -Mn1 -034	84.5(3)
Br1 -Mn1 -034	92.0(3)	032 -Mn1 -033	89.4(4)
Br2 -Mn1 -031	89.1(3)	032 -Mn1 -034	85.3(3)
Br2 -Mn1 -032	174.2(3)	033 -Mn1 -034	168.2(4)
Br2 -Mn1 -033	90.5(3)		

Figure A9. Bond lengths (Å) and angles (deg) in (BEDO-TTF)$_2$Br[MnBr$_2$(H$_2$O)$_4$](H$_2$O) (40)

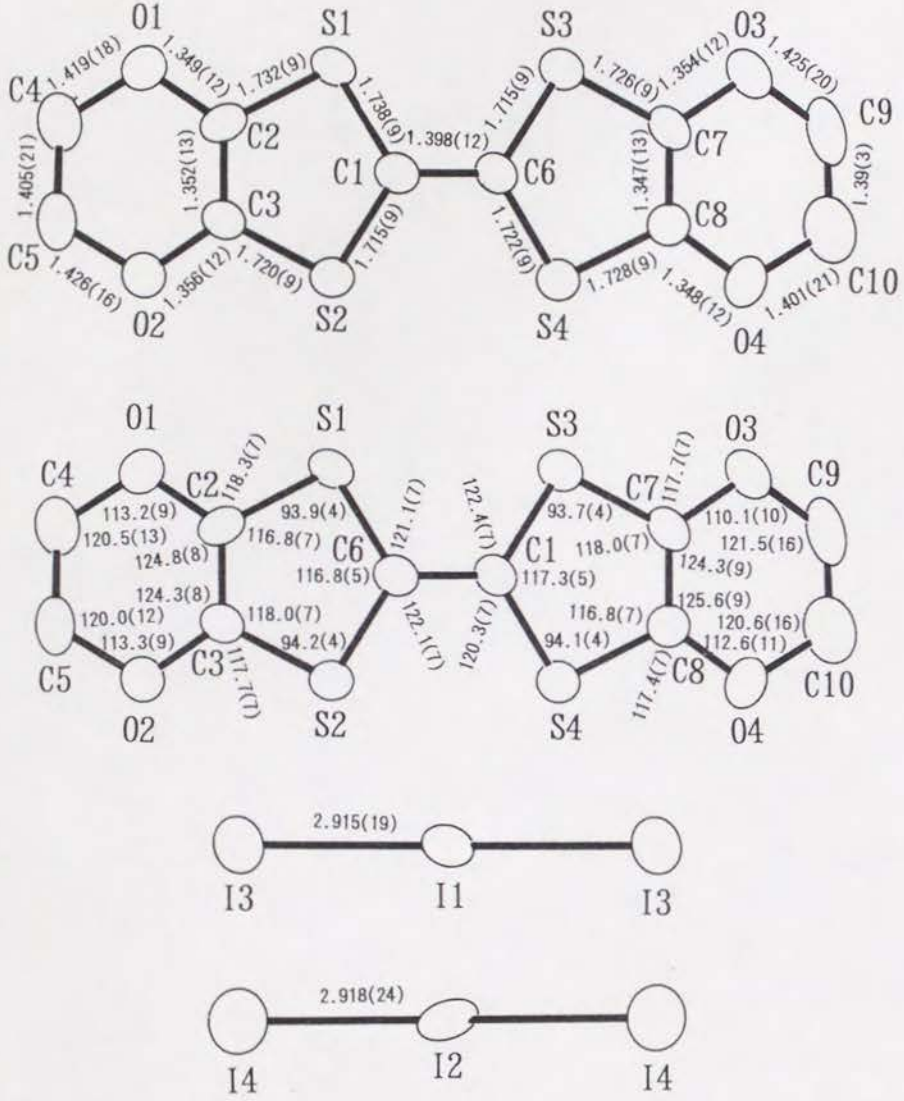

Figure A10. Bond lengths (Å) and angles (deg) in (BEDO-TTF)I_3 (42)

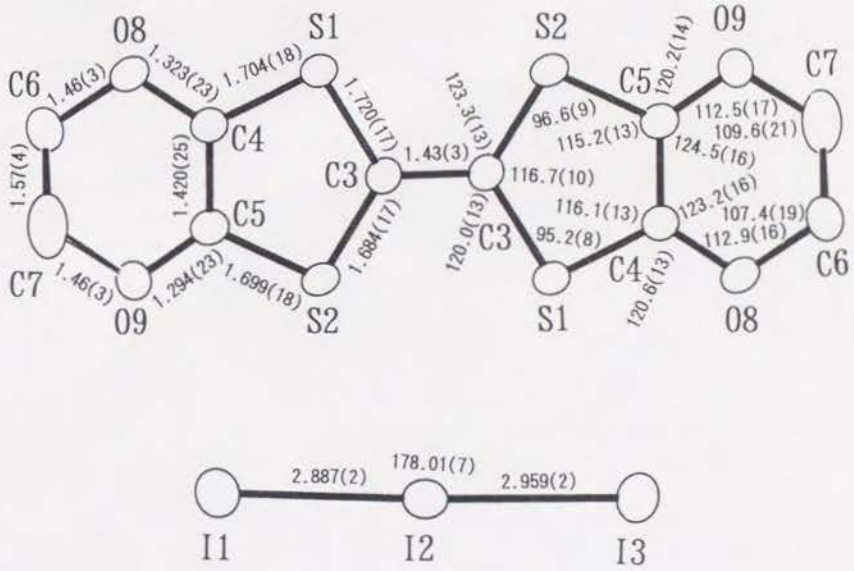

Figure A11. Bond lengths (Å) and angles (deg) in (BEDO-TTF)$(I_3)_2$ (43)